Volume 67C
Number 1
Jan.–Mar. 1963

Engineering and Instrumentation

U.S. DEPARTMENT OF COMMERCE

SECTION C

JOURNAL OF RESEARCH

NATIONAL BUREAU OF STANDARDS

Journal of Research
of the
National Bureau of Standards

C. Engineering and Instrumentation

JAN.-MAR. • 1963

VOLUME • 67C

NUMBER • 1

Editor: Martin Greenspan

Associate Editors: G. F. Montgomery, R. B. Jacobs

Publication dates:
Feb. 15, May 15, Aug. 15, Nov. 15, 1963

JOURNAL OF RESEARCH

The National Bureau of Standards Journal of Research reports research and development in the fields of activity shown at right. Also included from time to time are survey articles on topics closely related to the Bureau's scientific and technical program.

The Journal is published in four separate sections as follows:

A. Physics and Chemistry

Contains papers of interest primarily to scientists working in these fields. Issued six times a year. Annual subscription: domestic, $4.00; foreign, $4.75.

B. Mathematics and Mathematical Physics

Presents studies and compilations designed mainly for the mathematician and the theoretical physicist. Issued quarterly. Annual subscription: domestic, $2.25; foreign, $2.75.

C. Engineering and Instrumentation

Reports research and development results of interest chiefly to the engineer and the applied scientist. Issued quarterly. Annual subscription: domestic, $2.25; foreign, $2.75.

D. Radio Propagation

Reports work in radio propagation physics and upper atmospheric research. Issued six times a year. Annual subscription: domestic, $4.00; foreign, $4.75.

Functions and Activities

The functions of the National Bureau of Standards are set forth in the Act of Congress, March 3, 1901, as amended. These include the development and maintenance of the national standards of measurement and the provision of means and methods for making measurements consistent with these standards; the determination of physical constants and properties of materials, the development of methods and instruments for testing materials devices, and structures; advisory services to government agencies on scientific and technical problems; invention and development of devices to serve special needs of the Government; and the development of standard practices, codes, and specifications. The work includes basic and applied research development, engineering, instrumentation, testing, evaluation, calibration services, and various consultation and information services. The Bureau also serves as the Federal technical research center in a number of specialized fields. The scope of activities of the National Bureau of Standards is suggested in the following listing of the divisions and sections engaged in technical work.

Washington, D.C.

Electricity. Resistance and Reactance. Electrochemistry. Electrical Instruments. Magnetic Measurements. Dielectrics. High Voltage.
Metrology. Photometry and Colorimetry. Refractometry. Photographic Research. Length. Engineering Metrology. Mass and Scale. Volumetry and Densimetry.
Heat. Temperature Physics. Heat Measurements. Cryogenic Physics. Equation of State. Statistical Physics.
Radiation Physics. X-Ray. Radioactivity. Radiation Theory. High Energy Radiation. Radiological Equipment. Nucleonic Instrumentation. Neutron Physics.
Analytical and Inorganic Chemistry. Pure Substances. Spectrochemistry. Solution Chemistry. Standard Reference Materials. Applied Analytical Research. Crystal Chemistry.
Mechanics. Sound. Pressure and Vacuum. Fluid Mechanics. Engineering Mechanics. Rheology. Combustion Controls.
Polymers. Macromolecules: Synthesis and Structure. Polymer Chemistry. Polymer Physics. Polymer Characterization. Polymer Evaluation and Testing. Applied Polymer Standards and Research. Dental Research.
Metallurgy. Engineering Metallurgy. Microscopy and Diffraction. Metal Reactions. Metal Physics. Electrolysis and Metal Deposition.
Inorganic Solids. Engineering Ceramics. Glass. Solid State Chemistry. Crystal Growth. Physical Properties. Crystallography.
Building Research. Structural Engineering. Fire Research. Mechanical Systems. Organic Building Materials. Codes and Safety Standards. Heat Transfer. Inorganic Building Materials. Metallic Building Materials.
Applied Mathematics. Numerical Analysis. Computation. Statistical Engineering. Mathematical Physics. Operations Research.
Data Processing Systems. Components and Techniques. Computer Technology. Measurements Automation. Engineering Applications. Systems Analysis.
Atomic Physics. Spectroscopy. Infrared Spectroscopy. Solid State Physics. Electron Physics. Atomic Physics.
Instrumentation. Engineering Electronics. Electron Devices. Electronic Instrumentation. Mechanical Instruments. Basic Instrumentation.
Physical Chemistry. Thermochemistry. Surface Chemistry. Organic Chemistry. Molecular Spectroscopy. Molecular Kinetics. Mass Spectrometry.

Office of Weights and Measures.
Boulder, Colo.

Cryogenic Engineering Laboratory. Cryogenic Equipment. Cryogenic Processes. Properties of Materials. Cryogenic Technical Services.

Central Radio Propagation Laboratory

Ionosphere Research and Propagation. Low Frequency and Very Low Frequency Research. Ionosphere Research. Prediction Services. Sun-Earth Relationships. Field Engineering. Radio Warning Services. Vertical Soundings Research.
Radio Propagation Engineering. Data Reduction Instrumentation. Radio Noise. Tropospheric Measurements. Tropospheric Analysis. Propagation-Terrain Effects. Radio-Meteorology. Lower Atmosphere Physics.
Radio Systems. Applied Electromagnetic Theory. High Frequency and Very High Frequency Research. Modulation Research. Antenna Research. Navigation Systems.
Upper Atmosphere and Space Physics. Upper Atmosphere and Plasma Physics. Ionosphere and Exosphere Scatter. Airglow and Aurora. Ionospheric Radio Astronomy.

Radio Standards Laboratory

Radio Physics. Radio Broadcast Service. Radio and Microwave Materials. Atomic Frequency and Time-Interval Standards. Millimeter-Wave Research.
Circuit Standards. High Frequency Electrical Standards. Microwave Circuit Standards. Electronic Calibration Center.

U.S. DEPARTMENT OF COMMERCE
Luther H. Hodges, Secretary

NATIONAL BUREAU OF STANDARDS
A. V. Astin, Director

Order all publications from the Superintendent of Documents
U.S. Government Printing Office, Washington 25, D.C.

Use of funds for printing this publication approved by the Director of the Bureau of the Budget (June 19, 1961).

JOURNAL OF RESEARCH of the National Bureau of Standards—C. Engineering and Instrumentation
Vol. 67C, No. 1, January–March 1963

Method for Calibrating a Standard Volt Box

Bernadine L. Dunfee

(August 22, 1962)

A volt box provides several discrete ratios and permits the accurate measurement of direct voltages (maximum about 1,500 volts) through their reduction by suitable factors to values within the measuring capability of a potentiometer. The ratios of a volt box are measured against those of a standard using a "difference" technique. The standard volt box used at the National Bureau of Standards possesses those design features required for a ratio standard and lends itself to a "self-calibration" technique. This paper describes a method for measuring its ratios at rated and above rated voltage to an accuracy of 10 parts per million or better using a Direct Reading Ratio Set and a group of resistance standards. Although the method is described in its particular application to the NBS standard it can be used equally well in the measurement of other ratio networks. Errors that might appear in the measurements and procedures for evaluating their magnitudes are outlined and the derivation of a general expression that defines all ratios in terms of measured quantities is presented in an appendix. Comments and further details regarding the standard and its use are included.

1. Introduction

The value of a measured voltage, either direct or alternating, is derived from the national standard of emf. At the National Bureau of Standards the unit of voltage is maintained in terms of the mean value of emf of 48 saturated cells. This emf is only slightly larger than one volt so that the accurate measurement of larger voltages of any frequency usually requires the design of special ratio networks that can serve as voltage ratio standards, because of their stability and high accuracy. The volt box and the potentiometer with which it is used are classic examples in the measurement of moderately high direct voltages.

The volt box referred to here, as differentiated from other types of d-c ratio devices (or voltage dividers), provides several discrete ratios so that the voltage to be measured (maximum about 1,500 v) is reduced by a suitable factor to a value within the measuring capability of a potentiometer. Insertion of a volt box in a measuring circuit introduces an error in the measurement unless the volt box divides perfectly or the corrections to its nominal ratios are known and applied. In any event, each ratio must be measured, preferably at rated voltage and at a reduced voltage to evaluate the effects of self heating and leakage resistance.

The method of calibration employed at NBS utilizes a difference technique in which the potential at each binding post of a volt box under test is measured with respect to that at the corresponding binding post of the standard volt box, with both instruments connected in parallel and for the same nominal ratio. Special features must therefore be incorporated in the standard volt box to assure long term stability and the resistance sections must be arranged in a proper sequence with respect to magnitude so that a "self-calibration" procedure is possible and accurate to better than 10 parts per million (ppm). The standard volt box used at NBS, as well as a method developed for its calibration, have been described by Silsbee and Gross [1].[1]

A second method for calibrating the standard volt box was recently developed and has been under observation for more than a year. The associated circuitry and components have been incorporated in a semiportable test console and the only connections that need be made at the time of test are those to the d-c supply and to the volt box. The present paper describes this method and uses the NBS standard volt box to illustrate the technique. Additional comments are included on the use of the standard volt box in calibrating other volt boxes.

2. Comments on the Calibration of a Volt Box Against the Standard

A volt box consists, in general, of a large number of resistance coils connected in series. At both the low- and high-potential ends and at appropriate junctions along the resistor, taps are brought out to binding posts to form the high voltage side. The maximum voltage that can be applied between the zero post and any of the others is governed by the design of the resistance coils and is so marked at each binding post. In addition, the resistance of the lowest section is tapped at an appropriate point and

[1] Figures in brackets indicate the literature references at the end of this paper.

'eads are brought out from the zero potential end and this tap point to binding posts, forming the low voltage side for connection to a potentiometer. Any given voltage ratio is defined as the ratio of the voltage applied to the high side to that appearing across the low side. These ratios are integers and a given volt box, for example, may cover values from 1,500/1.5 to 3/1.5 if it is to be used with a 1.5-v potentiometer or values from 1,500/0.15 to 3/0.15 for a 150-mv potentiometer.

The test instrument is calibrated with reference to the standard in the circuit shown schematically in figure 1. The two volt boxes, having the same nominal ratio, are connected in parallel through leads l_1 and l_2 across a suitable d-c source. The measuring branch, consisting of a detector, a low range potentiometer, and a reversing switch (not shown), is inserted, in voltage opposition, into gaps identified at positions v_1, v_2, v_3, and v_4. For each position the output of the potentiometer is adjusted for a null on the detector so that at balance the potential difference between corresponding points on the two volt boxes is equal to that of the potentiometer. The potential differences v_1 and v_4 are small since they are essentially the potential drops in leads l_1 and l_2; similarly, if the volt box under test is of high quality, potential differences v_2 and v_3 will be small. Thus only moderate accuracy is required in the measurement of the potential differences in order to realize an extremely high accuracy for the values of ratio.

The equation that defines the ratio of the volt box under test in terms of the ratio of the standard and the measured potential differences may be derived as follows. Let the respective polarities be as shown in figure 1. By definition, the true ratio of the volt box under test is

$$N_{xt}=N_{xn}[1+\mu_x]=\frac{V}{V_{ab}} \tag{1}$$

where μ_x is the correction in proportional parts and N_{xn} is the nominal ratio.

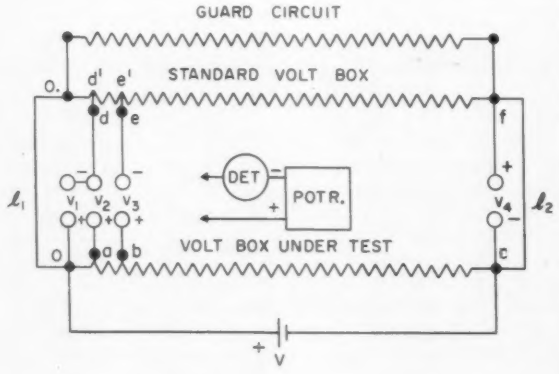

FIGURE 1. *Circuit for calibrating a volt box.*

Summing the potential drops around loop "badeb" gives

$$V_{ab}-v_2-V_{de}+v_3=0$$

or

$$V_{ab}=V_{de}+(v_2-v_3). \tag{2}$$

By definition, the true ratio of the standard volt box is

$$N_{st}=N_{sn}[1+\mu_s]=\frac{V_{df}}{V_{de}}$$

or

$$V_{de}=\frac{V_{df}}{N_{sn}[1+\mu_s]}$$

where N_{sn} is the nominal ratio of the standard and μ_s is the correction in proportional parts. Substituting this value in eq (2) gives

$$V_{ab}=\frac{V_{df}}{N_{sn}[1+\mu_s]}+(v_2-v_3). \tag{3}$$

Summing the potential drops around loop "defcod" we have

$$-V_{df}-v_4+V-v_1=0$$

or

$$V_{df}=V-(v_1+v_4).$$

When this expression is substituted in eq (3) V_{ab} becomes

$$V_{ab}=\frac{V-(v_1+v_4)}{N_{sn}[1+\mu_s]}+(v_2-v_3)$$

and if substituted in eq (1) the true ratio of the volt box under test becomes

$$N_{xn}[1+\mu_x]=\frac{VN_{sn}[1+\mu_s]}{V-(v_1+v_4)+N_{sn}[1+\mu_s](v_2-v_3)}.$$

On rearranging terms and remembering that $N_{xn}=N_{sn}\approx N_{sn}[1+\mu_s]$ the above expression becomes

$$[1+\mu_x]=\frac{[1+\mu_s]}{1-\dfrac{(v_1+v_4)}{V}+N_{sn}\dfrac{(v_2-v_3)}{V}}$$

so that

$$\mu_x=\mu_s+\frac{(v_1+v_4)}{V}-\frac{(v_2-v_3)}{V/N_{sn}}\text{ plus higher order terms.} \tag{4}$$

If v_1, v_2, v_3, v_4, and V are expressed in volts then, neglecting higher order terms, the correction to the nominal ratio is

$$\mu_x=\mu_s+\frac{(v_1+v_4)}{V}+\frac{(v_3-v_2)}{V/N_{sn}}\text{ in proportional parts.} \tag{5}$$

If v_1, v_2, v_3, and v_4 are expressed in microvolts and μ_s in ppm the correction is given in ppm. It should be noted that if the relative polarities of the supply voltage (V) and the potentiometer differ from those assumed in figure 1, the appropriate sign must be given to the recorded values of the measured quantities.

As will be seen later in the discussion on the calibration of the standard volt box, the measured resistances of all sections and their summations are referred to the resistance of the first section which is chosen to lie between junctions $d'-e'$. Thus the true ratio of the standard volt box, given as $\frac{V_{df}}{V_{de}}$ in the above derivation, is consistent with the measured ratio. (The effects of rod resistances,[2] such as o.d.', on the measured ratios are discussed in the section on errors.)

It is advisable that the potential drops in leads l_1 and l_2 be small in order to achieve the highest accuracy in the measured ratios without placing undue demands on the accuracy required in the measurement of the potential differences. A slight modification made in the test circuit would eliminate the lead effect and at the same time simplify the computation of test data. Referring to figure 2, let small resistances R_1 and R_2 be connected in the l_1 and l_2 branches with the d-c supply connected between their sliding contacts. The potential drops in the two sections of branch l_1, as well as those in branch l_2, are in opposition so that it is only necessary to adjust the respective sliders to achieve cancellation, which is indicated by a null on the detector connected at the v_1 and v_4 positions, respectively (see fig. 1). For this condition, the second term on the right of eq (5) becomes zero.

3. Standard Volt Box

A volt box must have several special features incorporated in its design if it is to serve as a standard in making ratio measurements to an accuracy of a few ppm. (1) Some provision must be made for reducing the effects from leakage paths to negligible amounts; (2) the selection and arrangement of the resistance wire must guarantee freedom from the effects of relative humidity as well as those arising from self-heating; (3) the corrections to the ratios should be small and the resistances of the tapped sections proportioned so that a "self-calibration" procedure of sufficient accuracy is applicable.

3.1. Leakage

The volt box is a high resistance network operating at rather high voltages so that careful consideration must be given to minimizing leakage paths into which a portion of the current may be diverted from points along the working resistance. Effects from such parallel paths may be reduced sufficiently by keeping the insulation resistance high. For example, if the total resistance of the high side is 250,000 ohms, the resistance of a leakage path bridging this section must be 2.5×10^9 ohms for an uncertainty no greater than 0.01 percent, and 2.5×10^{11} ohms if an error no greater than 1 ppm is required. This protection

[2] The rod resistances mentioned throughout the text refer to the leads which extend from the resistance sections to the binding posts where connections are made to the external circuit.

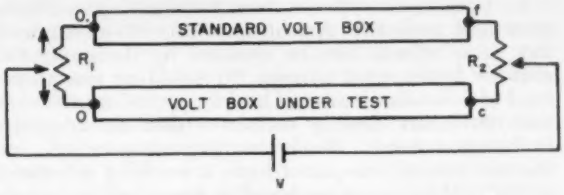

FIGURE 2. *Branches for compensating lead drops.*

may not be adequate in maintaining long-time stability because of possible accumulation of moisture and contamination across the insulating surface or possible deterioration of the insulation over long use. Additional protection must be provided by a guard network which, in effect, maintains the shields surrounding the resistance sections at the same potential as that of the resistance section within.

The standard volt box discussed here is equipped with a guarding resistance whose corresponding sections can be connected in parallel with the working circuit when the 15-v and higher ranges are used. Metal guard rings surrounding each binding post of the working resistance and connected to the corresponding binding post of the guarding resistance prevent leakage across and through the top panel. The working resistance is divided into sections of not more than 25,000 ohms with the resistance coils of each section mounted on separate insulating panels. Each of these insulating panels is fastened to the top panel through a metal block that is connected to the guard resistance and maintained at the appropriate potential to prevent leakage from one insulating panel to another. In use, leads that connect the standard volt box to the volt box under test and to the other parts of the measuring circuit carry their own shields which are maintained at their appropriate potentials through connections to the binding posts of the guard circuit.

3.2. Humidity and Self-Heating

Any effect from relative humidity on a properly guarded volt box originates at the resistance coils. It has long been known that certain insulating materials used for wire covering and for protective coatings of resistance coils are susceptible to changes in relative humidity and produce changes in the resistance of the coils. Although the effect might be expected to be negligible in materials available today or, if not, to be sufficiently suppressed in ratio devices, the matter must be considered if accuracies of a few ppm are desired. The particular standard volt box referred to in the original paper was found to have seasonal variations as large as 30 ppm as a result of changing humidity, so that provision was made for continuously supplying dry air at a pressure slightly higher than atmospheric. In 1960 a new unit was purchased in which the individual resistance coils are hermetically sealed. To date, no measurable seasonal variations because of changing humidity have been observed.

In theory, the effects from self-heating could be measured and the appropriate correction applied; but these effects can be avoided by designing the unit for lower rated current, by selecting the proper kind of resistance material and by providing the coils with sufficient cooling surface within an adequate exchange volume. Both the original standard and the one recently acquired have a working resistance of 333⅓ ohms/v and each coil is wound with a single layer of manganin wire taken from the same spool. There is sufficient freedom from self-heating that, with double rated voltage applied, the correction differs from that at reduced voltage by less than 5 ppm.

3.3. Self-Calibration Feature

The most difficult and critical problem encountered with any standard is the determination of its corrections to an accuracy considerably better than that required for the test instrument. The method should not only satisfy the immediate requirements in accuracy but should be capable of providing still better accuracy in the anticipation of future demands.

One of the most powerful measuring techniques available and one capable of the highest accuracy is that in which small differences are measured between like and nearly equal quantities. The circuit suggested by Silsbee and used in the designs of both standard volt boxes lends itself to this "difference" technique. Its arrangement and adaptation to difference measurements can be best understood by referring to figure 3. The circuit has 21 tapped sections beginning with the "0 to 0.15" section of 50 ohms and continuing to the "750 to 1500" section of 250,000 ohms.[3] This resistance chain can be considered as being formed of four groups M_1, M_2, M_3, and M_4 in which group M_1 serves as the first section of group M_2, M_2 as the first section of group M_3, and M_3 as the first section of group M_4. Being so considered the following pattern is observed. Each group contains six sections. The first five sections of any group have nominally equal resistances while the sixth section has a value nominally equal to the sum of the first five. It is possible, therefore, to measure the small differences between the first 50-ohm section and each of the remaining four sections of group M_1, and follow this by measuring the difference between the 250-ohm section and the sum of the first five sections. Since M_{n-1} forms the first section of M_n this measuring sequence can be repeated for each group in turn. Because of the continuity within a group and from one group to the next, the resistance of any portion summed from the zero end, compared with that of the first 50-ohm section can be computed from the nominal value of their ratio and the sum of the measured differences.

4. Direct Reading Ratio Set Test Method

With the rapid growth of standards laboratories evident in recent years, voltage ratio standards of the type discussed here are no longer the exclusive property of the National standardizing laboratory. The method recently adopted at NBS for calibrating the standard volt box and described herein makes use of equipment that is readily available in many of these laboratories. Thus, from the information that is given on both the theoretical and practical aspects of the method, the standards laboratory can perform the calibration without recourse to NBS. The method is not limited solely to those volt boxes having the particular sequence of sections indicated in figure 3 but can be used for any network in which the resistance of each section is nominally equal to the resistance of some combination of lower-valued sections. The only change lies in the defining equation and its derivation.

4.1. General Comments

A Wheatstone bridge network is used in which the successive difference measurements, referred to in the previous section, are made by inserting in turn each section or summation of sections in the unknown arm of the bridge. Aside from a d-c supply and detector, the only equipment required is a Direct

[3] The last section of 250,000 ohms is not present in the standard volt boxes at NBS. It is included here for completeness.

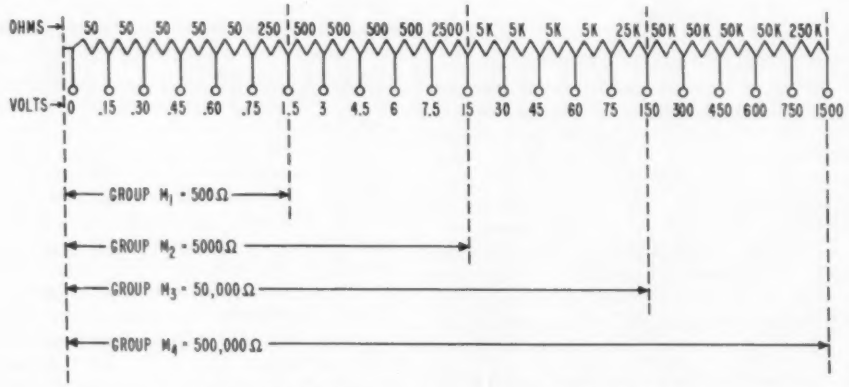

FIGURE 3. *"Self-calibrating" network of a standard volt box.*

Reading Ratio Set (DRRS) and a group of seven resistance standards: one each having the values 50, 200, 500, 2,000, and 5,000 ohms, and two having a value of 50,000 ohms. (Other types of resistors or resistance assemblies could be substituted for the standard resistors if they remain stable during the sequence of measurements.) The execution of the test is quite rapid and with the circuit incorporated in a suitable console a complete calibration including computation can be made in an hour by experienced personnel.

In the original method the test voltage was limited to some extent because of possible heating of the components. For example, measurements on the 50,000-ohm sections, if made at their rated voltage of 150 v, required a power dissipation of 2.25 w in one of the standard resistors. Since it is advisable to keep the power dissipation appreciably less than this amount, periodic calibrations were made at reduced voltage after it was initially established that changes arising from self-heating were negligible. The DRRS method has the advantage that all sections can be measured at their rated voltage. Under this condition the maximum power dissipation required of the standard resistor is 0.45 w. With some of the resistor assemblies now available the method can be extended to measurements at 200 percent rated voltage so that the overload capability of the standard volt box can be easily determined.

The method has a further advantage in that the positions of the supply and galvanometer (detector) relative to the circuit are such that the change in circuit resistance as seen by the galvanometer is quite small. Thus the damping and galvanometer response are little affected throughout the measurements.

4.2. Calibration Procedure

The measuring circuits are indicated schematically in figures 4a and 4b; the reversing switch for the supply is omitted to preserve simplicity. Resistances A and B represent the two arms of a DRRS (including leads) each having a nominal value of 100 ohms and S is a standard resistor always serving as a "Dummy" resistance and having a nominal value equal to that of the volt box section being measured. The guard branch that appears in figure 4b includes a resistance of about 80 ohms [4] in series with the appropriate guard section of the volt box; and the leads of the measuring circuit are of such length and size that at balance the DRRS reads near midscale.

Measurements on the first five sections are made with the circuit of figure 4a. The d-c supply is connected to the 1.5 binding post and the detector to the zero dot (0.) so that rod resistances l_1, l_2 . . . l_{n-1} appear in the A- and S-arms of the bridge rather than as part of the resistance being measured. Inequalities among the rod resistances can introduce errors in the measured ratios and are of greater significance when the low-valued sections are measured. There are three alternatives for locating the rod resistances: (1) both rods may be connected as part of the section being measured, (2) one rod may be so connected and the other located in the S-arm, and (3) they may be arranged as shown in figure 4a. The relative magnitudes of the rod resistances in the NBS standard volt box indicate figure 4a as the preferred connection.[5]

The remaining sections whose resistances are 250 ohms or more are measured in the network of figure 4b. (The rod resistances are expected to be negligible compared with the resistance of the section to which they are assigned.) The guard circuit of the particular standard volt box under discussion is not equipped with taps below the 15-v range so that it is used only on the ranges of 15 v and higher. Thus, for all successive resistances measured after the first five and to, but not including, the "15 to 30" section, the guard branch of figure 4b is not used. For all remaining measurements the guard branch is connected as shown in the figure.

The appropriate bridge network is balanced by adjusting the dials of the DRRS for a null on the detector as each section, or summation of sections, beginning with $R_{1,1}$ is inserted in succession in the "unknown" arm of the bridge. The procedure is as follows. With $S=S_{a1}=50$ ohms, the bridge of figure 4a is balanced with the first 50-ohm section

[4] The resistance per section of the guard of the volt box is 0.8 that of the working resistance.

[5] The influence of these rod resistances can be completely avoided by modifying the circuit so that the 50-ohm sections are measured as 4-terminal resistors. This technique is described in reference [2].

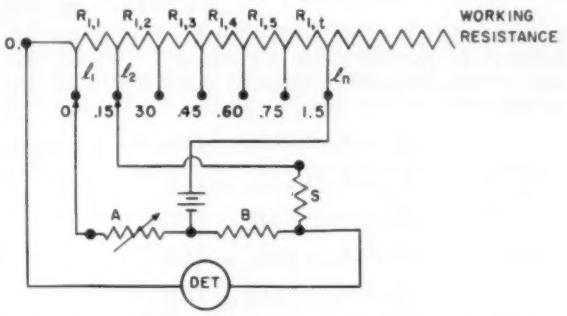

FIGURE 4a. *Circuit for measuring the lower-valued ratios.*

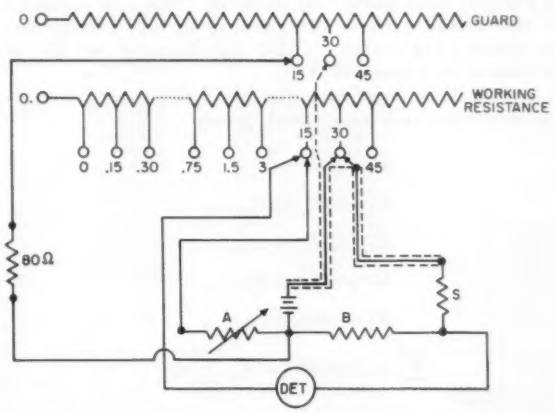

FIGURE 4b. *Circuit for measuring the higher-valued ratios.*

($R_{1,1}$) inserted in the unknown arm. In rapid sequence, each of the remaining four 50-ohm sections is inserted in turn and the bridge rebalanced in each instance. The resistance of each 50-ohm section can now be stated in terms of the resistance of $R_{1,1}$ and the measured difference, and the group can be summed to give $\sum_{k=1}^{k=5} R_{1,k}$ (computed). The next set of balances completes the series of measurements required for group M_1. It consists of two measurements using the appropriate circuit of figure 4b and with $S=S_{b1}=250$ ohms. The reference balance is made with the sum of the 50-ohm sections $\sum_{k=1}^{k=5} R_{1,k}$, having a nominal value of 250 ohms, connected into the unknown arm through the zero and 0.75 binding posts and is immediately followed by a measurement of $R_{1,t}$. This set of measurements provides a value of $R_{1,t}$ (sixth section) in terms of $\sum_{k=1}^{k=5} R_{1,k}$ and the measured difference. Since the value of $\sum_{k=1}^{k=5} R_{1,k}$ is obtained by summing the values from the first five measurements, straightforward substitution gives the value of $R_{1,t}$ in terms of $R_{1,1}$ and the sum of the measured differences. Adding this value of $R_{1,t}$ to the value of $\sum_{k=1}^{k=5} R_{1,k}$ (computed) gives the total resistance of group M_1 referred to the reference section $R_{1,1}$. These two sets of measurements expressed mathematically are as follows:

$$R_{1,1}=S_{a1}[1+(D_{1,1}-D_0)]$$
$$R_{1,2}=S_{a1}[1+(D_{1,2}-D_0)]$$
$$R_{1,3}=S_{a1}[1+(D_{1,3}-D_0)]$$
$$R_{1,4}=S_{a1}[1+(D_{1,4}-D_0)]$$
$$R_{1,5}=S_{a1}[1+(D_{1,5}-D_0)]$$

where $(D_{1,1}-D_0)$, $(D_{1,2}-D_0)$, etc., are the differences in proportional parts [6] as deduced from the readings of the DRRS; D_0 is the reading of the DRRS for an exact 1:1 ratio. (The significance of D_0 is explained in appendix A.)

Subtracting the first equation from each succeeding equation and from itself, gives

$$R_{1,1}=R_{1,1}$$
$$R_{1,2}=R_{1,1}+S_{a1}d_{1,2}$$
$$R_{1,3}=R_{1,1}+S_{a1}d_{1,3}$$
$$R_{1,4}=R_{1,1}+S_{a1}d_{1,4}$$
$$R_{1,5}=R_{1,1}+S_{a1}d_{1,5}$$
$$\sum_{k=1}^{k=5} R_{1,k}=5R_{1,1}+S_{a1}\sum_{k=1}^{k=5} d_{1,k}$$

[6] See appendix A.

where $d_{1,2}=(D_{1,2}-D_{1,1})$; $d_{1,3}=(D_{1,3}-D_{1,1})$ etc.

Since $S_{a1}=R_{1,1}$ closel y enough,

$$\sum_{k=1}^{k=5} R_{1,k}=5R_{1,1}\left[1+\sum_{k=1}^{k=5}\frac{d_{1,k}}{5}\right]. \qquad (6)$$

The second set of measurements stated in similar fashion is

$$\sum_{k=1}^{k=5} R_{1,k}=S_{b1}[1+(D_{1,s}-D_0)]$$
$$R_{1,t}=S_{b1}[1+(D_{1,t}-D_0)].$$

On subtracting, this gives

$$R_{1,t}=\sum_{k=1}^{k=5} R_{1,k}+S_{b1}d_{1,t} \text{ where } d_{1,t}=(D_{1,t}-D_{1,s}).$$

Substituting eq (6) in the above expression and remembering that

$S_{b1}=5R_{1,1}$ closely enough, $R_{1,t}$ becomes

$$R_{1,t}=5R_{1,1}\left[1+\sum_{k=1}^{k=5}\frac{d_{1,k}}{5}+d_{1,t}\right]. \qquad (7)$$

Adding eqs (6) and (7) and arranging terms gives

$$\sum_{k=1}^{k=5} R_{1,k}+R_{1,t}=10R_{1,1}\left[1+\sum_{k=1}^{k=5}\frac{d_{1,k}}{5}+\frac{d_{1,t}}{2}\right] \qquad (8)$$

which states the total resistance of group M_1 in terms of $R_{1,1}$ and the measured differences.

Group M_1, having a nominal value of 500 ohms and a true value given by eq (8), serves as the first section of group M_2 which, as in the case of group M_1, consists of five nominally equal sections plus a sixth section having a value nominally equal to the sum of the five sections (see fig. 3). The sequence of seven balances is now obtained for group M_2. In the first set of this sequence, with $S=S_{a2}=500$ ohms, each of the 500 ohm sections, beginning with group M_1 as the reference section, is inserted in the bridge to obtain five measurements. In the second set two balances are obtained, first with all 10 sections (2,500 ohms) in the unknown arm and then with the eleventh section (2,500 ohms) inserted; for this set, $S=S_{b2}=2{,}500$ ohms. Since group M_1 has a computed value given by eq (8), the summation procedure can be extended through group M_2 which contains all sections up to the 15 v tap and becomes the first section of M_3.

The same procedure is carried forward through groups M_3 and M_4 with resistance S always having a value nominally equal to that of the section being measured.

The mathematical treatment presented in this section attempts to clarify the significance of the computation process associated with the step-up procedure (sometimes called a bootstrap technique), which may be masked in the more formal approach given in appendix B.

4.3. Computations

The readings of the DRRS having been recorded, the summation of their differences can be computed according to the following equation (developed in appendix B) to give the correction to the nominal ratios of the standard volt box

$$N_{m,k}=N'_{m,k}\left[1+\frac{\sum_{k=1}^{k=5} d_{1,k}+\sum_{k=1}^{k=5} d_{2,k}\ldots+\sum_{k=1}^{k=5} d_{m-1,k}}{5}+\frac{d_{1,t}+d_{2,t}\ldots+d_{m-1,t}}{2}+\frac{\sum_{k'=1}^{k'=k} d_{m,k'}}{k}\right]. \quad (9)$$

Where $N_{m,k}$=true value of the ratios,
$N'_{m,k}$=nominal values of the ratios;
$d's$=measured differences in proportional parts.

The schedule of computation given in table 1 was derived, in effect, by applying eq (9) to successively increasing values of k and m. Its arrangement permits the computation of all corrections in a single process without having to apply the equation directly each time a ratio is determined. The summation of the differences within a set (five-set or two-set) are kept separate until the final manipulation. This is indicated by columns 4, 5, and 6. The d's are the differences within each set; the q's are the corresponding summations; and the r's refer to the separate quantities appearing in the final terms of eq (9). Column 7 is the summation of the sets for each successive ratio.

5. Test Console

After the test method was investigated for more than a year with the circuit assembled in "breadboard" fashion, a small test console was designed and built so that the set-up time for a test would be reduced to a minimum. The console, shown in the photograph and indicated in figure 5, houses the DRRS, the galvanometer with its damping resistance, a mercury stand to accommodate the standard resistors, the 80-ohm guard resistor and the battery reversing switch. The DRRS, located in the lower portion of the console, is connected to the circuit by short leads brought to three binding posts located on the vertical panel immediately above the terminals of the DRRS. (With this arrangement the DRRS can be easily removed and made available for other work.) The detector is a portable galvanometer mounted on a platform within the enclosure immediately above and to the left of the DRRS. The galvanometer scale is observed through an opening in the front panel and the damping resistance, permanently mounted on the inside, is adjustable in steps by a knob accessible to the operator. The mercury stand, located within the console on a platform adjacent to the detector and above the DRRS, can accommodate either a single resistor or several arranged in either series or parallel combination. A removable top permits ready access to all components and wiring.

As shown in the wiring diagram of figure 5, the battery reversing switch, accessible on the front panel, carries a two-conductor shielded cable that terminates at a fitting located on the side panel.

TABLE 1. *Schedule for computing corrections for the standard volt box*

1	2	3	4	5	6	7	8
Section in bridge arm	Resistor S	Reading of DRRS	$d's$	$q's$ $=\Sigma d's$	$\frac{r's}{}=\frac{\Sigma d's}{k}$	Correction referred to 0–0.15 section	Range
	Ohms					*ppm*	
0–0.15	50	$D_{1,1}$	$d_{1,1}=D_{1,1}-D_{1,1}=0$			$\mu_{1,1}=0$	0–0.15
0.15–0.30	50	$D_{1,2}$	$d_{1,2}=D_{1,2}-D_{1,1}$	$q_{1,2}=d_{1,2}$	$r_{1,2}=\frac{1}{2}q_{1,2}$	$\mu_{1,2}=r_{1,2}$	0–0.30
.30–0.45	50	$D_{1,3}$	$d_{1,3}=D_{1,3}-D_{1,1}$	$q_{1,3}=q_{1,2}+d_{1,3}$	$r_{1,3}=\frac{1}{3}q_{1,3}$	$\mu_{1,3}=r_{1,3}$	0–0.45
.45–0.60	50	$D_{1,4}$	$d_{1,4}=D_{1,4}-D_{1,1}$	$q_{1,4}=q_{1,3}+d_{1,4}$	$r_{1,4}=\frac{1}{4}q_{1,4}$	$\mu_{1,4}=r_{1,4}$	0–0.60
.60–0.75	50	$D_{1,5}$	$d_{1,5}=D_{1,5}-D_{1,1}$	$q_{1,5}=q_{1,4}+d_{1,5}$	$r_{1,5}=\frac{1}{5}q_{1,5}$	$\mu_{1,5}=r_{1,5}$	0–0.75
0–0.75	250	$D_{1,6}$	$d_{1,6}=D_{1,6}-D_{1,6}=0$				
0.75–1.5	250	$D_{1,7}$	$d_{1,7}=D_{1,7}-D_{1,6}$	$q_{1,7}=d_{1,7}$	$r_{1,7}=\frac{1}{2}q_{1,7}$	$\mu_{2,1}=\mu_{1,5}+r_{1,7}$	0–1.5
0–1.5	500	$D_{2,1}$	$d_{2,1}=D_{2,1}-D_{2,1}=0$				
1.5–3.0	500	$D_{2,2}$	$d_{2,2}=D_{2,2}-D_{2,1}$	$q_{2,2}=d_{2,2}$	$r_{2,2}=\frac{1}{2}q_{2,2}$	$\mu_{2,2}=\mu_{2,1}+r_{2,2}$	0–3.0
3.0–4.5	500	$D_{2,3}$	$d_{2,3}=D_{2,3}-D_{2,1}$	$q_{2,3}=q_{2,2}+d_{2,3}$	$r_{2,3}=\frac{1}{3}q_{2,3}$	$\mu_{2,3}=\mu_{2,1}+r_{2,3}$	0–4.5
4.5–6.0	500	$D_{2,4}$	$d_{2,4}=D_{2,4}-D_{2,1}$	$q_{2,4}=q_{2,3}+d_{2,4}$	$r_{2,4}=\frac{1}{4}q_{2,4}$	$\mu_{2,4}=\mu_{2,1}+r_{2,4}$	0–6.0
6.0–7.5	500	$D_{2,5}$	$d_{2,5}=D_{2,5}-D_{2,1}$	$q_{2,5}=q_{2,4}+d_{2,5}$	$r_{2,5}=\frac{1}{5}q_{2,5}$	$\mu_{2,5}=\mu_{2,1}+r_{2,5}$	0–7.5
0–7.5	2,500	$D_{2,6}$	$d_{2,6}=D_{2,6}-D_{2,6}=0$				
7.5–15	2,500	$D_{2,7}$	$d_{2,7}=D_{2,7}-D_{2,6}$	$q_{2,7}=d_{2,7}$	$r_{2,7}=\frac{1}{2}q_{2,7}$	$\mu_{3,1}=\mu_{2,5}+r_{2,7}$	0–15
0–15	5,000	$D_{3,1}$	$d_{3,1}=D_{3,1}-D_{3,1}=0$				
15–30	5,000	$D_{3,2}$	$d_{3,2}=D_{3,2}-D_{3,1}$	$q_{3,2}=d_{3,2}$	$r_{3,2}=\frac{1}{2}q_{3,2}$	$\mu_{3,2}=\mu_{3,1}+r_{3,2}$	0–30
30–45	5,000	$D_{3,3}$	$d_{3,3}=D_{3,3}-D_{3,1}$	$q_{3,3}=q_{3,2}+d_{3,3}$	$r_{3,3}=\frac{1}{3}q_{3,3}$	$\mu_{3,3}=\mu_{3,1}+r_{3,3}$	0–45
45–60	5,000	$D_{3,4}$	$d_{3,4}=D_{3,4}-D_{3,1}$	$q_{3,4}=q_{3,3}+d_{3,4}$	$r_{3,4}=\frac{1}{4}q_{3,4}$	$\mu_{3,4}=\mu_{3,1}+r_{3,4}$	0–60
60–75	5,000	$D_{3,5}$	$d_{3,5}=D_{3,5}-D_{3,1}$	$q_{3,5}=q_{3,4}+d_{3,5}$	$r_{3,5}=\frac{1}{5}q_{3,5}$	$\mu_{3,5}=\mu_{3,1}+r_{3,5}$	0–75
0–75	25,000	$D_{3,6}$	$d_{3,6}=D_{3,6}-D_{3,6}=0$				
75–150	25,000	$D_{3,7}$	$d_{3,7}=D_{3,7}-D_{3,6}$	$q_{3,7}=d_{3,7}$	$r_{3,7}=\frac{1}{2}q_{3,7}$	$\mu_{4,1}=\mu_{3,5}+r_{3,7}$	0–150
0–150	50,000	$D_{4,1}$	$d_{4,1}=D_{4,1}-D_{4,1}=0$				
150–300	50,000	$D_{4,2}$	$d_{4,2}=D_{4,2}-D_{4,1}$	$q_{4,2}=d_{4,2}$	$r_{4,2}=\frac{1}{2}q_{4,2}$	$\mu_{4,2}=\mu_{4,1}+r_{4,2}$	0–300
300–450	50,000	$D_{4,3}$	$d_{4,3}=D_{4,3}-D_{4,1}$	$q_{4,3}=q_{4,2}+d_{4,3}$	$r_{4,3}=\frac{1}{3}q_{4,3}$	$\mu_{4,3}=\mu_{4,1}+r_{4,3}$	0–450
450–600	50,000	$D_{4,4}$	$d_{4,4}=D_{4,4}-D_{4,1}$	$q_{4,4}=q_{4,3}+d_{4,4}$	$r_{4,4}=\frac{1}{4}q_{4,4}$	$\mu_{4,4}=\mu_{4,1}+r_{4,4}$	0–600
600–750	50,000	$D_{4,5}$	$d_{4,5}=D_{4,5}-D_{4,1}$	$q_{4,5}=q_{4,4}+d_{4,5}$	$r_{4,5}=\frac{1}{5}q_{4,5}$	$\mu_{4,5}=\mu_{4,1}+r_{4,5}$	0–750

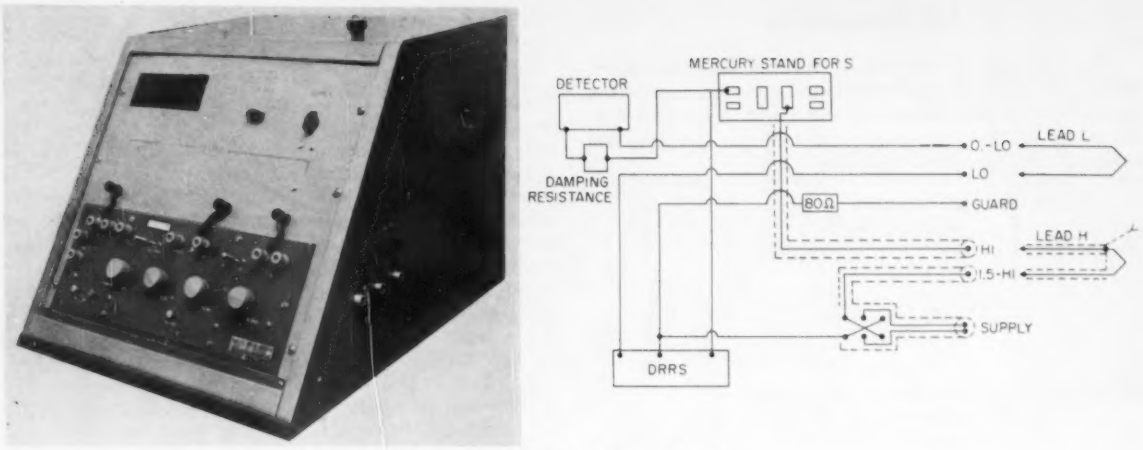

FIGURE 5. *Test console and layout.*

An external d-c supply is connected to this fitting with a pair of shielded leads equipped with a mating connector. The side panel also carries two single-conductor coax fittings, identified as "1.5-Hi" and "Hi," and three binding posts, identified as "0.-Lo," "Lo,", and "Guard."

When the first five sections of the standard volt box are measured separate unshielded leads are used to connect the terminals of the volt box (1.5 post, high-potential post of the section being measured, 0. post, and low-potential post of the section being measured) to the respective terminals of the console (1.5-Hi, Hi, 0.-Lo, and Lo). For all other measurements special leads H and L are used to connect the section under test as indicated in figure 5. When the guard of the volt box is used, the pigtail of lead H is connected to the high-potential terminal of the guard section and a connection is made from the "Guard" binding post to the low-potential terminal of the guard section. Otherwise, these last two connections are omitted.

6. Consideration of Errors

An examination of errors requires a careful study of all known effects that could render a measured value different from the true value within the specified accuracy. An appraisal of all components of the measuring circuit as well as a justification of approximations must be included, even though in this instance one would expect the associated errors to be negligible.

The first possible source of error to consider is the DRRS. As in the usual case, this type of error can be avoided by calibrating the instrument and applying corrections. Apart from this procedure, however, it should be emphasized that an error in the measured value is diluted when the values of the *ratios* are considered. For example, if each scale reading were in error by $\epsilon=1$ ppm and all errors were in such a direction as to add when computing each difference their contribution to the error of a given ratio, when summed within any one of the five-sets, would be

$$\frac{(k-1)2\epsilon}{k}=\frac{2(k-1)}{k}$$

where k is the number of summed sections. For $k=5$ the error would be $8/5=1.6$ ppm. Similarly, the error introduced in the measurements of the two-sets would be

$$\frac{2\epsilon}{2}=1 \text{ ppm.}$$

The maximum error would occur for the highest range since it contains all the sets. This would amount to only 9.4 ppm under these adverse conditions. Since the corrections to the DRRS used at NBS are less than 0.3 ppm and their signs and magnitudes have a random distribution, the errors in the ratio measurements are almost certain to be less than 1 ppm with no corrections applied to the dial readings.

A source of error is concealed in the base (or balance) equation used in appendix B to develop the general expression for the volt box ratios. Referring to appendix A, the exact base equation is given as

$$R_{m,k}=S\left[1+\frac{1}{1+\frac{l_2}{B_m}}\,(D_{m,k}-D_0)\right]$$

whereas, the approximate value used in the mathematical development in appendix B is

$$R_{m,k}=S[1+(D_{m,k}-D_0)].$$

The latter departs from exactness by an amount $\frac{l_2}{B_m}(D_{m,k}-D_0)$ but is of second order. For example, if $\frac{l_2}{B_m}$ were as large as 0.1 percent and $(D_{m,k}-D_0)$ rep-

resented a change of 500 ppm in the A-arm, the value for $R_{m,k}$ would be in error by only 0.5 ppm.

Another error is concealed through approximation in developing the general expression that defines the volt box ratios (appendix B) when it is assumed that the value of the "Dummy" resistor, including leads, is exactly equal to that of the section being measured. The error introduced through this assumption is second order since it is the product of two small terms. For example, consider the summation of the first five sections (refer to eq (6)).

$$\sum_{k=1}^{k=5} R_{1,k}=5R_{1,1}+S_{a1}\sum_{k=1}^{k=5} d_{1,k}.$$

If S_{a1} differs from $R_{1,1}$ and is given by $S_{a1}=R_{1,1}[1+\mu_1]$ the summation becomes

$$\sum_{k=1}^{k=5} R_{1,k}=5R_{1,1}\left[1+\sum_{k=1}^{k=5}\frac{d_{1,k}}{5}+\mu_1\sum_{k=1}^{k=5}\frac{d_{1,k}}{5}\right]$$

where the magnitude of the error is $\mu_1\sum_{k=1}^{k=5}\frac{d_{1,k}}{5}$.

If both μ_1 and the summation were as large as 500 ppm, the error would be only 0.05 ppm.

Another possible source of error arises if the resistance in any one arm changes during the measurements of a given set. This change could occur in the leads and contacts, for example, and its effect would be greatest when measuring the 50-ohm sections. A change of this nature can be considered as a change in D_0 and an estimate of the error it introduces in a measured ratio can be obtained by considering the measurements of the first set. Assume an extreme case in which the resistance of a given arm increases in equal increments after the first measurement so that for subsequent balances D_0 takes on new values. The measured values for the set become

$$\begin{aligned}
R_{1,1}&=S_{a1}[1+(D_{1,1}-D_0)]\\
R_{1,2}&=S_{a1}[1+D_{1,2}-(D_0+\epsilon)]\\
R_{1,3}&=S_{a1}[1+D_{1,3}-(D_0+2\epsilon)]\\
R_{1,4}&=S_{a1}[1+D_{1,4}-(D_0+3\epsilon)]\\
R_{1,5}&=S_{a1}[1+D_{1,5}-(D_0+4\epsilon)]
\end{aligned}$$

where ϵ is the change in D_0 between successive balances. After taking differences, any given sum within the set can be written as

$$\sum_{k'=1}^{k'=k} R_{1,k'}=kR_{1,1}\left[1+\sum_{k'=1}^{k'=k}\frac{d_{1,k'}}{k}-\sum_{k'=1}^{k'=k}\frac{(k'-1)\epsilon}{k}\right].$$

Thus an error in any ratio formed within the set is $\sum_{k'=1}^{k'=k}\frac{(k'-1)\epsilon}{k}$. For example, if a lead resistance increased in increments of 0.0001 ohm in the S-arm (50 ohms) the magnitude of the error introduced in the ratio $\frac{\sum_{k=1}^{k=5} R_{1,k}}{R_{1,1}}$ would be 4 ppm. If the usual precautions are taken, the probability of this kind of an occurrence is quite remote and could be easily observed from the detector response. A single, abrupt change would be more difficult to detect but an error from this cause can be avoided by taking a repeat set of measurements.

The final consideration involves those errors that arise from the unavoidable presence of the rod resistances. This source of error could be the most critical of any because of its insidious nature. Two errors must be examined when considering the rod resistances. If the rod resistances are equal they can introduce an error if, when the standard volt box is used, the connections differ from those made during the process of calibration. The second error occurs if the rod resistances differ in magnitude.

Consider the cause of the first error. When in use, the connections to the standard volt box are as shown in figure 6. There are no currents in rods l_1 and l_2; rod l_n, however, carries current by virtue of its connection to the supply. Thus the ratio of the standard in use is

$$N_s=\frac{\sum_{1}^{n} R_{n'}+l_n}{R_{1,1}}. \tag{10}$$

When the first five sections are measured (refer to fig. 4a) the rods are in the A- and S-arms. Thus, if the ratio under consideration were one confined solely to these sections, the measured ratio would be

$$N'_s=\frac{\sum_{1}^{n} R_{n'}}{R_{1,1}} \tag{11}$$

and eq (10) can be written as

$$N_s=N'_s+\frac{l_n}{R_{1,1}}=N'_s\left[1+\frac{l_n}{N'_sR_{1,1}}\right] \tag{12}$$

In the measurement and summing process through the higher ranges, the rod resistances form part of the section being measured. (See fig. 4b.) However, if the rod resistances are equal, their effects

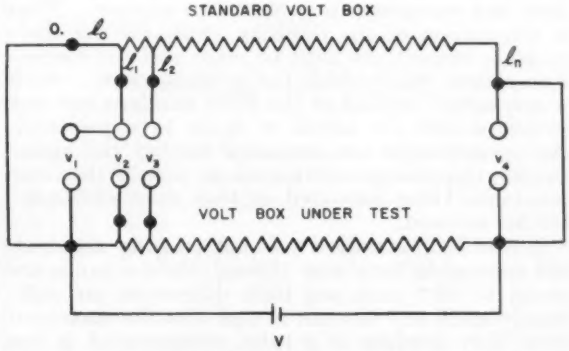

FIGURE 6. *Circuit emphasizing one effect from rod resistances.*

cancel and the difference between the ratio in use and the one measured is the same as that given in eq (12). It is apparent then that the ratio in use differs from the measured ratio by an amount equal to the rod resistance divided by the total resistance of the range used and occurs even though the rod resistances are equal. If the standard volt box were used as a 4-terminal voltage divider the above correction to the ratio in use would be $\frac{l_n+l_0}{N'_s R_{1,1}}$ since l_0 becomes part of the high voltage side.

The magnitude of an error arising from inequalities in the rod resistances depends on where the rods are located in the bridge network. As stated in section 4.2, there are three alternatives for connecting the rods and the choice of orientation is not as clearly indicated when measuring the 50-ohm sections as when measuring the higher-valued sections. For the purpose of analysis, consider the measurement of the low-valued sections and the particular connection shown in figure 4a.

For this condition, differences among the rod resistances may be considered as producing changes in D_0 so that, if the respective rod resistances are identified as l_1, l_2, etc., the measured resistances are

$$R_{1,1}=S_{a1}[1+D_{1,1}-D_0]$$

$$R_{1,2}=S_{a1}\left[1+D_{1,2}-D_0+\frac{l_2-l_1}{A}+\frac{l_3-l_2}{S_{a1}}\right]$$

$$R_{1,3}=S_{a1}\left[1+D_{1,3}-D_0+\frac{l_3-l_1}{A}+\frac{l_4-l_2}{S_{a1}}\right]$$

$$R_{1,4}=S_{a1}\left[1+D_{1,4}-D_0+\frac{l_4-l_1}{A}+\frac{l_5-l_2}{S_{a1}}\right]$$

$$R_{1,5}=S_{a1}\left[1+D_{1,5}-D_0+\frac{l_5-l_1}{A}+\frac{l_6-l_2}{S_{a1}}\right].$$

If the rod resistances are measured, their contribution to the error of any ratio can be evaluated. Comparable sets of equations can be formed for the other two cases and corresponding errors evaluated. If the successive values of rod resistances neither increase nor decrease, it cannot be stated categorically that one connection is preferred to another. Thus a comparison of the resulting errors for the three possible connections must be made and the connection chosen which yields the smallest errors. Such a comparison applied to the NBS standard volt box indicated that the circuit of figure 4a is preferred. As measurements are continued through the higher ranges, the rods are connected as part of the large resistance being measured so that their effects are further reduced.

In the NBS standard volt box recently acquired, rod resistances from zero through the 6-v range are about 5×10^{-4} ohm and their differences are sufficiently small and random in sign that the maximum error they produce in a ratio measurement is less than 0.3 ppm.

7. Summary

A particular type of voltage ratio standard and a method for its calibration are discussed. Although the method is described in its particular application to the NBS standard it can be used equally well in other networks. Errors that might appear in the measurement of its ratios and procedures for evaluating their magnitudes are outlined. With a standard volt box of proper design, the calibration method as set forth should yield results that are good to an accuracy of 10 ppm or better. This estimate of accuracy is based on the theoretical considerations of the circuit and its parameters, on the continued good agreement with those values of ratio obtained by the older method, and on other self-consistent tests.

The author appreciates the assistance of Rita McAuliff and Ronald Dziuba who made most of the measurements and constructed the test console.

8. Appendix A

8.1. Comments on the DRRS

Complete discussions on the DRRS and its use in the accurate measurement of d-c resistance are contained in references [2], [3], and [4] so that an elaborate treatment is not warranted. However, certain aspects are emphasized here in order to clarify the meaning of particular equations, as well as justify their use.

The DRRS is used principally in comparing two nearly equal resistances and under these conditions has an accuracy of about 1 ppm. It comprises two resistance arms of about equal magnitudes with one arm B' having a single-valued resistance (in most cases 100 or 1,000 ohms) and the other consisting of a fixed resistance in series with an adjustable section. The adjustable branch contains, in most cases, four resistance groups, each provided with a selector to vary the resistance and register the change on suitably marked dials. The resistance of the A'-arm can be varied by about 0.5 percent on either side of the B'-arm value to a least count of 1 ppm. The dials register in increasing numbers as resistance is added to the fixed portion of the A'-arm. Since the DRRS is used to measure differences between two nearly equal quantities, the dial readings can be translated to ppm or, as is often the case, the dials may be marked in ppm.

The reader should note carefully the form in which small corrections are recorded or used in derivations and computations. As usually constructed, a *change* of one step on the lowest dial of a four-dial DRRS corresponds to a change of 1 ppm in the ratio. At one particular balance of a measuring circuit the reading of the DRRS should be thought of simply as a four-digit number, such as 5472. If a second balance of the same circuit yields a DRRS reading of 5459 the measured ratio change is −13 ppm, this

being the first point at which the abbreviation "ppm" should be introduced. In recording data and computations (see table 1) it is convenient and space saving to enter DRRS readings as four-digit numbers, and ratio changes in ppm. In deriving equations, however, (and corrections based thereon) ratio changes should be expressed in proportional parts. A ratio change in proportional parts is one millionth of the change expressed in ppm. In the above illustration the ratio change is -0.000013 proportional parts. See reference [2] for further discussion of these terms.

8.2. Bridge Balance Equation

Figure 7 indicates a bridge network in which the adjustable arm of the DRRS is represented as a section of fixed resistance in series with a uniform slide wire of high resolution. Let B_m indicate the resistance of the B-arm of the DRRS, A_m the resistance of its A-arm for which $A_m=B_m$, l_2 and l_1 the respective lead resistances with $l_2 \neq l_1$, and S the resistance of a standard serving as the "Dummy" resistor. For convenience, let the DRRS be without error as previously determined from calibration.

Assume first that a standard resistor S_1, having a resistance equal to S, is inserted in the unknown arm and the bridge balances at some point for which the A- and B-arms of the DRRS are not equal. Let the resistance of the A-arm of the DRRS be A_0 for this balance condition. The equation of balance is given by

$$S=S\left[\frac{(A_0+l_1)}{(B_m+l_2)}\right]. \tag{13}$$

Thus A_0 is the resistance of the A-arm of the DRRS when the ratio arms (A- and B-) of the *bridge* are in a 1:1 ratio. Next, let S_1 be replaced by a resistance whose value is R and let A_R be the resistance of the A-arm of the DRRS under the new balance condition. The equation of balance is

$$R=S\left[\frac{(A_R+l_1)}{(B_m+l_2)}\right]. \tag{14}$$

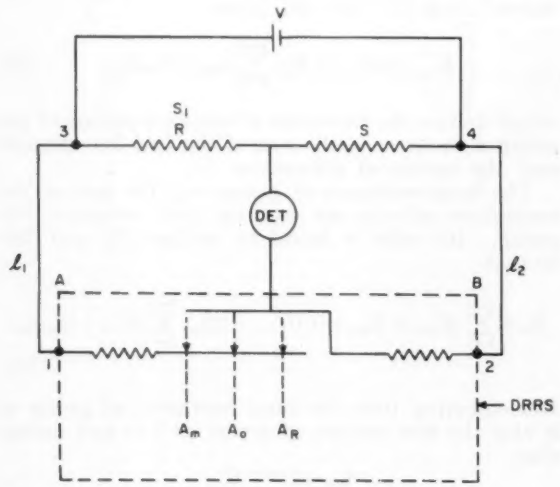

FIGURE 7. *Circuit indicating the DRRS with respect to the balance equation.*

Subtracting (13) from (14) and rearranging terms gives the value of R as

$$R=S+S\left[\frac{(A_R+l_1)}{(B_m+l_2)}-\frac{(A_0+l_1)}{(B_m+l_2)}\right]$$

$$=S\left[1+\frac{(A_R-A_0)}{(B_m+l_2)}\right]. \tag{15}$$

Since A_m and B_m equal the respective resistances of the A- and B-arms of the DRRS when $A_m=B_m$, let

$$A_R=A_m+\Delta_R$$

$$A_0=A_m+\Delta_0$$

where Δ_R and Δ_0 are small changes in the resistance of the slide wire. Equation (15) becomes

$$R=S\left[1+\frac{(A_m+\Delta_R)-(A_m+\Delta_0)}{B_m+l_2}\right]$$

which can be written as

$$R=S\left[1+\frac{\left(1+\frac{\Delta_R}{A_m}\right)-\left(1+\frac{\Delta_0}{A_m}\right)}{\left(1+\frac{l_2}{B_m}\right)}\right] \tag{16}$$

since $\frac{A_m}{B_m}=1$. Now the dials of the DRRS (assumed to be without error) indicate, in effect, that in going from a position corresponding to the resistance A_m to that of A_R, the resistance of the A-arm of the DRRS has changed by $\frac{\Delta_R}{A_m}$ in proportional parts; and similarly, in going from A_m to A_0 the resistance has changed by $\frac{\Delta_0}{A_m}$. Hence,

$$\frac{\Delta_R}{A_m}=(D_R-D_m) \text{ and } \frac{\Delta_0}{A_m}=(D_0-D_m)$$

where D_R, D_0 and D_m refer to the respective readings of the DRRS translated into proportional parts. Substituting these values in (16) gives

$$R=S\left[1+\frac{1}{1+\frac{l_2}{B_m}}(D_R-D_0)\right] \tag{17}$$

or, if $\frac{l_2}{B_m}$ is sufficiently small

$$R \approx S[1+(D_R-D_0)]. \tag{18}$$

In the notation used in developing the general expression given in appendix B, this corresponds to

$$R_{m,k}=S_{am}[1+(D_{m,k}-D_0)].$$

It should be noted that the concept of D_0 has been generalized for the purpose of this paper to indicate that setting on the DRRS for which the ratio arms between terminals 3 and 4 have a 1:1 ratio. In most uses of the DRRS, particularly in the comparison of resistance standards, arms A and B contain only the DRRS and D_0 is a constant, defined as the setting for which the A- and B-arms of the *DRRS* have a 1:1 ratio.

9. Appendix B

Referring to the text and to figure 3, the working resistance is considered as made up of four groups, with each group containing six sections. The first five sections of any one group have nominally equal resistances and the sixth section has a resistance nominally equal to five times this value (sum of the five sections). Counting from the low-potential end, the first section of each group (after the first) is formed by all the preceding sections connected in series. Any section, therefore, can be identified by two integers; the first, m, specifying the group to which the section belongs, and the second, k, specifying the position of the section within its group.

If the Wheatstone bridge of figure 4 is balanced as each of the first five sections of group m is inserted in succession in the unknown arm, then the resistance of the first section and of the kth section can be written as,

$$R_{m,1}=S_{am}[1+(D_{m,1}-D_0)] \tag{19}$$

and

$$R_{m,k}=S_{am}[1+(D_{m,k}-D_0)] \tag{20}$$

where

S_{am} is the resistance of S and has a nominal value equal to that of the volt box section being measured;

$D_{m,1}$ and $D_{m,k}$ are the readings of the DRRS in proportional parts [7] when the first and kth sections, respectively, of group m are inserted in the unknown arm;

D_0 is the reading that would be indicated on the DRRS if the Wheatstone bridge were in exact 1:1 ratio.

Subtracting (19) from (20) gives

$$R_{m,k}-R_{m,1}=S_{am}[D_{m,k}-D_{m,1}]$$

or

$$R_{m,k}=R_{m,1}+S_{am}d_{m,k} \tag{21}$$

where

$$d_{m,k}=[D_{m,k}-D_{m,1}]$$

The sum of the first five sections of group m is

$$\sum_{k=1}^{k=5} R_{m,k}=5R_{m,1}+S_{am}\sum_{k=1}^{k=5} d_{m,k} \tag{22}$$

since each section has the same nominal value and S_{am} is used throughout the set of measurements.

If now the resistor S_{am} is replaced by S_{bm} and the bridge is balanced first, with the five sections (connected in series) and then with the sixth section inserted in the unknown arm, we have

$$\sum_{k=1}^{k=5} R_{m,k}=S_{bm}[1+(D_{m,s}-D_0)] \tag{23}$$

and

$$R_{m,t}=S_{bm}[1+(D_{m,t}-D_0)] \tag{24}$$

where

$D_{m,s}$ is the reading of the DRRS when the sum of the five sections is inserted;

$D_{m,t}$ is the reading when the sixth section is inserted.

Subtracting (23) from (24) gives

$$R_{m,t}-\sum_{k=1}^{k=5} R_{m,k}=S_{bm}[D_{m,t}-D_{m,s}]$$

or

$$_{m,t}=\sum_{k=1}^{k=5} R_{m,k}+S_{bm}d_{m,t} \tag{25}$$

where

$$_{m,t}=[D_{m,t}-D_{m,s}].$$

Substituting (22) into (25) gives

$$R_{m,t}=5R_{m,1}+S_{am}\sum_{k=1}^{k=5} d_{m,k}+S_{bm}d_{m,t} \tag{26}$$

which defines the resistance of the sixth section of the group m in terms of the sum of the first five sections and the measured differences.

The total resistance of group m is the sum of the resistances of the six sections that comprise the group. Its value is found by adding (22) and (26) so that

$$R_m \equiv \sum_{k=1}^{k=5} R_{m,k}+R_{m,t}=10R_{m,1}+2S_{am}\sum_{k=1}^{k=5} d_{m,k}+S_{bm}d_{m,t} \tag{27}$$

Remembering that the total resistance of group m is also the first section of group $(m+1)$ and noting that

$$S_{am}=10^{m-1}R_{1,1}$$

and

$$S_{bm}=5\times 10^{m-1}R_{1,1}$$

[7] Strictly speaking, as emphasized elsewhere in the paper, $(D_{m,1}-D_0)$ and $(D_{m,k}-D_0)$ are the *differences* in proportional parts as deduced from the readings of the DRRS.

we have from (27)

$$R_{m+1,1}=10R_{m,1}+(2\times10^{m-1}R_{1,1})\sum_{k=1}^{k=5}d_{m,k}+(5\times10^{m-1}R_{1,1})d_{m,t}. \quad (28)$$

Equation (28) serves as the connecting link between one group and the next. If it is applied successively to increasing values of m, beginning with $m=1$, one finds that the resistance of the first section of any group m can be expressed in terms of the resistance of the first section of the first group and the measured differences by the general equation

$$R_{m,1}=10^{m-1}R_{1,1}+(2\times10^{m-2}R_{1,1})\left[\sum_{k=1}^{k=5}d_{1,k}+\sum_{k=1}^{k=5}d_{2,k}\ldots+\sum_{k=1}^{k=5}d_{m-1,k}\right]+(5\times10^{m-2}R_{1,1})[d_{1,t}+d_{2,t}\ldots+d_{m-1,t}]. \quad (29)$$

Equation (21) states that the resistance of the kth section of group m is

$$R_{m,k}=R_{m,1}+S_{am}d_{m,k}=R_{m,1}+(10^{m-1}R_{1,1})d_{m,k}$$

so that the sum of all resistances up to and including the kth section of group m is

$$\sum_{k'=1}^{k'=k}R_{m,k'}\equiv S_{m,k}=kR_{m,1}+(10^{m-1}R_{1,1})\sum_{k'=1}^{k'=k}d_{m,k'}. \quad (30)$$

Substituting (29) in (30) and factoring out $k\times10^{m-1}R_{1,1}$ gives

$$S_{m,k}=k\times10^{m-1}R_{1,1}\left[1+\frac{\sum_{k=1}^{k=5}d_{1,k}+\sum_{k=1}^{k=5}d_{2,k}\ldots+\sum_{k=1}^{k=5}d_{m-1,k}}{5}+\frac{d_{1,t}+d_{2,t}\ldots+d_{m-1,t}}{2}+\frac{\sum_{k'=1}^{k'=k}d_{m,k'}}{k}\right]. \quad (31)$$

Any given ratio of the volt box is defined as the ratio of the sum of all resistances up to the kth tap of group m to the resistance of the first section of the first group. Thus, by definition, any ratio of the volt box is $\frac{S_{m,k}}{R_{1,1}}$ so that, since $(k\times10^{m-1})$ is the nominal ratio, eq (31) can be written in the form

$$N_{m,k}=\frac{S_{m,k}}{R_{1,1}}=N'_{m,k}[1+\mu_{m,k}]$$

where $N'_{m,k}$ are the nominal ratios and $\mu_{m,k}$ are the corresponding corrections in proportional parts, computed from the difference terms that appear in eq (31). The corrections can be stated in ppm by multiplying by 10^6.

10. References

[1] Francis B. Silsbee and Francis J. Gross, Testing and performance of volt boxes, J. Research NBS **27,** 269 (1941) RP1419.

[2] Paul P. B. Brooks, Calibration procedures for direct-current resistance apparatus, NBS Mono. 39 (1962).

[3] James L. Thomas, Precision resistors and their measurement, NBS Circ. 470 (1948).

[4] Forest K. Harris, Electrical measurements (John Wiley & Sons, Inc., New York, N.Y., 1952).

(Paper 67C1-114)

JOURNAL OF RESEARCH of the National Bureau of Standards—C. Engineering and Instrumentation
Vol. 67C, No. 1, January-March 1963

Stability of Residual Thiosulfate in Processed Microfilm

C. I. Pope

(August 21, 1962)

The concentration of residual thiosulfate (hypo) in processed microfilm and its variation with storage humidity were measured. The initial thiosulfate concentration varied linearly with the image density up to a density of about 2. The rate of decomposition of the thiosulfate increased as the relative humidity increased. The concentration of thiosulfate in a silver-free area remained constant for nine months in film stored at 14-percent relative humidity but began to decrease within two weeks at 88-percent relative humidity. The residual thiosulfate in processed microfilm reacted with the silver in the image to form silver sulfide and the amount of sulfiding during aging at 88-percent relative humidity was measured. The residual thiosulfate concentration in microfilm was found to vary linearly with the silver concentration in the fixing bath. Potassium bromide, potassium iodide, and sodium chloride reacted with the residual silver thiosulfate complex making the thiosulfate soluble. Potassium bromide and iodide effected the complete elimination of thiosulfate.

1. Introduction

The use of microfilm for record purposes has increased rapidly during the past three decades and many microfilm records are intended for archival use. In the usual silver halide photographic process the image is fixed in a solution of sodium or ammonium thiosulfate and then the film is washed to remove the thiosulfate. If, due to inadequate washing, the residual thiosulfate concentration is excessive, the image may be damaged or destroyed since the thiosulfate reacts with the image silver to form silver sulfide and this reaction takes place rapidly at high relative humidities.

It is known that the thiosulfate concentration in freshly processed microfilm varies with the image density and that the thiosulfate decomposes during storage [1, 2, 5].[1] Data were needed on the decomposition of residual thiosulfate to determine the conditions under which the analysis for the residual thiosulfate could be expected to assess the potential damage to the image on storage.

The relationship of the residual thiosulfate content to the image density on freshly processed microfilm was measured for a wide range of densities. The decrease in the thiosulfate content and the amount of image silver sulfided during aging were measured. The effect of the nature of the fixing bath on the retention of thiosulfate during washing and the role of halide salts in removing thiosulfate from microfilm after fixation were investigated.

[1] Figures in brackets indicate the literature references at the end of this paper.

2. Preparation of Samples

Samples of 35 mm microfilm were cut in 10-in. lengths and exposed in an intensity scale sensitometer. The processing procedures were similar to those described in a previous paper [6]. The samples were developed 3 min, treated 30 sec in a stop bath, and fixed 6 min (3 min in each of two fresh baths). The processing was carried on at room temperature (22 to 28 °C) employing the solutions listed in the appendix, section 9.1. About 2 liters of fresh solution were used in each processing operation employing nominal 8 by 10-in. enameled-metal trays. Not more than eight samples were processed or treated at one time. The samples were continuously agitated by hand during processing. The samples were washed in a rapidly flowing stream of tap water at a constant temperature and for the required washing time to obtain the desired residual thiosulfate concentrations in processed microfilm or to measure the decrease of the thiosulfate concentration for different washing times. During the first minute of washing the tray was emptied three times to facilitate the removal of the fixing solution on the surface of the samples. At the end of the washing period the samples were taken up by one end, shaken to remove the surface water, and placed, emulsion side up, on clean white blotting paper to dry.

The samples had one unexposed area and six areas with various exposures, the area of each step being $^{15}/_{16}$ in. by 1¼ in. The exposure was controlled to obtain a density of approximately 0.3 in the area of least exposure and 4 to 4.5 in the area of greatest

exposure. The transmission density was measured with a densitometer calibrated against a step tablet measured by the American Standards Association method [3]. The density of the base and fog, measured on the unexposed area, was subtracted from the other density readings. In each run, several microfilm samples were given the same exposure in the sensitometer. Transmission density measurements were made on one step tablet of each kind and the others were used for the residual thiosulfate or sulfiding determinations. One square inch of film was cut from each step for the thiosulfate determination. The image densities from the same runs showed a variation of 0.00 to 0.03 in the low densities and 0.00 to 0.05 in the high. These variations in the image density in the same run were not large enough to cause a measurable difference in the thiosulfate and sulfiding determinations. The original thiosulfate determination was made within an hour after processing. The thiosulfate contents were generally the same for the same steps in the tablets in each run but there was an occasional variation of 1 $\mu g/in.^2$ in the low image densities and 1 to 3 μg in the high image densities when the thiosulfate concentrations were low but a variation of 2 to 5 μg in all image densities when the thiosulfate concentration was 60 to 70 μg.

The thiosulfate content in the processed microfilm was determined by the American Standards Association method [4] except that more standard solutions were used and the test samples and standards were allowed to stand 25 min instead of 15 min before examination. The turbidity or opalescence of the solutions was compared with the prepared standards visually. The test is very sensitive, being capabl of detecting one part of thiosulfate in one million. Standard samples for comparison were prepared by adding 2, 5, 7, 10, 15, 20, 25, 30, 35, 40, 45, 50, 55, 60, 65, 70, and 75 μg of sodium thiosulfate ($Na_2S_2O_3$) to the 10-ml mercuric chloride-potassium bromide test solution. The thiosulfate concentrations are expressed in terms of anhydrous sodium thiosulfate ($Na_2S_2O_3$) in micrograms per square inch ($\mu g/in.^2$).

3. Relationship of the Residual Thiosulfate Concentration to the Image Density

Step tablets of microfilm were washed until the unexposed step gave a negative test for thiosulfate and the step with the lowest image density, a positive test. This was accomplished by washing the tablets, after fixation, for 3 min in a rapidly flowing stream of tap water at 25 °C.

Figure 1 is a photograph of seven vials showing the turbidities formed in the mercuric chloride-potassium bromide test solution by the residual thiosulfate in one square inch of film taken from each of the seven steps of a typical step tablet. Viewing from left to right, the image densities of the samples ranged from 0.00 to 4.13 and their respective thiosulfate concentrations from 0 to 10 $\mu g/in.^2$ Though the precipitate is hardly perceptible in the photograph of the second vial, it was clearly visible during the test. A Coleman nephelometer was obtained and these experiments were repeated to compare the photoelectric method with the visual method in determining the relationship of the residual thiosulfate concentration to the image density.

The thiosulfate concentrations are plotted against the image densities in figure 2. One curve is typical for determination of the thiosulfate by the visual method and the other for the photoelectric method. The results from the nephelometer were higher in the high image densities. As shown in figure 2, the thiosulfate concentration varied practically linearly with image density up to a density of about 2 but tended to level off at the high image densities. Since the concentration of the residual thiosulfate is probably related to the amount of surface of the image silver this suggests that the surface of the silver in the high image densities does not increase proportionally with the increase in optical density. Scott [5] had previously reported that the residual thiosulfate in microfilm was roughly proportional to the image density. Thus, if the test for hypo concentration were made in a clear area, it would be possible to find no more than 5 μg of residual thiosulfate

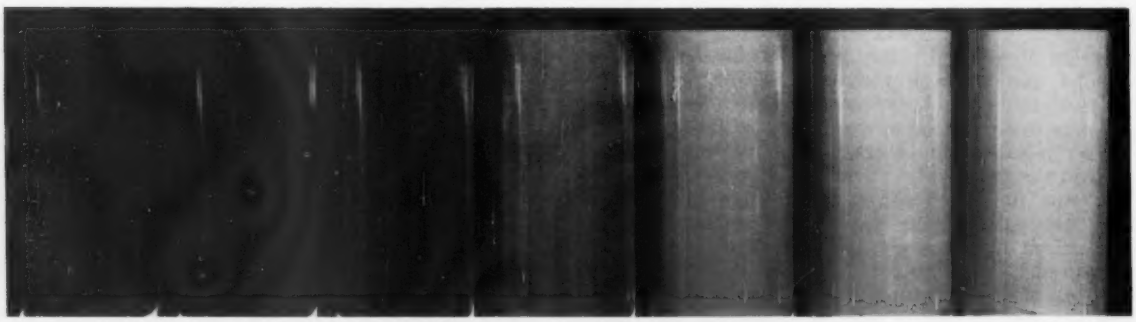

FIGURE 1. *Photograph showing the turbidity of the precipitate formed by the residual thiosulfate in the thiosulfate test solution, for different image densities.*

The image densities and their thiosulfate concentrations in $\mu g/in.^2$ shown in parentheses were as follows: left to right, 0.00 (0), 0.28 (less than 1), 0.44 (1), 0.88 (3) 1.67 (5), 3.74 (7), and 4.13 (10).

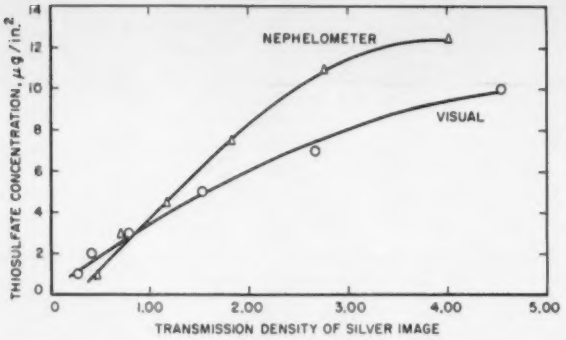

FIGURE 2. *Residual thiosulfate concentration versus transmission (image) density in processed microfilms A and B when the washing is stopped as close as possible to the point where the clear area (zero image density) just ceases to give a positive test for thiosulfate.*

per square inch as required by the American Standard specification for permanent record film [2] but, if the test were made in an area of high image density, well over that amount would be found.

The thiosulfate concentration during washing is shown in figure 3 for one microfilm for different image densities. Four step tablets were given the same exposure, developed and fixed together, and one step tablet was removed from the washing tray at 5, 10, 20, and 60-mm intervals. It was found that the thiosulfate concentration varied nearly linearly with the image density for each washing time.

One kind of microfilm had different washing characteristics than the four other microfilms investigated. The thiosulfate was almost completely removed by washing for 10 min, only 2 μg of thiosulfate per square inch remaining in the high image densities. The amount of image silver sulfided in this microfilm during fixation [6] was much less than in the other films. This suggests that there is some relationship between the sulfiding of the silver image during fixing and the retention of the thiosulfate during washing. When the other four microfilms were fixed in a bath containing 1 g of potassium iodide per liter, only 2 μg of thiosulfate per square inch remained in the high image densities after a 5-min wash and the sulfiding of the image silver during fixation was much less than normal.

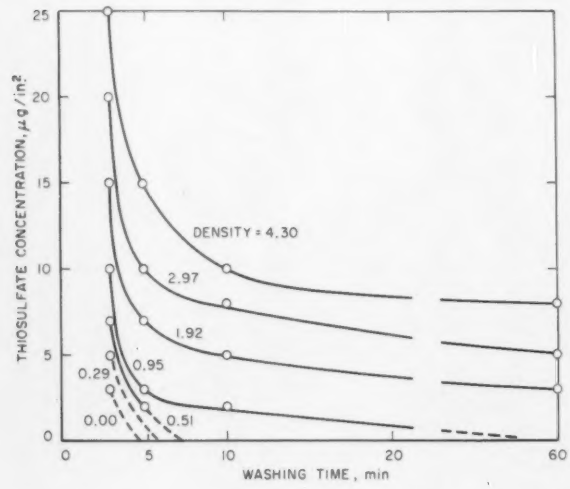

FIGURE 3. *Decrease in thiosulfate concentration during washing at 25 °C, for different image densities, for one microfilm. The image densities are noted on the curves.*

4. Effect of Humidity on the Stability of Residual Thiosulfate

Samples of microfilm were suspended on hooks above saturated salt solutions in sealed glass jars. Saturated solutions of the following salts were used to obtain the desired relative humidities: lithium chloride, $LiCl_2 \cdot H_2O$, for 14-percent relative humidity; sodium dichromate, $Na_2Cr_2O_7 \cdot 2H_2O$, for 53-percent; and barium chloride, $BaCl_2 \cdot 2H_2O$, for 88-percent. Sodium dichromate has been widely used to maintain the desired humidity in film storage cabinets. The saturated salt solutions were stored at room temperature ranging from 20 to 28 °C. It is recognized that changes in temperature cause slight changes in the relative humidities if, as in this case, the air is not stirred, but for the present study the relative humidities were taken to be 14, 53, and 88-percent.

The glass jars were right rectangular cylinders 13 in. long by 9 in. wide by 19 in. high, inside. The covers were sheet Lucite, ½ in. thick. Hooks of Lucite rod were fused to the cover. Sulfur-free rubber tubing was cut lengthwise and sealed to the top edge of the jars with rubber cement. This rubber gasket was coated with Cello-Grease (Fisher Scientific Co.) to effect a seal between it and the cover. A weight of several pounds rested on the cover during the aging. The glass jars were kept together in a closed light-tight cabinet. The bottom of the cabinet was 4½ in. from the floor and there was free air space at least 3 in. thick surrounding the jars. The temperature in the cabinet was recorded automatically.

4.1. Stability of Residual Thiosulfate in Silver-Free Microfilm

Samples of microfilm were cut 10 in. in length and, *without exposure*, were developed, stopped, and fixed. After fixation, they were washed 1½, 2, or 3 min at 25 °C to obtain different concentrations of residual thiosulfate. Samples containing 3 to 23 μg of thiosulfate per square inch were obtained by this procedure. The thiosulfate concentration was determined in six samples in each run and two of these were placed in each of the three glass jars having, respectively 14, 53, and 88-percent relative humidity. The thiosulfate concentration was measured on 1 $in.^2$ of each sample at selected time intervals during 9 months. Table 1 gives the tabulated results of five runs. The two samples in each jar generally had the

TABLE 1.—*Effect of relative humidity on the concentration of thiosulfate in clear or silver-free processed microfilm during aging at room temperature (20–30 °C) washed at 25 °C*

[Runs 1, 2, and 3 were fixed in a silver-free bath; run 4 in a bath containing 4 g of silver per liter; and run 5 in a bath containing 8 g of silver per liter.]

Relative humidity	Sample	Thiosulfate, μg/in.²					
Run 1, washed 2 min							
		Time after processing, days					
		0	14	28	83	149	269
%							
14	a	3	3	3	2	2	2
53	b	3	3	3	2	1	1
88	c	3	3	3	1	0	
Run 2, washed 1½ min							
		Time after processing, days					
		0	14	27	71	189	273
14	a	8	8	8	8	8	8
53	b	8	8	8	8	6	5
88	c	8	8	7	6	4	3
Run 3, washed 1½ min							
		Time after processing, days					
		0	14	28	83	149	269
14	a	10	10	10	10	10	10
53	b	10	10	10	7	7	6
88	c	10	9	8	5	4	2
Run 4, washed 3 min							
		Time after processing, days					
		0	14	37	65	181	274
14	a	10	10	10	10	10	10
53	b	10	10	10	10	9	9
88	c	10	9	8	7	5	3
Run 5, washed 3 min							
		Time after processing, days					
		0	27	59	185	279	
14	a	23	23	23	23	23	
53	b	23	23	23	23	23	
88	c	23	18	15	5	2	

same thiosulfate concentration with an occasional difference of 1 μg. The average value is reported in the table. The residual thiosulfate in silver-free processed microfilm was stable for 9 months at 14-percent relative humidity. A slight amount of decomposition was found in the higher thiosulfate concentrations after only 2 weeks at 88-percent relative humidity. Therefore, if tests are to be made on clear microfilm, they should be made within 2 weeks after processing if the samples are stored at about 90-percent relative humidity and within 2 months if they are stored at about 50-percent. When the samples were fixed in baths containing 4 and 8 g of silver per liter, respectively (runs 4 and 5 in table 1), the presence of this rather large amount of silver thiosulfate complex in the fixing bath *did not* materially affect the rate of decomposition of thiosulfate *in the silver-free area* of microfilm. In some runs, two samples were stored in a desiccator over anhydrous calcium sulfate and these always retained the same thiosulfate concentration as the two samples kept at 14-percent relative humidity.

4.2. Stability of Residual Thiosulfate for Different Image Densities

Step tablets of one microfilm were washed until the clear area ceased to give a positive test for thiosulfate. The densities of one step tablet in each

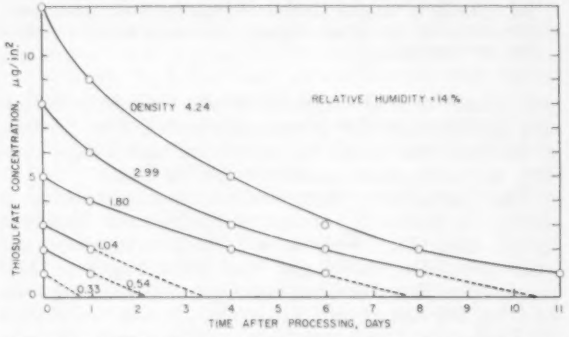

FIGURE 4. *Decrease of thiosulfate concentration in different image densities during aging at 14-percent relative humidity and room temperature (26 to 28 °C) for microfilm A.*

The image densities are noted on the curves.

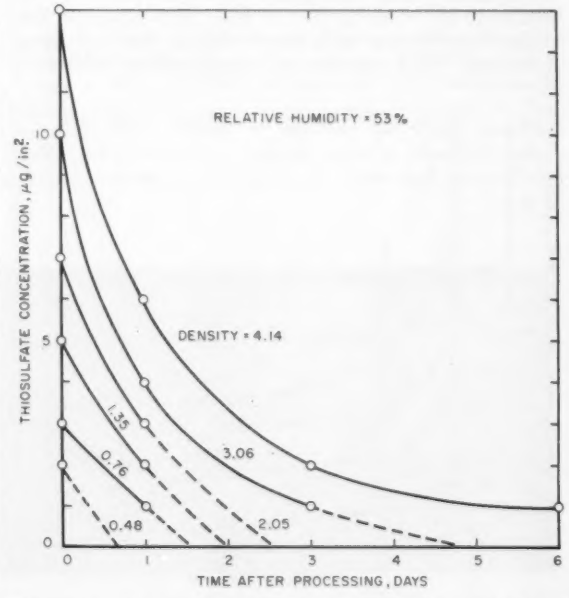

FIGURE 5. *Decrease of thiosulfate concentration in different image densities during aging at 53-percent relative humidity and room temperature (29 to 30 °C) for microfilm A.*

The image densities are noted on the curves.

run were measured and a square inch of film from each step of two tablets was analyzed for its thiosulfate content. The remaining samples were hung in one of the constant-humidity jars. At selected time intervals, the thiosulfate concentration was determined for each image density in one step tablet. The thiosulfate concentration versus time for each image density is shown in figure 4, for aging at 14-percent relative humidity; figure 5, for 53-percent; and figure 6, for 88-percent. The concentration of thiosulfate in most of the silver densities became zero during the test and the curves are extrapolated (dashed line) to zero concentration at an estimated time when the thiosulfate test would be negative. This was also done in figure 3. Figures 4, 5, and 6 show that the thiosulfate is unstable in the presence of silver and that the rate of reaction increases as the relative humidity increases. The rate of reaction was very high at the outset but diminished with time. In the highest image density no thiosulfate remained after 3 days at 88-percent relative humidity, and only 1 μg remained after 6 days at 53-percent, and 11 days at 14-percent. Figure 6 shows that within 6 hr at 88-percent relative humidity there is an appreciable decrease in the thiosulfate concentration.

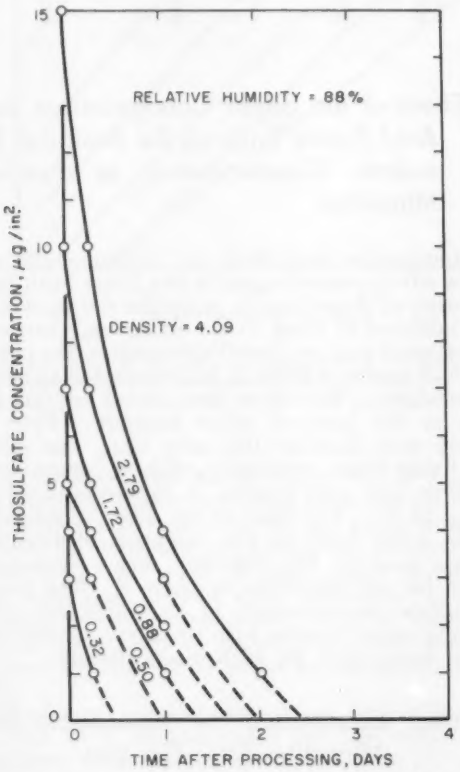

FIGURE 6. *Decrease of thiosulfate concentration in different image densities during aging at 88-percent relative humidity and room temperature (27–28 °C) for microfilm A.*

The image densities are noted on the curves.

For this reason the first thiosulfate determination for each run was made within an hour after processing.

Table 2 gives the thiosulfate concentration for step tablets with high initial concentrations of residual thiosulfate after 1 to 90 days at 88-percent relative humidity. The step tablets were washed 2½ min at 6 °C to obtain these high thiosulfate concentrations. In another run, step tablets from the same kind of microfilm used to obtain the data in table 2 were fixed in a bath containing 8 g of silver per liter and essentially the same results were obtained as those shown in table 2. This indicates that the stability of thiosulfate is not greatly affected by the silver thiosulfate complex formed during fixing in the presence of silver. Table 2 shows that the reaction of the thiosulfate with the image silver was faster in the higher densities where there was more available silver for sulfiding. The thiosulfate in the low image densities reacted if aged long enough.

TABLE 2. *Thiosulfate concentration in different image densities during aging at 88-percent relative humidity and room temperature (22–27 °C).*

Density	Thiosulfate Concentration, μg/in.²					
	Time after processing, days					
	0	1	9	21	59	90
0.00	27	25	25	23	13	10
.43	37	33	33	30	10	5
.68	40	35	33	27	4	1
1.17	45	40	35	22	0	0
2.06	50	40	27	0	0	0
3.16	55	43	10	0	0	0
4.39	63	43	2	0	0	0

The above experimental results show that the test for residual thiosulfate in image silver of processed microfilm should be made within an hour after processing. Even at 14-percent relative humidity the thiosulfate reacts slowly with the silver in the image.

5. Formation of Silver Sulfide in the Image at 88-Percent Relative Humidity

Residual thiosulfate in the processed film reacted with the image silver to form silver sulfide. Any thionates, if present, would also react with the image silver to form silver sulfide. The reaction was slow at low humidity but quite rapid at high humidity and continued until the silver or the thiosulfate was exhausted. The amount of sulfiding of the image silver during aging was determined in terms of optical transmission density of the silver which had been sulfided. The image silver remaining after aging was removed by a bleach, leaving the silver sulfide image or residue which was then reduced to silver. The process was carried on in daylight but not in direct sunlight.

The step tablets were treated 5 min in a dichromate bleach bath (see appendix 9.2), washed 10 min in tap water at 25 °C, treated 3 min in a clearing bath, fixed 3 min, and washed 10 min in running tap water. After the step tablets having an image of silver sulfide were dried, they were treated 2 to 3 min at 25 °C in a permanganate bleach bath (see appendix 9.3), rinsed 10 sec in running tap water, treated 2 to 3 min in a clearing bath at 15 °C, washed 10 min in running tap water at 15 °C, shaken to remove surface water, and hung to dry in the dark. The step tablets were then exposed for 10 min to a 100-w tungsten lamp at a distance of 12 in., developed 5 min at 20 °C, treated 1 min in the stop bath at 15 °C, washed 5 min in running tap water at 15 °C, shaken to remove excess water, and hung to dry. The step tablets then had an image of silver obtained by the reduction of the silver sulfide.

Eight step tablets were used in each run. The image densities were measured on one step tablet and the thiosulfate concentration was determined for each density of two tablets after processing and one tablet after aging. After processing, two tablets were treated in the thiosulfate eliminator described in appendix 9.1 to determine the amount of sulfiding of the silver image during fixation. Two tablets were aged at 88-percent relative humidity and treated in the thiosulfate eliminator. The two tablets that had been treated in the eliminator after processing and the two that had been aged and treated in the eliminator were bleached at the same time to obtain the silver sulfide image which was then reduced to the silver image.

Eight step tablets of one microfilm were fixed and washed 3 min at 25 °C to obtain low thiosulfate concentrations in the image densities. The results are shown in table 3. Two of the tablets were aged 6 days, at the end of which time all of the residual thiosulfate had disappeared. There was an increase in the amount of silver sulfided for all densities. The density of silver sulfided during aging is not shown directly in table 3 but may be obtained by subtracting the density of the silver sulfided during fixation from the density of silver sulfided during fixation and aging.

TABLE 3. *Density of the silver sulfided during fixation and by reaction with residual thiosulfate in the processed microfilm during aging at 88-percent relative humidity at room temperature*

Original density	Residual thiosulfate, μg/in.²		Density of silver image obtained by bleaching and reducing the silver sulfide image	
	After processing	After aging	Silver sulfided during fixation	Silver sulfided during fixation + silver sulfided by reaction with thiosulfate during 6 days at 88% rh(25–26 °C)
0.00	0	0	0.00	0.00
.32	2	0	.01	.02
.54	3	0	.02	.04
.98	5	0	.05	.07
1.88	7	0	.09	.14
3.00	10	0	.15	.21
4.43	15	0	.22	.30

Eight step tablets of one microfilm were fixed and washed 3 min at 3.5 °C to obtain high thiosulfate concentrations in the image densities. Two tablets were aged 27 days. The results are shown in table 4. Some of the thiosulfate remained in the low densities after 27 days but none was left in the high densities. The data in tables 3 and 4 show that the residual thiosulfate in processed microfilm reacts readily with the image silver to form silver sulfide at 88-percent relative humidity.

TABLE 4. *Density of the silver sulfided during fixation and by reaction with residual thiosulfate in the processed microfilm during aging at 88-percent relative humidity at room temperature*

Original density	Residual thiosulfate, μg/in.²		Density of silver image obtained by bleaching and reducing the silver sulfide image	
	After processing	After aging	Silver sulfided during fixation	Silver sulfided during fixation + silver sulfided by reaction with thiosulfate during 27 days at 88% rh(23–27 °C)
0.00	35	15	0.00	0.00
.38	45	15	.01	.08
.62	47	10	.02	.12
1.06	50	3	.05	.22
1.95	55	0	.10	.33
3.08	60	0	.15	.39
4.46	70	0	.20	.46

6. Effect of the Silver Concentration in the Acid Fixing Bath on the Residual Thiosulfate Concentration in Processed Microfilm

Experiments were made to determine the effect of the silver concentration in the fixing bath on the retention of thiosulfate in microfilm during washing. The addition of silver to the fixing bath causes the formation of a silver thiosulfate complex, the presence of which makes it difficult to remove the thiosulfate by washing. The silver was added to the fixing bath in the form of silver bromide. Four step tablets were fixed at the same time, one each in four fixing baths containing different concentrations of silver, and were washed in the same pan for 10 min at 25 °C. The effect of the silver concentration in the fixing bath on the retention of thiosulfate during washing for different image densities is shown for one microfilm in figure 7. The residual thiosulfate concentration in the microfilm during washing *varied linearly* with the silver concentration in the fixing bath for each image density.

7. Total Elimination of Thiosulfate From Microfilm After Fixation

Complete elimination of the thiosulfate is necessary for the determination of the amount of sulfiding of the silver image during fixation and aging.

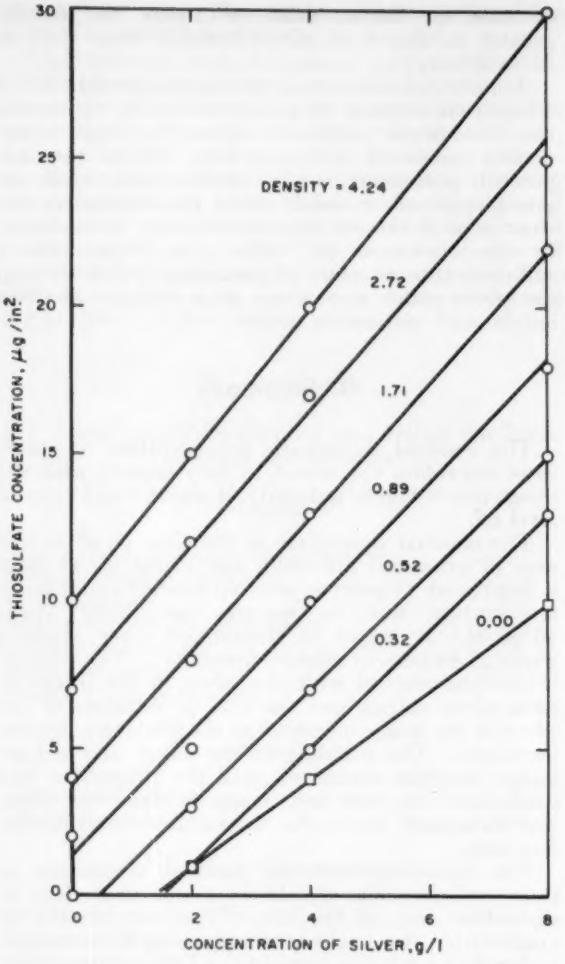

FIGURE 7. *Effect of the silver concentration in the fixing bath on the concentration of residual thiosulfate for different image densities after a 10-min wash at 25 °C, on one microfilm.*

A residual thiosulfate concentration of 2 or 3 μg/in.² will give a measurable increase in silver sulfide during aging as shown in table 3 for the low image densities. Washing for 1 hr will not completely remove thiosulfate from the areas of high image density of most microfilms. Even after treatment in alkali solutions, tablets still contained traces of thiosulfate in these areas, and an investigation was made to find how the thiosulfate could be completely eliminated.

A hydrogen peroxide-ammonium hydroxide solution has been recommended for the removal of thiosulfate from photographic materials [7]. Step tablets were fixed and washed 3 min, treated 10 min in the thiosulfate eliminator at 20 °C, and washed 15 min at 25 °C. The formula for the eliminator was as follows:

Hydrogen peroxide (30%)	50 ml
Ammonium hydroxide (28%)	10 ml
Water to make	1 liter

The image densities and residual thiosulfate concentrations are given in table 5 for fixation in a silver-free bath and a bath containing 8 g of silver per liter. The thiosulfate concentrations were about the same as those obtained when the microfilm was washed for 1 hr in running tap water, as indicated in figure 3. The concentrations of thiosulfate were slightly higher in the step tablet fixed in the bath containing silver, showing that more of the silver thiosulfate complex was retained in the emulsion. The hydrogen peroxide did not oxidize all of the thiosulfate bound in the silver thiosulfate complex in the high image densities.

TABLE 5. *Thiosulfate concentration in different image densities after treatment in the hydrogen peroxide and ammonium hydroxide solution following fixation*

Silver-free fixing bath		Fixing bath +8 g of silver per liter	
Density	Thiosulfate	Density	Thiosulfate
	μg/in.²		μg/in.²
0.00	0	0.00	0
.21	0	.18	0
.39	0	.40	0
.74	1	.80	2
1.58	2	1.72	4
2.64	4	2.98	7
4.36	7	4.74	10

It was found that the thiosulfate in the silver thiosulfate complex ion could be oxidized in solution by hydrogen peroxide in the presence of sodium chloride, potassium bromide, and potassium iodide. To demonstrate this, the following test solution was used, the chemicals being added in the order listed:

Water	400 ml
Silver nitrate, $AgNO_3$	0.5 g
Ammonium hydroxide (28%)	20 ml
Sodium thiosulfate, $Na_2S_2O_3 \cdot 5H_2O$	0.2 g
Hydrogen peroxide (30%)	25 ml
Water to make	500 ml

A black precipitate of silver sulfide was formed when the above solution was acidified with concentrated nitric acid. The nitric acid decomposed the silver thiosulfate complex forming silver sulfide. However, when a sufficient concentration of the halide salts was added before acidification by nitric acid, no dark precipitate or brownish coloration resulted, showing that the thiosulfate had been released from the silver thiosulfate complex ion and oxidized by the peroxide. The halide salts were dissolved in 25 ml of water and added to the above test solution.

The following approximate amounts of the halide salts were found necessary to eliminate the thiosulfate silver complex ion:

Sodium chloride	8 g
Potassium bromide	0.5 g
Potassium iodide	0.8 g

The silver in the silver thiosulfate complex ion appears to react with the halide ion to form silver halide thereby releasing the thiosulfate anion according to the following equation:

$$Ag(S_2O_3)_2^{---} + \text{Halide ion} \rightarrow AgHalide + 2S_2O_3^{--}$$

The small amount of silver halide is soluble in the excess halide present. This is apparently how sodium chloride in sea water assists in removing thiosulfate from processed photographic materials after fixation. The effectiveness of the different halide ions in eliminating the silver thiosulfate complex ion increases as the solubility of their silver salts decreases.

Step tablets of microfilm having a high image density (about 4.5) were fixed in a bath containing 8 g of silver per liter, washed 3 min in running tap water at 25 °C, and treated for 10 min at 25 °C in one of the following solutions: 6-percent sodium chloride, 3-percent potassium bromide, or 0.15-percent potassium iodide, and were washed 15 min in running tap water at 25 °C. The thiosulfate was completely eliminated in all image densities by the solutions of potassium bromide and potassium iodide. The sodium chloride solution left 1 μg of thiosulfate per square inch in an image density of 1.6 and 3 μg in the highest image density of 4.5, showing that sodium chloride does not remove the last traces of thiosulfate in the highest image densities.

A 0.15-percent solution of potassium iodide precipitated the silver in the silver thiosulfate complex ion as silver iodide in the emulsion. This released the thiosulfate which, in turn, was readily washed out of the emulsion. Any silver halide in the emulsion is reducible to silver. A sample of unexposed microfilm was developed, stopped, fixed in a bath containing 8 g of silver per liter, washed in tap water for 3 min at 25 °C, treated in a 0.15-percent solution of potassium iodide, and washed 15 min at 25 °C in running tap water. For the reduction of the silver iodide to silver the sample was bleached in the permanganate bleach solution, cleared, dried, exposed to sunlight 30 min, and developed. An image density of 0.07 was obtained, showing that the silver in the silver thiosulfate complex ion had been precipitated as silver iodide in the emulsion by the potassium iodide. The experiment above was repeated except that the sample of microfilm was treated in a 0.10-percent potassium bromide solution but silver bromide could not be detected in the emulsion, evidently due to the greater solubility of silver bromide over that of silver iodide.

A 3-percent solution of potassium bromide and a 4.5-percent solution of potassium iodide eliminated the thiosulfate completely from the high image density areas of the microfilm. When the 4.5-percent potassium iodide solution was used, no precipitated silver iodide could be detected in the clear area of the emulsion which may be explained by the "common ion" effect, i.e., there was a sufficient concentration of potassium iodide to keep the silver iodide in solution as a complex of silver iodide and potassium iodide.

8. Summary

The residual thiosulfate concentration in processed microfilm was found to vary linearly with the image density up to a density of about 2 and then to level off.

The residual thiosulfate in the clear or silver-free area of processed microfilm was stable for at least 9 months at 14-percent relative humidity and room temperature but, in samples containing about 10 μg/in.², it began to decompose after about 2 weeks at 88-percent relative humidity. The residual thiosulfate reacted with the silver in the image to form silver sulfide and the rate of sulfiding of the silver in the image increased as the relative humidity increased. The sulfiding of the silver in the high image densities continued until the thiosulfate was exhausted. In very low image densities the silver was exhausted when the thiosulfate concentration was high.

The thiosulfate test for residual thiosulfate in processed microfilm should be made on a clear or silver-free area of the film. The test should be made within two weeks after processing if the sample is stored at a relative humidity as high as 90 percent. However, if the film is stored at a relative humidity of 14 percent or lower, the residual thiosulfate test on the clear area of microfilm is valid for at least 9 months after processing. Samples of silver-free microfilm can be stored in a desiccator if delay in making the thiosulfate test cannot be avoided. The residual thiosulfate test on microfilm having high image densities should be made within 1 hr after processing.

In the case of one kind of microfilm involved in this study the thiosulfate was removed rapidly and almost completely in the high silver image densities during washing and the sulfiding of the image silver was much lower than that of the other four microfilms investigated. When potassium iodide was added to the fixing bath the thiosulfate in the other four microfilms also washed out rapidly in the high density silver image areas and the amount of the silver image sulfided was negligible. There appears to be a relationship between the sulfiding of the

mage silver during fixation and the retention of the thiosulfate during washing.

The hydrogen peroxide-ammonium hydroxide thiosulfate eliminator did not remove all of the silver thiosulfate complex ion unless potassium bromide was added to decompose it. The chloride, bromide, and iodide ions in a thiosulfate eliminator decomposed the silver thiosulfate complex ion, releasing the thiosulfate ion which was then readily removed by washing or oxidation. A 3-percent solution of potassium bromide or a 4½-percent solution of potassium iodide eliminated thiosulfate from microfilm which had been fixed in a bath containing 8 g of silver per liter.

9. Appendix

9.1. Formulas for Developing and Fixing the Silver Image in the Microfilm

Developer

Monomethyl *p*-aminophenol sulfate	3.1 g.
Sodium sulfite, anhydrous	45.0 g.
Hydroquinone	12.0 g.
Sodium carbonate, anhydrous	67.5 g.
Potassium bromide	1.9 g.
Water to make	1 liter.

Dilute 1 to 1 before use.

Stop Bath

Acetic acid, glacial	12 ml.
Water to make	1 liter.

Acid Fixing Bath

Sodium thiosulfate, $Na_2S_2O_3 \cdot 5H_2O$	240.0 g.
Sodium sulfite, anhydrous	15.0 g.
Acetic acid (28%)	48 ml.
Boric acid	7.5 g.
Potassium aluminum sulfate, $KAl(SO_4)_2 \cdot 12H_2O$	15.0 g.
Water to make	1 liter.

Acid Fixing Bath containing 8 g of silver per liter

Above acid fixing bath	1 liter.
Silver bromide	13.9 g.

Thiosulfate Eliminator

Water	300 ml.
Hydrogen peroxide (30%)	50 ml.
Ammonium hydroxide (28%)	10 ml.
Potassium bromide	1.0 g.
Water to make	1 liter.

After fixation or aging the sample of film was washed 3 min in running tap water, treated 10 min in the above solution, bathed for 2 min in a 1-percent solution of sodium sulfite, and washed 15 min in running tap water.

9.2. Formulas for the Bleaching Process in Which the Silver of the Photographic Image Is Removed and the Silver Sulfide Is Left as a Residue in the Emulsion Layer

Bleach Bath

Potassium dichromate	5.0 g.
Sulfuric acid (95%)	5.0 ml.
Water to make	1 liter.

Clearing Bath

Sodium sulfite, anhydrous	50.0 g.
Sodium hydroxide	1.0 g.
Water to make	1 liter.

Fixing Bath

Sodium thiosulfate, $Na_2S_2O_3 \cdot 5H_2O$	240 g.
Sodium carbonate, anhydrous	5 g.
Water to make	1 liter.

9.3. Formulas for Reducing the Silver Sulfide Residue in the Gelatin Layer to Silver

Bleach Bath

Potassium permanganate	5.0 g.
Sodium chloride	10.0 g.
Acetic acid, glacial	50 ml.
Water to make	1 liter.

Clearing Bath

Sodium bisulfite	50.0 g.
Potassium bromide	12.0 g.
Water to make	1 liter.

Developer

2,4-Diaminophenol Dihydrochloride	5.0 g.
Sodium sulfite, anhydrous	30.0 g.
Water to make	1 liter.

Stop Bath

Same as used in section 9.1

9.4. Quality of the Chemicals Used for the Formulas Listed in This Appendix

All of the solutions were made up with distilled water. The following chemicals were of reagent quality meeting ACS specifications: ammonium hydroxide, acetic acid, barium chloride, boric acid, potassium bromide, potassium dichromate, potassium permanganate, sodium chloride, sodium carbonate, sodium hydroxide, sodium sulfite, and sulfuric acid. Lithium chloride, hydrogen peroxide, and sodium dichromate were of reagent grade. The monomethyl *p*-aminophenol sulfate, hydroquinone, potassium

aluminum sulfate, sodium thiosulfate, and sodium bisulfite conformed to American Standard Specifications for Photographic Grade Chemicals. The silver bromide was Fisher, purified. The 2,4-Diaminophenol Dihydrochloride was Eastman Kodak Cat. No. P–614.

10. References

[1] E. P. Przybylowic, C. W. Zuehlke, and A. E. Ballard, An evaluation of the Crabtree-Ross procedure for residual hypo in processed film, Phot. Sci. Eng. **2,** No. 3, 148 (1958).

[2] American Standard Specifications for Photographic Films for Permanent Records, PH1.28–1957 (American Standards Association, Inc., 10 East 40th St., New York 16, N. Y.).

[3] American Standard Diffuse Transmission Density, PH2.19–1959 (American Standards Association, Inc., 10 East 40th St., New York 16, N. Y.).

[4] American Standard Method for Determining the Thiosulfate Content of Processed Black-and-White Photographic Film and Plates, PH4.8–1958 (American Standards Association, Inc., 10 East 40th St., New York 16, N. Y.).

[5] Peter Scott, The permanence of photographic silver film with special emphasis on microfilm, Proceedings of the National Microfilm Association, p. 179–202, 1958 (National Microfilm Association, Annapolis, Md.).

[6] C. I. Pope, Formation of silver sulfide in the photographic image during fixation, J. Research NBS **64C,** 65 (1960).

[7] J. I. Crabtree, G. T. Eaton, and L. E. Muehler, The elimination of hypo from photographic images, Am. Phot. **35,** No. 4, 272 (1941).

(Paper 67C1–115)

JOURNAL OF RESEARCH of the National Bureau of Standards—C. Engineering and Instrumentation
Vol. 67C, No. 1, January-March 1963

Equipment for Single Crystal Growth from Aqueous Solution

John L. Torgesen, Avery T. Horton, and Charles P. Saylor

(September 25, 1962)

The growing of large single crystals of high quality from solution requires the precise control of supersaturation and the avoidance of thermal and mechanical shock. Uniform growth conditions and cleanliness need to be maintained. Good seed crystals are necessary and the accidental introduction or generation of new nuclei should be prevented insofar as possible. In the apparatus and equipment assemblies here described, the crystal-growth bath is designed for uniform growth conditions and the exclusion of contamination. The support for the crystals provides for convenient mounting of the seeds, holds the crystals firmly, and allows their easy removal with minimum damage. A new reversing rotation mechanism promotes equal washing of the crystal surfaces and achieves uniform temperature and composition of the solution without, at the same time, producing significant mechanical stresses in the crystals. The temperature controller gives regulation of the temperature an order of magnitude more sensitive than those hitherto used and provides for stepless change of temperature. The crystals are thus free from liquid inclusions found to result from sudden acceleration of growth. The electrolytic conductance of ionic solutions may be used as a precise and sensitive measure of solution concentration and supersaturation. The crystal-growth procedures which are reported have resulted in the production of very good single crystals of a considerable variety of chemical phases.

1. Introduction

The procedure for growing large single crystals of a chemical phase from its solution in an appropriate solvent requires that a limited number of crystals be maintained in a metastable solution, that is, a solution that possesses some degree of supersaturation. Unstable conditions of supersaturation are to be avoided whereby spontaneous nucleation would result in a shower of small volunteer crystals. The procedure further requires the maintenance of supersaturation despite the removal of dissolved solute as it deposits on the faces of the growing crystal. The latter requirement may be satisfied by one of the following three general methods: (1) Removing solvent from the system as by evaporation; (2) changing the temperature of the solution in the direction toward decreasing solubility of the phase; and (3) adding solution of higher solute content while depleted solution is withdrawn to be strengthened.

This paper describes in some detail the apparatus and equipment which has been assembled to grow large single crystals from solution under closely controlled and reproducible conditions. The changing-temperature technique was preferred to solution-addition because it requires less complex equipment and to solvent-evaporation because it seemed more amenable to control.

Many reports have appeared in the literature on methods for growing crystals from solution [1–6].[1] We have drawn fully from the experience of others and have devised modifications and revisions to meet rather exacting requirements which we believe contribute (1) to close control of the system for the production of single crystal specimens of high quality and (2) to the reproductibility of growth conditions for studies on habit changes and the inclusion of impurities in crystals grown from purposely contaminated systems.

[1] Figures in brackets indicate the literature references at the end of this paper.

2. Crystal Growth Assembly

2.1. Crystal Bath

Single crystals are grown from solution contained in large glass jars 12 in. in diameter, 12 in. in height, and approximately 4½ gal in capacity. Jar covers of methyl methacrylate resin support the rotation mechanism and the temperature indicating and control devices. The jars are supported in metal frames which contain flat bottom heaters to distribute heat uniformly over the entire bottom surface and inhibit volunteer crystal growth. The bottom heater is constructed of either a bank of 25 small (15 w) lamps evenly distributed over the area of the frame or a flat spiral of coiled Nichrome wire.

The crystals are supported on glass pins situated near the ends of the arms of a "crystal tree" or "spider". The general aim is to provide support offering a minimum of interference with the external growth surfaces. When seed crystals are large it is preferable to employ twin pins to prevent rota-

tion of the crystal on its mount. The crystal tree (fig. 1) is constructed of glass rod and has three rows of four arms each, thus accommodating a total load of 12 crystals. Thin sleeves of polytetrafluoroethylene, covering the pins, are excellent in preventing adherence between the crystal and its support. By using a jig to fuse the pair of pins to the tree arm and a guide in drilling the seed crystals, trouble-free, even interchangeable, mounting and easy "harvesting" of the grown crystals are attained.

To promote efficient stirring of the bath and produce uniform solution temperature and concentration, the crystal tree is provided with vanes of flat glass. Two designs have been used, the first comprising plates attached between vertically adjacent tree arms at an angle of approximately 45° to the tree axis and also tilted at about the same angle. A second and more satisfactory design involves hanging the plates on the arms on glass tubing which acts as a hinge. The plates change position depending on the direction of rotation and continuously promote a transfer of solution from top to bottom in the jar.

A demountable T-joint attaches the crystal tree to the shaft of the rotation mechanism and a mercury seal at the lid of the bath prevents the loss of solvent vapor, contamination of the solution from the outside, and corrosion of bearings and other metal parts of the rotation mechanism.

Figure 1, a photograph taken during an actual growth operation with an insulation blanket momentarily removed, shows the details of the crystal tree assembly described above. The glass-cotton insulation blanket has a zipper closure for ready inspection of the crystals during growth.

2.2. Reversing Rotation Mechanism

In order that all surfaces of the growing crystal be washed approximately equally with the solution to promote uniform growth, it is necessary to provide a mechanism for rotation of the crystal tree in both directions. Two different devices have been used. The one employs a system of relays operated by a synchronous motor and cam to periodically stop a stirring motor, reverse the field connections, and start the motor in the reverse direction. A similar device has been described [2]. It has the disadvantage that rotational speeds must be slow, since the rotation starts suddenly and at full speed and the resulting jerk induces mechanical stress in the crystals and threatens the fracture of parts of the glass tree or possible jarring the crystals from their mounts. A more satisfactory rotation device employs a rack-and-pinion mechanism. The gear-rack, moved back and forth by eccentric attachment to the shaft of a slow speed motor, imparts, through the pinion gear on the tree shaft, an approximately sinusoidal rate of rotation to the crystal tree. The arrangement gives gradual deceleration and acceleration on either side of the reversal point and avoids undue mechanical stress in the growing crystals and the equipment assembly.

A drawing of the rotation mechanism is shown in figure 2.[2] Dimensions given here are nominal and not critical. The speed and the number of revolutions of the crystal-tree shaft in one direction are, of course, dependent on the speed of the motor, the length of the driver arm, and the diameter of the pinion gear. The arrangement shown provides a maximum speed of approximataly 25 rpm and the crystal tree is rotated through about four complete revolutions between changes of direction. The height of the frame should allow removal of the motor without other dissembly. Shafts must be slightly undersize to pass through the bearings. Commercial gear-racks must be smoothed by milling a thin cut on the three plain sides. It is important that the knuckle be placed on the tree shaft in good alinement with the driver arm bearing, and it is advisable to mill a small flat on the shaft to receive the set-screw which holds the knuckle in place. The small phosphor-bronze spring, placed behind the shoe, holds the gear-rack snugly against the pinion gear, yet allows some play to prevent binding. Good quality gear-grease is essential for smooth operation.

Ball bearings are not absolutely essential for the crystal tree and driver-arm shafts, although they contribute markedly to trouble-free operation. Units equipped with porous bronze sleeve bearings throughout have given admirable service and their alinement for the crystal-tree shaft is more easily accomplished.

It is recommended that the motor[3] be equipped with spiral gears in the gear-reduction train and that the position of the driver arm on the motor shaft be changed periodically to distribute wear in the gear train. Spur gears have stripped after several months of continuous operation.

3. Temperature Control

Of primary importance for the production of single crystal specimens of high quality by growth from solution is the control of temperature. Momentary temperature fluctuations, resulting in interrupted and accelerated growth rates, produce veils of mother liquor inclusions which lie parallel to the crystal faces on which deposition occurs. In addition, when the temperature-changing technique is employed, we have found that finite changes in temperature of a few hundredths of a degree will again induce the inclusion of mother liquor pockets. The close control of temperature at a given instant, together with a slow and continuous change in the temperature to maintain a uniform degree of supersaturation, can do much to minimize this effect.

3.1. Proportioning Temperature Controller

A proportioning type temperature controller, in which heat is supplied to the system in direct relation

[2] The design of this mechanism is based on that of a similar device observed in operation in the laboratories of the Brush Development Company, now a subsidiary of the Clevite Corporation, Cleveland, Ohio.
[3] Bodine, Type KCI-22 RM.

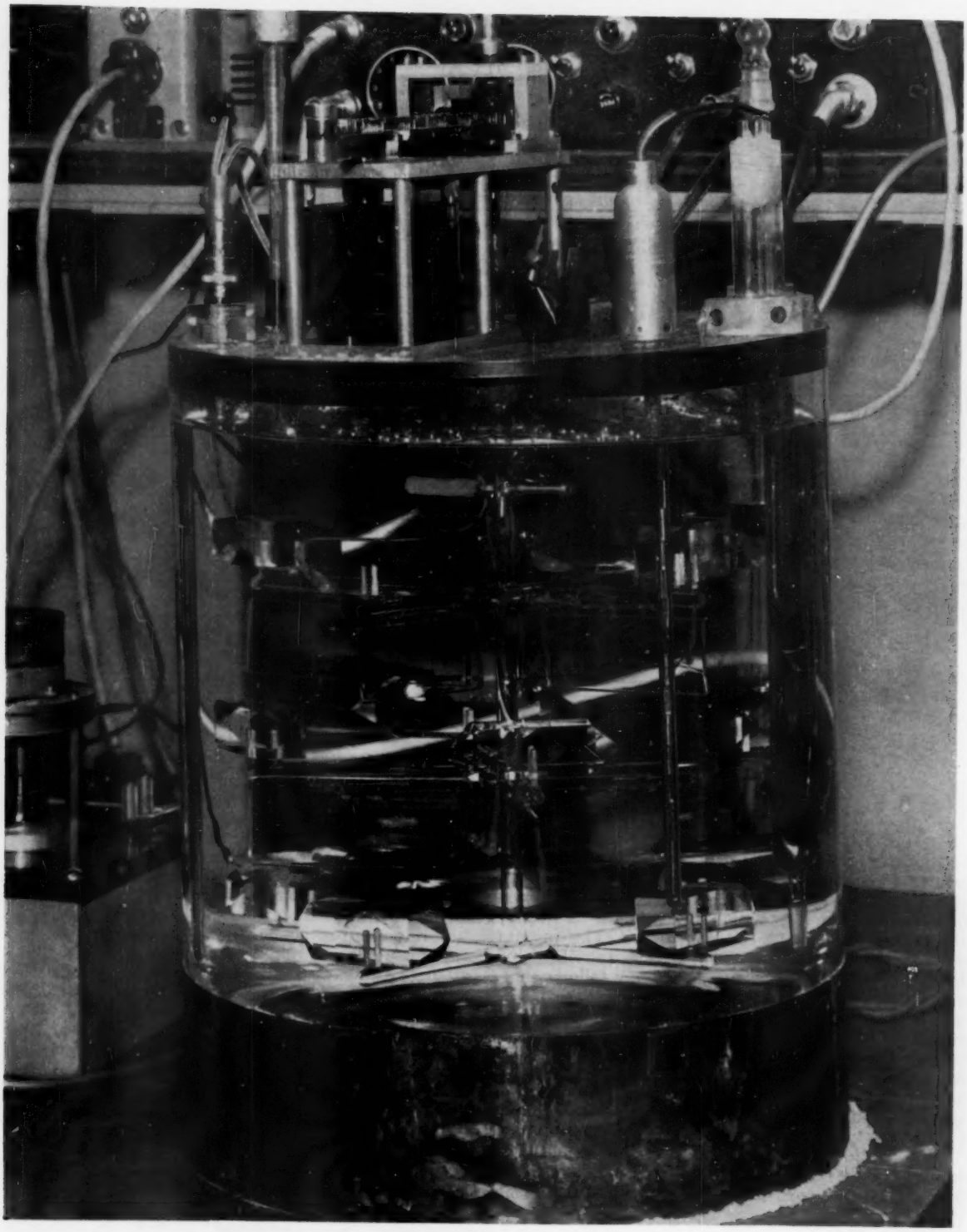

FIGURE 1. *Crystal growth assembly.*

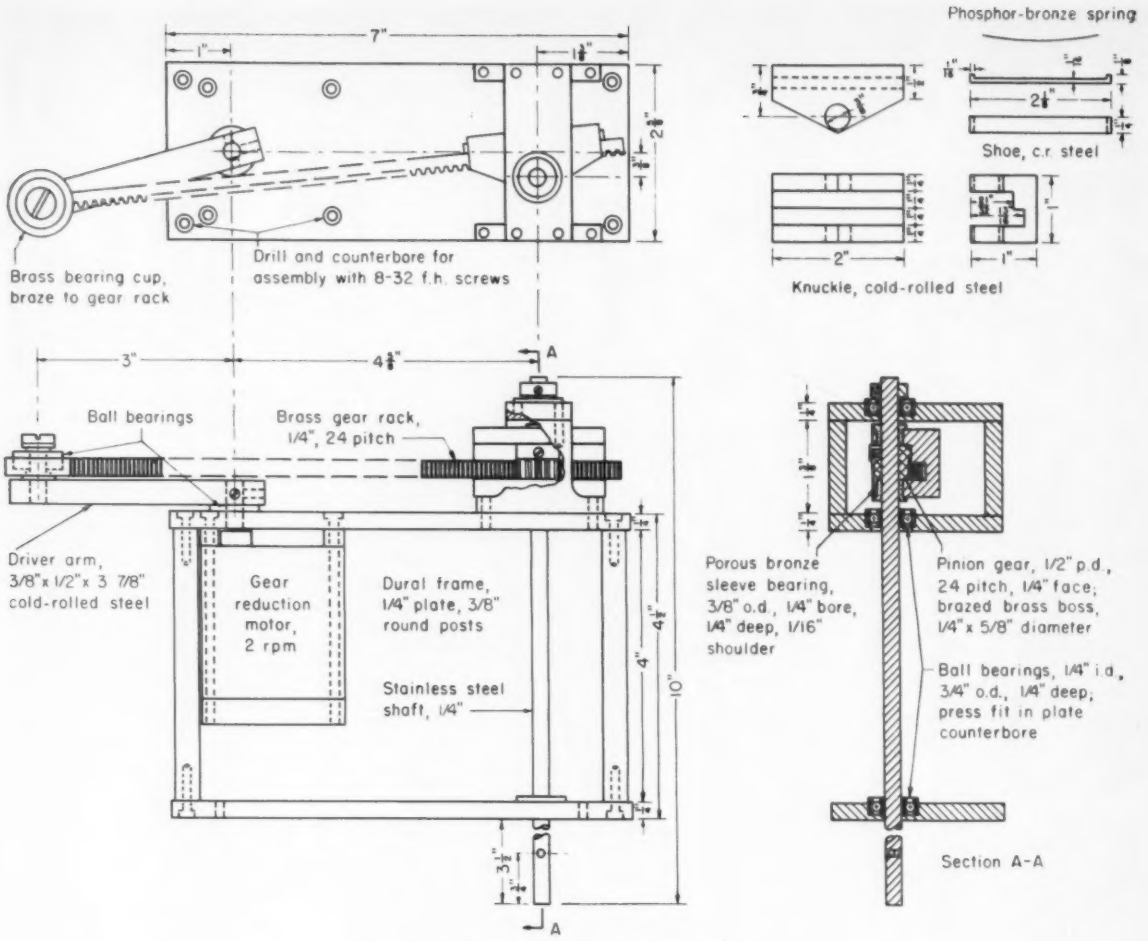

FIGURE 2. *Reversing rotation mechanism.*

to the departure of temperature from the desired point, is generally regarded as superior to an on-off circuit. The great majority of our crystal growth operations have been conducted with a time-proportioning "saw-tooth" controller. The instrument is similar in principle to one described by Ransom [7] and its construction closely follows that of the controller designed by Sargent [8]. The instrument time-modulates the electrical energy supplied to control heaters proportionally to any temperature departure from the control point. In conjunction with a commercial power supply,[4] a commercial amplifier of 10^5 to 10^6 gain,[5] and a specially-built Wheatstone bridge, a "saw-tooth" relay, whose circuit is shown in figure 3, is used.

The temperature-sensing element is a platinum coil, similar in construction to a platinum resistance thermometer to provide rapid response and coil stability, connected as one arm of the Wheatstone bridge. The adjacent arm is a variable resistance adjustable to the desired control point. The bridge is energized with direct current from dry cells, and the bridge output is coupled to a converter and a-c amplifier. The amplified bridge signal (d-c output) is fed to the saw-tooth relay circuit to change the potential level of the saw-tooth voltage whose frequency corresponds to a selected duty cycle. As shown in figure 3, an appropriate R-C circuit is used to generate the saw-tooth voltage, the circuit being shorted periodically and momentarily by a microswitch operated with a cam and 10 rpm synchronous motor. The duty cycle is thus of 6 sec duration. The change in potential level operates the control relay, S_2, and switches power to the control heaters.

The potential level of the saw-tooth voltage is adjusted with coarse (R_9) and fine (R_{17}) control potentiometers, while the spring tension on the plate relay (S_2) is adjusted, so that the relay is closed 50 percent of the duty cycle when the error

[4] DC Power Supply, Model 28M, Lambda Electronics Co., Huntington, Long Island, New York.
[5] Brown Elektronic Amplifier, Model 356358-1, Minneapolis-Honeywell Regulator Co., Brown Instruments Division, Philadelphia, Pa.

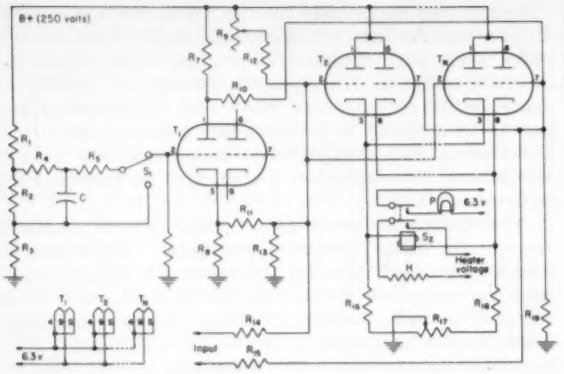

FIGURE 3. *Time-proportioning sawtooth relay.*

R_1—150 kohm, ½ w
R_2, R_4—47 kohm, ½ w
R_3—3 meg, ½ w
R_5—10 kohm, ½ w
R_6—10 meg, ½ w
R_7, R_8—68 kohm, ½ w
R_9—2.5 meg potentiometer
R_{10}, R_{11}—1.2 meg, ½ w
R_{12}, R_{13}—0.82 meg, ½ w
R_{14}—4.7 meg, ½ w
R_{14}, R_{15}—0.47 meg, ½ w
R_{16}, R_{18}—2 kohm, 10 w
R_{17}—2 kohm potentiometer
T_1—5751
T_2, T_3—5814A
C—4 μf, oil impregnated paper
S_1—SPDT microswitch, cam operated, 10 rpm synchronous motor
S_2—DPST sensitive plate circuit relay, 2500-ohm coil
P—Pilot lamp
H—Heater

voltage (bridge signal) is zero (bridge output shorted). Subsequent error voltages from the bridge will shift the potential level of the saw-tooth voltage up or down so that the percentage of time per duty cycle that the control heater is energized, is dependent on the magnitude and sign of the error voltage.

In normal operation the potential drop across the relay coil varies linearly with time from about 20 to 10 v during the six-second duty cycle, except for a momentary (¼ sec) 50-v spike at the beginning of the cycle. The latter provides assurance that the relay closes and power is supplied to the heaters. Spring tension on the relay is adjusted to provide release and opening the heater circuit at about the mid-point in the normal operating range.

The sensitivity of the controller to changes in temperature is dependent on the degree of amplification of the bridge signal. It is found that an amplification factor of approximately three-quarters maximum provides a control band, from full off to full on, corresponding to a temperature interval of 0.010 to 0.015 °C. Temperature control of the crystal baths to ±0.002 °C is obtained.

Four units as described above have been in service for a number of years. Their performance has been very satisfactory for the extended periods required in crystal growth experiments. They are composed of mechanical relays, switches, motors, and common electronic components which are subject to failure, and failure of temperature control is disastrous to crystal growth experiments. Electronic tubes of the best quality are used and these are tested for performance and life expectancy whenever possible, that is, at the completion of each crystal growth experiment. Figure 3 shows some choice as to the number of 5814A tubes in parallel to supply current to the relay coil. While one tube would probably do the job, we actually use four in parallel as a precaution against failures. It has been our experience that the units may be depended upon to operate continuously without breakdown for periods up to 6 months. We have not conducted growth operations to exceed more than one-half this period. Our laboratory is provided with an independent and regulated a-c power supply, separate and distinct from the building supply, to avoid interruptions in electrical service.

3.2. Continuous Temperature Change

Growth of single crystals from solution by the temperature-changing technique, and this usually means lowering the temperature as growth proceeds, requires that the setting of the Wheatstone bridge in the control circuit must be changed. Initially this was done manually, decreasing the resistance in the setting arm of the bridge by an amount proportional to the desired change in temperature. The twice-daily change of 0.02 to 0.04 °C in earlier growth operations led to inclusions of mother liquor in certain areas of the crystals. This was particularly true in the case of ammonium dihydrogen phosphate, where inclusions of varying size and up to almost 1 mm in length, appearing in the position of the advancing prism corner, marked each temperature shock to which the system was subjected. The effect demanded an arrangement whereby the temperature could be changed continuously.

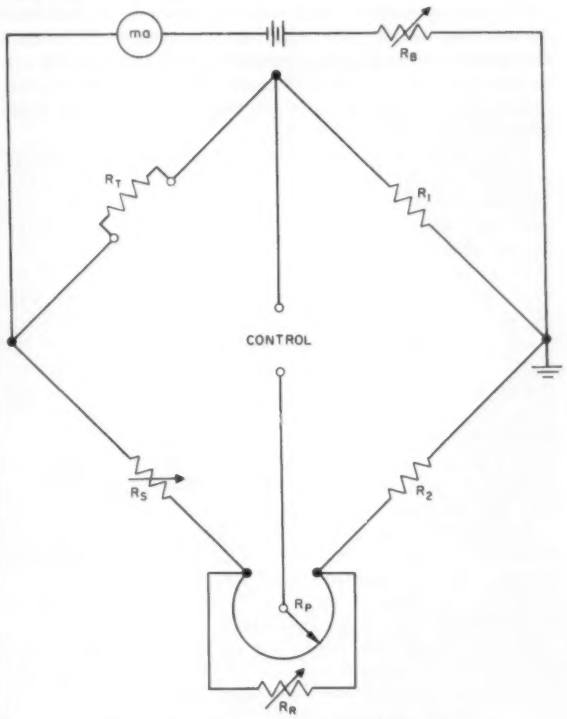

FIGURE 4. *Modified Wheatstone bridge.*

Transfer of resistance from one arm of the bridge to another, as with a slide-wire potentiometer driven by a synchronous motor, will unbalance the bridge continuously and cause the temperature control point to shift. The rate of temperature change may be governed by the size of a shunt across the potentiometer. We have constructed several bridges of this type in accordance with the diagram given in figure 4. Precision components are employed since satisfactory performance depends on resistor stability, slide-wire uniformity, low contact resistance in the switches, etc.

The ratio arms of the bridge, R_1 and R_2, consist of two 50-ohm precision resistors (General Radio Type 500). A decade resistor of 1.0 ohm-per-step in series with one of 0.1 ohm-per-step (both General Radio Type 510) plus a fixed precision resistor of 25 ohms constitute the setting arm of the bridge, R_S. A platinum coil of 25.5 ohms resistance at 0 °C and a temperature coefficient of 0.1 ohm per degree C is the fourth arm, R_T, and the temperature-sensing element of the control system. As stated above, this coil is constructed in the same manner as a precision resistance thermometer in order that it have low lag and adequate sensitivity. A 100-ohm 10-turn potentiometer (Beckman Instrument Co.), R_P, is connected as shown. The slider must be in the output circuit to avoid variable contact resistance in the bridge circuit. A similar bridge [9], but constructed with the slider contact in the bridge circuit in one arm to add or remove resistance, gave some contact resistance trouble. The shunt, R_R, is a 0.1 ohm-per-step decade resistance unit (General Radio Type 510). A 0.1 turn-per-day synchronous motor and gear train drives the slider, transferring resistance in normal temperature-dropping operation from the setting arm to one ratio arm. A dial mounted on the drive shaft indicates position and is necessary in making small temperature adjustments.

The circuit does not give a change in temperature precisely linear with time due principally to bridge balance relationships with the resistors small and near the same size. A slight nonlinearity is introduced also by the fact that the sensing-arm resistance is not strictly linear with temperature. However, at the maximum setting of the shunt, with R_S set to control the temperature in the neighborhood of 50 °C, the deviation from linearity is less than 3 percent as the slider is moved from one extreme position to the other. Actually, the bridge may be made practically linear by increasing the resistance in the ratio arms sufficiently. Such revision would, however, require a large d-c supply to maintain sufficient current (20 ma, controlled by R_B) for adequate sensitivity in the control system.

The control range of the bridge described is from 0 to 100 °C approximately. The rate of temperature change, over a maximum of 100 days without resetting R_S, is from 0 to 0.15 °C per day in steps of 0.015 °C per day approximately.

Of the total heat supplied to the baths for maintenance of temperature near 50 °C, about 50 percent is supplied continuously through the bottom heaters and variable transformers. The controlled heat is supplied through two finger heaters introduced through and supported by the lid of the bath. The finger heaters are of Nichrome wire wound on a mica strip and enclosed in a glass tube which has been silvered on the inside. The silver coating effects better radiation of heat and, when grounded, serves as a shield to prevent 60-cycle radiation from interfering with conductivity measurements used to determine the solution concentration and supersaturation [10].

The temperature of the crystal-growth baths is measured with platinum resistance thermometers and a Type G–1 Mueller thermometer bridge (Leeds and Northrup No. 8067). A four-pole, silver-contact selector switch, accommodating several thermometers, makes convenient the transfer from one thermometer to another. Future plans include the installation of a multipoint recorder system of adequate sensitivity to provide a more complete history of crystal-growth operations and a warning system.

3.3. Measurement of Solution Concentration

The electrolytic conductance of ionic solutions has been found to be a precise and sensitive measure of the concentration of these solutions at a given temperature in the saturation region. The measurements are made with an immersion conductance cell of new design (shown at the extreme right in fig. 1) and they provide a means to monitor with precision the growth conditions of supersaturation which obtain during the crystal-growth operation. Details on the design of conductance cells, the measurement procedures, and conductivity data for ammonium dihydrogen phosphate solutions are given in a concurrent publication appearing elsewhere [10].

4. Crystal Growth Procedure

Sufficient solution is prepared from distilled water and solute of the best available quality to fill the crystal-growth jar to within an inch or two of the top. The concentration of the solution corresponds to saturation at the desired growth temperature. The solution is filtered hot through fritted glass filters to remove insoluble material, which may run as high as several hundredths of 1 percent even in analytical reagent grade materials. On transfer to the growth jar, the temperature is raised well above that corresponding to saturation (usually 4 to 5 °C) to insure complete solution and the absence of nuclei which would induce volunteer growth. In this step a separate jar lid is used which holds a motor stirrer and long glass propeller. The temperature control and measurement devices are inserted and, using conductivity measurements or a pilot crystal as a guide, the temperature is decreased to the saturation point. Meanwhile seed crystals which have been cut or cleaved from parent single crystal material or which have been grown in crystallizing dishes to sufficient size (usually by solvent-evaporation methods) are drilled and mounted on the crystal tree which has been attached to its own lid and rotation mechanism. Drilling can usually be done with

ordinary steel twist drills and a small variable-speed drill press, with the seed crystal immersed in a saturated solution of the same material. For crystals which cleave readily, dental burrs with an inverted-cone shape have been used successfully. With seed crystals not large enough for mounting on twin pins, single pins have been used. In these cases it is advisable to place a short length of small plastic tubing on the pin and above the seed to assist in holding the seed in place during the planting operation and in the early stages of growth.

When saturation conditions have been established in the bath, the temperature is raised slightly and the seeds are planted by simple exchange of equipment. The bath temperature is held above saturation for a few hours until the seeds have dissolved slightly, as evidenced by the first noticeable rounding at the corners and edges. This is done to remove the small individual crystals which may be on the surface of the seed as a result of cutting or drilling operations and would tend to induce polycrystalline growth. The temperature is then lowered to the saturation point and the temperature-dropping procedure begun.

The temperature-dropping program selected depends on the temperature coefficient of solubility of the solute, the number, habit, and size of the crystal seeds, the growth habit and mechanism including the type and number of self-perpetuating growth centers, and the degree of supersaturation that will induce spontaneous nucleation. In the absence of previous knowledge, caution is recommended with a new material until some information on the behavior of the system has been gained. If high quality material is the goal, one does not normally expect to push growth rates from solution to exceed a deposition of 1 mm per day normal to the fastest growing crystal face. This condition will lead to quite different temperature programs for different materials. For ammonium dihydrogen phosphate the area of actively growing crystal does not increase with growth time from uncontaminated solutions. As the saturation concentration versus temperature curve is roughly linear over the range used, the temperature program consists of a constant dropping rate after the habit is fully established. The initial seed will have additional imperfections, pits, and vicinal faces that grow very much faster than an established pyramid face, so initially much lower supersaturations are needed.

On one occasion in an effort to accelerate the growth of ammonium dihydrogen phosphate crystals of 2 cm diam, we increased the temperature drop-rate to 0.2 °C per day. Growth on (101) faces became polycrystalline, with small individual crystals originating particularly from corners and edges. The supersaturation in this experiment increased to better than 10 percent. We normally grow ammonium dihydrogen phosphate crystals in the temperature range from 40 to 50 °C at a temperature-dropping rate of approximately 0.10 °C per day under which conditions deposition on the (101) faces is approximately 0.5 mm per day. With much smaller seed crystals of uranyl nitrate hexahydrate, sodium chlorate, etc., the temperature-dropping rate in initial stages of growth does not exceed 0.02 °C per day.

Finished crystals are taken individually from the crystal tree, dried quickly with soft paper tissue, and, if the growth temperature has been as much as 5 to 10 °C above ambient laboratory temperature, they are transferred to a warm air-bath for subsequent slow cooling to avoid thermal shock and cracking. In this operation the evaporation of adhering solution and subsequent growth leaves the crystal faces far from perfect. For an improvement on this technique we have often immersed the crystals immediately in 50–50 propylene glycol-water mixture at essentially the same temperature as the crystal bath, followed by washing in ethyl alcohol. In some cases etching of the crystal surface has been observed.

A high degree of preservation of the surfaces would involve the transfer of the crystal from the growth medium to an inert medium at exactly the same temperature, avoiding as much as possible both deposition and dissolving the crystalline material while the adhering solution is removed from contact with the crystal faces. The inert medium must neither etch the crystal surfaces nor "salt-out" dissolved solute. It may be miscible or immiscible with the saturated solution. In the latter case, it would appear that a considerable density difference would enhance the removal of solution. Our experiments in this connection have not resulted in a procedure to be recommended.

5. Conclusion

With crystal-growth units assembled as described above, we have successfully grown single crystal specimens of ammonium dihydrogen phosphate, potassium dihydrogen phosphate, uranyl nitrate hexahydrate, strontium dichromate, sodium chlorate, sodium nitrate, and oxalic acid dihydrate. In representative cases these single crystals have been judged to be excellent so far as control of dislocations, twinning, and inclusion of foreign substances are concerned. This judgment has been largely based upon single crystal X-ray diffraction, optical examinations between crossed polarizers, microscopical searches for discontinuities or inclusions, and the observation of reflections from cleavage surfaces. Corroborative information has come from chemical or spectrochemical analysis for impurities present in the mother liquor but not definitely detectable in the crystals. Imperfections associated with the junction between seed and growth are not considered in this context.

The procedures have been followed in a great many experiments on the growth of ammonium dihydrogen phosphate in the presence of selected impurities. The equipment has performed satisfactorily for us and its design and assembly are presented for those with an interest in the growth of large single crystals from aqueous solution.

We express appreciation to Herbert Lowey for expert machine work in the construction of various parts of the equipment, in particular the reversing rotation mechanism. We are very much indebted to Jack Sargent[6] for his assistance in the design of the temperature-control relay.

[6] Now with Panellit, Inc., Chicago, Ill.

6. References

[1] A. C. Walker and G. T. Kohman, Trans. Am. Inst. Elec. Engrs. **67,** 12 (1948).
[2] A. N. Holden, Discussions Faraday Soc. **1949,** No. 5, 312.
[3] A. E. Robinson, Discussions Faraday Soc. **1949,** No. 5, 315.
[4] A. C. Walker, J. Franklin Inst. **250,** 481 (1950).
[5] H. E. Buckley, Crystal Growth, Ch. 2, (John Wiley & Sons, Inc., New York, N.Y., 1951).
[6] A. V. Shubnikov and N. N. Shefta', Growth of Crystals, Vol. **1** (1958) Consultants Bureau, Inc. New York, N.Y. (First Conference on Crystal Growth of the Institute of Crystallography, Academy of Sciences USSR, 1956).
[7] F. A. Ransom, Control Eng. **1,** 1 (1952) (McGraw-Hill Book Co., Inc., New York, N.Y.).
[8] J. Sargent (unformal communication, 1955).
[9] T. W. Thomas and L. G. Finch, J. Sci. Instr. **34,** 118 (1957).
[10] J. L. Torgesen and A. T. Horton, J. Phys. Chem. **67,** (1963).

(Paper 67C1–116)

JOURNAL OF RESEARCH of the National Bureau of Standards—C. Engineering and Instrumentation
Vol. 67C, No. 1, January–March 1963

An Automatic Multichannel Correlator

Robert F. Brown, Jr.

(September 25, 1962)

Very early in the Infrasonic Research Program of the U.S. National Bureau of Standards, it became apparent that the only way to differentiate between local meteorological pressure variations and the infrasonic signals from distant sources was through the relative time of arrival of the pressure disturbance at pickups spaced several miles apart. The "Multichannel Correlator" is an analog computing instrument that was designed to detect these infrasonic signals.

At each pickup the pressure variations are converted to FM audio signals which are transmitted over leased telephone lines to the correlator. At the correlator these FM signals are demodulated and recorded on a one-fourth inch per minute multichannel magnetic tape. The recorded data frequency range is 0.02 to 1.0 cycles per second and the pressure range is 0.1 to 50 dynes per square centimeter. Ten-minute blocks of data are read from the tape and amplitude equalized to a constant root mean square value. A programed time-delay device produces the equivalent delays appropriate to a continuous horizontal azimuth search for velocities in the range of 280 to 400 meters per second. The correlator output is a continuous record of the average of the rectified sum of the delayed channel signals.

1. Multichannel Correlator

The multichannel correlator is an analog computing instrument which produces an output proportional to the average of the cross correlations between pairs of its inputs. It was built in an attempt to mechanize signal detection in a noisy environment. The inputs were from several microbarograph pickups located in the Washington area. The only available criterion for the presence of signal was waveform congruence, at an appropriate time delay, between data channels. Experience had shown that within one data channel there was no way to tell signal from noise. Both signals and background noises could show semiperiodic structure or random waveforms. They could occur anywhere in a wide frequency spectrum. They showed both rapid and slow rise and decay of energy levels. Thus a signal waveform was completely unpredictable and looked like the background noise on any one channel. Also, a type of noise associated with weather phenomena could maintain waveform congruence while passing through the area but would have a very low velocity, frequently local wind speed. Therefore, the time delay search range was restricted to include only velocities of 280 to 400 m/sec. The correlator has five operational sections; data storage, sampling readout, time delay, amplitude equilization, and detection.

Figure 1 is a photograph of the complete Multichannel Correlator. The equipment fills most of a three section rack. The left hand section holds the data recorder and readout. The center section holds the delay system and amplitude equalizers. The right hand section holds the detector, output recorder and auxiliary equipment.

FIGURE 1. *Front view of the automatic multichannel correlator.*

2. Data Storage Section

The correlator has five data inputs and a time input. The data inputs are in the form of frequency-modulated audio carriers. The FM is demodulated

665368—63——3

and the resulting analog data are recorded on a magnetic tape. The five tracks of data are recorded in parallel on the tape. The range of frequencies of interest is from 0.02 c/s to 1.0 c/s. By using a tape speed of 0.25 in. per minute (about 0.004 ips), the recorded wavelengths on the tape lie between 0.2 in. and 0.004 in. This is the same range of wavelengths as is used in conventional recording. The recording is done using a-c biasing and the bias frequency used is about 80 c/s.

A sixth track on the magnetic tape is used for recording the time signal. The time signal consists of a 1.0 sec pulse recorded every 5 min. The hour pulse is identified by adding another 1.0 sec pulse displaced by 10 sec.

Figure 2 is a photograph of the data storage and sampling readout section. The storage tape travel is from the supply spool, across the writing table, record head, drive capstan, readout heads, and onto the takeup spool.

The tape moves so slowly that it can easily be written on with a brush or a felt ink marker. Thus comments such as local weather conditions, calibration data, or date and time marks can be written directly on the storage tape. The only precaution is that the tape motion across the recording head should not be disturbed. For these reasons the writing table was provided ahead of the recording head. The tape was mechanically isolated from writing disturbances by lateral guides and a friction pad.

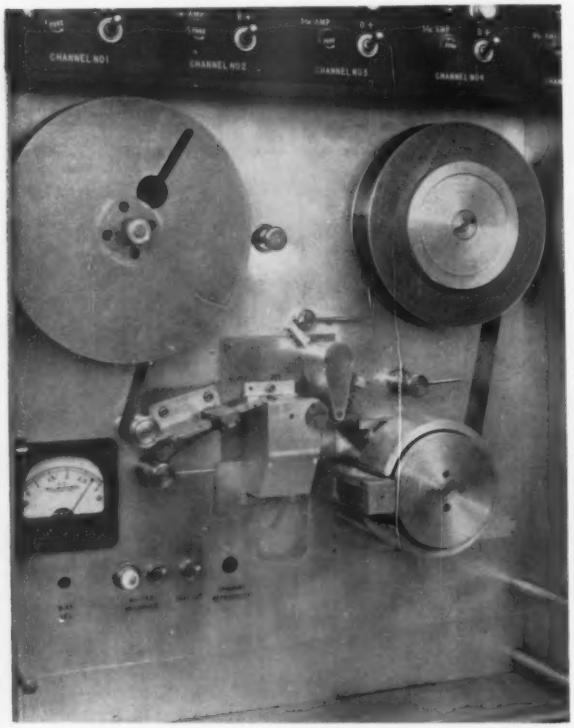

FIGURE 2. *Closeup view of the data storage section.*

The recording head stack is of conventional construction as are the drive capstan and pressure roller.

3. Sampling Readout

The sampling readout occurs at the cylinder around which the tape makes a 90° turn. In this cylinder are mounted four readout head blocks with their gaps accurately located 90° apart. The circumference of the cylinder is 10 in. In operation it revolves counter-clockwise at 3 rps. This makes the playback head-to-tape velocity 30 ips, which gives reasonable head output levels. Each head contacts the tape for 2½ inches, which corresponds to 10 min. of recorded data. The outputs of the four heads sampling a recorded data channel are added in series. Thus, the sampled readout consists of a continuous sequence of data blocks, each containing the equivalent of 10 min. of original recorded signal.

The tape was recorded at 1/240 ips and is read at 30 ips. This high speed readout translates the input frequency spectrum upwards by a factor of 7200:1. Thus the original 0.02 c/s to 1.0 c/s becomes 144 c/s to 7200 c/s. Also, the time delays between channels, necessary to bring the signal waveforms into coincidence, are reduced by the same 7200:1 factor. For example consider two microbarographs placed 10 miles apart. They have about a 48 sec direct line transit delay. The equivalent relative delay needed after sampling is only 6.7 msec.

The data are read out at 12 samples per second. Each head is in contact with the tape for 2.5 in. so that any given datum point on the tape continues to be sampled for 10 min. The effect is to produce 7,200 samples of any given datum point. In the limit this would allow the trial of 7,200 different data computations.

A synchronizing pulse is produced during each sample. This pulse can be phased to correspond with any position along the 10 min sample.

4. Time Delay Section

By means of the tape loop and the map linkage, variable time delays are introduced into each channel corresponding to a systematic search for signal correlation at all azimuths and over a range of velocities appropriate to acoustic signals. Relative time delays are introduced into all five data channels but not the time channel. Figure 3 is a photograph of the time delay mechanism. The time delay is produced by using a tape loop with moveable playback heads. The loop is formed of 40 in. of 1 in. wide magnetic tape. It runs at a speed of 30 ips. The five data outputs from the storage readout are re-recorded in parallel on the tape loop. Each data track has an independently moveable readout head. The heads can be displaced a maximum of ¾ in. for a maximum change in time delay of 25 msec. This is the equivalent of 180 sec in the original data time scale.

The time delay is programed by a map and push-rod linkage. The program includes only those time delays appropriate to acoustic phase velocities across the microbarograph array. Plane wavefronts are assumed and no corrections are made for local topography. This program is achieved by the following mechanism. A scale map of the microbarograph sites is mounted in a pair of gimbals with the plane of the map at the gimbal axis. The push-rods operate from the map positions of the sites, and are displaced along their axes when the map is tilted. The push-rods in turn vary the position of the playback heads along the tape loop. In the neutral position, map plane perpendicular to push-rod axes, all playback heads are in line and there is no relative time delay. This corresponds to an infinite horizontal velocity or to a signal which comes straight down form overhead. As the map is tilted away from neutral some heads are advanced and others retarded from the neutral position. This corresponds to searching in the direction of greatest retardation for the presence of signals having a velocity which is a function of the amount of retardation.

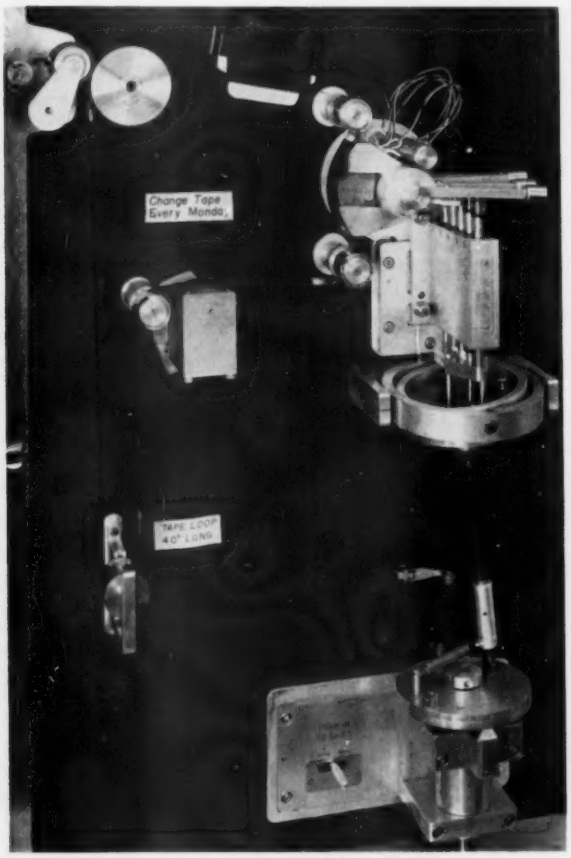

FIGURE 3. *Closeup view of the time delay mechanism.*

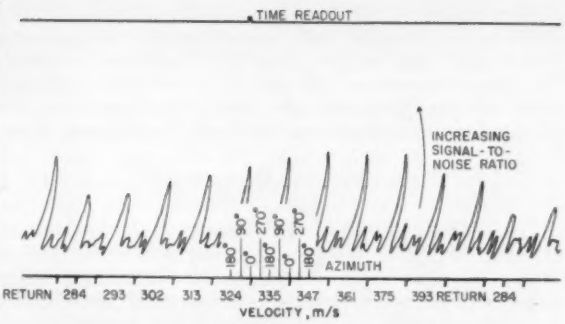

FIGURE 4. *Sample output record for the correlator.*

Since the map is mounted in gimbals, it can be tilted toward any azimuth; or, at a given tilt, it can be rotated through a complete circle or azimuth sweep. The time delay program rotates the map tilt continuously, taking 15 sec for a complete azimuth sweep. At the same time as it is rotating, the map tilt angle is slowly changing from an angle corresponding to a velocity of 400 m/sec to an angle corresponding to a velocity of 280 m/sec. The total change in tilt angle takes 10 azimuth sweeps or 2.5 min. An eleventh azimuth sweep is used to return the velocity program to its starting point. Figure 4 shows a sample output record for one complete azimuth-velocity search pattern. At the search rate used, any signal in the original recording will yield an output for at least three successive azimuth-velocity searches.

Each azimuth sweep takes 15 sec. At 12 data samples per second there are 180 data samples per azimuth sweep (360°). Ignoring all other factors this gives an azimuth resolution of 2°. In automatic search this resolution is seldom achieved. But the automatic search can be stopped and the mechanism moved by hand to any desired point in the program.

5. Amplitude Equalization

The original input data amplitude range covers over 60 db. Under "quiet" conditions the background may fall as low as 0.1 to 0.2 dyne cm^{-2}. Under "noisy" conditions the background can exceed several hundred dyne cm^{-2}. Since this is recorded as direct analog data on the magnetic tape, the tape's own dynamic range becomes the limiting factor. This has been set at 0.2 to 50 dyne cm^{-2}. To cover this wide range of data levels, automatic amplitude equalization or automatic gain controls were used.

The amplitude of each channel is independently and automatically adjusted to the same rms voltage. This is done by two stages of thermistor controlled feedback amplifiers. One stage is between the sampling readout and the tape loop delay. This stage can reduce a 60 db input amplitude range to a 20 db range. This eases the dynamic range requirement of the delay system. The other stage comes after the delay system, reducing the 20 db delay

output range to 0.5 db. As a result all input levels, from the equipment self noise level to tape saturation come out within 0.5 db of the same level. The time constant of the equalizer and the averaging time of the detector are both approximately 10 min, referred to the time scale of the original data.

6. Signal Detection

In an ideal situation the output would be zero at all search points except for the one representative of the signal. This would require that the noise present be completely incoherent at all times and the signal be of such a character as to be incoherent at all search points except that point of full coherence. This ideal situation cannot exist in a practical device since it would require as one prerequisite an infinite sample length. Since the sample length is finite and there are a limited number of inputs, there is also a real probability of correlation in the noise. The output of the correlator is useful, in spite of the nonideal operation, since noise correlations tend to occur at random, while the azimuth is searched. It is this repetitive output for signal that allows it to be identified in the presence of noise.

For the following analysis it is assumed that the map linkage is stopped at the point which introduces the ideal relative time displacements for signal correlation.

Let the correlator have n inputs I_i, each of which is the sum of signal S_i and noise N_i. These inputs are operated on by compressor circuits which equalize all inputs to the same rms level. Therefore the outputs of the compressors are $E_i=C[I_i/(\overline{I_i^2})^{1/2}]$. The channels are added in a resistive adder whose output is $E_A=[1/(n+2)]\Sigma E_i$, this adder being chosen for calibration convenience. The adder output may be detected by a square law rectifier, averaged, and displayed on a graphic recorder. The recorder deflection D is therefore another averaged quantity $D=\overline{E_A^2}$. Combining these several operations gives as a result

$$D=[C/(n+2)]^2\left[n+\sum_{i\neq j}\overline{(I_iI_j)}/(\overline{I_i^2})^{1/2}(\overline{I_j^2})^{1/2}\right].$$

The Pearson correlation coefficient r_{ij} is defined as

$$r_{ij}=\overline{I_iI_j}/(\overline{I_i^2})^{1/2}(\overline{I_j^2})^{1/2},$$

so that the recorder deflection can be written as

$$D=[C/(n+2)]^2\left(n+\sum_{i\neq j}r_{ij}\right).$$

An average correlation coefficient $\bar{r}$ can be defined by

$$\bar{r}=\left[\sum_{i\neq j}r_{ij}\right]/[n(n-1)]$$

resulting in $D=[C/(n+2)]^2[n+n(n-1)\bar{r}]$.

To establish a scale for the output recorder it is necessary to note that removal of all inputs but one results in a constant output of $D=C^2/9$. With $\bar{r}=0$, $D=C^2/[(n+2)^2/n]$; or for $n=4$, $D=C^2/9$ and for $n=5$, $D=C^2/9.8$. Thus, the one input case gives the same deflection as zero correlation for four inputs and is a close approximation for five inputs. The deflection for $\bar{r}=1$ is established by injecting the same signal into all inputs simultaneously. For operational use the constant term was suppressed so that the recorder scale would be direct reading in $\bar{r}$.

Returning to r_{ij} and substituting S_i+N_i for I_i gives

$$r_{ij}=\overline{(S_i+N_i)\,(S_j+N_j)}/[\overline{(S_i+N_i)^2}]^{1/2}[\overline{(S_j+N_j)^2}]^{1/2}$$

or, assuming that $\overline{S_iN_i}=\overline{S_iN_j}=\overline{N_iN_j}=0$,

$$r_{ij}=\overline{S_iS_j}/[(\overline{S_i^2}+\overline{N_i^2})(\overline{S_j^2}+\overline{N_j^2})]^{1/2}.$$

The signal-to-noise ratio R_i can be defined as $R_i^2=\overline{S_i^2}/\overline{N_i^2}$ and, if it is assumed that $S_i=S_j$, then $r_{ij}=R_iR_j/[(R_i^2+1)(R_j^2+1)]^{1/2}$. The correlator output is now seen to be a function only of the number of input channels and the signal-to-noise ratio at each input.

If all the input noise levels are approximately the same, then it is convenient to think of an average input signal-to-noise ratio R. The operating recorder output then can be taken as $D\propto R^2/(1+R^2)$ and it is this scale that is used in estimating input signal-to-noise ratio.

The original detector was an approximately square-law device. Although it was an excellent detector, its operating point and range were variable enough to be a maintenance problem. A simple full-wave rectifier has since been used with excellent results. Comparison tests have shown it to be approximately equivalent to the square-law device for detection. Both have detected signals at a signal-to-noise ratio of 1/4, $\bar{r}=1/17$. The linear detector has the disadvantage that the output indication is not calibratable in terms of signal-to-noise ratio as is the square-law detector.

7. Auxiliary Devices

The synchronizing pulse produced with each data sample has been used for three purposes. Originally it was used to generate a blanking pulse to eliminate the overlap region between sample ends. The data samples are taken continuously with the beginning of a sample immediately following the end of the preceeding sample. There is no gap or blank between samples. Thus, when the delay playback heads are displaced to give a relative delay, there is a short region when the leading head is reading the beginning of a sample and the trailing head is reading the end of a sample. This region of nonreal inputs was accordingly blanked from the detector's memory. Subsequent tests showed that the contribution from this region to the output was so small as to be unnoticeable; therefore, the blanking feature was eliminated.

The second use of the synchronizing pulse is in reading out the time pips. The sync-pulse generates a gate about 0.5 msec long. The time pulse reads out as a 0.14 msec pulse. As the storage tape moves through the sampler, the position of the time pulse will pass through the position of the gate. A coincidence circuit is used to compare the position of the time pulse with the gate. The two will show coincidence for about 36 samples or 3 sec. The output of the coincidence circuit throws a time marking pen on the output recorder. Thus, the recorder time track has a 3 sec mark every 5 min. These marks identify the data interval being processed.

The third use of the synchronizing pulse is a recent development. Using it to trigger a gated detector connected to the sampler output allows the creation of a graphic anolog replica of the input data in real time. Divorced from the correlator it forms a gated-readout device for low speed magnetic tape recordings. It is not the same as a flux sensitive readout but can perform essentially the same function.

Another use of the gated readout which has been suggested is in signal enhancement. Once a signal has been detected by the correlator the search mechanism can be stopped and set to the optimum azimuth and velocity. The storage tape can be backed up and rerun through the sampler. Now, if the gated readout is connected to the adder output, it will read out a graphic replica of the "best correlating fit." This improves the signal-to-ratio by $(n)^{1/2}$ over the original data channels. For our 5 channel system this amounts to 7 db. This is not a large increase but, having once identified the presence of a signal, it may allow a better study of the signal's character.

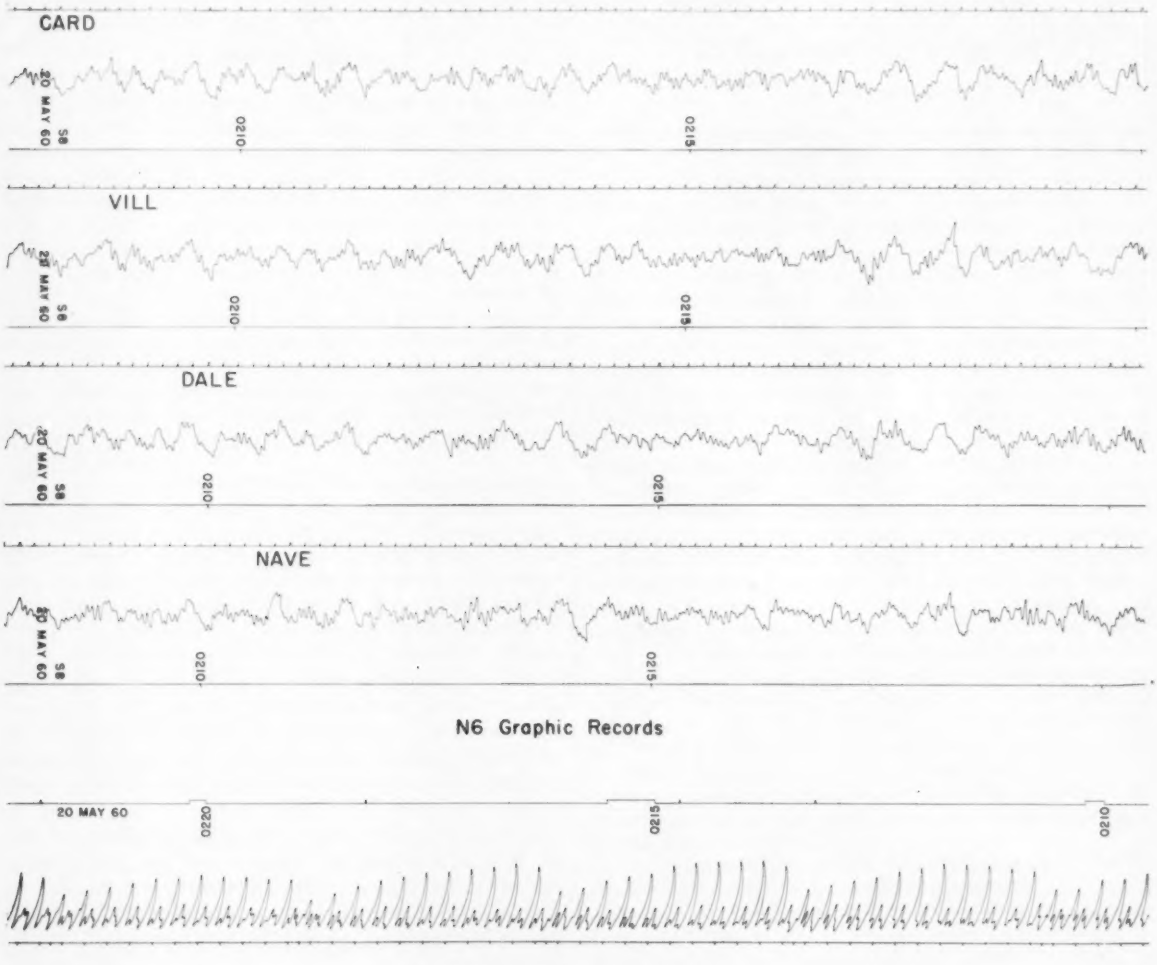

FIGURE 5. *Graphic records and correlator output for a tornado signal.*

As an example of signal detection by the correlator, figure 5 shows the graphic recordings and correlator output for the May 20, 1960 acoustic signal reported in "Intrasonic Disturbance in the Atmosphere," NBS Technical News Bulletin, December 1960.

(Paper 67C1–117)

The correlator exists as a functional device primarily due to the skill and efforts of the following persons. The basic concepts used in the device were originated by Daniel P. Johnson and the late Peter Chrzanowski. The device was designed and proven out chiefly by Harry Matheson, Irving Levine, and Henry Schmidt.

JOURNAL OF RESEARCH of the National Bureau of Standards—C. Engineering and Instrumentation
Vol. 67C, No. 1, January–March 1963

Elastic Constant—Porosity Relations for Polycrystalline Thoria

S. Spinner, F. P. Knudsen, and L. Stone

(October 23, 1962)

The relations between the elastic constants and porosity for about 300 thoria specimens have been determined. Both Young's and the shear modulus for each specimen were obtained by a dynamic resonance method. From these two moduli, Poisson's ratio was computed. The decrease in the elastic constants with increasing porosity was greater than would be expected from the theory. This greater decrease for the experimental values is attributed to the fact that the specimens do not conform to the idealized assumptions of the theory.

1. Introduction

Polycrystalline metals, which are formed by cooling from the molten state, ordinarily result in a material of essentially zero porosity. Consequently, metallurgists who are interested in the relation between microstructure and the macroscopic properties of such materials are generally concerned with the effect of the grains (size, shape, possible orientation) on these (macroscopic) properties. On the other hand, in materials which are formed by sintering—this includes some metals as well as ceramic materials—zero porosity is seldom achieved, so that ceramists studying the relation between microstructure and macroscopic properties of sintered materials must be concerned with the effect of porosity as well as granular structure on macroscopic properties.

The effect of porosity on the elastic properties has been the subject of considerable experimental [1,2,3] [1] and theoretical [4,5,6,7,8] investigation. The primary purpose of the present study is to present data on this relationship (between porosity and elastic constants) obtained from polycrystalline ThO_2 specimens. The reasons for the choice of ThO_2 specimens are twofold. In the first place, very little data of this type are available for ThO_2. In the second place, since ThO_2 is a cubic crystal, its thermal expansion is isotropic. Consequently, thermally induced intergranular stresses, such as may exist in Al_2O_3, for instance, are not present. It would appear, then, that the porosity—elastic constant relationship developed with ThO_2 would come closer to the "ideal" situation. It will be seen later, however, that other complicating factors affected the results to such a degree that this supposed advantage was effectively rendered of minor importance.

[1] Figures in brackets indicate the literature references at the end of this paper.

2. Experimental Procedure

2.1. Specimens

All the specimens used in this study were hydrostatically cold pressed and sintered at 1,750 °C for 17 hr. All the specimens were sintered in the same furnace at the same time. The specimens were placed in the center of the (large) furnace in such a manner as to minimize any possible temperature gradients from specimen to specimen. As a further precaution to insure uniform heat treatment, the various groups and subgroups of specimens (to be described) were interspersed in the furnace so that no group would tend to receive a different heat treatment from any other group. A range of porosities was obtained in each of three different groups of specimens in the following manner. In the first group, all the initial particle sizes were from 0 to 2 μ. The lowest porosity was obtained by using no filler, and increasingly higher porosities were obtained by using increasing amounts of filler in the cold pressing process. The filler burned out on firing. This group is designated as Group I. The second group, designated as Group II, was of 2 to 4 μ particle size, and the range of porosities was obtained in the same manner. The filler used in all cases consisted of 250–325 mesh unsulfonated styrene—divinyl benzene beads. In the third group, designated as Group III, no filler at all was used, the range of porosities being obtained by using increasingly larger particle sizes to form the specimens. It is seen that the lowest porosity specimens of Groups I and II (in which no filler was used) also comprise the lowest porosity specimens in Group III.

The range of porosities for each group could be divided into subgroups of the same nominal porosity. Because of the large total number of specimens measured, 293, it was more convenient and also facilitated clarity of presentation, to show the data in terms of these subgroups rather than in terms of individual specimens. In some cases, however, when

it was believed to be important, statistical analysis was performed on the basis of individual specimens rather than on the basis of subgroups.

The first three columns of table 1 give the specimen designation, number of specimens, and average porosity in each subgroup having the same nominal porosity. The fourth column gives the standard deviation of the porosity of each subgroup. The first two numbers of the specimen designation indicate the particle size and the third number indicates the nominal percentage by volume of filler used. (i.e., 0–2–6 means that the particle size was from 0 to 2 μ and 6 percent filler was used, 12–24–0 means that particle size was from 12 to 24 μ and no filler used).

It is also noted from the table that in Group III, the largest particle size (24 to 44μ) resulted in specimens of slightly (but not significantly) lower average porosity (26.08%) than those of the next smaller particle size (13–24μ) which gave specimens having an average porosity of 26.19 percent.

After firing, the specimens were ground to the shape of rectangular bars about $6\times\frac{1}{2}\times\frac{3}{4}$ in. The dimensions of each of the finished specimens[2] were uniform to 0.001 in.

Spectrochemical analysis on samples from representative subgroups showed the following impurities: —Al, about 0.01 percent, Si, <0.01 percent, Ni, about 0.005 percent, Mg, <0.005 percent, Fe, <0.001 percent, Sn, present in one sample (7–13–0–7), <0.005 percent. Elements looked for and the presence of which was questionable were Ag and Ca. Elements looked for and not detected were Au, B, Ba, Be, Bi, Co, Cr, Pb, Sb, Ti, V. There appeared to be no significant chemical differences between the different groups and subgroups of specimens. Also the purity of the starting powder, as measured on one group (0 to 2μ) was not significantly different from that of the finished specimens.

2.2. Method

The elastic moduli were determined by the dynamic resonance method previously described [9]. Resonance frequencies were determined to an accuracy of about 1 part in 4,000. For each specimen, the fundamental of four different resonance frequencies was determined. These were

(1) flexural, flatwise vibration
(2) flexural, edgewise vibration
(3) longitudinal
(4) torsional.

Young's modulus was computed independently from the first three types of vibration (Y_1, Y_2, Y_3, respectively) and the shear modulus was computed from the torsional mode. The equations for these computations have also been previously described [9]. The time involved in making these numerous and rather cumbersome calculations ($293\times4=1{,}172$ calculations), as well as most other analysis of the data, was considerably reduced by the use of an automatic computer.

The porosity, P, in volume fraction of pores, was obtained from the equation,

$$P=1-\frac{\rho_s}{\rho_0}$$

where ρ_0, the theoretical or zero porosity density, is taken as 10.0 g/cm.[3] [3] and ρ_s, the density of a particular specimen, was obtained from the mass, and volume, calculated from the dimensions.

[2] The starting ThO_2 powder was supplied by the Norton Co., Worcester, Mass.; the particle separation was done by Dr. S. C. Lyons of the Georgia Kaolin Co.; the cold pressing and sintering was done by Norton Co., and the grinding to the final dimensions was done at NBS.

[3] This value is based on the X-ray data of Lang and Knudsen [10], who measured ThO_2 from the same source as used here, obtaining 10.01 g/cm^3 and the A.S.T.M. value (also based on X-rays) of Swanson and Tatge [11] who give 9.991 g/cm^3 on high purity ThO_2.

TABLE 1. *Elastic constants and porosities of thoria specimens of this investigation*

	Specimens	Number n	Porosity	$\sigma(P)$ [a]	Young's modulus (flatwise) Y_1	$\sigma(Y_1)$ [a]	Shear modulus G	$\sigma(G)$ [a]	Poisson's [b] ratio μ	Young's modulus (edgewise) Y_2	$\sigma(Y_2)$ [a]	Young's modulus (Longitudinal) Y_3	$\sigma(Y_3)$ [a]
			%		*Kilobars*		*Kilobars*			*Kilobars*		*Kilobars*	
Group I	0- 2- 0	29	3.73	0.09	2296	7	894.1	2.3	0.284	2233	9	2296	7
	0- 2- 6	6	7.97	.06	1992	18	785.1	5.4	.269	1985	17	2004	19
	0- 2-12	5	13.74	.04	1520	94	620.7	26.3	.225	1543	84	1565	84
	0- 2-18	6	19.15	.20	1029	83	461.0	20.4	.112	1049	78	1073	78
	0- 2-24	3	23.91	.29	779.1	37	365.8	11.0	.065	798.3	39	818.2	35
	0- 2-30	2	33.40	.63	167.6	19	114.5	4.3	−.270	182.1	14	191.7	15
Group II	2- 4- 0	46	7.15	.53	2120	6	830.5	2.0	.276	2117	8	2127	7
	2- 4- 6	6	12.27	.12	1835	3	724.0	1.3	.267	1835	4	1841	4
	2- 4-12	5	16.43	.10	1604	17	638.4	3.1	.256	1609	11	1611	12
	2- 4-18	5	22.05	.48	1248	18	507.6	4.5	.229	1261	16	1257	11
	2- 4-24	6	28.50	.37	816.6	39	353.3	7.9	.156	829.4	36	827.9	35
	2- 4-30	6	33.36	.61	681.0	48	294.8	15.5	.155	692.7	53	691.1	44
	2- 4-36	6	39.44	.38	410.6	16	193.4	5.8	.062	428.3	17	429.5	15
Group III	4- 7- 0	39	17.27	.80	1565	8	622.6	2.6	.257	1577	7	1580	7
	7-13- 0	39	23.66	.33	1200	6	484.2	2.0	.239	1215	5	1213	20
	13-24- 0	40	26.19	.47	1029	9	417.4	3.0	.232	1038	7	1037	7
	24-44- 0	44	26.08	.23	985.9	8	401.8	2.7	.227	995.5	6	997.8	6

[a] Indicates standard deviation of value in column immediately to left.
[b] Computed from corresponding Y and G values from $\mu=Y/2G-1$.

3. Results

The complete data for the specimens are given in table 1. It seems desirable to clarify the following two points at the outset. The first concerns the procedure for obtaining the averages and standard deviations of the porosities and elastic moduli of each subgroup given in table 1. For the porosities, which constitute the independent variable, the standard deviation for a particular subgroup is merely a measure of the range of porosity for that subgroup, and a large value for the standard deviation implies no lack of accuracy in that variable. The average and standard deviation of the porosity of each subgroup, then, was computed directly in the conventional manner. On the other hand, the standard deviation of the associated elastic moduli, the dependent variable, should be a measure of the precision of the data. Consequently, one wishes to know, not the average and standard deviations of the directly determined values of moduli for a subgroup, but rather the average and standard deviation of the moduli that would be associated with the average value of the porosity of that subgroup. This corresponds geometrically to moving the directly determined point for each specimen along a line parallel to the overall porosity-modulus relation for all the specimens of a group until it meets the vertical line through the average porosity for the subgroup in which that specimen is included. This process is represented by the equation,

$$E_a = E_b \pm \Delta P(dE/dP)$$

where E represents the generalized elastic modulus (whether Young's modulus, Y, or shear modulus, G) and the subscripts, a and b, represent the adjusted and unadjusted values of that modulus. ΔP is the difference in porosity between the value for a particular specimen (of given E_b) and the average for the subgroup containing that specimen. The $+$ or $-$ sign in the equation depends upon whether E_b is at a higher or lower porosity than the average for the subgroup. Average and standard deviations of E_a were then obtained in the usual manner and are the ones given in table 1.

The values of dE/dP for the different subgroups used in the equation were obtained in two different ways depending upon whether the subgroups consisted of a small (six or less) or large (about 40) number of specimens.

In the subgroups containing a small number of specimens, where an insufficient number was available to establish a reliable slope for that subgroup, a second degree equation was fitted by least squares to the data representing the particular modulus-temperature relationship for all the individual specimens (not subgroups) comprising a group. dE/dP for each subgroup was then obtained in the conventional manner, by substituting the average value of porosity for that subgroup into the derivative of the related porosity-modulus equation. The adequacy of these second degree representations of the data will be demonstrated later.

For the larger subgroups, a sufficient number of specimens and a sufficient range of porosity was involved for a satisfactory slope to be computed on the basis of the specimens of each subgroup. A typical plot of such modulus-porosity relation is shown in figure 1. It can be seen from the figure that a linear least squares fit would give a reliable value of dE/dP for the data. Also, the standard deviation of the ordinate given by the computer along with the least squares equation gives the standard deviation of the elastic modulus directly.

This procedure for both large and small subgroups assumes that ΔP is linear over the range of any particular subgroup. This assumption is seen to be justified by figure 1 for a typical large subgroup and would certainly hold for the smaller subgroups having a smaller range of porosities.

The second point concerns the three independently computed values of Young's modulus. It is clear that if the equations for these computations are self-consistent, and the specimens conform to the basic assumptions of the equations, namely that they be homogeneous and macroscopically isotropic, then the values of Young's modulus from the three types of vibration (flatwise flexural, edgewise flexural and longitudinal) must agree within the accuracy of measurement of the relevant parameters (resonance frequency and dimensions). This agreement should be on the order of about 0.2 percent for the specimens of this investigation.

That this is clearly not the case here may be seen from table 2 which gives typical values of Young's modulus computed from these three types of vibration for individual specimens. Since previous work [12, 13] has shown that for materials which are more homogeneous than those used here, annealed glass and steel, the values of Young's modulus computed

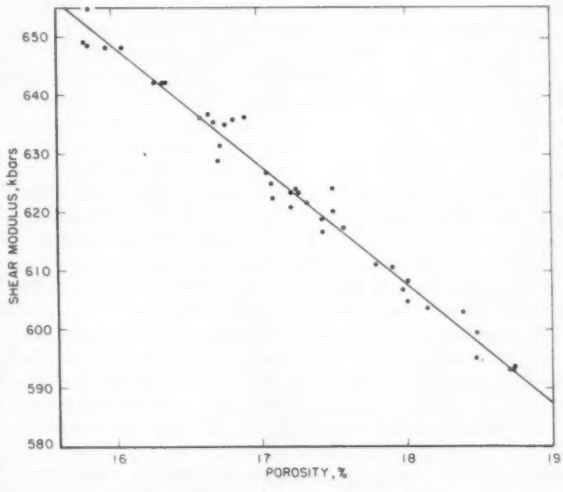

FIGURE 1. *Typical data of an elastic modulus versus porosity for a large subgroup 4–7–0.*

The line is drawn through the linear least square fit for the date, G = −2032P + 973

from these three types of vibration do agree to within the expected figure, one must conclude that it is the lack of uniformity of the specimens (due to nonuniform distribution of the pores throughout the specimens or some other cause) rather than inconsistency in the equations that is responsible for the lack of such agreement found here.

TABLE 2. *Typical data showing different values of Young's modulus obtained from three types of vibration*

Specimen	Young's modulus		
	Y_1	Y_2	Y_3
	Kilobars	*Kilobars*	*Kilobars*
2-4-6-1*	1834	1837	1842
2-4-6-2	1826	1825	1831
2-4-12-1	1634	1634	1640
2-4-12-2	1618	1620	1622
2-4-18-1	1225	1244	1242
2-4-18-2	1241	1248	1248
2-4-24-1	795	809	812
2-4-24-2	811	831	826
2-4-30-1	630	653	654
2-4-30-2	632	620	621
2-4-36-1	440	458	458
2-4-36-2	354	370	374

*First three digits indicate starting particle size and nominal porosity. Last digit indicates particular specimen.

This conclusion is strengthened by the following additional information. Almost all the specimens were cut laterally in half and reground for further experimentation after measurement. This work will be described in later publications. A small section was also removed from the middle for microscopic analysis. Y_1 and density for all the cut and reground specimens were obtained in the same manner as already described. Not only did the densities and Young's moduli (Y_1) of the two halved specimens not agree with each other but the averages of these values for the two halves often did not agree with those for the specimen from which they were formed. This disagreement was greater for the more porous specimens. In general, the best agreement in Y_1, Y_2, and Y_3 was associated with specimens having the lowest porosities. (This observation is in accordance with the idea that nonuniform distribution of pores is the main cause of lack of uniformity of the specimens, for where the overall porosity is low, any departure from uniformity should have less effect on the bulk specimen.) Lang [3] also found this lack of agreement in Y_1, Y_2, and Y_3, not only for ThO_2, but for sintered materials in general.

Thus, although the precision (the average difference between repeated measurements) of Y_1, Y_2, and Y_3 is usually better than 0.2 percent, nevertheless, the accuracy, using the agreement in these moduli as a criterion, is considerably less than this, being about 1 to 4 percent depending on the porosity; and for the shear modulus, G, though no such criterion is available, since G was computed on the basis of only one resonance frequency, the same figure for the accuracy probably applies inasmuch as the same factors are involved. The precision of the values of G is on the same order as for Y_1, Y_2, and Y_3.

This lack of agreement in Y_1, Y_2, and Y_3 to within the expected limit and associated lower accuracy for the elastic moduli must not be confused with the standard deviations of the elastic moduli of the subgroups given in table 1. These standard deviations are a measure of the scatter of the points for any given porosity and, although this scatter is undoubtedly a reflection of the nonuniformity of the specimens, it is not a direct measurement of this nonuniformity.

In fact, this scatter, represented by the standard deviations of the elastic moduli in table 1, may mask the real differences in Y_1, Y_2, and Y_3 for individual specimens by making it seem that these values of Young's modulus "agree" if the standard deviations are taken into account. Indeed, it is possible for Y_1, Y_2, and Y_3 to disagree by amounts greater than indicated here and still have standard deviations far less than those in table 1; and conversely, one may have much better agreement in Y_1, Y_2, and Y_3 and yet have standard deviations larger than those in table 1.

This disagreement in Y_1, Y_2, and Y_3 requires that some choice be made as to what value of Young's modulus shall be taken as representative of the specimens in subsequent analysis. One may choose some appropriate average or select that value which is believed most "accurate." Y_1 was finally chosen as the representative value mainly because it is usually the easiest one to obtain experimentally and seems the one most appropriate to compare with shortened specimens which were subsequently fabricated from the large ones, and for which the flatwise flexural resonance frequency is often the only one that can be detected. Further reference to Young's modulus, then, applies to Y_1 and the subscript will be dropped. It is recognized that this choice is somewhat arbitrary but it may be seen from table 1 that had some other value of Young's modulus been selected on some reasonable basis, then, although individual points might vary somewhat, the trends to be shown would not be affected.

The Young's modulus-porosity and shear modulus-porosity relations for all three groups are shown graphically in figures 2 and 3 respectively. Each point for this investigation represents a subgroup given in table 1. It is seen that for both Young's modulus and shear modulus, the data divides itself into two sets. The upper curve in each figure represents the data for Groups II and III while the lower curve is for Group I. The lines drawn through the points are the solutions of the second degree least squares equations for all the individual specimens (not subgroups) of a group. The equation for the upper line in figure 2 is for the specimens of Group II, and is given by

$$Y=3437P^2-6978P+2606.$$

The equation for the lower line in figure 2 is for the specimens of Group I, and is

$$Y=4036P^2-8762P+2621.$$

The shear modulus-porosity equations for Groups II and I, which form the upper and lower curves of figure 3, are respectively,

$$G=1155P^2-2540P+1008$$

and

$$G=693.3P^2-2885P+1001.$$

No similar equations for the specimens of Group III were developed because it can be seen from the figures that the equations developed for Group II give a satisfactory fit for Group III as well as the group on which they are based. It is also recalled that the original purpose of these equations was to obtain values of dE/dP for the small subgroups and all the subgroups of Group III contained a sufficient number of specimens for dE/dP to be determined on the basis of a linear least squares fit for each subgroup.

On the basis of these equations and the graphs, the "best estimate" of the values of Young's and shear modulus of ThO_2 at zero porosity, Y_0 and G_0, (the "theoretical" elastic moduli corresponding to the "theoretical" density) are given as

$$Y_0=2610 \text{ kilobars and } G_0=1006 \text{ kilobars.}$$

From these values of Y_0 and G_0, Poisson's ratio at zero porosity, μ_0 may be computed from the well-known equation for isotropic materials, $\mu=\frac{Y}{2G}-1$, to be 0.297. Values of Poisson's ratio at the different porosities for all subgroups may be similarly computed using the values of Y and G for that subgroup. These values are given in table 1 and are plotted in figure 4. The same division in the data previously observed for Young's and the shear modulus as a function of porosity is also seen to hold for Poisson's ratio, the upper curve being for Groups II and III and the lower curve for Group I. Apparently, whatever factor or factors are causing the specimens of Group I to show different Young's and shear modulus-porosity characteristics from those of Groups II and III also manifest themselves for Poisson's ratio as a function of porosity. The greater decrease in Poisson's ratio found for Group I is not a consequence of the fact that the decreases of Young's and the shear modulus for Group I are larger than for Groups II and III, but of the fact that the relative decrease in Young's modulus is greater than the relative decrease in the shear modulus by a larger amount for Group I than for Groups II and III.

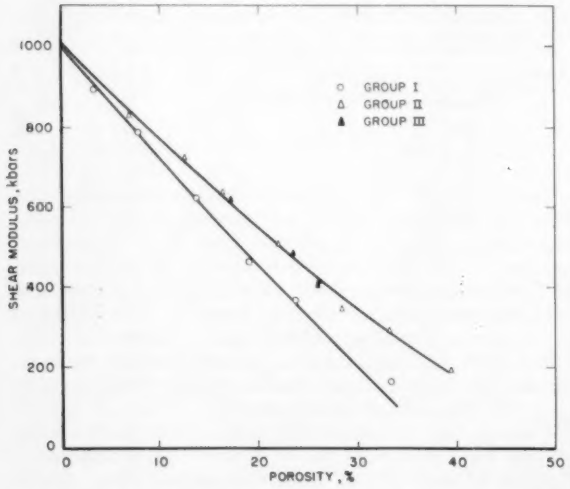

FIGURE 2. *Young's modulus versus porosity for all the ThO_2 specimens of this investigation.*
Each point represents a subgroup in table 1.

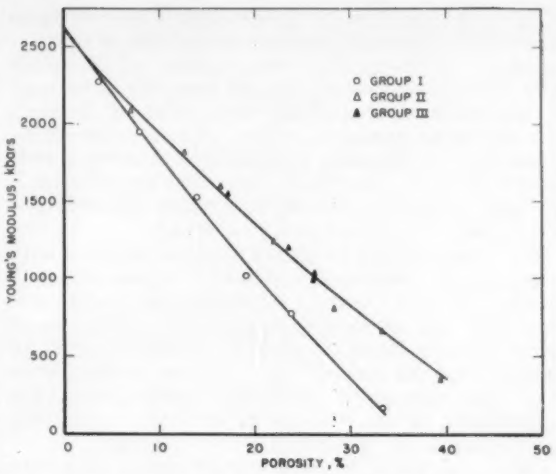

FIGURE 3. *Shear modulus versus porosity for all the ThO_2 of this investigation.*
Each point represents a subgroup in table 1.

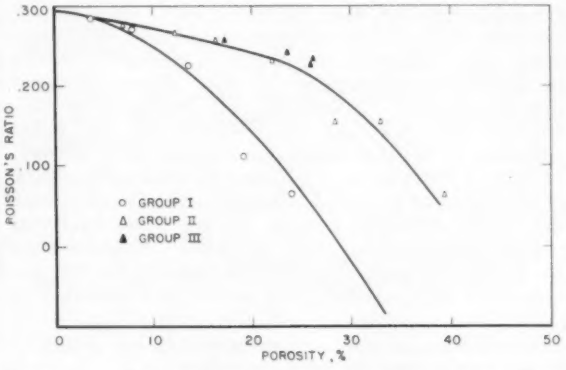

FIGURE 4. *Poisson's ratio versus porosity for all the ThO_2 specimens of this investigation.*

The larger scatter in the data for Poisson's ratio than for Young's and the shear modulus is not unexpected, since in the computation of Poisson's ratio from these two moduli, its accuracy is reduced by an order of magnitude from that of Young's and the shear modulus. Thus, the negative value of the 0–2–30 subgroup is probably not correct even though it is in line with the trend for Group I. (In this subgroup, μ computed from Y_2 or Y_3, is also negative but by a smaller amount.)

The tendency for Poisson's ratio to decrease with increasing porosity is in qualitative agreement with Hashin's [8] and Dewey's [4] theoretical predictions. However, the large decrease in the experimental values (above about 15 percent porosity) is not in accordance with theory. As indicated earlier, however, the specimens probably depart from the assumptions of the theories to such an extent that even a qualitative agreement is encouraging.

Using the value of Y_o for each group, one may plot Y_s/Y_o where Ys is the value of Y for a specimen at any given porosity, and compare the results of this investigation with those of other investigations on some other sintered materials, plotted on a similar basis. These are shown in figure 5.

Lang's data for Al_2O_3 is typical of a fairly large group for this material, as summarized recently by Knudsen [14]. It is interesting to note that Barducci and Cabarat's [1] results for fritted bronze are in such good agreement with those obtained here for Groups II and III. However, here too, although the decrease in modulus for all these materials is in qualitative agreement with theory, the large differences in Y_s/Y_o as a function of porosity for the different materials, as well as the two separate curves for different groups of the same material in this investigation, and for Al_2O_3, indicate that the specimens probably do not conform to the assumptions of the theory and render any attempt at quantitative comparison with the various theoretical formulations (at least, over an extended porosity range) a somewhat dubious procedure.

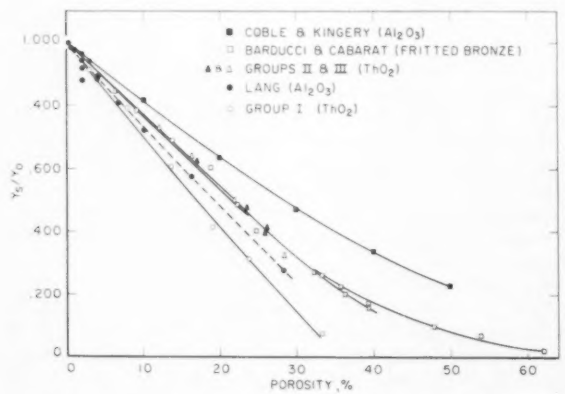

FIGURE 5. *Relative change in Young's modulus versus porosity for various experimental investigations with different sintered materials.*

Recognizing the limitations involved, it might still be instructive to compare some experimental and theoretical results on the basis of a linear approximation. For this purpose, we consider only the relative slopes at zero porosity, $-1/E_o\ (dE/dP)$, of the experimental and theoretical relationships. Such a comparison seems realistic since one of the major assumptions of the theories, namely no interaction between pores, is most likely to be realized experimentally as zero porosity is approached. Also, such a comparison should be of more than academic interest because it can be seen from figures 2, 3, and 5 that the porosity-modulus relationships depart only slightly from linearity up to about 15–20 percent porosity which encompasses the range of interest in most practical applications.

These comparisons are shown in tables 3 and 4. A description of the procedures for obtaining the numerical values in these tables is given in the appendix.

TABLE 3. *Comparison of some experimental and theoretical values of the relative decrease in the shear modulus,* $-1/G_o$ (dG/dP), *at zero porosity*

Experiment			Theory	
Source	Material		Dewey	Hashin, Mackenzie, Kerner
Group I	ThO_2	2.88	1.67	1.90
Groups II and III	do	2.52	1.67	1.92
Lang	Al_2O_3	2.80	1.67	1.97
Coble and Kingery	do	2.20	1.67	1.94

TABLE 4. *Comparison of some experimental and theoretical values of the relative decrease in Young's modulus with porosity,* $-1/Y_o$ (dY/dP), *at zero porosity*

Experiment			Theory	
Source	Material		Gatto	Hashin, Mackenzie, Kerner
Group I	ThO_2	3.34	2.32	2.00
Groups II and III	do	2.68	2.32	2.01
Cabarat and Barducci	Fritted bronze	2.68	2.32	----
Lang	Al_2O_3	3.07	2.32	2.00
Coble and Kingery	do	2.00	2.32	2.01

Inspection of the tables shows that generally, the relative decrease in elastic moduli found experimentally is greater than the theoretical equations predict. The only exception to this is for the data of Coble and Kingery [2] who obtained a decrease in Young's modulus slightly greater than Gatto's [3] theoretical value. Coble and Kingery [2] also noted that the experimental values of other investigators generally decreased more rapidly with porosity than the theoretical expectations.

Concerning the separation in the porosity-modulus curves for the specimens of Group I from those of Groups II and III, it does not appear that this is due to chemical differences, as has already been noted. Furthermore, the possibility of the effect of different methods of forming the pores, one from

filler and one from different starting particle sizes, must be discounted since the pores of the specimens of Groups II and III were formed in different ways while the pores of Group I were formed in the same way as for Group II.

It has already been suggested [15] that the greater decrease for the experimental values obtained by Lang [3] over the theoretical predictions was due to the fact that the pores were not spherical. Also, the possibility cannot be overlooked that factors other than porosity (such as grain size, grain orientation, nature of grain boundaries, etc.) may also affect the elastic moduli. If however, it is assumed that the more rapid decrease in moduli with increasing porosity for the experimental curves over the theoretical ones is due mainly to the nonsphericity of the pores, then it seems reasonable that the greater decreases in moduli for one set of experimental results over another will be associated with those groups of specimens having pores with greater departures from sphericity. Thus the pores of the specimens of Group I should depart from being spherical to a greater degree than those of Groups II and III. The pores of the specimens of Group I might also be more interconnected in some type of channelized structure than those of Groups II and III. A more definite answer to this problem will probably come from microscopic analysis which will be dealt with in a future publication.

It does seem that since the specimens of Groups II and III were prepared under a wide variety of conditions (more nearly resembling those in actual practice) while the specimens of Group I were prepared under rather specialized conditions, that the elastic constant-porosity curves for Groups II and III are typical for ThO_2 while the departure of the curves for Group I from this pattern is due to some unusual structural peculiarity in these specimens. Further evidence in support of this conclusion is that the curves for Groups II and III fall more or less in the middle of other experimental relations, and are in better general agreement with various values reported for ThO_2 [16, 17, 18, 29, 20].

4. Appendix

Experimental values for the relative decrease in Young's and the shear modulus with porosity at zero porosity were obtained in the following manner:

For the specimens of this investigation the values were obtained analytically from the appropriate second degree equations given in the text.

Corresponding values for Lang's results were similarly obtained from second degree equations fitted to his data by Wachtman [15].

The values for Coble and Kingery's results were obtained from a graphical fit to their original data using $Y_0=3861$ kilobars and $G_0=1517$ kilobars.

Barducci and Cabarat's value for $-1/Y_0\ (dY/dP)$ was taken as equal to that for Groups II and III because it can be seen from figure 3 that there is no significant difference in these two sets of data at low porosities.

Theoretical values of $-1/G_0\ (dG/dP)$ were obtained in the following manner:

Dewey's expression for the relation between G and P is,

$$G/G_0=1-\frac{5}{3}P,$$

then $-1/G_0\ (dG/dP)\cong 1.67$.

MacKenzie's corresponding equation is

$$G/G_0=1-5\left(\frac{3B_0+4G_0}{9B_0+8G_0}\right)P$$

so that $-1/G_0\ (dG/dP)=5\left(\frac{3B_0+4G_0}{9B_0+8G_0}\right)$.

Kerner's equation is,

$$G/G_0=1-5\left(\frac{3B+4G}{9B+8G}\right)P.$$

MacKenzie's and Kerner's equations are seen to differ only in that MacKenzie's equation depends upon B and G at zero porosity, whereas Kerner's equation depends upon B and G at porosity P. The two equations become identical as zero porosity is approached so that $-1/G_0\ (dG/dP)$ from either of these equations is the same.

Hashin's equation has been shown by Weil [21] to reduce to the following form as zero porosity is approached,

$$G/G_0=1-\left[\frac{15(1-\mu)}{7-5\mu}\right]P$$

and $-1/G_0(dG/dP)=\left[\frac{15(1-\mu)}{7-5\mu}\right]$.

From the well-known equations relating the elastic moduli for isotropic materials, it may also be shown that Hashin's equation is equal to Kerner's and MacKenzie's as zero porosity is approached. Consequently, the numerical values of $-1/G_0\ (dG/dP)$ from Hashin, MacKenzie and Kerner are the same.

Most theoretical formulations (this includes Hashin, MacKenzie, and Kerner) give relations for the bulk modulus as well as the shear modulus as a function of porosity whereas most experimental investigations (such as this one) are in terms of Young's modulus and the shear modulus as a function of porosity. However, from the equations mentioned in the preceding paragraph which are related in such a way that if any two elastic constants are known the others may be computed, one may deduce theoretical equations for Young's modulus as a function of porosity so that experimental and theoretical values of $-1/Y_0\ (dY/dP)$ may be compared.

The equations of MacKenzie, Kerner, and Hashin (Hashin's equation again, as simplified by Weil [21]

for the bulk modulus at very low porosities) are respectively,

$$B/B_0=1-\left(1+\frac{3B}{4G_0}\right)P,$$

$$B/B_0=1-\left(1+\frac{3B}{4G}\right)P$$

and

$$B/B_0=1-\frac{3(1-\mu)}{2(1-2\mu)}P.$$

As was the case for the shear modulus relationships, it is obvious that MacKenzie's and Kerner's equations become identical as zero porosity is approached; and it can also be shown that Hashin's equation becomes equivalent to these two as zero porosity is approached.

Following now the procedure just mentioned, one deduces the following equation for Young's modulus from Hashin's equation,

$$Y/Y_0=(1-P)\left[1-\frac{(1+\mu)}{6(7-5\mu)}(39-45\mu)P+\ldots\right]$$

(Higher order terms are negligible for small values of P.)

Then

$$1/Y_0(dY/dP)=(1-P)\left[-\frac{(1+\mu)}{6(7-5\mu)}(39-45\mu)\right]$$
$$-\left[1-\frac{(1+\mu)}{6(7-5\mu)}(39-45\mu)P\right]$$

and at zero porosity

$$-1/Y_0(dY/dP)=\left[\frac{(1+\mu)}{6(7-5\mu)}(39-45\mu)+1\right].$$

Since Kerner's, MacKenzie's, and Hashin's equations for the bulk modulus are equivalent as zero porosity is approached, the numerical values of $-1/Y_0(dY/dP)$ from the above equation would also apply to the other two.

The values of B_0 and μ_0 used in these equations were derived from the more directly determined values of Y_0 and G_0.

Dewey also gives an equation for Y as a function of P but this equation is not consistent with her relations for G and μ as a function of P, and is not used.

Gatto's value of $-1/Y_0(dY/dP)$ was derived from his graph which is the same as the one used by Coble and Kingery.

The authors are indebted to H. J. Foster and W. E. Tefft for valuable assistance in much of the mathematical development in the appendix.

5. References

[1] S. Barducci and R. Cabarat, Mesures statiques et dynamiques du module de Young de materiaux frittes, Rev. Met. **LI** [3] 149–153 (1954).

[2] R. L. Coble and W. D. Kingery, Effect of porosity on physical properties of sintered alumina, J. Am. Ceram. Soc. **39** [11] 377–385 (1956).

[3] S. M. Lang, Properties of high-temperature ceramics and and cermets—elasticity and density at room temperature, NBS Mono. No. 6 (1960), Ceram. Abstr., p. 201i (Aug. 1960).

[4] Jane M. Dewey, The elastic constants of materials loaded with non-rigid fillers, J. Appl. Phys. **18** [6] 578–581 (1947).

[5] J. K. Mackenzie, "The elastic constants of a solid containing spherical holes, Proc. Phys. Soc. (London) **63B** [1] 2–11 (1950).

[6] E. H. Kerner, The elastic and thermo-elastic properties of composite media, Proc. Phys. Soc. (London) **69B** 808–813 (1956b).

[7] F. Gatto, Influence of small cavities on velocity of sound in metals, Alluminio **19** [1] 19–26 (1956).

[8] Zvi Hashin, The elastic moduli of heterogeneous materials, J. Appl. Mechanics ASME Paper No. 61–WA–39, Presented at Ann. Mtg. of ASME (N.Y., Nov. 1961).

[9] S. Spinner and W. E. Tefft, A method for determining mechanical resonance frequencies and for calculating elastic moduli from these frequencies, Proc. ASTM **61** 1221–1238 (Phila., Pa., 1961).

[10] S. M. Lang and F. P. Knudsen, Some physical properties of high density thorium dioxide, J. Am. Ceram. Soc. **39** [12] 415–423 (1956).

[11] H. E. Swanson and Eleanor Tatge, Standard X-ray diffraction powder patterns, Vol. I, NBS Circ. No. 539 (June, 1953), Ceram. Abstr. 1956, p. 173c (Aug.).

[12] S. Spinner, Elastic moduli of glasses by a dynamic method, J. Am. Ceram. Soc. **37** [5] 229–234 (1954).

[13] S. Spinner, T. W. Reichard, and W. E. Tefft, A comparison of experimental and theoretical relations between Young's modulus and the flexural and longitudinal resonance frequencies of uniform bars, J. Research NBS **64A** 147 (1960).

[14] F. P. Knudsen, Effect of porosity on Young's modulus of alumina, J. Am. Ceram. Soc. **45** [2] 94–95 (1962).

[15] J. B. Wachtman, Jr., Mechanical and electrical relaxation of lattice imperfections in a fluorite structure, Doctorate Thesis submitted at University of Maryland (1961).

[16] I. E. Campbell (editor), High temperature technology, John Wiley & Sons, Inc., 48 (1956) (Personal communication to R. J. Runck from O. J. Whittemore, Jr.).

[17] J. B. Wachtman, Jr., W. E. Tefft, D. G. Lam, Jr., and C. S. Apstein, Exponential temperature dependence of Young's modulus for several oxides, Phys. Rev. **122** [6] 1754–1759 (Jan. 1961).

[18] James F. Wygant, Elastic and flow properties of dense, pure oxide refractories, J. Am. Ceram. Soc. **12** [34] 374–380 (1951).

[19] C. E. Curtis and J. R. Johnson, Properties of thorium oxide ceramics, J. Am. Ceram. Soc. **2** [40] 63–68 (1957).

[20] N. A. Weil (editor), Studies of the brittle behavior of behavior of ceramic materials, Armour Research Foundation Contract Report No. 8203–17, 82–90 (Feb. 1962).

(Paper 67C1–118)

JOURNAL OF RESEARCH of the National Bureau of Standards—C. Engineering and Instrumentation
Vol. 67C, No. 1, January–March 1963

An Oxygen Partial Pressure Warning Instrument*

Lewis Greenspan

(October 1, 1962)

An instrument has been developed to monitor partial pressure of oxygen in the respiratory air supply to an aviator. The requirements for the application are small size, light weight, capability for measuring oxygen partial pressure with an accuracy of ±5 millimeters Hg and response times less than 15 seconds. The instrument utilizes an oxygen absorber in one arm. Theory of the instrument is discussed and expressions for response and response time are derived. A prototype measuring 9⅝ × 7⅝ × 7¼ inches and weighing about 13 pounds is described and performance data given. The prototype measures oxygen partial pressure within ±4.5 millimeters Hg from sea level to 45,000 feet with response time from 5 to 124 seconds. It may be used either as a warning device or as an indication. Means for improving response time are discussed.

1. Introduction

In order to maintain the well-being and efficiency of personnel in high-altitude aircraft, it is necessary that they be supplied with air for breathing, having a near-sea-level equivalent oxygen content. Where cabin pressure is not maintained at or near sea level equivalent, mixtures of air and oxygen or pure oxygen are metered by oxygen regulators to the personnel. Though air containing insufficient oxygen may have a very deleterious effect on a person, he is often completely unaware of the deficiency. It is, therefore, necessary to have an instrument to warn flying personnel of the lack of sufficient oxygen in the breathing air supply, which may be detected by a measure of the oxygen partial pressure in either the inhaled or exhaled breath.

Such an instrument must be capable of measuring the partial pressure of oxygen in the range of 65 to 112 mm Hg (depending on whether the oxygen content of the exhaled or inhaled breath is to be measured) to within about 5 mm Hg. It must perform the measurement and indication operation within about 15 sec due to the short time of useful consciousness when breathing ambient air at high altitude.[1] In addition, such an instrument must be small and lightweight for use in aircraft.[2]

An oxygen-partial-pressure indicating and warning instrument, meeting most of these requirements, has been developed and constructed. It is based on the critical-flow pneumatic bridge described by W. A. Wildhack.[3] It is roughly analogous to a Wheatstone bridge where orifice or nozzle elements are the analogs of the resistance elements and a differential pressure gage is the analog of the galvanometer. When the bridge is balanced, that is, when the nozzle or orifice area ratios of the two arms are equal, the pressure difference across the bridge is zero. When a specific absorber is incorporated into one branch of a balanced bridge, between the upstream and downstream elements, pressure unbalance, approximately proportional to the partial pressure of the absorbed gas constituent, occurs and is measured by the differential pressure gage.

---

*This project was supported by the Bureau of Naval Weapons, Department of the Navy.

[1] Journal of Applied Physiology **1**, 490 (1949) Interval of useful consciousness at various altitudes, F. H. Hall.

[2] Whereas no currently available instrument was adequate for this purpose in June 1958, when this development was begun, electrochemical and polarigraphic type oxygen detectors which may meet requirements have since become available.

[3] Review of Scientific Instruments, Vol. **21**, No. 1, 25–30, January 1950; A versatile pneumatic instrument based on critical flow, W. A. Wildhack.

2. Theory

2.1. General Steady State Theory

Whenever critical flow exists in a nozzle or orifice, the upstream volumetric flow is independent of the pressure downstream of the nozzle or orifice. For a nozzle, the flow is given by

$$F_1 = CA\left(\frac{2n}{n+1}\right)^{1/2} r_c^{1/n}\left(\frac{P_1}{\rho_1}\right)^{1/2} \tag{1}$$

where

F_1=entrance volumetric flow
C=discharge coefficient
A=nozzle throat area
n=ratio of specific heats
r_c=ratio of throat to upstream pressure at critical flow=

$$\left(\frac{2}{n+1}\right)^{\frac{n}{n-1}}$$

P_1=entrance pressure
ρ_1=entrance gas density.

Equation (1) holds whenever the ratio of downstream pressure to upstream pressure is equal to or less than r_c. For dry air, under standard conditions, r_c=0.528. It varies only to a minor degree with temperatures and pressures here of interest.

Consider now a pneumatic bridge containing four critical flow elements (i.e., nozzles) and a specific gas absorber, shown schematically in figure 1. Let the critical flow elements have areas of A_{1x}, A_{2x}, A_{1y}, and A_{2y}. F_{1x}, F_{2x}, F_{1y}, and F_{2y} are the corresponding entrance volume flows to each of the elements. P_1 is the entrance pressure to the bridge. P_{2x} is the pressure in the x-branch (the absorber branch) between the upstream and downstream elements and P_{2y} is the pressure in the y-branch between the upstream and downstream elements.

With reference to the upstream nozzle of the y-branch of the bridge, eq (1) becomes

$$F_{1y} = CA_{1y}\left(\frac{2n}{n+1}\right)^{1/2} r_c^{1/n}\left(\frac{P_1}{\rho_{1y}}\right)^{1/2}. \tag{2}$$

Values of $\left(\frac{2n}{n+1}\right)^{1/2} r_c^{1/n}$ are tabulated in table 1 for several gases. In addition, values for each gas relative to nitrogen are also given. It can be seen from table 1 that for oxygen,

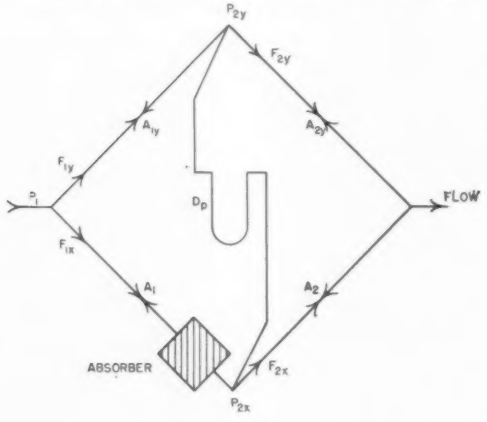

FIGURE 1. *Schematic bridge arrangement.*

nitrogen, and air (as well as other gases), these values are essentially the same. Therefore let Z be a constant defined as follows:

$$Z=C\left(\frac{2n}{n+1}\right)^{1/2} r_c^{1/n}. \tag{3}$$

TABLE 1. *Gas constants at 300 °K for discharge coefficients of unity*

Gas	n C_p/C_v	r_c $\left(\frac{2}{n+1}\right)^{\frac{n}{n-1}}$	Z $\left(\frac{2n}{n+1}\right)^{1/2} r_c^{1/n}$	Z/Z_{N_2}
Nitrogen	1.401	0.5281	0.6849	1.0000
Dry air	1.4017	.5280	.6850	1.0001
Oxygen	1.396	.5289	.6840	0.9987
Carbon dioxide	1.2878	.5480	.6651	.9711
Hydrogen	1.405	.5274	.6856	1.0010
Water vapor	1.333	.5399	.6732	0.9829

The mass flow through the upstream nozzle of the y-branch is given by

$$\rho_{1y}F_{1y}=A_{1y}ZKP_1\sqrt{\frac{M_1}{T_{1y}}} \tag{4}$$

where ρ_{1y} is the density of the entrance gas in the y-branch.

K is a constant defined by the equation $\rho_{1y}=\frac{K^2M_1P_1}{T_1}$

M_1 is the molecular weight of the entrance gas

T_{1y} is the absolute entrance temperature in the y-branch.

The mass flows through the other nozzles similarly are given by

$$\rho_{2y}F_{2y}=A_{2y}ZKP_{2y}\sqrt{\frac{M_{2y}}{T_{2y}}} \tag{5}$$

$$\rho_{1x}F_{1x}=A_{1x}ZKP_1\sqrt{\frac{M_{1x}}{T_{1x}}} \tag{6}$$

$$\rho_{2x}F_{2x}=A_{2x}ZKP_{2x}\sqrt{\frac{M_{2x}}{T_{2x}}}. \tag{7}$$

The mass flow of gas absorbed in the x-branch is given by

$$\rho_AF_{1x}=A_{1x}ZKP_A\frac{M_A}{\sqrt{M_{1x}T_{1x}}} \tag{8}$$

where ρA is the density of oxygen in the entrance gas, P_A is the partial pressure of the absorbed constituent and M_A its molecular weight.

Since there are no sources or sinks in the y-branch

$$\rho_{1y}F_{1y}=\rho_{2y}F_{2y} \tag{9}$$

and

$$M_{2y}=M_1=M_{1x}. \tag{10}$$

Solving for P_{2y} in (4) and (5) yields

$$P_{2y}=\frac{A_{1y}}{A_{2y}}P_1\sqrt{\frac{T_{2y}}{T_{1y}}}. \tag{11}$$

Since there is a sink in the x-branch

$$\rho_{2x}F_{2x}=\rho_{1x}F_{1x}-\rho_A F_{1x}. \tag{12}$$

Solving for P_{2x} in (6), (7), and (8) gives

$$P_{2x}=\frac{A_{1x}}{A_{2x}}P_1\sqrt{\frac{M_1T_{2x}}{M_{2x}T_{1x}}}-\frac{A_{1x}}{A_{2x}}P_A\frac{M_A}{\sqrt{M_1M_{2x}}}\sqrt{\frac{T_{2x}}{T_{1x}}}. \tag{13}$$

The differential pressure across the bridge, D_p, is P_{2y} less P_{2x} or

$$D_p=P_1\left(\frac{A_{1y}}{A_{2y}}\sqrt{\frac{T_{2y}}{T_{1y}}}-\frac{A_{1x}}{A_{2x}}\sqrt{\frac{M_1T_{2x}}{M_{2x}T_{1x}}}\right)+P_A\frac{A_{1x}}{A_{2x}}\frac{M_A}{\sqrt{M_1M_{2x}}}\sqrt{\frac{T_{2x}}{T_{1x}}}. \tag{14}$$

Assume that the bridge is balanced, that is, $\frac{A_{1y}}{A_{2y}}=\frac{A_{1x}}{A_{2x}}=\frac{A_1}{A_2}$, and that the temperatures are all equal, that is, $T_{1x}=T_{1y}=T_{2x}=T_{2y}=T$. Equation (14) then becomes

$$D_p=P_1\frac{A_1}{A_2}\left(1-\sqrt{\frac{M_1}{M_{2x}}}\right)+P_A\frac{A_1}{A_2}\frac{M_A}{\sqrt{M_1M_{2x}}}. \tag{15}$$

If the molecular weight of the gas is not significantly changed by the removal of the absorbed constituent, that is, where $M_1=M_{2x}$, eq (15) becomes

$$D_p=\frac{A_1}{A_2}P_A\frac{M_A}{M_1}. \tag{16}$$

Thus it follows that the pressure difference across the bridge is a direct linear function of the partial pressure of the absorbed constituent. For air at atmospheric conditions, this linear approximation, would lead to a 5 percent error.

2.2. Speed of Response

Adequate speed of response is an essential requirement in the application being considered. To estimate the response of the instrument to a step change in the input conditions, where the inlet pressure goes from P_0 to P_1 and the inlet partial pressure of the absorbed constituent goes from P_{A_0} to P_A, assume that the entire bridge is maintained at constant temperature so that $T_{1y}=T_{2y}=T_{1x}=T_{2x}=T$. The mass of gas between the two nozzles in the nonabsorber branch of the bridge (the y branch) is $\rho_{2y}V_y$, where V_y is the total gaseous volume of the y branch between the inlet and outlet nozzles. The rate of change of mass is given by

$$V_y\frac{d\rho_{2y}}{dt}=\rho_{1y}F_{1y}-\rho_{2y}F_{2y}. \tag{17}$$

Substituting (4) and (5) into (17), and, integrating and evaluating constants, we obtain

$$P_{2y}=\frac{A_{1y}}{A_{2y}}\left[P_0e^{-\frac{A_{1y}Z\sqrt{Tt}}{V_yK\sqrt{M_{1y}}}}+\sqrt{\frac{M_1}{M_{2y}}}P_1\left(1-e^{-\frac{A_{1y}Z\sqrt{Tt}}{V_yK\sqrt{M_{1y}}}}\right)\right]. \tag{18}$$

Now in the y-branch, the major volume, the ballast volume, is in a side branch not directly in the flow path from the upstream to downstream nozzle. This actual flow path is very

small (of the order of 2cm³ in volume). Therefore, except for slight diffusion from the ballast volume, the gas composition flowing from the outlet nozzle is the same as the gas composition flowing into the inlet nozzle and it is assumed that $M_{2y}=M_1$. Equation (18) therefore becomes

$$P_{2y}=\frac{A_{1y}}{A_{2y}}\left[P_0 e^{-\frac{t}{C_1}}+P_1\left(1-e^{-\frac{t}{C_1}}\right)\right] \tag{19}$$

where

$$\frac{1}{C_1}=\frac{A_{2y}Z\sqrt{T}}{V_y K\sqrt{M_1}}.$$

In the x-branch (absorber branch) the flow is through a packed absorber which has the effect of providing essentially a nonturbulent and nonmixing flow. When the composition of the inlet gas changes, a boundary is formed in the absorber container between downstream gas of the old composition and upstream gas of the new composition. This boundary travels down the absorber tube until it reaches active absorber, at which point the oxygen begins to be removed. The time ω required for the boundary to travel from the absorber container inlet to the active absorber is defined by the following expression.

$$\int_0^{\omega}\frac{P_{2x}}{P_1}\,dt=\frac{\omega F_{1x}}{V_A U} \tag{20}$$

where V_A is the volume of the voids in the absorber container and U is the ratio of consumed absorber to total absorber. Equation (20) may be also expressed as

$$\omega=\frac{V_A U}{F_{1x}}\overline{\frac{P_{2x}}{P_1}} \tag{21}$$

where $\overline{\frac{P_{2x}}{P_1}}$ is the average value of $\frac{P_{2x}}{P_1}$ per unit time during ω. Assuming no pressure drop through the absorber, the rate of change of mass in the x-branch is given by

$$V_x\frac{d\rho_{2x}}{dt}=\rho_1 F_{1x}-\rho_{A_2}F_{1x}\frac{P_1}{P_{2x}}-\rho_{2x}F_{2x} \tag{22}$$

where ρA_2 is the density of oxygen in the x-branch just upstream of the active absorber. For $0\leqq t\leqq\omega$, we have

$$\rho_{A_2}=\frac{P_{A_0}}{P_0}P_{2x}\frac{M_A}{T}K^2 \tag{23}$$

and for $\omega\leqq t\leqq\infty$, we have

$$\rho_{A_2}=\frac{P_A}{P_1}P_{2x}\frac{M_A}{T}K^2. \tag{24}$$

For $t\leqq\omega$, eq (22) becomes,

$$V_x=\frac{d\rho_{2x}}{dt}=A_{1x}ZK\sqrt{\frac{M_1}{T}}P_1-A_{1x}ZK\frac{M_A}{\sqrt{M_1T}}\frac{P_{A_0}}{P_0}P_1-A_{2x}ZK\sqrt{\frac{M_{2x}}{T}}P_{2x}. \tag{25}$$

$$\frac{dP_{2x}}{dt}=\frac{A_{1x}Z\sqrt{T}\sqrt{M_1}P_1-A_{1x}Z\sqrt{T}\frac{M_A}{\sqrt{M_1}}\frac{P_{A_0}}{P_0}P_1-A_{2x}Z\sqrt{T}\sqrt{M_{2x}}P_{2x}}{V_xKM_{2x}} \tag{26}$$

Integrating and evaluating constants, we obtain,

$$P_{2x}=\frac{A_{1x}}{A_{2x}}\left[\left(P_0\sqrt{\frac{M_0}{M_{2x}}}-P_{A_0}\frac{M_A}{\sqrt{M_0M_{2x}}}\right)e^{-\frac{t}{C_2}}+\left(P_1\sqrt{\frac{M_1}{M_{2x}}}-\frac{P_{A_0}}{P_0}P_1\frac{M_A}{\sqrt{M_1M_{2x}}}\right)\left(1-e^{-\frac{t}{C_2}}\right)\right] \tag{27}$$

where

$$\frac{1}{C_2}=\frac{A_{2x}Z\sqrt{T}}{V_xK\sqrt{M_{2x}}}.$$

Equation (27) depicts the pressure in the absorber branch of the bridge subsequent to discrete changes in inlet gas conditions up to the time ω. For $t\geq\omega$, eq (22) becomes

$$V_x\frac{d\rho_{2x}}{dt}=A_{1x}ZK\sqrt{\frac{M_1}{T}}P_1-A_{1x}ZK\frac{M_A}{\sqrt{M_1T}}P_1-A_{2x}ZK\sqrt{\frac{M_{2x}}{T}}P_{2x}. \tag{28}$$

$$\frac{dP_{2x}}{dt}=\frac{A_{1x}Z\sqrt{T}\sqrt{M_1}P_1-A_{1x}Z\sqrt{T}\frac{M_A}{\sqrt{M_1}}P_A-A_{2x}Z\sqrt{T}\sqrt{M_{2x}}P_{2x}}{V_xKM_{2x}} \tag{29}$$

Integrating and evaluating constants, we obtain,

$$\begin{aligned}P_{2x}=&\frac{A_{1x}}{A_{2x}}\left(P_0\sqrt{\frac{M_0}{M_{2x}}}-P_{A_0}\frac{M_A}{\sqrt{M_0M_{2x}}}\right)e^{-\frac{t}{C_1}}\\&+\frac{A_{1x}}{A_{2x}}\left(P_1\sqrt{\frac{M_1}{M_{2x}}}-\frac{P_{A_0}}{P_0}P_1\frac{M_A}{\sqrt{M_1M_{2x}}}\right)\left(1-e^{-\frac{t}{C_1}}\right)\\&+\frac{A_{1x}}{A_{2x}}\left(\frac{P_{A_0}}{P_0}P_1-P_A\right)\frac{M_A}{\sqrt{M_1M_{2x}}}\left(1-e^{-\frac{(t-\omega)}{C_1}}\right).\end{aligned} \tag{30}$$

Equation (30) depicts the pressure in the absorber branch of the bridge for periods greater than ω following a discrete change in inlet gas conditions. For a balanced bridge $\left(\frac{A_{1x}}{A_{2x}}=\frac{A_{1y}}{A_{2y}}=\frac{A_1}{A_2}\right)$, the differential pressure across the bridge, D_p, is given by

$$\begin{aligned}D_p=\frac{A_1}{A_2}\Bigg[&P_0e^{-\frac{t}{C_1}}-\left(P_0\sqrt{\frac{M_0}{M_{2x}}}-P_{A_0}\frac{M_A}{\sqrt{M_0M_{2x}}}\right)e^{-\frac{t}{C_1}}\\&+P_1\left(1-e^{-\frac{t}{C_1}}\right)-P_1\left(\sqrt{\frac{M_1}{M_{2x}}}-\frac{P_{A_0}}{P_0}\frac{M_A}{\sqrt{M_1M_{2x}}}\right)\left(1-e^{-\frac{t}{C_1}}\right)\Bigg],\end{aligned} \tag{31}$$

for $t\leq\omega$, and by

$$\begin{aligned}D_p=\frac{A_1}{A_2}\Bigg[&P_0e^{-\frac{t}{C_1}}-\left(P_0\sqrt{\frac{M_0}{M_{2x}}}-P_{A_0}\frac{M_A}{\sqrt{M_0M_{2x}}}\right)e^{-\frac{t}{C_1}}+P_1\left(1-e^{-\frac{t}{C_1}}\right)\\&-P_1\left(\sqrt{\frac{M_1}{M_{2x}}}-\frac{P_{A_0}}{P_0}\frac{M_A}{\sqrt{M_1M_{2x}}}\right)\left(1-e^{-\frac{t}{C_1}}\right)-\left(\frac{P_{A_0}}{P_0}P_1-P_A\right)\frac{M_A}{\sqrt{M_1M_{2x}}}\left(1-e^{-\frac{(t-\omega)}{C_1}}\right)\Bigg]\end{aligned} \tag{32}$$

for $t\geq\omega$.

It is apparent from (31) and (32) that if $\frac{A_{2y}}{V_yM_1}=\frac{A_{2x}}{V_xM_{2x}}=\frac{A_2}{VM}$, the response of the instrument is exponential. Though the volume V_y cannot be made exactly equal to $V_x\frac{M_{2x}}{M_1}\frac{A_{2y}}{A_{2x}}$, because M_1 is not a constant, it is made approximately so and the expression for the bridge response to a discrete change in inlet gas conditions for $t\leq\omega$ is approximately given by

$$\begin{aligned}D_p=\frac{A_1}{A_2}\Bigg[&P_0\left(1-\sqrt{\frac{M_0}{M_{2x}}}\right)+P_{A_0}\frac{M_A}{\sqrt{M_0M_{2x}}}\Bigg]e^{-\frac{t}{C}}+\frac{A_1}{A_2}\Bigg[P_1\left(1-\sqrt{\frac{M_1}{M_{2x}}}\right)\\&+P_A\frac{M_A}{\sqrt{M_1M_{2x}}}\Bigg]\left(1-e^{-\frac{t}{C}}\right)+\frac{A_1}{A_2}\frac{M_A}{\sqrt{M_1M_{2x}}}\left(\frac{P_{A_0}}{P_0}P_1-P_A\right)\left(1-e^{-\frac{t}{C}}\right);\end{aligned} \tag{33}$$

where $\frac{1}{C}=\frac{A_2 Z\sqrt{T}}{VK\sqrt{M}}$ and for $t \gtrless \omega$,

$$D_p=\frac{A_1}{A_2}e^{-\frac{\omega}{C}}\left[P_0\left(1-\sqrt{\frac{M_0}{M_{2x}}}\right)+P_{A_0}\frac{M_A}{\sqrt{M_0 M_{2x}}}\right]e^{-\frac{(t-\omega)}{C}}$$
$$-\frac{A_1}{A_2}e^{-\frac{\omega}{C}}\left[P_1\left(1-\sqrt{\frac{M_1}{M_{2x}}}\right)+P_A\frac{M_A}{\sqrt{M_1 M_{2x}}}\right]e^{-\frac{(t-\omega)}{C}}+\frac{A_1}{A_2}\left[P_1\left(1-\sqrt{\frac{M_1}{M_{2x}}}\right)\right.$$
$$\left.+P_A\frac{M_A}{\sqrt{M_1 M_{2x}}}\right]-\frac{A_1}{A_2}\left(1-e^{-\frac{\omega}{C}}\right)\left(P_A-\frac{P_{A_0}}{P_0}P_1\right)\frac{M_A}{\sqrt{M_1 M_{2x}}}e^{-\frac{(t-\omega)}{C}}. \quad (34)$$

Substituting

$$\frac{A_1}{A_2}\left[P_0\left(1-\sqrt{\frac{M_0}{M_{2x}}}\right)+P_{A_0}\frac{M_A}{\sqrt{M_1 M_{2x}}}\right]=D_{p_0} \quad (35)$$

and

$$\frac{A_1}{A_2}\left[P_1\left(1-\sqrt{\frac{M_1}{M_{2x}}}\right)+P_A\frac{M_A}{\sqrt{M_1 M_{2x}}}\right]=D_{p_1} \quad (36)$$

into eqs (33) and (34), where D_{p_0} and D_{p_1} are the steady-state bridge indications corresponding to the initial and final inlet conditions, respectively, we have

$$D_p=D_{p_1}+\frac{A_1}{A_2}\frac{M_A}{\sqrt{M_1 M_{2x}}}\left(\frac{P_{A_0}}{P_0}P_1-P_A\right)+\left[D_{p_0}-D_{p_1}-\frac{A_1}{A_2}\frac{M_A}{\sqrt{M_1 M_{2x}}}\left(\frac{P_{A_0}}{P_0}P_1-P_A\right)\right]e^{-\frac{t}{C}} \quad (37)$$

where $t \lesssim \omega$. For $t \gtrless \omega$, we have

$$D_p=D_{p_1}+\left[D_{p_0}-D_{p_1}+\left(e^{-\frac{\omega}{C}}-1\right)\frac{A_1}{A_2}\frac{M_A}{\sqrt{M_1 M_{2x}}}\left(\frac{P_{A_0}}{P_0}P_1-P_A\right)\right]e^{-\frac{t}{C}}. \quad (38)$$

Substituting the indication at which a warning is achieved, D_{pw} for D_p, in (37) and (38), we may solve for the time necessary to achieve a warning, t_w.

$0 \lesssim t_w \lesssim \omega$

$$t_w=-C\ln\frac{D_{p_w}-D_{p1}-\frac{A_1}{A_2}\frac{M_A}{\sqrt{M_1 M_{2x}}}\left(\frac{P_{A_0}}{P_0}P_1-P_A\right)}{D_{p_0}-D_{p_1}-\frac{A_1}{A_2}\frac{M_A}{\sqrt{M_1 M_{2x}}}\left(\frac{P_{A_0}}{P_0}P_1-P_A\right)} \quad (39)$$

$\omega \lesssim t_w \lesssim \infty$

$$t_w=-C\ln\frac{D_{p_w}-D_{p_1}}{D_{p_0}-D_{p_1}+\left(e^{-\frac{\omega}{C}}-1\right)\frac{A_1}{A_2}\frac{M_A}{\sqrt{M_1 M_{2x}}}\left(\frac{P_{A_0}}{P_0}P_1-P_A\right)}. \quad (40)$$

A special case of (39) and (40) is obtained when either $\frac{P_{A_0}}{P_0}=\frac{P_A}{P_1}$ (the percentage of oxygen remains constant) or when $\omega=0$. In these cases we have

$0 \lesssim t_w \lesssim \infty$

$$t_w=-C\ln\frac{D_{p_w}-D_{p_1}}{D_{p_0}-D_{p_1}}. \quad (41)$$

The time constant C of the instrument constructed was approximately 119 sec. Based on an assumption that one half of the volume of the absorber container remained void after filling with absorber, it is estimated that ω could vary from 0 to 47 sec under steady inlet

pressure conditions. Under these circumstances the time to warn was excessively large. A number of improvements could be made to reduce the time necessary to achieve a warning.

One method of reducing t_w is to reduce the time constant C. Better packing of the absorber in the absorber container would reduce V, but not to any appreciable extent since the volume of the pressure switch is also involved in V. Increasing A_2 or reducing the volume of absorber container would reduce the allowable operating time between refills of fresh absorber. Some improvement in C may be achieved by better packing of absorber or by obtaining a pressure switch with a smaller internal volume, but to a great extent it is determined by the operating time desired between absorber refills.

Another method of reducing t_w is to reduce ω. This is likewise influenced by the desired operating time between absorber refills but more complete filling of the absorber container has a greater influence on ω than on the time constant C, because the internal volume of the pressure switch is not involved in the determination of ω.

Another method of improving ω is to reverse the flow through the absorber container after one half of the normal operating time between absorber refills had expired. This would have the effect of halving the maximum value of ω. Another method would be to have the inlet tube in the absorber container advance through the absorber during operation at a rate greater than the rate of absorber consumption. This would have the effect of essentially restricting ω to the value of 0.

Another method of reducing t_w would be to restrict the maximum value of D_{p_0} to a value only slightly greater than D_{p_w}. Various methods of restricting D_{p_0} may be used. One method was used in this instrument and demonstrated its feasibility though it did not reduce t_w to acceptable limits in all cases.

The method of controlling D_{p_0} in this instrument was to close off the inlet to the bridge by means of a solenoid valve whenever D_p exceeded some value D_{p_A} and to reopen the solenoid valve whenever D_p was less than some preset value D_{p_B}. Both D_{p_A} and D_{p_B} were greater than D_{p_w}. A second microswitch located within the pressure switch and set just above the warning indication microswitch, was used to actuate the solenoid valve. Closing or opening the solenoid valve, while inlet conditions are steady, does not change the molecular weight of the inlet gas or the percent of oxygen in the inlet gas. Therefore, D_{p_A} is given by

$$D_{p_A}=\frac{D_{p_A}}{D_{p_0}}\frac{A_1}{A_2}P_0\left(1-\sqrt{\frac{M_0}{M_{2r}}}+\frac{P_{A_0}}{P_0}\frac{M_A}{\sqrt{M_0M_{2r}}}\right). \tag{42}$$

Since the only initial conditions appearing in (39), (40), or (41) are D_{p_0} and $\frac{P_{A_0}}{P_0}$, D_{p_A} or D_{p_B} may be substituted directly for D_{p_0} since $\frac{P_{A0}}{P_0}$ is not changed.

An estimate of the effect on the time to warn created by this method may be made for specific conditions. Assume that $D_{p_A}=D_{p_B}$, and that $D_{p_w}=43.8$ mm Hg which corresponds to an oxygen partial pressure of 110 mm Hg at 35,000 ft. If we switch from O_2 to air at 35,000 ft we have the following time to warn

	Time to warn in sec with $\omega=0$	Time to warn in sec with $\omega=59.5$
No solenoid modification	78. 2	102
$D_{p_A}=53.8$	35. 9	68. 6
$D_{p_A}=45.0$	4. 7	13. 9

Since D_{p_A} is not equal to D_{p_B}, there is a period of time during which the solenoid valve is closed, during which time, the instrument is incapable of sensing changes in inlet conditions.

Therefore to the above estimated times would have to be added some fraction of the time that the solenoid valve remained closed. For this system to operate optimally, it is necessary for D_{p_A} and D_{p_B} to be very near each other and only slightly larger than D_{p_w}. The limits to which this system may be pushed depend primarily on the sensitivity of the pressure switch available.

3. Description of Instrument

Figure 2 shows a schematic diagram of the pneumatic system of the instrument constructed to give a warning whenever the inlet partial pressure of oxygen decreases below a predetermined value.

Test gas, the oxygen partial pressure of which is to be determined, enters the inlet (1). About half of the flow goes through the bypass orifice (2) directly to the main valve (3) and on to the vacuum pump (4). The rest of the test gas goes through the solenoid valve, (5), through a filter (6) and into the inlet of the orifice block (7). In the orifice block, the gas again splits into two roughly equal streams, one of which traverses the y-branch while the other traverses the x-branch of the bridge.

The y-branch flow passes through the y-branch inlet orifice (8) and out of the orifice block. From there it goes to a ballast volume (9), and then to one side of a differential pressure switch (10), to a self-sealing pressure tap (11) and back into the orifice block. It then passes through the y-branch outlet orifice (12) and, joining the flow from the x-branch, flows from the outlet of the orifice block, is met and augmented by the bypass flow and discharges through the main valve (3) into the vacuum pump. The x-branch flow goes through the x-branch inlet orifice (13), out of the orifice block, through the absorber container (14) to the other side of the differential pressure switch (10) and to a self-sealing pressure tap (15) and back into the orifice block where it traverses the x-branch outlet orifice (16) and then merges with the y-branch flow and proceeds as previously described.

The vacuum pump induces a flow through the orifice block containing the four orifices which make up the pneumatic bridge. The filter is used upstream of the orifice block to maintain orifice cleanliness. The differential pressure switch across the bridge senses the bridge indication and initiates the warning. The ballast volume compensates for the absorber bolume so that $\frac{V_y}{A_{2y}}=\frac{V_x}{A_{2x}}$. The self-sealing pressure taps allow introduction of a differential pressure gage for reading directly the differential bridge pressure.

In order to minimize the warning time, the maximum instrument indication is kept near the indication necessary to cause a warning. This is accomplished by stopping the flow to the inlet of the bridge by means of the solenoid valve whenever the differential pressure across the bridge exceeds the warning pressure by some fixed amount. The continuing flow from the bridge causes a reduction in the inlet pressure as well as the inlet oxygen partial pressure, thereby decreasing the differential pressure across the bridge until the solenoid valve reopens. The action of the solenoid valve is controlled by the differential pressure switch through a microswitch that is set to operate at a pressure just slightly above the warning pressure. The bypass orifice maintains a continuous flow of test gas, regardless of on-off position of the solenoid valve, directly to the vacuum pump.

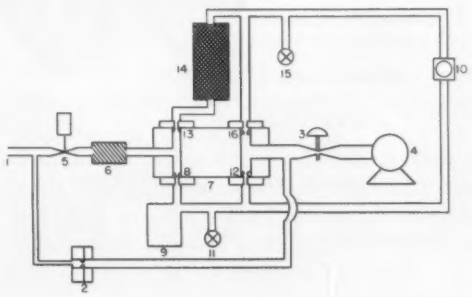

FIGURE 2. *Schematic diagram of model 2.*
1=inlet; 2=by-pass orifice; 3=main valve; 4=vacuum pump; 5=solenoid valve; 6=filter; 7=orifice block; 8=y-branch inlet orifice; 9=ballast volume; 10=pressure switch; 11=self-sealing pressure tap; 12=y-branch outlet orifice; 13=x-branch inlet orifice; 14=absorber container; 15=self-sealing pressure tap; 16=x-branch outlet orifice.

Figure 3 is a front view of the actual instrument, without the absorber container connected and figure 4 is a view of an assembled and disassembled absorber container.

The instrument as constructed weighs 11¾ lb, exclusive of the absorber or ballast volumes. The filled absorber container weighs between 1½ and 1⅝ lb of which 1.15 lb is the weight of the empty container. Over 5 lb of the weight of the instrument is contributed by the vacuum pump and motor. The major dimensions of the instrument are 9⅝ in. long, 7⅛ in. deep and 7⅝ in. high.

Orifices are used in lieu of the nozzles since orifice flow measurements indicated that these orifices had nozzlelike critical flow characteristics. The outlet orifices were made by drilling a hole in 0.008 in. thick phosphor bronze blanks with a 0.006 in. drill. The inlet orifices were fabricated in like manner with a 0.004 in. drill and the diameter of the y-branch inlet orifice was enlarged by etching in nitric acid until the desired $\frac{A_{1y}}{A_{2y}}$ ratio was obtained. With these orifices, the y-branch flow was approximately 74 cm³/min and the x-branch was approximately 62 cm³/min. The orifice area ratios for both branches $\frac{A_1}{A_2}$ are approximately 0.377.

The orifice block is made of aluminum and measures roughly 2½ in. by ⅞ in. by ¾ in. The block is of one piece construction with two orifice recesses on each of the two largest faces. At the ends (inlet and outlet) are machined fittings to take rigid tubing. There is an aluminum fitting for each of the recesses which is attached to the face with three allen-head screws. O-rings provide a leak-tight seal between fitting and orifice disk and between the latter and the block. The heat capacity and high conductivity of the block tends to maintain the orifices at a uniform temperature.

The absorber container is made of three interchangeable elements, an aluminum tube and two aluminum end caps. At each end, the inner wall is slightly tapered. Each cap is constructed to slip into an end of the tube and is held in place by three set screws which extend

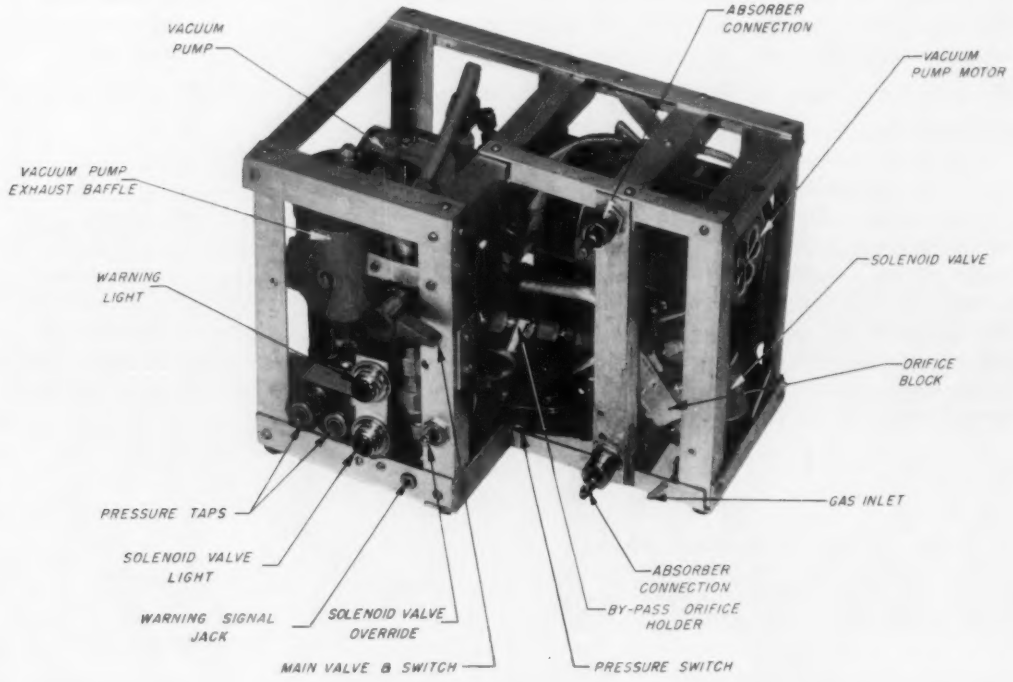

FIGURE 3. *Front view.*

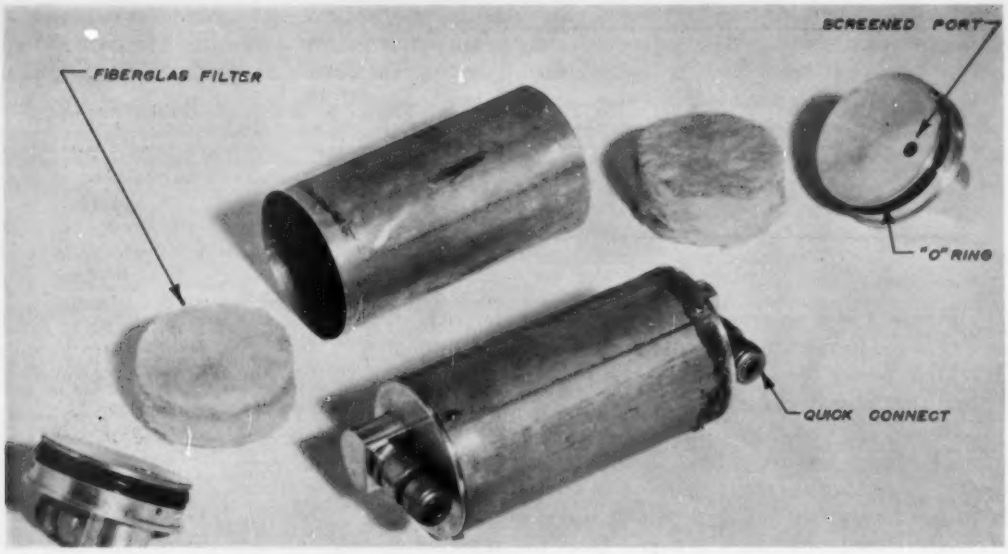

FIGURE 4. *Absorber container assembled and unassembled.*

through threaded holes in the wall of the container. Each cap has three set screw holes, an O-ring groove and a quick-connect self-sealing female fitting at the top which communicates with the necessary holes in the underside of the cap. The hole in the underside of the cap has a fine screen filter.

When the absorber container is filled with absorber, fiberglass plugs, the same diameter as the i.d. of the tube are placed under each cap to retain the absorber. O-rings seal the cap to the tube and set screws help in the alining of the caps so that the absorber container quick-connects mate with the male quick-connects on the instrument proper.

An oil-wetted vane-type vacuum pump is used as the final downstream element of the instrument. By means of this pump, the critical flow conditions necessary to the operation of the instrument are maintained. The pump exhaust is fitted with a special baffle which permits operation in any position without loss of oil. Included with the pump, in one integral unit, is a 27 v d-c motor, rated at 7 amp.

The differential pressure switch, used to actuate both the warning signal and the solenoid valve, is a slack diaphragm type with two separately adjustable microswitches.

The valve used to decrease the response time is a 24 v d-c direct-acting solenoid valve with a $\frac{1}{16}$ in. orifice.

Downstream of the solenoid valve is a sintered bronze filter in the shape of a flower pot which is sealed to the inside of a lucite tube by means of O-rings.

The bypass orifice used to insure a continuous flow from the gas source irrespective of whether the solenoid valve is open or closed, has an area approximately equal to the sum of the inlet orifice areas. It was made and is retained in a metal block in the same manner as the bridge orifices. It is connected between the inlet to the solenoid valve and the inlet to the main valve.

In its present form, the instrument contains no permanent ballast volume to compensate for the volume of the absorber container. A connection is provided for attachment of an external volume. A glass bottle containing glass beads was used to adjust the volume to its proper value. If containers of absorber become standardized, a permanent fixed ballast volume can be added to the instrument. Otherwise, a permanent adjustable volume can be added.

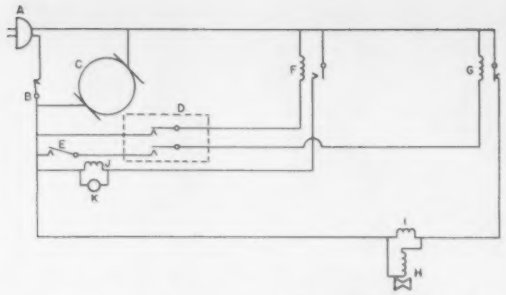

FIGURE 5. *Electrical schematic diagram.*
A=power input; B=main switch; C=vacuum pump motor; D=pressure switch; E=solenoid override switch; F=normally open relay; G=normally closed relay; H=solenoid valve; I=solenoid signal light; J=warning light; K=warning signal jack.

Figure 5 is a schematic diagram of the electrical circuitry of the instrument. Electric energy in the form of 28 v d-c enters the instrument through a nonpolar recessed male receptacle, A. Main power then goes to the main microswitch, B, and then to the vacuum-pump motor, C, and the other controls.

One of the two microswitches in the differential pressure switch, D, actuates a relay, F, which energizes a warning light, J, and miniature phone jack, K, both on the face of the instrument. The other microswitch actuates another relay, G, which energizes a second signal light, I, on the face of the instrument and the solenoid valve, H. This relay, G, is operated in a normally closed position. A signal from the pressure switch, through the relay, closes the solenoid valve. In the absence of a signal from the pressure switch the solenoid valve remains open as long as the power is on. A solenoid valve override switch, E, is provided on the instrument face, which interrupts the signal from the pressure switch to the solenoid relay thereby holding the solenoid valve open.

The chemical selected as the oxygen absorber is cobaltous oxide (CoO), which combines with oxygen to form cobaltic oxide (Co_2O_3). It is not readily available commercially but can be produced by heating cobaltous carbonate at 640 °F in vacuum for several hours. The chemical reactions involved are

$$CoCO_3 \rightarrow CoO + CO_2$$
$$4CoO + O_2 \rightarrow 2Co_2O_3$$

Theoretically, 1.6 pounds of cobaltous carbonate should produce 1 lb of cobaltous oxide, which in turn should combine with 0.1 lb of oxygen, or about 32 liters of oxygen at standard conditions. Based on the flow rate in the x-branch of this instrument, one pound of chemical absorber would be adequate for 8½ hr of operation with 100 percent oxygen at standard conditions. Perfect and complete conversion of cobaltous carbonate into cobaltous oxide is not achieved. Neither can a container of absorber be used until all of the cobaltous oxide is converted into cobaltic oxide. But on the other hand, neither is operation with 100 percent oxygen at standard conditions likely. Based on observed consumption, it was estimated that 1 lb of absorber chemical should be adequate for 8 to 10 hr of operation.

There was a tendency for the cobaltous oxide powder to pack, thereby presenting too great a resistance to the flow of gas. This was overcome as follows: Cobaltous carbonate, 0.15 lb, was thoroughly mixed with 10 cm^3 of water and then pressed into disks 2⅜ in. in diameter and ⅝ in. thick in a piston cylinder arrangement with a force of 50 tons. The disks were then converted to cobaltous oxide under vacuum in a glass chamber at 640 °F. The vacuum and temperature conditions were maintained until the liberation of carbon dioxide and water vapor became negligible (indicated by a reduction in pressure to ½ mm Hg or less). After cooling, the disks were transferred from the conversion chamber to the instrument absorber container in a nitrogen-filled glove box.

The conversion is accompanied by a color change from orange to green, the disks shrink slightly in size, and escaping carbon dioxide makes them porous. This porosity makes it possible for the subsequent gas flow to come into contact with virtually all of the chemical. The disk allows more chemical absorber to be packed into less volume than is possible with powder. Even when the disks break up, they fracture into large pieces which do not pack.

Reactivation of cobaltic oxide into cobaltous oxide is accomplished by continuously flushing the expended disks with hydrogen in a sealed chamber maintained at a temperature 550 °F or higher. The effluent is passed through a cold trap which condenses out the water vapor. The process is continued until the rate of water condensation has become negligible.

Absorber charges of approximately ½ lb were generally used. It is estimated that the absorber container will hold about three quarters of a pound of absorber when packed to the optimum.

4. Performance

4.1. Method of Determining Performance Characteristics

In order to determine performance characteristics, the instrument was operated with input gases which were controlled in composition and pressure. Input pressures were measured by means of an absolute pressure gage, connected at the input to the instrument, and control was obtained by manipulation of valves. Composition was also controlled by valve manipulation on flow lines coming from different cylinders of known gases. The mixed gases were sampled by a Model E–2 Beckman Oxygen Analyzer before entering the instrument. The oxygen analyzer was maintained at the same pressure as the input to the instrument and therefore gave a measure of the partial pressure of oxygen entering the instrument. Tanks of oxygen air, nitrogen, and carbon dioxide were used, as well as a water saturator.

In order to measure response time, solenoid valves were placed in the gas supply lines with appropriate switches so that discrete changes of composition could be made. The 28 v d-c warning signal was used to operate a relay which stopped an electric clock. The reading of the electric clock gave the time to warn directly. Instrument response was read with a mercurial manometer with a zero to 800 mm Hg range and a resolution of 0.1 mm Hg.

Figure 6 is a composite graph of data taken on three different days. Table 2 is a comparison of this data with theoretically expected performance given by (15).

This data indicates that the instrument response is less than theoretically expected. This is probably due to the incomplete absorption of the oxygen by the absorber and to the pressure drop upstream of the inlet orifices such that the inlet partial pressure of oxygen to

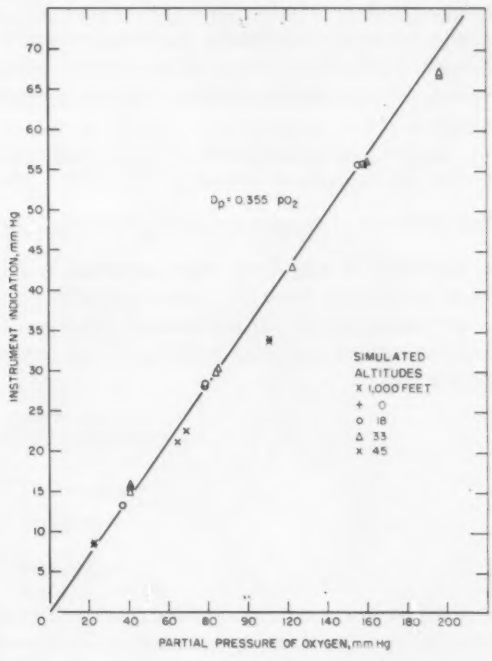

FIGURE 6. *Test data.*
Instrument response versus partial pressure of oxygen.

these orifices is actually less than that in the sample. The instrument response is nominally linear except in cases where the mass ratio of oxygen to test gas approaches unity; here the vacuum pump fails to maintain critical flow across the outlet orifice in the x-branch which produces a further reduction in instrument response.

TABLE 2. *Comparison of measured values with theoretically expected values*

Altitude	Partial pressure of oxygen	Percentage of oxygen by volume	Measured bridge output			Theoretical expected bridge output	Ratio of output indication to partial pressure of oxygen
			6/13/60	7/1/60	8/8/60		
1000 ft	*mm* Hg	*Percent*	*mm* Hg	*mm* Hg	*mm* Hg		
0	159.5	20.9	55.8			62.7	0.350
18	37.0	9.8	13.3			14.9	.359
18	78.8	20.9	28.1			31.0	.357
18	78.8	20.9		28.5		31.0	.362
18	155.9	41.4	55.7			61.1	.357
18	159.0	42.2		55.8		62.3	.351
33	41.2	20.9	15.2			16.2	.369
33	41.2	20.9			15.3	16.2	.371
33	41.3	20.9		15.0		16.2	.363
33	84.1	42.8	29.8			32.9	.354
33	85.5	43.4		30.3		33.5	.354
33	122.7	62.3			42.9	47.4	.350
33	160.0	81.4	56.2			61.0	.351
33	196.8	100.0			67.0	74.1	.340
33	197.2	100.0		67.0		74.3	.340
33	197.2	100.0	67.1			74.3	.340
45	23.2	20.9			8.8	9.1	.379
45	23.2	20.9		8.6		9.1	.371
45	64.3	58.1			21.3	24.9	.331
45	69.0	62.3		22.5		26.7	.326
45	110.7	100.0		33.8		41.7	.305
45	110.9	100.0			34.1	41.8	.307

4.2. Linearity and Altitude Dependence

The indicated differential pressure is dependent primarily on the oxygen partial pressure and secondarily on the ratio of oxygen partial pressure to total gas pressure. If this latter ratio is constant, the indication is linear and independent of altitude. In actual use, this ratio is not constant; therefore, where the altitude (inlet pressure) is constant, this effect shows up as a nonlinearity in response and where the partial pressure of oxygen is constant, this effect shows up as an altitude (inlet pressure) dependent response. As a warning device, where only one value of oxygen partial pressure is of interest, only the altitude effect is of any concern.

If the inlet gas mixture contains only oxygen and nitrogen, then a computation using (15) yields the theoretical extent of this effect, which is a maximum of 7 percent of the indication. For mixtures of oxygen enriched air where $0.209 \leq \frac{P_A}{P_1} \leq 1.00$, the maximum theoretical variation in linearity at any fixed inlet pressure is 5.4 percent of the indication. For systems which vary in altitude from sea level to 45,000 ft, the maximum theoretical variation in indication at any fixed oxygen partial pressure is 4.6 percent of the indication. Table 3 gives the measured and theoretical variation in linearity for the data in table 2 for altitudes of 18,000, 33,000, and 45,000 feet.

TABLE 3. *Linearity*

Altitude	Variation in linearity of indication in percent of indication	
	Measured	Theoretical
1000 ft		
18	2.3	2.8
33	8.7	3.9
45	21.6	3.9

We may determine the altitude effect at any particular partial pressure of oxygen by drawing individual altitude curves. As an example, the maximum altitude effect at 74 mm Hg oxygen partial pressure for altitudes from 18,000 to 45,000 ft is 10 percent. The theoretical value for these conditions is 3 percent.

Determinations of linearity and altitude effects were based on measurements of inlet pressure, partial pressure of oxygen, and the indicated differential pressure of the instrument, each of which had experimental errors. It is likely that the actual variations in linearity and altitude dependence are less than the computed maxima.

4.3. Sensitivity

Figure 6, which is a composite of data on the instrument performance, also includes a straight line going through the origin, $D_p = 0.355\ pO_2$. This is the straight line representation of the data below 45,000 ft. The experimental sensitivity of the instrument is approximately 2.82 mm Hg oxygen partial pressure per/mm Hg instrument indication.

4.4. Repeatability

a. As Partial Pressure Indicator

We may determine the repeatability of the instrument by comparison of the output indication divided by the partial pressure of oxygen values for similar points (same altitude with near oxygen partial pressures) in different runs. The 8th column of table 2 gives these values. It shows an average repeatability to within 1.1 percent with a maximum deviation of 2.2 percent.

b. As a Warning Device

As a warning device the range of oxygen partial pressure causing a warning is a function of the altitude dependence, repeatability of indication at warning point, and repeatability of pressure switch operation. It was determined that the differential pressure, when decreasing, at which the pressure switch operates to give a warning, is 25.1 to 25.4 mm Hg. Combining this information with data taken from figure 6 yields the results in table 4. For an increasing differential pressure, this pressure switch always removes the warning before the differential exceeds 27.4 mm Hg. This fact, in connection with figure 6, gives the oxygen partial pressure necessary to remove a warning as shown in table 4. At pressure altitudes from sea level to 45,000 ft, a warning is given when the partial pressure of oxygen decreases to 74.1 ± 4.5 mm Hg. The warning is always removed before the oxygen partial pressure increases to 85.6 mm Hg.

The solenoid valve, operated by the second pressure switch, is set to operate at a differential pressure somewhat above 85 mm Hg.

TABLE 4. *Oxygen partial pressures for warning*

based on figure 6

Altitude	Partial pressure of oxygen causing warning	Maximum partial pressure of oxygen necessary to remove warning
1000 ft		
0	73.5 to 74.2	79.5
18	69.6 to 70.6	76.0
33	70.1 to 72.2	77.6
45	77.6 to 78.7	85.6

4.5. Speed of Response

a. As a Partial Pressure Indicator

Since the volume of the differential pressure gage influences the time constant of the instrument, either the gage volume must be specified or the time constant given for the instrument

without a gage. The time constant was determined without a differential pressure gage by using the warning feature to determine when a particular indication had been reached. With a typical absorber charge, the time constant of the instrument without a gage is approximately 119 sec. With a time constant of 119 sec, it would take 94 sec to achieve a warning when the inlet gas is changed from air to nitrogen at sea level.

The volumes introduced by the filled absorber containers were not identical because the containers were not uniformly nor completely filled. Techniques could be evolved for more complete packing and this would of course, reduce the time constant.

b. As a Warning Device

A number of runs were made using the instrument as a warning device. The times required to achieve a warning following a discrete change in inlet gas composition are given in table 5. It is believed that a reduction of the volume between the solenoid valve and the orifice block will decrease these warning times since reducing this volume decreases dead time.

TABLE 5. *Measured times necessary to achieve a warning*

Altitude	Inlet gas		Time to warn in seconds
	Initial	Final	
1,000 ft			
0	Air	N_2	15.5
0	Air	N_2	5
0	Air	N_2	12
0	Air	N_2	11
0	Air	N_2	16
0	Air	N_2	124
0	Air	N_2	72
0	Air	N_2	27
35	O_2	N_2	27.5
35	O_2	Air	35
35	O_2	Air	48
39	O_2	Air	57
45	O_2	Air	23.5
45	O_2	Air	19.5

4.6. Absorber Life

The instrument was operated with absorber charges of approximately ½ pound. This, theoretically should have provided 3,200 mm Hg oxygen partial pressure-hours of operation. In actual practice, these absorber charges provide only about 1,200 mm Hg-hr of operation. As presently adjusted the solenoid valve operation limits the average oxygen partial pressure to about 90 mm Hg. This should provide 13 hr of operation with a ½-lb absorber charge.

4.7. Contaminating Vapors and Gases

Runs were made with entrance gases passing through a water saturator. This introduced water vapor into the gas mixture. It was found that water vapor was absorbed by the chemical thereby increasing the bridge output over that obtained with dry gas. When the saturator was removed, the instrument indication decreased below the normal dry gas value, presumably because some of the absorbed water vapor was being liberated by the chemical. Use of carbon dioxide as one of the inlet constituents produced results similar to the water vapor, indicating that it, too, was absorbed by the chemical.

If varying amounts of water vapor and carbon dioxide were to be present in the inlet gas, compensation mechanisms would have to be employed or a more specific absorber used.

5. Conclusion

An oxygen partial pressure warning device has been built that will indicate whenever the oxygen partial pressure in air oxygen mixtures is less than 74.1 ± 4.5 mm Hg at altitudes from sea level to 45,000 ft. The instrument is fundamentally rugged and is moderate in size and weight. The times required to obtain the necessary indication in response to a decrease in oxygen partial pressure are very variable and usually exceed the 15 sec desired of such an instrument.

Further reduction in the size, weight and warning time of this type instrument, as well as increased reliability are possible. The likelihood also exists that the range of oxygen partial pressure causing an indication can be reduced. This instrument demonstrates the practicality of using a critical flow pneumatic bridge as an airborne oxygen warning device. It also demonstrates the practicality of using this particular bridge for dynamic gas analysis.

The instrument is capable of measuring the partial pressure of any gas for which an absorber exists. The purpose of the y-branch is merely to serve as a nonabsorber reference. As a gas analysis instrument a separate x-branch could be provided for each constituent to be measured. By reading the differential pressure between the y-branch and each of the x-branches, multiplicity of gas constituents in a gas stream could be measured simultaneously. The bridge would always possess one more branch than the number of constituents to be measured.

This instrument can also be used to study the absorption characteristics of materials in environments of known gas composition and pressure. The differential pressure is a measure of the rate of absorption occurring, under the existing conditions.

(Paper 67C1–119)

JOURNAL OF RESEARCH of the National Bureau of Standards—C. Engineering and Instrumentation
Vol. 67C, No. 1, January-March 1963

New Fast-Opening, Large-Aperture Shutter for High-Speed Photography*

E. C. Cassidy and D. H. Tsai

(October 5, 1962)

A fast-opening, large-aperture, high-transmittance shutter has been developed. This shutter consists essentially of a metallic foil in a capacitor discharge circuit. The opening action is obtained when the foil is buckled and compressed laterally by the electromagnetic forces which accompany the heavy surge current through the circuit, during a transient discharge. A shutter made up of two foils in a loop arrangement may be opened to an area 1 inch × 3 inches in less than 45 microseconds. Some of the factors affecting the design and operation of the shutter are briefly discussed. These factors include the electrical energy input to the foil, the circuit parameters, and the materials and the size of the foil. Some experimental results are also given.

1. Introduction

In recent years a number of high speed photographic shutters have been developed (see for example, references [1] [1] through [6]). Of these, the Kerr-cell and Faraday type shutters [1,2] both open and close in the submicrosecond range. They are, however, characterized by poor light transmission. Reference [4] describes a shutter which opens and closes a 1.6 mm slit in about 15 μsec. References [5] and [6] are closing shutters which require 20 to 30 μsec to close. This paper describes a fast-opening, large aperture, high transmittance shutter. The shutter consists of a piece of metallic foil clamped between two electrodes in a capacitor discharge circuit. The foil is placed in front of a camera so that the camera lens is completely covered. When a heavy current is passed through the foil during the discharge of the capacitor, each current filament in the foil reacts with the magnetic field set up by the other current filaments. The direction of the force is such that the filaments are drawn together [7]. As a result, the edges of the foil are compressed toward the center filament, and the fast-opening action is achieved.

An improved arrangement consists of two foils mounted side by side in the same plane (but insulated from each other along their common edge) and clamped to a common conductor at the top and to two electrodes at the bottom. The foils thus form the two arms of a loop circuit. When current is passed through the foils, each foil is compressed by the electromagnetic forces described above, and, in addition, each foil is repelled by the other because they carry current in opposite directions [7]. The opening action is therefore faster.

Typically, a shutter with foils in a loop arrangement opens to an area 1 in. × 3 in. in less than 45 μsec. The initiation of the opening action may be controlled to within 1 μsec. When this shutter is used in conjunction with a high-speed camera and a suitable closing shutter, it gives precise control of the initiation and duration of an exposure, and permits photographic observation of any portion of a high speed event with a high percent of light transmittance.

2. Experiments

Experiments have been made to test the performance of several shutters of both the single- and the looped-foil type with foils of different materials and dimensions. Figure 1 is a schematic drawing of the discharge circuit with a looped-foil shutter. In this model, the foils were mounted on opposite sides of a thin piece of transparent plastic. The foils overlapped slightly in order to prevent the passage of light at the center. The plastic piece served to support the clamps at the top and the bottom, and to insulate the two bottom clamps (and the foils) from one another. The clamps were made rather massive in order to reduce distortion when tightened, and to provide good electrical contact with the foils.

The shutter assembly was installed in series with a high-voltage capacitor and a spark gap which served as a switch [8]. The capacitor was charged by means of a high voltage power supply. The spark gap was fired by means of a thyratron trigger circuit which supplied a high-voltage pulse to break down the spark gap. With this setup, the initiation of the discharge could be controlled to within 1 μsec. The duration of the discharge, for the foils tested, ranged from about 10 μsec to about 50 μsec. The motion of the foils due to the discharge was observed by means of a high-speed framing camera, focused on the foils.

Figures 2a and 2b show a single-foil shutter before and after the passage of current. With an aluminum foil, 1 in.×3 in.×0.0005 in. thick, it was found that the width could be compressed from 1 in. to ⅛ in. in about 100 μsec.

Figure 3 shows the experimental apparatus with two 2 in.×3 in.×0.0005 in. aluminum foils installed in the loop arrangement. In this setup, the foil

*This work was sponsored by the Advanced Research Projects Agency under Order No. 20-61.

[1] Figures in brackets indicate the literature references at the end of this paper.

665368—63——5

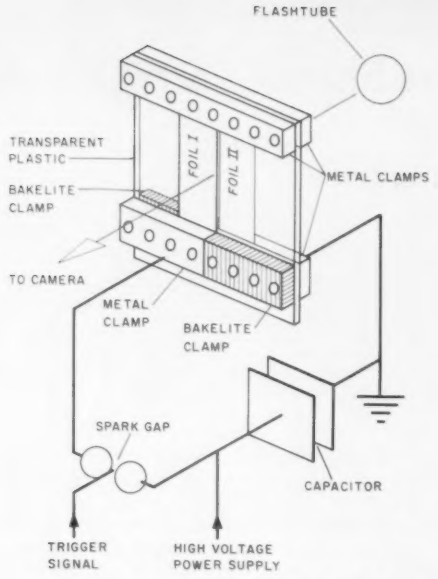

FIGURE 1. *Schematic drawing of the discharge circuit with a looped-foil shutter.*

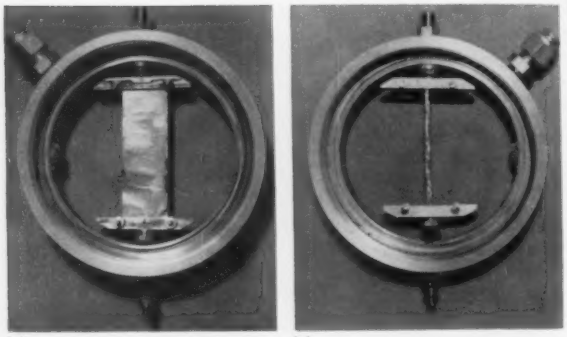

(a) (b)

FIGURE 2. *A single foil shutter before discharge (a), after discharge (b).*

holder and the spark gap assembly were mounted on a 15 μf, 20 kv, energy storage capacitor. The opening action of a shutter of this design, with two aluminum foils (1 in.$\times$3 in.$\times$0.001 in.), is shown by the framing camera record in figure 4. Here the framing camera was focused on the foils, and the opening action was silhouetted by backlighting the foils with a flashtube. This particular shutter opened to a 1 in. $\times$ 3 in. area in about 50 μsec.

3. Results and Discussion

The opening action of the shutter (the motion of the foils) is controlled by the magnitude and duration of the electromagnetic forces, and by the mass and stiffness of the foil. The rather complex prob-

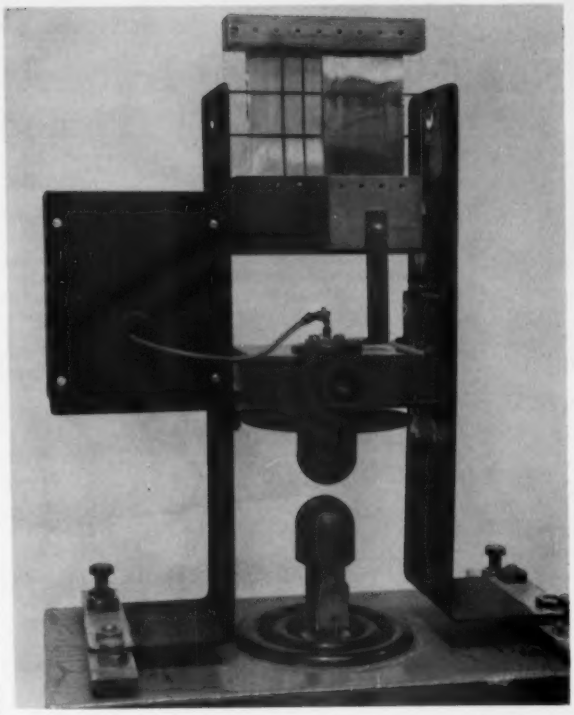

FIGURE 3. *A looped-foil shutter (before discharge) installed in the experimental setup.*

lems of solving the equation of motion for the foil and of optimizing the speed of the opening action were not undertaken in the present investigation. However, the qualitative effects of some of the design and operating parameters on the opening of the shutter were examined in an effort to determine conditions of more favorable operation. In the following paragraphs, the results of this investigation are briefly discussed, and some typical experimental results are presented.

Optimum energy input—The speed of the opening action of the shutter may be increased by increasing the current through the foil [7]. However, with a given foil and discharge circuit, the maximum speed of the action is limited by two practical considerations: (1) the total electrical energy input to the foil must not be so high as to cause combustion of the foil,[2] because the flash from the combustion which is sometimes accompanied by an arc discharge would expose the film in the camera; (2) the electromagnetic forces at any instant should not be so high as to cause excessive stresses in the foil, because this could shatter the foil and interrupt the current path, and consequently reduce the driving electromagnetic forces. These considerations, therefore, determine the "optimum" energy input to a foil.

The "optimum" energy input depends primarily on the thermochemical and the mechanical (stress-

[2] All of the energy input goes into heating of the filaments because the heat loss during the disharge is negligible.

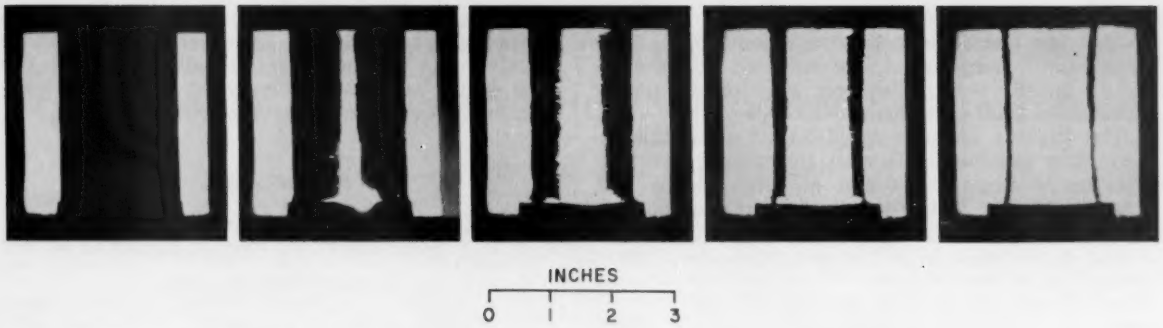

FIGURE 4. *Opening action of a looped-foil shutter (20 μsec between frames).*

strain relationship) properties of the foil material. For a given foil the "optimum" energy level may be obtained by a trial-and-error method, by adjustment of the initial energy stored in the capacitor. Experience has shown that for a given material the "optimum" energy (initial stored energy) per unit mass of foil remained approximately constant. For example, experiments, with a given discharge circuit, showed that the "optimum" energies per unit mass for the copper and aluminum foil used were approximately 4.7×10^5 j/lb and 9.9×10^5 j/lb, respectively. It was also found, of three materials tested (copper, aluminum, and Monel), that copper and aluminum were limited by burning, whereas Monel was limited by shattering.

Effect of circuit parameters—The capacitance, resistance, and inductance of the circuit affect the current as well as the duration of the discharge. These parameters therefore affect the impulse to the foil and the distribution of the impulse during the discharge. The problem of obtaining the "optimum" impulse (highest force without shattering or burning, shortest discharge time) from a given level of stored energy is difficult, and a satisfactory solution was not obtained in the present investigation. However, experimental tests showed the following results, which may be of interest to one who is seeking more favorable operating conditions.

With a given foil, for which the energy input was held fixed at the "optimum" level, a change in the capacitance in the circuit had essentially no effect on the opening of the shutter over the range tested (from 15 to 30 μf). As for the resistance in the circuit, it would seem that, for faster opening action, a lower resistance would be desirable, inasmuch as a lower resistance would allow a higher current, and thus a higher electromagnetic force. However, the resistance in the shutter circuit is mainly that of the foils. If the size of the foils is kept the same, then the resistance can be changed only by changing the material (or the resistivity) of the foil. This, of course, involves a change in the "optimum" energy and in the mass (density) of the foil. To determine the effect of changing the resistance (foil materials), therefore, one must balance the effects of these concurrent changes. In the present investigation, experiments were performed with two shutters, one with copper foils and the other with aluminum foils. The dimensions of the foils in each case were 1 in. × 3 in. × 0.001 in. For the copper foils, the "optimum" stored energy was 923 j, the density was 8.9 g/cm^3, and the resistivity was 1.8×10^{-6} ohm-cm; for the aluminum foils, these values were 528, 2.7, and 2.8×10^{-6}, respectively. It was concluded, from a consideration of these changes, that the shutter with aluminum foils should open faster. The experimental results showed that this was indeed the case. The shutter with aluminum foils opened to an area 1 in. × 3 in. in about 48 μsec, while the shutter with copper foils required about 60 μsec to open to the same area. Aluminum foil is also a good choice because of its availability and low cost.

The inductance of the circuit is determined primarily by the geometry of the circuit, and is not easily adjustable in an actual experiment. The effect of inductance was therefore not investigated experimentally. However, generally speaking, a low inductance results in a high peak current and a short duration of discharge. For fast-opening action, therefore, the inductance in the circuit should be minimized. The inductance should not, however, be so low that the peak current and thus the compressive force and the mechanical stresses in the foil become excessive and cause shattering of the foil.

Effect of size of the foil—In the present work, the length of the foil was considered as fixed by the size of the camera aperture, and was not investigated. As for the thickness of the foil, some experiments were performed with aluminum foils of the same width (1 in.) but different thicknesses (0.0005 in. and 0.001 in.). The results showed that the shutter with the thicker foils opened faster. This result was expected inasmuch as the electromagnetic forces on the foil filaments are proportional to the current squared [7] (and thus to the thickness squared), while the mass per filament is directly proportional to the thickness. The stiffness is not a factor if the foil is kept thin enough to permit buckling, because after the initial buckling of the foil the stiffness is

greatly reduced. It was concluded, therefore, that if the electromagnetic forces, obtained at the "optimum" energy input, are sufficient to cause the foil to buckle, then the shutter with foils of greater thickness should open faster.

The highest opening speed achieved in the experiments was obtained with the widest foils, the foils tested being plane and of three widths: 1.0, 1.5, and 2.0 in. With the 2 in. foils, in the loop arrangement, the inner edges of each foil attained an initial speed of 1.7×10^4 in./sec, and the shutter opened to an area of 1 in. $\times$ 3 in. in about 42 μsec. The 1.5 and 1.0 in. foils required 50 μsec and 57 μsec, respectively, to open to the same area. These results were also expected inasmuch as increasing the width of the foil allows a greater current, without affecting the mass per filament or the stiffness of the foil. Increasing the width should, therefore, increase the opening speed of the shutter. Another advantage of a wider foil is that the interruption of the current path, caused when the edges of the foil are torn from the clamping electrodes in the process of opening, is less significant for a wider foil. The foil should therefore be as wide as is practical with the stored energy available. Another, possibly more effective, way of increasing the width and hence the force would be to use a corrugated foil. This, however, was not done in this investigation.

References

[1] P. Fayolle and P. Naslin J. SMPTE **60,** 603 (1953).
[2] H. E. Edgerton and C. W. Wyckoff, J. SMPTE **56,** 398 (1951).
[3] A. W. Hogan, J. SMPTE **56,** 635 (1951).
[4] P. A. Kendall, A high-speed electromechanical shutter, U.S. Naval Ordnance Laboratory, White Oak, Md., NAVWEPS 7362.
[5] H. E. Edgerton and F. I. Strabola, Rev. Sci. Instr. **27,** 162 (1956).
[6] Model 234, Beckman and Whitley, Inc., San Carlos, Calif.
[7] F. W. Sears, Electricity and Magnetism, p. 267 (Addison-Wesley Press, Inc., Cambridge, Mass., 1951).
[8] E. H. Cullington, W. G. Chace, and R. L. Morgan, Lovotron—a low voltage triggered gap switch, Instrumentation for Geophysical Research No. 5, AFCRC–TR–55–227 (Sept. 1955).

(Paper 67C1–120)

JOURNAL OF RESEARCH of the National Bureau of Standards—C. Engineering and Instrumentation
Vol. 67C, No. 1, January-March 1963

Equations for the Radiofrequency Magnetic Permeameter

Cletus A. Hoer and Alvin L. Rasmussen

(October 25, 1962)

The rf permeameter is an impedance transformer for measuring toroidal-shaped magnetic materials at radiofrequencies. Several equations already exist for calculating permeability (μ') and dissipation factor ($\tan\delta$) from measured input impedances of the permeameter. The results from these equations do not agree with each other except over a small range of $\tan\delta$. In this paper the permeameter is represented by its equivalent T-network and an exact solution for μ' and $\tan\delta$ is obtained in terms of the input impedances and the impedance of a calibration core. The resulting equations are valid for all values of μ' and $\tan\delta$ for the conditions discussed in the paper. Values of μ' and $\tan\delta$ calculated from these exact equations are compared with those calculated from previous equations, and these results, differing as much as several orders of magnitude, are shown graphically. A frequency range from 0.1 to 50 Mc/s and a $\tan\delta$ range from 0.0005 to 5 are covered.

1. Introduction

Since the development of the radiofrequency permeameter[1] [1, 2, 3, 4][2] several equations have been derived for calculating the permeability (μ') and dissipation factor ($\tan\delta=\frac{\mu''}{\mu'}$ where μ' and μ'' are related by the complex permeability, $\mu^*=\mu'-j\mu''$) of toroidal-shaped magnetic materials. In all of these derivations various assumptions have been made about the transformer characteristics of the permeameter. Although useful in the design and application of the rf permeameter, these assumptions have led to a number of expressions each of which gives correct values of μ' and $\tan\delta$ for only a limited range of $\tan\delta$. The equations here derived are valid for all values of μ' and $\tan\delta$ for the conditions discussed in section 2. Problems arising from assuming certain characteristics of the transformer are circumvented by analyzing the equivalent T-network corresponding to the permeameter. It is assumed that the arms of the equivalent network are not a function of the load impedance. A low loss toroidal-shaped magnetic material is used as an impedance standard in evaluating the T-network. The T-network yields a set of exact equations which have been used in determining values of μ' and $\tan\delta$ for $\tan\delta$ ranging from very low loss (0.0005) to very high loss (5.0). These values agree within experimental error with those obtained by other methods not using a permeameter. An evaluation of all permeameter formulas shows that the former equations for $\tan\delta$ are in error as much as several orders of magnitude for low loss materials, and that one of these equations for μ' is in error as much as an order of magnitude for high loss materials.

The use of the permeameter makes the measurement of many magnetic materials possible in the frequency range of 0.1 to 50 Mc/s. These results are not readily obtained using other techniques.

[1] See appendix A for a description of the rf permeameter.
[2] Figures in brackets indicate the literature references at the end of this paper.

2. Derivation of the Exact Equation

A brief derivation of the permeameter equations for μ' and $\tan\delta$ is given in eqs (1) through (11). The rf permeameter is an impedance transformer and can be represented by the T–network shown in figure 1.

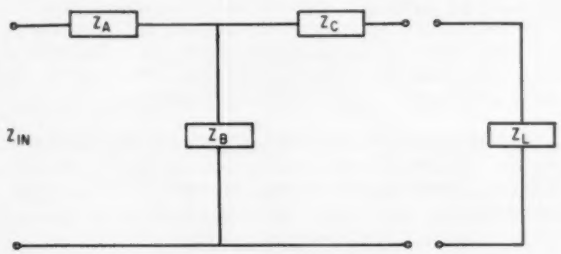

FIGURE 1. *Equivalent T-network for rf permeameter.*

The input impedance is $Z_{in}=Z_A+\frac{Z_B(Z_C+Z_L)}{Z_B+Z_C+Z_L}$, where Z_A, Z_B, and Z_C are the impedances[3] of the arms of the T-network, and Z_L is the impedance added to the secondary. If the input impedance is measured with three different known values of Z_L, an equation for any unknown Z_L may be derived eliminating Z_A, Z_B, and Z_C, the source of error in previous derivations. Let the input impedance be measured using the following definitions:

$Z_1=Z_{in}$ when the secondary is open; $Z_L=\infty$.
$Z_0=Z_{in}$ when the secondary is closed without a sample enclosed; $Z_L=0$ (this corresponds to the output terminals being shorted in fig. 1).
$Z_{s'}=Z_{in}$ when the secondary is closed with a known or standard impedance sample enclosed; $Z_L=Z_S$, where Z_S is the impedance of the standard sample minus the reactance of the space it replaces.

[3] The impedance due to the shorting plate is included in Z_C.

$Z_f = Z_{in}$ when the secondary is closed with an unknown sample enclosed; $Z_L = Z_u$, where Z_u is the impedance of the unknown sample minus the reactance of the space it replaces.

When a sample is enclosed in the secondary to measure Z_f or $Z_{f'}$, it is assumed that there is negligible direct coupling with the primary and that there is no significant change in the distributed capacitance of the secondary. If there is no measurable change in Z_1 when a sample is placed in the open secondary, then the coupling and change in distributed capacitance are negligible.

Expressing the input impedance in terms of Z_A, Z_B, Z_C, and Z_L gives

$$Z_1 = R_1 + j\omega L_1 = Z_A + Z_B, \tag{1}$$

$$Z_0 = R_0 + j\omega L_0 = Z_A + \frac{Z_B Z_C}{Z_B + Z_C}, \tag{2}$$

$$Z_{f'} = R_{f'} + j\omega L_{f'} = Z_A + \frac{Z_B(Z_C + Z_S)}{Z_B + Z_C + Z_S}, \tag{3}$$

$$Z_f = R_f + j\omega L_f = Z_A + \frac{Z_B(Z_C + Z_u)}{Z_B + Z_C + Z_u}. \tag{4}$$

From these equations the unknown impedance, Z_u, may be written

$$Z_u = Z_S \left(\frac{Z_{f'} - Z_1}{Z_{f'} - Z_0}\right)\left(\frac{Z_f - Z_0}{Z_f - Z_1}\right). \tag{5}$$

The product of the first two factors on the right is a constant for a permeameter at a given frequency. Defining this complex calibration constant as $\omega(x + jy)$ we have

$$\omega(x + jy) = Z_S \left(\frac{Z_{f'} - Z_1}{Z_{f'} - Z_0}\right). \tag{6}$$

By substituting (6) into (5) and expressing Z_u in terms of μ' and tan δ, (5) becomes

$$\omega L_a[\mu' \tan \delta + j(\mu' - 1)] = \omega(x + jy)\left(\frac{Z_f - Z_0}{Z_f - Z_1}\right), \tag{7}$$

where L_a=equivalent air inductance of the sample.[4] Solving (7) for μ' and tan δ gives [5]

$$\mu' - 1 = \frac{(x/y)B + A}{(R_{f1})^2 + (\omega L_{f1})^2}\left(\frac{y}{L_a}\right) \tag{8}$$

$$\tan \delta = \frac{(x/y)A - B}{(x/y)B + A}\left(\frac{\mu' - 1}{\mu'}\right) \tag{9}$$

where

$$A = R_{f0}R_{f1} + \omega^2 L_{f1}L_{f0}$$

$$B = \omega L_{f0}R_{f1} - \omega L_{f1}R_{f0}.$$

The calibration constants x and y may be expressed in terms of μ' and tan δ of the standard core. Z_S may be written

$$Z_S = \omega L_{as}[\mu'_s \tan \delta_s + j(\mu'_s - 1)].$$

Then from (6) we have

$$y = \frac{L_{as}[E(\mu'_s - 1) - F\mu'_s \tan \delta_s]}{(R_{f'0})^2 + (\omega L_{f'0})^2} \tag{10}$$

$$\frac{x}{y} = \frac{F(\mu'_s - 1) + E\mu'_s \tan \delta_s}{E(\mu'_s - 1) - F\mu'_s \tan \delta_s}, \tag{11}$$

where

$$E = R_{f'0}R_{f'1} + \omega^2 L_{f'1}L_{f'0}$$

$$F = \omega L_{f'0}R_{f'1} - \omega L_{f'1}R_{f'0}.$$

Primed subscripts and quantities with subscript s refer to the standard of known impedance.

Assuming that the load impedance does not change the characteristics of the T-network, these equations should be exact for all values of μ' and tan δ. The accuracy of the resulting answers appears to be limited only by the accuracy of the device used to measure the input impedances, the reproducibility of the secondary "short," and the accuracy of the standard impedance Z_S. Reducing errors due to the impedance measuring device has been discussed in the literature [1, 3].

The present secondary shorting arrangement is silver-to-silver surface contact formed under high and relatively evenly distributed pressure exerted by a cap which is screwed onto the permeameter (fig. 2). This arrangement yields a contact resistance

FIGURE 2. *An rf permeameter showing silver to silver contact surfaces.*

[4] $L_a = 2\times$(height in meters)$\times$ln(outside diameter/inside diameter)$\times 10^{-7}$ henrys.

[5] The double subscripts denote differences, for example $R_{f1} = R_f - R_1$, $L_{f1} = L_f - L_1$.

which is reproducible to a precision approximately equal to or greater than that of the impedance measuring devices presently used. The error introduced by calibrating the permeameter with a known impedance may be minimized by choosing the proper calibration core.

3. Approximate Equations for Low Loss Samples

The working eqs (8) through (11) can be simplified considerably for low loss samples. These approximate equations are also useful in determining the desired characteristics of a standard calibration core. Equations (8) through (11) may be expressed in terms of resonating capacitance and Q by letting

$$Q_1=\omega L_1/R_1 \quad Q_0=\omega L_0/R_0 \quad Q_f=\omega L_f/R_f \quad Q_{f'}=\omega L_{f'}/R_f$$

$$C_1=1/\omega^2 L_1 \quad C_0=1/\omega^2 L_0 \quad C_f=1/\omega^2 L_f \quad C_{f'}=1/\omega^2 L_{f'}.$$

If the assumption is made that the square of each Q is much greater than one, that is

$$Q_1^2 \gg 1 \quad Q_0^2 \gg 1 \quad Q_f^2 \gg 1 \; QQ_{f'}^2, \quad \gg 1,$$

and that $\tan\delta \ll 1$, then (8) and (9) reduce to

$$\mu'-1=\frac{y}{L_a}\frac{L_{f0}}{L_{f1}}=\frac{y}{L_a}\frac{C_1}{C_0}\frac{C_{0f}}{C_{1f}} \tag{8a}$$

$$\tan\delta=\left(\frac{x}{y}-\frac{B}{A}\right)\left(\frac{\mu'-1}{\mu'}\right) \tag{9a}$$

where B/A reduces to

$$\frac{B}{A}=\frac{R_{f1}}{\omega L_{f1}}-\frac{R_{f0}}{\omega L_{f0}}=\frac{C_f}{C_{0f}C_{f1}}\left\{\frac{C_{0f}}{Q_1}+\frac{C_{f1}}{Q_0}-\frac{C_{01}}{Q_f}\right\}.$$

Also (10) and (11) reduce to

$$y=(\mu_s'-1)L_{as}\frac{L_{f'1}}{L_{f'0}}=(\mu_s'-1)L_{as}\frac{C_0}{C_1}\frac{C_{1f'}}{C_{0f'}} \tag{10a}$$

$$\frac{x}{y}=\frac{\mu_s'}{\mu_s'-1}\tan\delta_s+\frac{F}{E} \tag{11a}$$

where F/E reduces to

$$\frac{F}{E}=\frac{R_{f'1}}{\omega L_{f'1}}-\frac{R_{f'0}}{\omega L_{f'0}}=\frac{C_{f'}}{C_{0f'}C_{f'1}}\left\{\frac{C_{0f'}}{Q_1}+\frac{C_{f'1}}{Q_0}-\frac{C_{01}}{Q_{f'}}\right\}.$$

The results from (8a) through (11a) agree with the results from (8) through (11) to better than 1 percent for the NBS permeameters, provided that $\tan\delta<0.1$. In part 4 it is suggested that the calibration core have a low loss. The calibration constants x and y may then be calculated from (10a) and (11a).

4. Reference Sample or Calibration Core

The reference sample presently used at the National Bureau of Standards to find the calibration constants x and y is a stable low loss powered iron carbonyl SF core. The most accurate determination of y can be made if the calibration core is machined to have an L_a such that either $L_{f'1}/L_{0f'}$ or $C_{f'1}/C_{0f'}$ in (10a) approaches unity, depending on whether inductance or capacitance measurements are being made. Since y and C_0/C_1 do not change greatly over the frequency range of 0.1 to 50 Mc/s, one calibration core may be cut to have an L_a that will be near optimum for calibration over this frequency range.

The most accurate determination of x/y may be made by using a core with the lowest possible value of $\tan\delta_s$. The value of x/y for the National Bureau of Standards permeameters is of the order of 0.01. Examination of (11a) shows that if $\tan\delta_s$ is much less than 0.01, say 0.0001, x/y is approximately independent of $\tan\delta_s$ in which case $x/y \approx F/E$ and only an approximate value of $\tan\delta_s$ need be known. Therefore, the permeameter may be calibrated with a minimum of error by choosing a very low loss material having a permeability that is stable with time and temperature and having an optimum value of L_a.

The permeability μ_s' and loss tangent $\tan\delta_s$ of the SF calibration core were determined in the frequency range of 1.0 to 50 Mc/s as follows. The core was measured in demountable coils and coaxial lines below 1.0 Mc/s on a Maxwell-type bridge and in variable length re-entrant cavities above 50 Mc/s. The μ_s' remained constant from 0.1 to 100 Mc/s. To obtain a curve of $\tan\delta_s$ between 1.0 and 50 Mc/s the curve above 50 Mc/s was extended down and the curve below 1 Mc/s was extended up to make a smooth transition as shown in figure 3.

From (8a) and (10a) it can be shown that any error, $\Delta\mu_s'$, in μ_s' will produce an error, $\Delta\mu'$, in the μ' of any measured sample of an amount

$$\Delta\mu'=\Delta\mu_s'\frac{\mu'-1}{\mu_s'-1}. \tag{12}$$

The percent error in μ' is approximately equal to the percent error in μ_s'.

Likewise it can be shown from (9a) and (11a) that any error, $\Delta\tan\delta_s$, in $\tan\delta_s$ will produce an error, $\Delta\tan\delta$, in the $\tan\delta$ of any measured sample of an amount

$$\Delta\tan\delta=\Delta\tan\delta_s\frac{\mu_s'}{\mu_s'-1}\frac{\mu'-1}{\mu'}\approx\Delta\tan\delta_s. \tag{13}$$

Therefore if a more accurate determination of μ_s' and tan δ_S is made later, the μ' and tan δ of previously measured samples may easily be corrected using (12) and (13).

5. Q-Meter Measurements

Since the permeameter is often measured on a Q-meter, it is of value to note that most of the corrections to the measured Q and C due to residuals in the Q-meter cancel out when using (8a) through (11a). A Q-meter circuit including the residuals R_m, L', L_c, and R_v is shown in figure 4. The effective Q, Q_e, and the effective capacitance, C_e, can be expressed in terms of the indicated Q, Q_i, and indicated capacitance, C_i, as

$$C_e=\frac{C_i}{1-\omega^2 L_m C_i} \tag{14}$$

$$Q_e=\frac{Q_i(1-\omega^2 L_m C_i)}{1-\omega C_i Q_i(R_m+R_G')-\omega^2 L_c C_i} \tag{15}$$

where

$$L_m=L'+L_c$$

and

$$R_G'=\frac{(\omega^2 L_c C_i-1)^2}{\omega^2 C_i^2 R_v}.$$

In obtaining (14) and (15) it is assumed that

$$R_v^2 \gg \left(\frac{1-\omega^2 L_c C_i}{\omega C_i}\right)^2.$$

If each capacitance in (8a) and (10a) is replaced by the corresponding corrected expression from (14), the resulting equation for $\mu'-1$ is identical to (8a) in which indicated values of capitance are used. The corrections cancel.

If each capacitance and Q in (9a) and (11a) is replaced by the corresponding corrected expression from (14) and (15) the resulting expression for tan δ becomes

$$\tan\delta=\left(\frac{x}{y}\frac{B}{A}+K\right)\left(\frac{\mu'-1}{\mu'}\right) \tag{16}$$

where K is a correction term which becomes significant above about 10 Mc/s.

$$K=\omega^2 L_c\left[\frac{C_f}{C_{0f}C_{f1}}\left\{\frac{C_1C_{0f}}{Q_1}+\frac{C_0C_{f1}}{Q_0}-\frac{C_fC_{01}}{Q_f}\right\}\right.$$
$$\left.-\frac{C_{f'}}{C_{0f'}C_{f'1}}\left\{\frac{C_1C_{0f'}}{Q_1}+\frac{C_0C_{f'1}}{Q_0}-\frac{C_{f'}C_{01}}{Q_{f'}}\right\}\right] \tag{17}$$

Each Q and capacitance in (16) and (17) is the indicated value as read on the Q-meter. Note that L_c is the only residual appearing in the correction term. The corrections due to L', R_m, and R_v cancel. Tan δ may be corrected either with (17) or by correcting each indicated Q with the expression

$$Q_e=\frac{Q_i}{1-\omega^2 L_c C_i}$$

and using these corrected values of Q in (9a) and (11a).

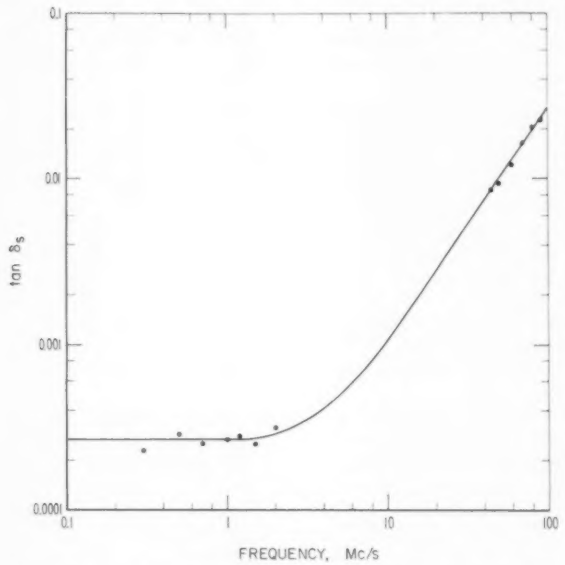

FIGURE 3. *Carbonyl SF calibration core,* tan δ_s *versus frequency showing demountable coil results (0.1 to 2.0 Mc/s) and re-entrant cavity results (45 to 100 Mc/s).*

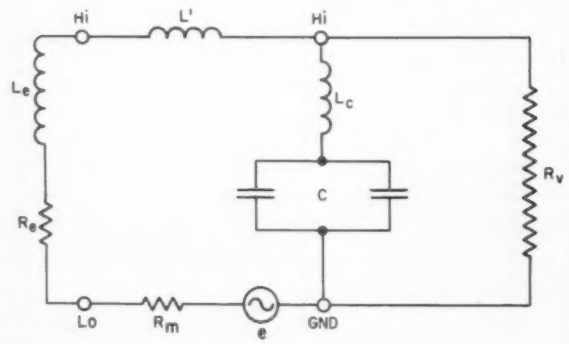

FIGURE 4. Q *meter approximate equivalent measuring circuit.*

6. Comparison With Previous Permeameter Equations

The following eqs. (18) through (24) have been used in the past to evaluate μ' and tan δ from permeameter data using the Q-meter.

From circuit (a) and assumptions 1, 2, and 3 (fig. 5) Haas [1] derived (18) and (19).

$$\mu'-1=\frac{K}{L_a}\frac{C_{0f}}{C_{f1}} \tag{18}$$

$$\tan\delta=\frac{C_{01}C_{f1}}{C_{0f}}\left[\frac{1}{C_{f1}^2}\left(\frac{C_f}{Q_f}-\frac{C_f^2C_1}{C_1^2Q_1}\right)-\frac{1}{C_{01}^2}\left(\frac{C_0}{Q_0}-\frac{C_0^2C_1}{C_1^2Q_1}\right)\right]. \tag{19}$$

Because (19) becomes negative when measuring relatively low loss materials, McKnight [2] derived (20) using circuit (b) and assumptions 1, 2, and 3

$$\tan\delta=\frac{C_{01}C_{f1}}{C_{0f}}\left[\frac{1}{C_{f1}^2}\left(\frac{C_f}{Q_f}-\frac{C_1}{Q_1}\right)-\frac{1}{C_{01}^2}\left(\frac{C_0}{Q_0}-\frac{C_1}{Q_1}\right)\right]. \tag{20a}$$

Equation (20a) reduces to (19) plus $2/Q_1$

$$\tan\delta=\tan\delta_{(19)}+2/Q_1. \tag{20b}$$ [6]

In another attempt to correct the error of (19), Rasmussen, Enfield, and Hess [3] derived eq (21) from circuit (c) and assumptions 1, 2, 3, 4, and 5. In the primary section the losses of the winding were separated from those of the material. Tan δ is here defined as μ''/μ', not as $\mu''/(\mu'-1)$ as was done in [1] and [2].

$$\tan\delta=\left(\tan\delta_{(19)}+2\frac{R_P}{X_P}\right)\frac{\mu'-1}{\mu'}. \tag{21}$$

[6] Subscripts on tan δ refer to equations giving the associated expression for tan δ.

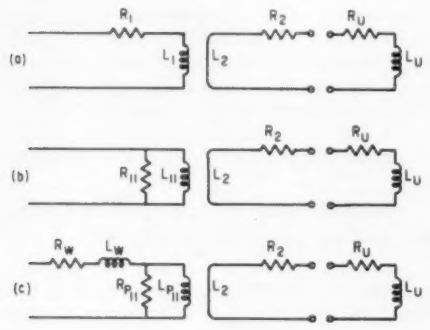

ASSUMPTIONS

1. $R_1^2 \ll \omega^2 L_1^2$
2. $R_2^2 \ll \omega^2 L_2^2$
3. $(R_2+R_U)^2 \ll \omega^2(L_2+L_U)^2$
4. $(R_p/X_p)^2 \ll 1$
5. $2(R_p/X_p)\ \text{TAN}\ \delta_{(19)} \ll 1$
6. $2(R_p/X_p)\ \text{TAN}\ \delta_{(24)} \ll 1$

FIGURE 5. *Circuits used and assumptions made in deriving equations (18) through (24).*

R_p and X_p are the series resistance and reactance of the primary material.

Since assumption 3 is not valid when measuring relatively high loss samples, Rasmussen and Hess [4] derived (22) through (25), using circuit (c) and assumptions 1, 2, 4, and 6.

$$\mu'-1=\frac{K'}{L_a}\frac{C_0}{C_1}(D-1) \tag{22}$$

$$\tan\delta=\left(\tan\delta_{(24)}+2\frac{R_P}{X_P}\right)\frac{\mu'-1}{\mu'} \tag{23}$$

where

$$\tan\delta_{(24)}=\frac{\frac{1}{C_{f1}}\left(\frac{C_1}{Q_f}-\frac{C_f}{Q_1}\right)D-\frac{1}{C_{01}}\left(\frac{C_1}{Q_0}-\frac{C_0}{Q_1}\right)}{D-1} \tag{24}$$

and

$$D=\frac{\frac{C_{01}}{C_0}C_fC_{f1}}{C_{f1}^2+\left(\frac{C_1}{Q_f}-\frac{C_f}{Q_1}\right)^2} \tag{25}$$

A number of samples with losses ranging from 0.0005 to 5.0 were measured in the permeameter and the resulting data evaluated using eqs (8) and (9), and (18) through (23). The resulting values of μ' and tan δ for 5 of these samples are shown in figure 6. Also included are μ' and tan δ as measured in a coaxial line. Below 15 Mc/s, samples F3, P1, and P2 could no longer be measured in the coaxial line because of their low resistance.[7] To increase the resistance to a value within the limits of the measuring system, the volume of the material was increased by adding a number of cores of the same material to the coaxial line. In this way an average value of tan δ for each material was obtained at several frequencies below 15 Mc/s. These results are in close agreement with tan δ obtained by measuring individual samples in the permeameter and evaluating the data with eq (9), the exact expression for tan δ.

A study of the results from the different equations (with $\mu' \cong 4$ to 4,000 and tan $\delta \cong 0.0005$ to 5.0) shows that the equations may be used within the following limitations:

(1) Equation (18) can be used for all values of μ' provided tan δ does not exceed approximately 0.1. For tan δ greater than 0.1, (18) gives values for μ' that are too high.

(2) Equation (22) gave correct results for μ' in the range of μ' and tan δ studied. ($\mu' \cong 4$ to 4,000 and tan $\delta \cong 0.0005$ to 5.0).

(3) Equations (19), (20), (21), and (23) can be used for tan δ in the approximate range of 0.1 to 1.0, with the exception of (23) which can be used up to at least 5.0.

[7] The equivalent series resistance of the sample is $\omega\mu' L_a \tan\delta$.

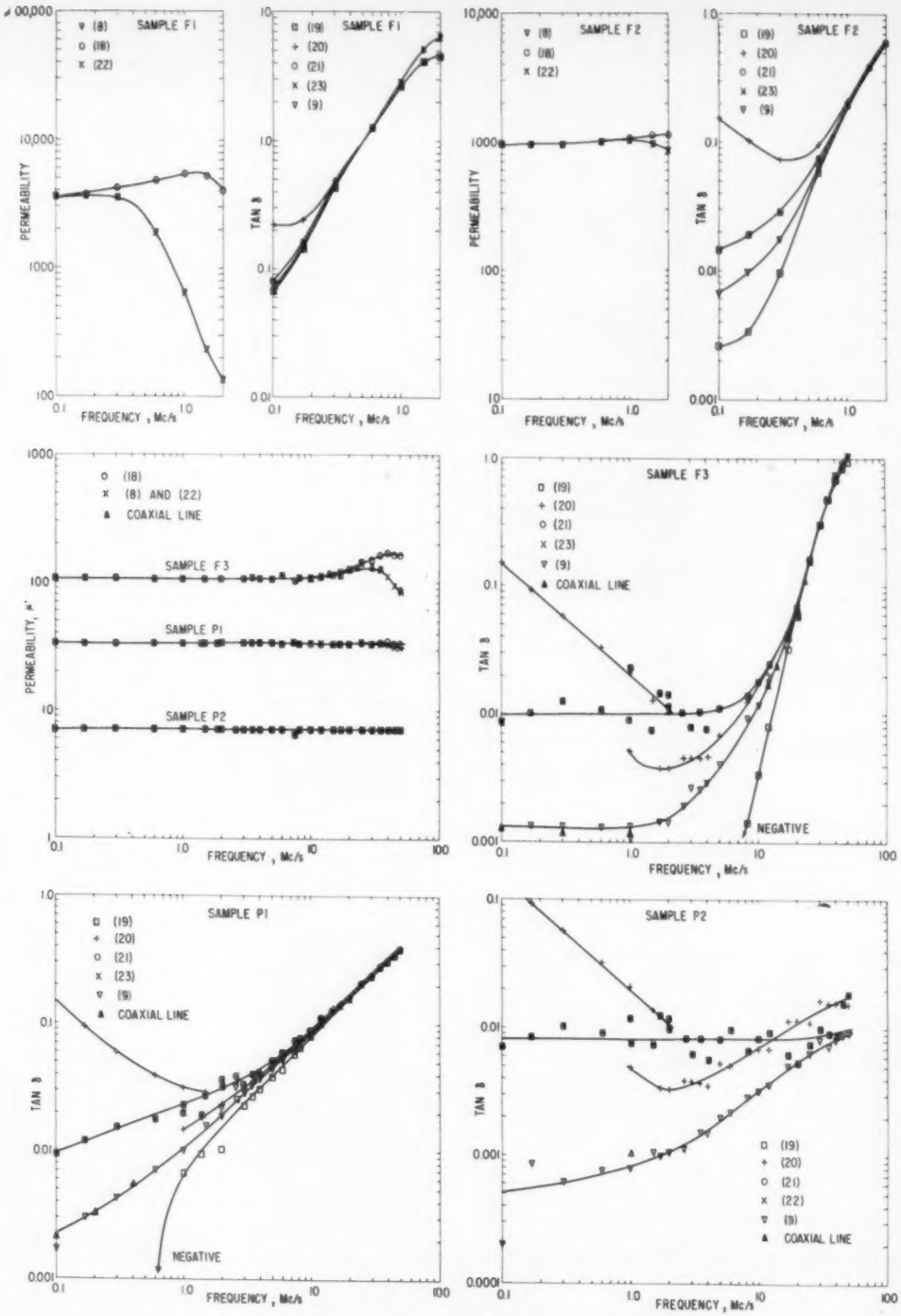

FIGURE 6. *Three ferrite samples (F1, F2, and F3) and two powdered iron samples (P1 and P2) measured in rf permeameters on a Maxwell type bridge (0.1 to 2.0 Mc/s) and on a Q meter (1.0 to 50 Mc/s).*

The data were evaluated using the different equations discussed in the text. The coaxial line values below 2.0 Mc/s were found by filling a coaxial line with a number of like samples and obtaining a value of μ' and tan δ for the group representing the average of the values for the individual cores. (Typical sample size: OD = 1.00, ID = 0.60, H = 0.16 inches.)

(4) The exact equations (8) and (9) can be used for values of μ' and tan δ at least within the range of $\mu' \cong 4$ to 4,000 and tan $\delta \cong 0.0005$ to 5.0.

(5) The approximate eqs (8a) and (9a) agree with (8) and (9) to better than 1 percent for tan $\delta < 0.1$.

The authors thank Mr. W. A. Pittman for making the many measurements and calculations.

7. Appendix A. Description of the RF Permeameter

The rf permeameter is an impedance transformer. It has a wound powered iron or stable ferrite toroidal core as a primary and a coaxial shorting enclosure as a secondary which envelops both the primary and a toroidal test sample core in such a manner that the magnetic field is concentric with the coaxial structure. Primaries, provided with connectors for terminals at one end of the enclosure, have different input impedances depending upon the frequency of interest and cover a range of at least 20 kc/s to 50 Mc/s. The core to be tested is inserted into the permeameter secondary where it is surrounded by a nearly uniform current sheet. Relatively small impedance changes in the secondary are easy to detect at the input to the primary. Because the form of the test core is toroidal, corrections for demagnetization effects are not necessary.

In making measurements, the primary of the permeameter is placed in an arm of an impedance bridge or across the terminals of a Q meter. The input impedance of the primary of the permeameter is measured, first with permeameter secondary open, second with permeameter secondary shorted without a sample, and third with permeameter secondary shorted with either a standard or unknown sample enclosed. From these data, the initial permeability (μ') and the dissipation factor (tan $\delta = \mu''/\mu'$), i.e., the reciprocal of the Q of the material, are derived.

8. Appendix B. Accuracy Check Using Metal Rings

At radiofrequencies a metal ring or toroid has an impedance which can be calculated from its physical dimensions and the resistivity of the metal. Such a ring would be an ideal standard of impedance for calibrating the permeameter provided that the impedance of the ring was within the impedance range of the permeameter. It can be shown that the inductance and resistance of a metal ring at radiofrequencies are

$$L = 2(H-\delta) \ln \frac{OD-\delta}{ID+\delta} 10^{-9} \text{ henry} \quad (26)$$

$$R = \frac{\rho}{\pi\delta}\left[\ln \frac{OD-\delta}{ID+\delta} + \frac{(H-\delta)(OD+ID)}{(OD-\delta)(ID+\delta)}\right] \text{ohm} \quad (27)$$

where

$$\delta = \frac{1}{2\pi}\sqrt{\frac{\rho 10^9}{f}}, \text{ skin depth in cm,}$$

ρ = resistivity, Ω cm,

f = frequency in cycles/second,

OD, ID, H = outside diameter, inside diameter, height in cm.

Several brass and copper rings were made and used in an attempt to calibrate the permeameter, but the results lacked precision. The impedance of the metal rings and the Q of the permeameter with a ring enclosed were too low for accurate determination of the calibration constants x and y.

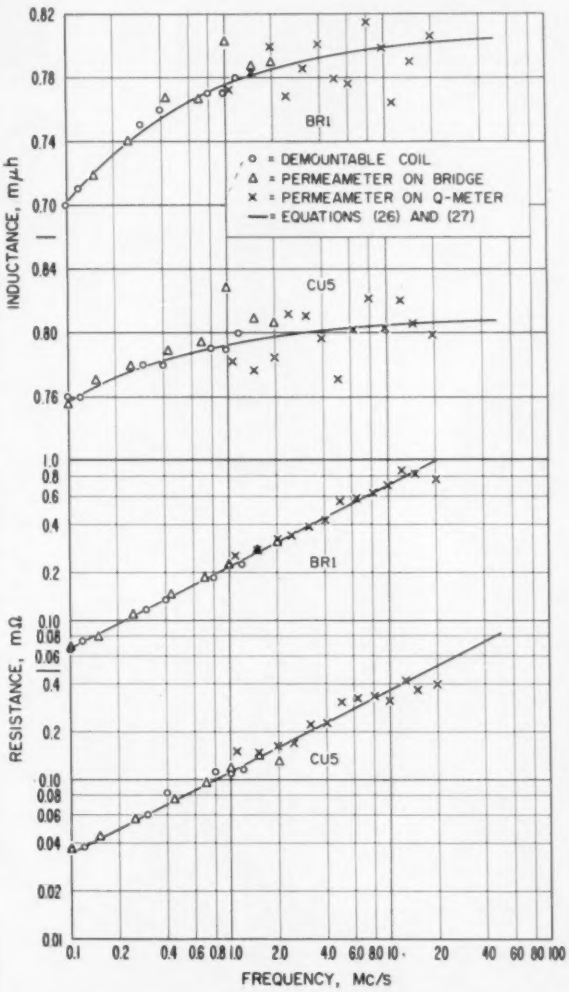

FIGURE 7. *Resistance and inductance of a brass (BR1) and a copper (CU5) ring as measured in a demountable coil and in the permeameter.*

The solid lines are calculated from equations (26) and (27).

It was decided that the metal rings would not make good calibration cores, but that they could be used to check the accuracy of the permeameter when using the exact equations. Figure 7 shows the results of the measured values of inductance and resistance versus frequency of two brass and two copper rings of different size. The rings were measured in the permeameter on a Maxwell-type bridge from 0.1 to 1.0 Mc/s and on a Boonton Q meter 260–A from 1.0 to 50 Mc/s. The SF core described in part 4 was used as the calibration core. The data were evaluated with the exact equations in the form

$$R-j\omega L=\omega(x+jy)\left(\frac{Z_f-Z_0}{Z_f-Z_1}\right). \tag{28}$$

The rings were also measured in a demountable coil [5] from 0.1 to 1.0 Mc/s on the Maxwell type bridge to compare the results of the permeameter and demountable coil with each other as well as with the results from (26) and (27).

As figure 7 shows, the results of the permeameter are in complete agreement with that from the demountable coil and from (26) and (27) within the precision of the measuring devices. The precision obtained for both the permeameter and the demountable coil is approximately 20 ph for L and 0.02 mΩ for R from 0.1 to 1.0 Mc/s on the bridge. The precision obtained from the permeameter on the Q-meter is approximately 50 ph for L and 0.1 mΩ for R.

9. References

[1] Haas, P. H., A radio frequency permeameter, J. Research NBS **51,** 221–228 (Nov. 1953) RP2454.

[2] McKnight, G. P., Permeameter for radio frequencies, Elec. Mfg. **52,** No. 4, 150 (Oct. 1953).

[3] Rasmussen, A. L., A. W. Enfield, and A. E. Hess, Advances in the design and application of the radio frequency permeameter, J. Research NBS **56,** 261–268 (May 1956) RP2673.

[4] Rasmussen, A. L., and A. E. Hess, RF permeameter techniques for testing ferrite cores, Elec. Mfg. **61,** No. 5, 86 (May 1958).

[5] Danielson, B. L., and R. D. Harrington, A technique for reducing errors in permeability measurements with coils. Proc. IRE **48,** No. 3, 365–366 (March 1960).

(Paper 67C1–121)

JOURNAL OF RESEARCH of the National Bureau of Standards—C. Engineering and Instrumentation
Vol. 67C, No. 1, January–March 1963

Publications of the National Bureau of Standards*

Selected Abstracts

Elastic constants of rutile (TiO_2), J. B. Wachtman, Jr., W. E. Tefft, and D. G. Lam, Jr., *J. Research NBS* **66A** (*Phys. and Chem.*) *No. 6, 465 (Nov.–Dec. 1962) 70 cents.*
The six elastic constants (and six elastic compliances) of rutile were determined in the kilocycle per second frequency range by a resonance method. The standard deviations range from 0.2 percent for s_{11} to 4.3 percent for s_{13}.

Reaction of hardened portland cement paste with carbon dioxide, C. M. Hunt and L. A. Tomes, *J. Research NBS* **66A** (*Phys. and Chem.*) *No. 6, 473 (Nov.–Dec. 1962) 70 cents.*
The effect of age, water-cement ratio, and evaporable water content on the reaction of hardened cement paste with carbon dioxide was investigated, using small cylinders of cement paste. The rate and extent of the reaction are subject to manipulation by varying the evaporable water content of the paste. Pastes of different age and water-cement ratio tend to dry at different rates, and this tendency exerts an important indirect effect on carbonation.
According to the CO_2–H_2O stoichiometry of carbonation, other phases can react while calcium hydroxide is still present, but the possibility of preferential attack on calcium hydroxide at low levels of carbonation should be considered. Water-cement ratio, particularly when the paste is very dense, may make a difference in the relative accessibility of different phases to carbon dioxide.

Reliability of a system in which spare parts deteriorate in storage, G. H. Weiss, *J. Research NBS* **66B** (*Math. and Math. Phys.*) *No. 4, 157 (Oct.–Dec. 1962) 75 cents.*
The problem which we consider in the following paper is the calculation of the lifetime statistics of a component with n spares with the proviso that redundant elements can fail in storage. It is assumed that failed components are instantaneously replaced. Similar models have been considered before in the literature, particularly by Proschan and collaborators, who were interested in determining the optimal spare parts kit for a system of components in series, given a fixed amount of capital to provide the spare parts. If it is assumed that components do not deteriorate in storage then the calculation of the distribution of time to failure is simple since it is just the sum of individual failure times. In the present situation the calculations are somewhat more complicated, and we have only succeeded in finding a solution when the reliability functions for on-line failures and for in-storage failures are exponential. In other cases we prescribe algorithms for the solution.

A model for the viscoelastic behavior of rubberlike polymers including entanglement effects, R. S. Marvin and H. Oser, *J. Research NBS* **66B** (*Math. and Math. Phys.*) *No. 4, 171 (Oct.–Dec. 1962) 75 cents.*
A model representing the mechanical *response* of a rubberlike polymer is derived, using the same molecular concepts of entropy elasticity and a viscous parameter expressing interactions between polymer molecules employed by Rouse, Bueche, and Zimm in their molecular theories. Since the model developed here represents the mechanical response of a chain, rather than the chain itself, it can be modified more easily than these strict molecular theories to include effects due to entanglements between chains which modify the character of the viscosity-molecular weight relationship at a critical molecular weight.
This modification is introduced, the results for both steady-state and transient response functions are calculated, and these results compared with experiment for the "Standard" polyisobutylene. The agreement indicates that the same "entanglements," whatever their precise nature, are responsible for the proportionality of viscosity to M3.4 for a high molecular weight polymer, the equilibrium compliance, and the pseudoequilibrium compliance at intermediate times or frequencies.

RF impedance probe measurements of ionospheric electron densities, J. A. Kane, J. E. Jackson, and H. A. Whale, *J. Research NBS* **66D** (*Radio Prop.*) *No. 6, 641 (Nov.–Dec. 1962) 70 cents.*
The Aerobee-Hi rocket NASA 4.07 obtained vertical electron density profiles in the ionosphere simultaneously by the Seddon CW propagation technique and by an RF impedance probe technique. The experimental goal was to assess the performance of the RF probe against the accurate values from the CW method. In the RF probe method, the electron density N was derived from the dielectric constant K of the medium at a frequency f=7.75 Mc/s. If the earth's magnetic field is neglected, the relation between these quantities may be given as $K=1-(81N/f^2)$. An expression for the dielectric constant including the effects of the earth's magnetic field is derived. The fractional error introduced by neglecting the earth's field is of the order of $(f_H/f)^2$ where f_H is the electron gyrofrequency.
It was concluded that, with allowance for the positive ion sheath around the rocket, the RF impedance probe can yield reliable values of electron density. These values were obtained from changes in the capacitive part of the probe's impedance. Small, apparently anomalous changes in the resistive part were also observed.

On the geometrical optics of curved surfaces with periodic impedance properties, C. J. Marcinkowski and L. B. Felsen, *J. Research NBS* **66D** (*Radio Prop.*) *No. 6, 699 (Nov.–Dec. 1962) 70 cents.*
In a previous publication, a two-dimensional Green's function has been derived for a circular cylinder whose surface impedance around the periphery deviates from a constant value by a sinusoidal variation of small amplitude α. Here, this solution is evaluated asymptotically in the illuminated region under the assumption that the cylinder radius is large compared with the wavelength of the incident field. The asymptotic result is interpreted in terms of geometrical optics generalized to apply to cylindrically curved, convex reflection gratings, and comprises the first and higher order diffracted rays associated with a plane grating, together with geometrical divergence coefficients accounting for the surface curvature. General properties of the spectrum of reflected rays are observed. The behavior of the first-order diffracted rays, and in particular their domain of existence as a function of surface periodicity, is discussed in detail.

On the limitations of geometrical optics solutions for curved surfaces with variable impedance properties, C. J. Marcinkowski and L. B. Felsen, *J. Research NBS* **66D** (*Radio Prop.*) *No. 6, 707 (Nov.–Dec. 1962) 70 cents.*
In the preceding paper, the authors have presented an asymptotic solution for the field in the illuminated region of a large circular cylinder whose surface impedance around the periphery deviates from a constant value by a sinusoidal variation of small amplitude α. To $O(\alpha)$, the reflected field comprises a specularly reflected ray and two first-order diffracted rays characteristic of a curved convex reflection grating. If the surface impedance varies "slowly," these three rays can be combined into a single specularly reflected ray having a reflection coefficient which depends solely on the local impedance at the reflection point. The "slowness" conditions necessary for the validity of this local reflection principle of geometrical optics are investigated and interpreted in physical terms. The results are presented in a manner which suggests their applicability to general, gently curved surfaces with slowly varying impedance properties.

Chemistry of cement. Proceedings of the fourth international symposium, Washington, 1960, *NBS Mono. 43, Vol. I (Aug. 31, 1962), $5.75; Vol. II (Sept. 27, 1962), $5.50. The two volumes are available at $11.25 a set.*
This two-volume Monograph contains the complete texts of all papers given at the Fourth Internal Symposium on the Chemistry of Cement, held in Washington, D.C., October 2–7, 1960. The publication represents one of the most complete reference works available on the subject, and presents the latest information in most of the fields of cement chemistry research. Topics covered, divided according to session titles: Volume I, Chemistry of clinker, chemistry of hydration of cement compounds, and chemistry of hydration of portland cement; Volume II, Properties of cement paste and concrete destructive processes in concrete, chemical additions and admixtures, and special cements.

Tables of Eisenstein functions. Vibrational contributions to the thermodynamic functions, J. Hilsenrath and G. G. Ziegler, *NBS Mono. 49 (July 12, 1962), $2.75.*
Tables are presented for the contribution of a harmonic oscillator to the free energy function, enthalpy function, entropy, and heat capacity of gases. Dimensionless values of the Planck-Einstein functions are given as a function of $X=Hc/kT$ for $X=0.0010(.0001)\ 0.1500(.001)\ 4.000(.01)\ 10.00(.2)\ 16.0$. A second table which gives the contributions in cal/mole °K directly as a function of frequency μ, and temperature T, was computed using the values 1.43880 for the second radiation constant hc/k, and 1.98717 for the universal gas constant R. The arguments for the latter table are spaced at 10 wave number intervals from 100 cm^{-1} to 4000 cm^{-1}.

Bibliography on atomic transition probabilities, B. M. Glennon and W. Wiese, *NBS Mono. 50 (Aug. 1, 1962), 35 cents.*
A bibliography on atomic transition probabilities is presented. The papers are arranged according to elements and stages of ionization, and the method employed and class of transitions are indicated behind each reference. Only articles on discrete transitions, both permitted and forbidden, are listed. Also included is a supplementary list of papers dealing with transition probabilities from a general point of view, a table showing the availability of numerical material on the individual atoms and ions, and a table of conversion factors

Systems of electrical units, F. B. Silsbee, *NBS Mono. 58 (Sept. 20, 1962), 30 cents.*
The various systems of measurement, with their respective sets of units, used in the literature on electricity and magnetism are described in detail. Their historical development is summarized. The manner in which each is derived from either of the two alternative points of view of the experimentalist and the theoretician is compared and contrasted. The desirability of recognizing both points of view in international standardization, particularly when discussing rationalization, is pointed out. The present status of the absolute measurements on which all electrical units are based is reported, and tables are included for the conversion of equations and numerical values from one system to another.

A survey of the techniques for measuring the radio refractive index, R. E. McGavin, *NBS Tech. Note 99 (May 1962) 30 cents.*
The radio refractive index can be measured either directly or indirectly. The former method is utilized by radio frequency refractometers; the latter method involves measurement of temperature, pressure and humidity and conversion to refractive index. In terms of convenience and accuracy the direct method is superior; however, lack of the universal use of refractometers requires the use of weather service type of data for the bulk of refractive index structures. Meteorological sensing is limited mainly by the inaccuracy in measuring humidity which under ideal conditions appears to limit the accuracy to $\pm$ 1.0 N. Gradient measurements utilizing radiosondes reflects an accuracy no better than $\pm$ 3 N units. Radio frequency refractometers are capable of accuracies as much as an order of magnitude better than that achieved by meteorological sensors. Lightweight refractomenters have been devised for balloon-borne and dropsonde measurements reflecting accuracies inferior to the conventional refractometer but superior to the radiosonde.

A tabulation of the thermodynamic properties of normal hydrogen from low temperatures to 540 °R and from 10 to 1500 psia, Supplement A (British units), J. W. Dean, *NBS Tech. Note 120A (June 1962) 45 cents.*
Pressure, volume, temperature, internal energy, enthalpy, and entropy of normal hydrogen gas have been tabulated along isobars in 2 °R temperature steps. The range covered is from the saturation temperature to 540 °R and from a pressure of 10 to 1500 psia. The source of data is Research Paper 1932 of the National Bureau of Standards Journal of Research. The method is described by which the data presented in Research Paper 1932 is reduced to properties directly useful for engineering calculations. A method is also described for estimating the effects of ortho-para compositions upon the tabulated properties.
Tabular values are presented in the dimensional units of the British system. The tabulations are also available in the dimensional units of the metric system as Technical Note No. 120.

General characteristics of linear strain gage accelerometers used in telemetry, P. S. Lederer, *NBS Tech. Note 150 (June 1962) 40 cents.*
This paper presents a summary of pertinent information, theoretical and experimental, on the design characteristics, performance capabilities and limitations of strain gage accelerometers used in telemetry. Properties and characteristics of unbonded and bonded types of strain gage accelerometers are discussed.

A general survey of the semiconductor field, G. W. Reimherr, *NBS Tech. Note 153 (Aug. 1962) 30 cents.*
This survey presents a listing of some of the properties and applications of a number of single-element and binary compound inorganic semiconductors. Brief mention is made of other types of semiconductors (ternary compounds, mixed crystals, alloys, ferrites, and organics). The toxicity problem presented by many semiconductors is noted.

The thermodynamic properties of helium from 3 to 300 °K between 0.5 and 100 atmospheres, D. B. Mann, *NBS Tech. Note 154 (Jan. 1962) 50 cents.*
The specific volume, enthalpy, entropy, and internal energy values of helium are presented in tabular form as functions of pressure and temperature.
Data are tabulated in one degree Kelvin increments for forty isobars between 0.5 atmosphere and 100 atmospheres. A comparison with previously published data is made where applicable.
An expression is presented which represents the pressure-density-temperature surface based on previously published data.
The tabulation is presented in the dimensional units of the metric system, but is also available in the dimensional units of the British system (Supplement A).

The heat capacity of diamond at high temperatures, A. C. Victor, *J. Chem. Phys.* **36,** *No. 7, 1903–1911 (Apr. 1962).*
The enthalpy of gem diamonds has been measured from 273 to 1073°K using a "drop" method and a Bunsen ice calorimeter. The derived heat-capacity values, which are believed to be accurate to $\pm$ 0.5 percent, are used to calculate the thermal functions of diamond above 298.15°K. Values of C_v° (harmonic) derived from the present investigation and recent measurements of the thermal expansion and the elastic constants of diamond are compared with theoretical treatments. Reasonably good agreement in the temperature range of this study can be obtained with a single Debye function ($\Theta_D=1860$) obtained from the measured elastic constants. Extrapolation of the data gives $\Theta_\infty=1880\pm10$.

Millimeter wave techniques, W. Culshaw, *Book, Advances in Electronics and Electron Physics* **XV,** *197–263 (Academic Press, Inc., New York, N.Y., 1961).*
The importance of millimeter waves both in research and in technology is outlined, and the difficulties experienced in the exploitation of these short wavelengths are made evident.

Considerable attention is given to transmission and measurement problems, since conventional waveguide methods have serious limitations at short mm wavelengths. Optical and quasi-optical methods are discussed, and applications of mm wave interferometers and a mm wave spectrometer are considered and diffraction effects treated in detail. The great potential use of the mm wave Fabry-Perot interferometer in precision measurements, and in maser research is made evident. Total reflection phenomena at mm wavelengths are presented and applications such as attenuation standards, phase changers, and polarizers are discussed. A re-entrant biconical spherical resonator is considered for operation at mm and sub-mm wavelengths, at high orders of interference. Expressions for the Q and shunt impedance are given, and results indicate that it could have direct application to the mm wave generation problem, and to solid state research at these wavelengths. Finally some practical aspects of mm wave detection and possible levels of sensitivity are given, together with some concluding remarks on millimeter wave research.

Plastics, G. M. Kline, *Encyclopedia Americana* **XXII,** *221–229 (1962 Ed.).*
The article currently published in the Encyclopedia Americana has been revised and expanded to include new developments in materials, processes, and applications. New sections have also been added on stereospecific polymerization, irradiated plastics, and graft and block copolymers.

The influence of temperature and pressure on the rheological properties of polymers, R. S. Marvin, *J. Japan Soc. Testing Materials, Rheology Issue* **11,** *303–307 (May 1962).*
The influence of temperature and pressure on viscosity and their corresponding influence on time dependent rheological properties is reviewed in terms of the free volume theory. Measurements obtained at the National Bureau of Standards on the effect of pressure on the dynamic bulk nodulus of natural rubber and poly(vinyl acetate) are used to illustrate the usefulness of the free volume concept and to give some clues as to its validity. The results for natural rubber seem to agree very well with the predictions of the free volume theory; those for poly(vinyl acetate) show an unexplained discrepency which indicates the need for further studies of other polymeric systems.

Extension of the Flory-Rehner theory of swelling to an anisotropic system, S. D. Bruck, *J. Polymer Sci.* **55,** *29–31 (Dec. 1961).*
The Flory-Rehner treatment of isotropic swelling of crosslinked amorphous networks has been modified to apply to oriented, semi-crystalline structures. The new parameters introduced can be readily determined from the dimensional changes of small segments of fibers in a suitable solvent using a microscope equipped with a micrometer eyepiece or with a photomicrograph assembly. Unlike other methods, this technique enables the attainment of swelling equilibria usually within 30 minutes. Preliminary experiments conducted on a series of crosslinked fibers substantiate the validity of this modification of the Flory-Rehner equation.

The international standard of light, R. P. Teele, *J. Opt. Soc. Am.* **52,** *No. 7, 826 (July 1962).*
In 1931 Wensel et al., reported the practical realization of the suggestion, made in 1908 by Waidner and Burgess, that a blackbody radiator at the freezing point of pure platinum be used as a standard of light. Subsequently such a standard was adopted internationally, effective January 1, 1948. From 1957 to the present time investigations of factors affecting the reproducibility of the standard have been conducted at the National Bureau of Standards. The previous work was extended to include crucibles and sight tubes of different dimensions and immersed to various depths, and the use of various freezing patterns. The application of corrections for the necessary viewing aperture, for the temperature drop in the walls of the sight tube, and for the unimmersed portion of the sight tube, enable us to evaluate the ideal blackbody radiator from observed values obtained with practical radiators. Appropriate modification of the freezing pattern yields improved precision. It is found that the standard is reproducible to well within 0.1 percent. It is planned to present a complete discussion and results in the Journal of Research of the NBS.

Polymer degradation (by heat, oxidation and radiation), in unsolved problems in polymer science, L. A. Wall, *ASD Tech. Report 62–283, pp. 32–36 (Mar. 1962).*
The Committee of Macromolecular Chemistry of the National Academy of Sciences—National Research Council has requested this Survey of the Problems in Polymer Degradation.

Infrasonic pressure waves associated with magnetic storms, P. Chrzanowski, J. M. Young, G. Greene, and K. T. Lemmon, *J. Phys. Soc. Japan* **17,** *Suppl. A–II, 9–13 (1962).*
Pressure waves with predominant periods between 20 and 80 seconds and amplitudes up to 8 dyne/cm² have been recorded with a quadrilateral microphone array near Washington, D.C., during intervals of high magnetic activity. These waves have a trace velocity along the earth's surface higher than the local speed of sound and show diurnal-directional properties consistent with a source on the night side of the earth. A high degree of association with large values of the planetary magnetic index K_p hs been established.

Characterization of textile yarns for use under ballistic impact conditions, J. C. Smith, *Proc. Symp. Personnel Armour, U.S. Naval Research Laboratory I, 1–21 (Oct. 4–5, 1961).*
This paper shows how textile materials for personnel armor can be selected using criteria derived from theories on transverse impact of long textile yarns. These theories introduce the concepts of longitudinal and transverse critical velocities defined as velocities just sufficient to cause immediate rupture in a yarn struck transversely or impacted in tension. An extension of the theory shows that the longitudinal and transverse critical velocities of a textile yarn depend upon the shape of its stress-strain curve, and are greatest when the curve is linear. An expression is derived for the initial rate at which a yarn absorbs energy from a projectile impacting it transversely. Arguments based on this expression suggest that a yarn most suitable for use in personnel armor should have a high transverse critical velocity and a high breaking tenacity.
Critical velocity estimates are calculated for some textile yarns using stress-strain data obtained at impact speeds near 45 m/sec. The longitudinal critical velocities range in value from 165 m/sec for acetate yarn to approximately 300 m/sec for some vinal, rayon tire cord, acrylic and nylon yarns. Transverse critical velocities for these materials are two to three times higher.

Effect of gamma radiation on chemical structure of plastics, V. J. Krasnansky, M. S. Parker, and B. G. Achhammer, *SPE Trans.* **1,** *133–138 (July 1961).*
Twelve plastics representing various chemical structures were studied as part of a program to determine the utility of plastics as packaging materials in the high energy radiation preservation of food. The plastics were exposed to selected dosages of Cobalt-60 gamma radiation, in vacuum and in air. Gas evolution and changes in infrared spectra as a result of irradiation were used to hypothesize the relative stability of these plastics to irradiation. On the basis of these criteria it was found that plastics containing conjugated ring systems, ionic linkages, and chlorine in side groups were the most stable.

Thermal degradation of polymers at temperatures up to 1200° C, S. L. Madorsky, *Soc. Chem. Ind. Mono. No. 13, 60–74 (1961).*
A study was made of the thermal degradation of polymers in a vacuum and in some cases in helium at atmospheric pressure, using 10 to 50 mg samples. Polymethylene, a noncrosslinked polymer, when heated for about half an hour in a vacuum or in helium at 500° C, vaporizes without leaving a residue. The volatile products consist of a series of saturated and unsaturated hydrocarbons of various molecular weights. At 800° C and higher, pyrolysis gives similar results; however, the products are more fragmented, and the higher the temperature and pressure the greater is this fragmentation. Polytrivinylbenzene, which is a highly crosslinked polymer, and poly(vinylidene fluoride), which is one that develops cross-

linkings during pyrolysis, both yield on heating in a vacuum at any pyrolysis temperature various volatile fragments and a more or less carbonized residue. Here too, as in the case of polymethylene, a higher temperature produces greater fragmentation of the volatile products. The more volatile products were analyzed by mass spectrometry, and the less volatile products were tested for their average molecular weight by a microcryoscopic method. Elemental analysis of residues were made by a microchemical method.

Charge-storage techniques for pulse-height analysis, L. Costrell and R. E. Brueckman, *Nuclear Electronics* (*Intern. Atomic Energy Agency*) **II,** *29–39* (*1962*).
The low duty cycles of many pulsed accelerators make necessary high pulse rates within the bursts in order to accumulate adequate data in a reasonable time. Not only do economic factors, as influenced by expensive machine time, dictate the use high pulse rates, but purely technical considerations often make experiments unfeasible unless the pulses per burst are so numerous as to exclude the use of conventional pulse-height analyzers. For these reasons much effort has been devoted to development of high speed pulse-height analyzers for use with pulsed accelerators. Much of this work has been directed toward producing what we term a "charge-storage analyzer" based on work conducted at the National Bureau of Standards. We have developed a charge-storage analyzer that is in operation with the NBS 180 Mev synchrotron on a nuclear absorption experiment for which the obstacles would otherwise be formidable. The analyzer uses temporary electrostatic storage for the accumulation of pulse-height data during the machine bursts. During the dead intervals between bursts the contents of the temporary storage are analyzed and transferred into a convential magnetic core memory. The use of this technique for nanosecond pulses is discussed and data is presented to show its feasibility.

Glass Dewars for optical and other studies at low temperatures, L. J. Schoen and H. P. Broida, *Rev. Sci. Instr.* **33,** *No. 4, 470–473* (*Apr. 1962*).
A small, rugged glass Dewar using a liquid nitrogen cooled metal shield is described. This Dewar is relatively inexpensive to construct and to modify, stores helium with only a moderate loss rate, and can be adapted for a wide variety of low temperature experiments. Two other Dewars, in which vapor-cooled radiation shields replace liquid nitrogen cooled shields, also are described. Helium loss rates show that a liter of liquid helium will keep these Dewars at 4°K for about 5 to 10 hr.

Distillation analysis, R. T. Leslie and E. C. Kuehner, *Anal. Chem. Suppl.* **34,** *No. 5, 50R–56R* (*Apr. 1962.*).
The world literature concerning laboratory distillation and related subjects that appeared in 1958–1959 is summarized. The survey covers the construction and testing of laboratory stills for use at atmospheric and low-pressure, and for microdistillation. Applications to special problems, both organic and inorganic, are discussed briefly, and theoretical and mathematical papers concerning column design and operation are mentioned. Studies of the vapor-liquid equilibria of azeotropic and nonazeotropic systems are summarized.

Displacement and strain-energy distribution in a longitudinally vibrating cylindrical rod with a viscoelastic coating, P. Hertenlendy, *J. Appl. Mech.* **29,** *Series E, 47–52* (*Mar. 1962*).
A numerical solution by R. M. Davies of the Pochhammer frequency equation is used to determine the displacement and strain-energy distribution across the cross section of an infinite elastic circular cylindrical rod for a number of wave lengths of the first, second, and third modes of symmetrical longitudinal wave propagation. With these results the effect of a thin uniform layer of viscoelastic material is investigated. The four viscoelastic parameters of the coating are reduced to one in the definition and computation of upper and lower bounds of the loss factor, and the application of results to experimental work is discussed.

Catalytic effects of thermocouple materials, L. O. Olsen, *SAE J. Paper No. 524G,* **70,** *No. 5, 94* (*May 1962*).
It has long been recognized that under some conditions certain noble metal thermocouples produce erroneous indications when immersed in gas streams containing oxygen and combustible gases. These errors have been shown to be caused by catalysis of the gaseous mixture on the surfaces of the thermocouple elements. The object of this investigation was to determine the magnitude of the catalytic effects of all of the commonly used thermocouple materials in lean mixtures of hydrogen, carbon monoxide, propane, and methane in air. The effects of catalysis were determined under three different experimental methods.

Wires of platinum, palladium, iridium, platinum plus 15% iridium, and the two elements of the Platinel thermocouple were found to catalyze the combustion of mixtures of hydrogen, carbon monoxide, and propane in air. Combustion of methane-air mixtures was not initiated by these materials at temperatures up to 1800°F. Experiments with gold, silver, Chromel, Alumel, and constantan wires showed no catalysis of any mixture at temperatures of the wires up to 1800°F. Base-metal thermocouples are therefore recommended for accurate determinations of temperatures of gaseous mixtures containing combustible materials.

Characteristics of some air-turbine handpieces, D. F. Taylor, R. R. Perkins, and J. W. Kumpula, *J. Am. Dental Assoc.* **64,** *No. 6, 794–805* (*June 1962*).
A method and equipment were developed for the simultaneous measurement of the speed and torque of dental air turbine handpieces. The power output characteristics of several models of handpieces were studied under a variety of conditions. The effect of air pressure upon speed and torque, and some effects of instrument size and balance upon speed were investigated. Increased air pressure was found to increase both the maximum speed and maximum torque attained but to be more effective in increasing torque. Within clinical limits, the size of the instrument was found to have negligible effect upon power output in comparison to the effect of dynamic balance.

Tensile shear strength of adhesive bonded metals as a function of the rate of loading, D. A. George, H. R. Butzlaff, and J. Mandel, *Symp. on Adhesion and Adhesives, Am. Soc. Testing Materials Spec. Tech. Publ. No.* **271,** *47–53* (*1961*).
A round-robin test program was devised by ASTM Committee D–14 on Adhesives to study the effects of the rate of loading on the ultimate tensile shear strength of metal-to-metal adhesive-bonded lap-shear specimens. Two metals, three adhesives, two overlap lengths and four rates of loading were studied. The tensile shear specimens tested at rates of stressing from 600–2000 psi per minute showed very little change in strength due to the rate of stressing. For a given rate of stressing the rate of strain which was observed by changes in crosshead speed increased as the modulus of elasticity of adhesives decreased. It is not possible, therefore, to express one rate of stressing as being equivalent to a particular rate of strain for adhesives that have different moduli of elasticity.

Vacuum system for use with a microbalance, G. F. Rouse, *Book, Vacuum Microbalance Techniques, ed. R. F. Walker,* **2,** *59–69* (*Plenum Press, Inc., New York, N.Y., 1962*).
A vacuum system constructed for use with a fused-silica torsion microbalance is described. Recent developments in high vacuum apparatus and technique are incorporated into its design. The system can be outgassed at 425° C and can be used in connection with experiments which must be carried out at elevated temperatures. Its use makes it possible to perform an experiment under very clean conditions and at pressures less than 10^{-8} mm Hg.

Creep of pure-gum rubber vulcanizates from indentation-time measurements, L. A. Wood and F. L. Roth, *Rubber Tech. Conf.* (*London, England, 1962*).
The compliance J (limit of the ratio of strain to stress at zero deformation) has been determined from measurements of the indentation of a flat rubber surface by a rigid sphere, as a function of time t and temperature T. The results are subjected to two successive operations: (1) J is multiplied by the absolute temperature T and (2) an empirically-determined quantity is added to the logarithm of the time at each

temperature to make the values of JT agree as well as possible. For natural rubber from 25° to −40° C of the shift required appears to correspond to a constant "activation energy" of 38 kcal/mole; from −40° to −60° C the shift is in quite good agreement with that predicted by the equation of Williams, Landel, and Ferry. Butyl rubber yields an activation energy of 20 kcal/mole, while styrenebutadiene rubber gives a value of 22 kcal/mole. The resulting curve of JT against log t shows a sigmoid form with an increase of slope over 2–3 decades and a decrease at higher values. There is usually an extended region of nearly constant slope corresponding to the conditions of normal use of rubber products. For natural rubber this slope is 1–2% per decade; for the synthetics it is appreciably higher, reaching a value of 15% per decade for nitrile rubber.

The ideal Lovibond color system, D. B. Judd, G. J. Chamberlin, and G. W. Haupt, *J. Opt. Soc. Am.* **52,** *No. 7, 813–819 (July 1962).*
Lovibond red, yellow, and blue glasses, widely used as color standards in industry, are assigned numerals in accord with the basic plan of marking each glass with the number of unit glasses of the same type through which light must be passed to produce its color. It is possible to compute from the spectral transmittances of the unit glasses defining the Lovibond scales the CIE specification of the color produced by all combinations of any number of unit glasses. Such specifications were computed in 1939 not only for all ideal red, yellow, and blue Lovibond glasses illuminated by CIE sources B (representing noon sunlight) or C (representing average daylight) but also for two-part (red-yellow, yellow-blue, or blue-red) combinations thereof. The present paper gives the results of such computations for CIE source A (representing gas-filled incandescent lamps). Although actual Lovibond glasses must unavoidably depart somewhat from this definition of the ideal Lovibond system, the computed color specifications serve to indicate with good reliability not only the CIE specification of the color produced by single glasses and two-part combinations, but also the choice of Lovibond glasses required to produce a color of any desired chromaticity within the gamut of the system.

Single-trace sweep adapter for transistor-curve tracers, L. J. Swartzendruber, *Rev. Sci. Instr.* **33,** *No. 5, 560–562 (Aug. 1961).*
A simple relay circuit, adaptable to curve tracers, that provides a single-trace sweep is described. The adapter allows the low-frequency current-voltage characteristics of many devices to be observed at high currents without large heating effects.

Proton magnetic resonance in clay minerals, R. L. Blaine, *Highway Research Board Bull. No. 287, 44–55 (June 1962).*
Energy absorption line widths at the proton resonance frequency associated with free water (H_0) were determined for a number of clays and related materials at room temperature. The line widths were calculated from the horizontal distance between the peaks of the maximum and the minimum of the derivative absorption curves obtained with a 1720-gauss proton-magnetic-resonance apparatus. Line widths in the order of decreasing proton mobility were found to be approximately three gauss for pyrophylites, six gauss for kaolins and halloysites, nine gauss for a sepiolite, and eleven to twelve gauss for a bayerite and a bauxite. Illites and montmorillonites gave only narrow line widths (0.3 to 0.7 gauss) in the semi-dry state, but exhibited some less mobile hydrogen (line width of 2–3 gauss) after drying at 200° C. Except for bayerite, bauxite, and sepiolite, the clays did not exhibit the wide lines normally associated with either hydroxide groups or water of crystallization or as determined for brucite and gibbsite. A sample of montmorillonite frozen with liquid nitrogen and slowly thawed in the apparatus indicated that greatly increased proton mobility began at about −70° C.

Ultra-high vacuum ultraviolet monochromator, L. Marton, J. A. Simpson, J. A. Suddeth, and L. B. Leder, *1961 Trans. 8th Natl. Vacuum Symp., 2d Intern. Congress, Ed. L. E. Prauss, P. 633–639 (Pergamon Press, Inc., New York, N.Y., 1962).*
A 1-meter, normal incidence vacuum ultraviolet monochromator having a sample chamber pressure of approximately 1 x 10^{-9} mm Hg is described. The entrance and exit slits are on the Rowland circle while the center floats. Wavelength is scanned by moving the grating along the circle. All moving parts are external to the vacuum chamber. The high vacuum conditions are obtained by several stages of differential pumping from the lamp housing to the sample chamber. The entire monochromator is of stainless steel with welded joints. Interesting vacuum features are the flange design, liquid nitrogen traps and rotary sea.

Constitution diagram for 16% Cr-2% Ni stainless steel, C. R. Johnson and S. J. Rosenberg, *Trans. Quart. Am. Soc. Metals* **55,** *No. 2, 277–286 (June 1962).*
A constitutional diagram was constructed for the 16% Cr–2% Ni stainless steels containing up to 1.23 percent carbon, from data obtained by metallographic examinations, thermal analysis, dilatometry, X-ray diffraction, microhardness measurements, and electron microscopy.

Effect of surface roughness on the oxidation rate of iron, A. G. Eubanks, D. G. Moore, and W. A. Pennington, *J. Electrochem. Soc.* **109,** *No. 5, 382–389 (May 1962)*
An investigation was made of the effect of surface roughness on the oxidation rate of iron in air at 800° C. Specimens of ingot iron were grit blasted to give surfaces of different textures. The roughened specimens were found to oxidize more slowly than smooth ones, the difference in rate becoming greater with increasing roughness. The smooth specimens oxidized parabolically with a certain rate constant at the beginning; however, with continued oxidation, roughness developed on the metal surface and a change in the rate constant occurred. Specimens of high-purity iron with smooth surfaces, on the other hand, not only remained smooth throughout a three-hour oxidation period, but they also oxidized parabolically with a single rate constant.
It was found that the reduction in rate due to roughening was not caused by surface contamination, or by surface cold work, but by voids that form in the scale layers on roughened surfaces. These voids apparently act as diffusion barriers for iron ions and, thereby, lower the rate at which roughened specimens oxidize.

On the theory of diffraction grating interferometers, H. Mendlowitz and J. A. Simpson, *J. Opt. Soc. Am.* **52,** *No. 5, 520–524 (May 1962).*
One-dimensional diffraction-grating theory is developed in vector notation. First-order expressions are derived for the effects of the rotation of the grating about an arbitrary axis upon the diffracted beam. These results are applied to the three-grating interferometer whose characteristics are given in some detail. Generalization to moiré patterns or to any number of gratings with arbitrary separations is indicated.

Effect of oleophobic films on fatigue crack propagation, W. L. Holshouser and H. P. Utech, *Am. Soc. Testing Materials Proc.* **61,** *749 (1961).*
Sharply notched rotating beam specimens were used to evaluate the effect of oleophobic films formed by dodecyl alcohol on the rate of fatigue crack propagation in 4340 steel, 17–7 PH stainless steel, 6061–T6 aluminum alloy, and a copper—1.75% beryllium alloy. The number of cycles required to propagate the crack was increased by the presence of the organic compound by factors ranging from 1.4 to 5.0. This effect is attributed to the ability of compounds of this type to form films that protect the metal from oxygen and water vapor in the atmosphere.

Strange sounds in the atmosphere, Part II, R. K. Cook and J. M. Young, *Sound—Its Uses and Control* **1,** *No. 3, 25–33 (May–June 1962).*
This is the second installment of the popular-scientific account whose first installment was prepared about two months ago. We describe infrasonic waves associated with microbaroms, earthquakes, magnetic storms, and tornados. Material for the second article is drawn from the open technical literature, including scientific papers in Helvetica Physica Acta, Archiv fur Meterologie usw., Nature, etc.

665368—63——6

Time resolved electron optical image of a pulsed atomic beam in flight, L. Marton, S. R. Mielczarek, and D. C. Schubert, *J. Appl. Phys.* **33,** *No. 4, 1613–1614 (Apr. 1962.)*
The electron optical schlieren method for study of gas behavior at very low pressures has been applied in stroboscopic fashion to produce photographs of chopped atomic beam pulses in flight. A photograph is shown of a cadmium atomic beam pulse moving at approximately 300 meters/sec. with maximum atomic density corresponding to about 2.10^{-6} mm Hg equilibrium pressure. The potential usefulness of this technique for study of accommodation coefficients on aerodynamic surfaces is described briefly.

Second breakdown in transistors, H. A. Schafft and J. C. French, *IRE Trans. Electron Devices* **ED–9,** *No. 2, 129–136 (July 1962).*
"Second breakdown" in transistors has been characterized as an abrupt reduction in V_{CE}, at a collector current designated by I_M, when the transistor is swept through its V_{CE} vs I_C characteristics. A critical review of the literature concerning this phenomenon and a more complete description of its characteristics are given. It appears that "second breakdown" is a more fundamental property of the transistor than has previously been thought. Each of the mechanisms thus far considered in the literature, in particular the "pinch-in" effect and p-n-p-n action, has been examined and found inadequate. The apparent dependence of the initiation of the phenomenon on the quantity of energy absorbed, and on the ambient temperature, indicates that it may be related to some thermal mechanism. This points to the importance of examining "second breakdown" in terms of energy dissipated rather than in terms of voltage or current as has been done to date.

Preservation of edge detail in metallography, W. P. Hayes, Jr., N. Tighe, and H. B. Kirkpatrick, *Metal Progress* **81,** *No. 3, 112 (Mar. 1962).*
Extremely fragile surface layers have been retained on metallographic sections as the result of the described modified version of a well known technique.

Microsize magnetic field probes with axial symmetry, C. A. Shiffman, *Rev. Sci. Instr.* **33,** *No. 2, 206–207 (Feb. 1962).*
Magnetic field probes occupying less than 10^{-3} cc and having axially symmetric response have been developed for use at liquid nitrogen temperatures and below. The probes are made by drawing a microscopic boule of bismuth from the melt, using a wire which ultimately serves as a pair of leads at one end. A second wire is fused to the other end by ohmic heating.

Optical studies at high pressures using diamond anvils, C. E. Weir, A. Van Valkenburg, and E. Lippincott, *Book, Modern Very High Pressures Techniques, ed. R. H. Wentorf, Jr., p. 51–69 (Butterworth & Co., London, England, 1962.)*
A pressure cell capable of maintaining pressures up to 160,000 atmospheres has been constructed using a pair of type II diamonds for studies in the infrared, visible and ultraviolet spectrum. Temperature variations from 175° to −30° C can be obtained with the cell. Major effects observed in the infrared spectrum of substances under pressure include shifts in absorption bands to both higher and lower frequencies, occurrence of new band as well as elimination of existing bands, the splitting of bands and changes in apparent band intensities. Examples of these effects using the infrared spectra of sodium nitrite, calcite, succinic acid, ice and ferrocene are given.

Stress-strain relationships in yarns subjected to rapid impact loading. 9. Effect of yarn structure, J. C. Smith, J. M. Blandford, P. J. Shouse, and K. M. Towne, *Textile Res. J.* **32,** *472–480 (June 1962).*
Samples of high-tenacity deacetylated cellulose acetate yarn were braided or plied and twisted by various amounts. Stress-strain data were obtained on these yarns at conventional rates of straining and under conditions involving transverse and longitudinal impact at velocities of about 40 m/sec. Strain wave propagation velocities were also measured. The effects of twisting and braiding were the same at high rates of straining and at conventional rates of straining. The addition of twist or braid caused the following effects. The initial slope of the stress-strain curve and the strain wave propagation velocity decreased. The bend in the curve at the yield stress became less sharp so that the stress-strain curve became more linear. The breaking tenacity decreased and the breaking elongation increased. The work required to break unit mass of yarn material remained unchanged. The calculated value of the longitudinal critical velocity at which a specimen breaks immediately upon impact in tension remained unchanged. Calculated transverse critical velocities tended to decrease as the yarn was twisted or braided.

Stress corrosion of high strength case aluminum alloys, F. M. Reinhart and W. F. Gerhold, *Corrosion* **18,** *No. 4, 158 (Apr. 1962).*
The unsatisfactory performance in marine environments of high strength sand cast 220–T4 aluminum alloy in vital load carrying applications and the paucity of published information on the heat treatment and resistance to stress corrosion cracking of the alloy prompted this investigation. The purpose was twofold: to determine whether variations in the heat treatment of 220 alloy would improve its resistance to stress corrosion cracking; and to compare the stress corrosion resistance of other high strength cast alloys with that of the 220T–4 alloy. Specimens of the alloys were stressed at 75 percent of their yield strengths while being intermittently immersed in a sodium chloride-hydrogen peroxide solution. The period of exposure was usually 60 days unless earlier failure occurred. Variations of magnesium contents between 9.1 and 12.7 percent did not affect the low resistance of alloy 220–T4 to stress corrosion cracking. Slow quenching from the solution heat treating temperature slightly improved the resistance of alloy 220–T4 to stress corrosion cracking. A sensitizing treatment or prolonged natural aging rendered the alloy more susceptible to stress corrosion cracking. The resistance to stress corrosion cracking of alloys A356–T61 and 357–T6 was rather uniform and was considerably better than that of 220–T4 alloy. The resistance to stress corrosion cracking of the other alloys investigated was poor.

Phase-modulated calibrator for testing phase meters, M. C. Thompson, Jr., *Rev. Sci. Instr.* **33,** *563–564 (May 1962).*
A device is described which may be used to measure the frequency response characteristics of phase meters, both electronic and electro-mechanical.

A procedure for estimating eigenvalues, N. W. Bazley and D. Fox, *J. Math. Phys.* **3,** *469–471 (May–June 1962).*
A new procedure is given for calculation of lower bounds to the eigenvalues of self-adjoint operators. Calculation of the lower bounds is reduced to the solution of linear algebraic problems.

Physical standards of emittance and reflectance, J. C. Richmond (*Proc. Conf. Radiative Transfer from Solid Materials, Boston, Mass., Dec. 12–13, 1960), Book, Radiative Transfer from Solid Materials, ed. H. H. Blau, Jr., and H. Fischer, Sec. 111, pp. 142–153 (The Macmillan Co., New York, N.Y., 1962).*
The work being done at the National Bureau of Standards on the development of specimens stable in emittance is briefly described. The fundamental laws of radiation involved in the measurement of emittance are reviewed and a limited glossary of terms is given.
The reflectance standards issued by the National Bureau of Standards are also briefly described.

A combined analog-digital differential analyzer (CADDA), W. D. Urban, W. R. Hahn, Jr., and H. K. Skramstad, *Proc. Combined Analog Digital Computer Systems Symp., Phila., Pa., Dec. 1960, 2d item (1960).*
In a paper presented at the 1959 EJCC, one of the authors described a concept of using both analog and digital techniques to produce a differential analyzer which combines the analog advantages of high speed and continuous representation of variables with the digital capability of high precision and large dynamic range. This paper deals with a study of the problems in the design, construction, and use of integrators

and multipliers employing this concept. The mathematical basis for the design is reviewed, and the construction and operation of the equipment is described.

Some properties of dirty contacts on semi-conductors and resistivity measurements by a two terminal method, G. G. Harman and T. Higier, *J. Appl. Phys.* **33,** *2198 (July 1962).*
The surface and bulk properties of semiconductors have been studied by a two-terminal method using dirty contacts. These contacts are defined as ones that are easily applied and removed and that are separated from the bulk by surface states, oxides, adhered gasses and chemical films. The method essentially involves measuring the resistance-voltage characteristics from the millivolt range up to about 100 v. In the process it is possible to separate the bulk from the surface effects, calculate the surface barrier height and thickness from tunneling equations, and determine whether the barrier is a surface film or due to metal-semiconductor contact potential difference. In addition the resistivity can be measured for difficult materials such as SiC and GaAs. The effect of work-damaging or etching the semiconductor surface can be readily evaluated. Various possible electrode systems are discussed. Efforts were concentrated on silicon carbide and silicon, but the techniques are applicable to all types of semiconductors.

A property of linear frequency modulation, A. J. Goldman, *Proc. IRE* **50,** *No. 7, 1711 (July 1962).*
(A fact useful in connection with chirp radars is that a linear FM signal of arbitrary envelope, when passed through a suitable network with linear delay characteristic, suffers a reversal of the linear FM and a Fourier transformation of the functional form of the envelope. It is shown here that no other FM signal and delay network are related in this way, i.e., in respect to Fourier transformation of the arbitrary envelope, reversal of a summand of the input phase, and reproduction of the complementary summand.)

The thermal properties of powder insulators in the temperature range 300°–4°K, D. Cline and R. H. Kropschot, *(Proc. Conf. Radiative Transfer from Solid Materials, Boston, Mass., Dec. 12–13, 1960), Book, Radiative Transfer from Solid Materials, ed. H. H. Blau, Jr., and H. Fischer, Sec. I, pp. 61–81 (The Macmillan Co., New York, N.Y., 1962).*
The transport of heat through dielectric powders and dielectric-metallic powder mixtures is investigated theoretically and experimentally for temperatures below 300° K. The most general formulation of the problem results in a non-linear integro-differential equation that is not solvable in closed form; however, a much simpler formulation is made for evacuated powders that allows certain qualitative conclusions. An attempt is made to separate out the radiative and solid heat conduction. Experimental procedures and results are reviewed.

Reference tables for 40% iridium-60% rhodium versus iridium thermocouples, G. F. Blackburn and F. R. Caldwell, *Book, Temperature, Its Measurement and Control in Science and Industry* **3,** *Pt. 2, 161–175 (Reinhold Publ. Corp., New York, N.Y., 1962).*
In a program to establish reference tables for several alloys of iridium and rhodium against iridium, the work has been completed on 40% iridium-60% rhodium. Tables have been prepared giving emfs for temperatures in degrees Fahrenheit from 32° F to 3800° F and in degrees Celsius (centigrade) from 0° C to 2100° C, and temperatures in these units with emf in millivolts as the argument. They are based on the average emfs measured on eight thermocouples, made from three lots of wire obtained in 1955, 1958, and 1960.
Measurements at temperatures 32° F to 2500° F were made in a platinum-wound furnace of conventional design, using a Pt-10% Rh vs Pt thermocouple to measure temperature. From 1950° F to 3800° F (thus overlapping the upper end of the lower range), the furnace used was an iridium block heated by electric induction. Blackbody conditions prevailed in the cavity in which the test thermocouple was inserted, and enabled measurement of the temperature with an optical pyrometer

The cement reference laboratory (1929–1959), J. R. Dise, *Am. Soc. Testing Materials Proc.* **59,** *369 (1959).*
Recent changes in the scope of its operations have stimulated numerous inquiries about the functions of the Cement Reference Laboratory. Therefore, as a record which may be of special interest to those engaged in the testing of cements and concretes, and of general interest to those engaged in the testing of other materials, a report has been prepared which covers the origin, purpose, and development of each of the present responsibilities of the Reference Laboratory.

International coordination of measurement, A. G. McNish, *Sci. Math. Weekly* **2,** *No. 3, 28–29 and 35 (Sept. 1961).*
International coordination of measurement standards permits scientists in one country to relate their measurements to those made by scientists in another country. Such coordination is provided by the International Bureau of Weights and Measures and the General Conference on Weights and Measures. In October 1960 the Conference redefined the meter in terms of a wavelength of light from krypton 86. Efforts are now being made to arrive at an atomic definition of the second.

The calibration at the National Bureau of Standards of mass standards for ultramicroanalysis, L. B. Macurdy, *Book, Vacuum Microbalance Techniques, ed. R. F. Walker,* **2,** *165–175 (Plenum Press, Inc., New York, N.Y., 1962).*
Measurements may be made with a precision of tenths or hundredths of a microgram. Small weights suffer from an unfavorable surface to mass ratio and should be checked from time to time. This may be done by the regular procedures used in weight calibration, provided a suitable selection of nominal weight values exist in each set.

Post office mechanization, B. M. Levin, M. C. Stark, and P. C. Tosini, *Elec. Eng.* **80,** *No. 2, 105–110 (Feb. 1961.)*
The introduction of mechanical equipment into the Post Office for the sorting and handling of mail makes feasible the development of procedures for maintaining precise data regarding the status of mail being sorted. These are the data needed by a computer that would regulate the flow of mail throughout the sorting process. Such a computer would control the flow of mail on conveyor belts, would make decisions regarding the type of sorting done by each sorting machine and would change these decisions when conditions warrant. The introduction of such a computer should improve service and reduce costs.

Rate of vaporization of refractory substances, J. J. Diamond, J. Efimenko, R. F. Hampson, and R. F. Walker, *(Proc. 4th Intern. Symp. Reactivity of Solids), Book, Reactivity of Solids, ed. J. H. de Bower, et al., p. 725 (Elsevier Publ. Co., Amsterdam, The Netherlands, 1961).*
The more important factors affecting the rate of vaporization of solid systems are summarized. Techniques for measuring the rates of vaporization of refractory substances at temperatures in the 1600–3000° C range are briefly described. The techniques pertain to measurements both in vacuum and in the presence of foreign gases. Some of the factors and the experimental techniques are illustrated by brief reference to studies of the vaporization of platinum and aluminum oxide.

A nomograph for selecting light balancing filters for camera exposure of color films, C. S. McCamy, *Med. Biol. Illustration, London, England* **11,** *No. 1, 13–15 (Jan. 1961).*
A nomograph is given for rapid selection of filters for color photography. The nomograph provides for a very large number of combinations of films and light sources in a simple form, permits the easy interpolation of new films, light sources, or filters, indicates which filters would be most nearly satisfactory when an ideal filter is not available, indicates the general nature of abnormal combinations for special effects, and provides a convenient conversion from color temperature to reciprocal color temperature. The nomograph is based on the assumption that the color balance of color films, the chromaticity of the illumination, and the effect of filters can be characterized adequately on a scale of reciprocal color temperature and that the change of reciprocal color temperature by a given filter is a constant.

Young's modulus of single crystal corundum form 77 °K to 850 °K, J. B. Wachtman, Jr., W. E. Tefft, and D. G. Lam, Jr., *Book, Mechanical Properties of Engineering Ceramics, p. 221–223 (Interscience Publ. Inc., New York, N.Y., 1961).*
An equation is proposed to represent the temperature dependence of Young's modulus. This equation fits data on some corundum single crystals very well.

A controller for maintaining a constant rate of vaporization in fractional distillation, E. C. Kuehner and R. T. Leslie, *Anal. Chem.* **34,** *No. 9, 1155–1156 (Aug. 1962.)*
A controller for maintaining a constant rate of vaporization from the pot of a fractionating column is described. To show the performance of the controller, a comparison is made of the constancy in efficiency of a still during controlled and uncontrolled test runs.

A method for determing mechanical resonance frequencies and for calculating elastic moduli from these frequencies, S. Spinner and W. E. Tefft, *Am. Soc. Testing Materials Proc.* **61,** *1221–1238 (1961).*
Part I describes the techniques for exciting, detecting, and measuring the mechanical resonance frequencies of specimens. These resonance frequencies have many useful diagnostic applications (for quality control, for instance) even when the elastic moduli are not calculated from them. Part II describes the methods for calculating the various elastic moduli from the appropriate resonance frequencies.

The dynamic compressibility of a rubber-sulfur vulcanizate and its relation to free volume, J. E. McKinney, H. V. Belcher, and R. S. Marvin, *Trans. Soc. Rheology* **4,** *347–362 (1960).*
The dynamic bulk compliance of natural rubber—12 sulfur was measured for varying static pressure (0 to 1000 bar), temperature (−30 to +70° C), and frequency (50 to 1000 cps). The data can be represented by reduced frequency or temperature plots, assuming viscosity is proportional to exp (1/), a fractional free volume which is a linear function of temperature and pressure. The temperature-frequency reduction fits the "universal" WLF constants, and the temperature-pressure reduction term is practically the same as that found by Singh and Nolle for polyisobutylene.

Suggested arrangement of mirrors to form multiple reference angles, J. B. Saunders, *J. Opt. Soc. Am.* **51,** *No. 8, 859–862 (Aug. 1961).*
A reference angle is described that forms, by successive or multiple reflections, a multiplicity of equal optical angles having common vertices. This angle may be used as a standard for calibrating circular scales either with an autocollimator or an interferometer. The angle can be adjusted in an interferometer to a very high accuracy. If the faces of the mirrors are 6 inches long, an error of 0.1 fringe corresponds to an error in the angle of 0.02 second of arc.

D–C differential current meter, E. Niesen, *Rev. Sci. Instr.* **32,** *No. 12, 1407–1408 (Dec. 1961).*
A technique is described using a commercial clip-on d-c milliammeter to make sensitive differential current measurements.

High-energy X-ray spectrometer using large anticoincidence sodium iodide crystals, J. M. Wycoff, *Proc. Total Absorption Gamma-Ray Spectrometry Symp., Gatlinburg, Tenn., May 19, 1960, p. 201–210 (1960).*
A 9-in.-dia by 6.25-in.-long crystal has been used in a total absorption spectrometer for X-rays in the 5- to 100-Mev range. The well-collimated X-rays are directed onto the side and along a diameter of the main crystal. On the exit side, a 6.75 x 3.63 in. NaI crystal has been set in anticoincidence to detect radiations above 0.6 Mev. The combination of the large crystal and the anticoincidence crystal has improved considerably the resolution for high-energy X-rays over the resolutions obtained with various combinations of crystals that were summed to provide a total absorption pulse. The final test of the resolution (and detailed response function shape) will come from activation curve and (p, γ) data. The initial indications of the improved resolution will be demonstrated by the comparison of the shapes of pulse-height distributions produced by 90-Mev bremsstrahlung spectra transmitted by a 604-cm water attenuator. This spectrum has a characteristic dip at 22 Mev due to giant resonance nuclear absorption which required good resolution for its detailed observation.

Determination of the dissociation equilibria of water by a conductance method, H. C. Duecker and W. Haller, *J. Phys. Chem.* **66,** *No. 2, 225–229 (Feb. 1962).*
Electrical conductivity measurements have been made at various temperatures on electrophoretically purified water with varying impurity content. The temperature coefficients of conduction are determined at 18 and 25° C for each fraction. An expression is derived for the activation energy of conduction of dilute aqueous solutions as a function of electrical conductivity. Upon substitution of the calculated activation energies of conduction into this expression, the theoretical conductivity of pure water is calculated to be $.0373 \times 10^{-6}$ ohm^{-1} cm^{-1} at 18°, a volume 3% lower than predicted by Kohlrausch sixty years ago. The dissociation constants for water calculated from this value, the equivalent conductance of the ions and the density, however, agree with those determined from the E.M.F. of galvanic cells.

The rapid selector and other NBS document retrieval studies, J. L. Pike and T. C. Bagg, *Proc. National Microfilm Assoc., Annual Meeting, Wash. D.C., Apr. 25–27, 1962, XI, 213–227 (Annapolis, Md., 1962).*
Rapid Selectors are electro-mechanical devices for reproducing selected frames from reels of coded microfilm.
A brief history of the Rapid Selector development and a description of the various models is given.
Several other document retrieval problems studied at the National Bureau of Standards are described.

Determination of oxidation rates of air-blown asphalts by infrared spectroscopy, J. R. Wright and P. G. Campbell, *J. Appl. Chem.* **12,** *256–266 (June 1962).*
Oxidation rates for eight air-blown asphalts were determined by measuring the change in infrared absorption at 5.88 microns with time of exposure to the radiant energy of a carbon-arc. While all the asphalts oxidized at different rates, those from the same geographical areas had similar rates; those from different areas varied considerably. The pattern of oxidation was generally the same for each of the eight asphalts, in that there was an induction period followed by a steady oxidation rate until near the failure point, beyond which time the oxidation rate accelerated until film failure as denoted by asphalt film cracking. An inverse relationship was found between the rate of oxidation and the accelerated weathering durability of each asphalt.

Thermocouple materials, F. R. Caldwell, *Book, Temperature, Its Measurement and Control in Science and Industry* **3,** *Pt. 2, 81–134 (Reinhold Publ., Corp. New York, N.Y., 1962).*
Thermocouple materials are considered that are used primarily as immersion temperature sensors in the range from 0° C up. Included are the conventional thermocouples that have survived since the beginnings of the art of thermoelectric temperature measurement, newer noble metal thermocouples, and thermocouples of refractory metals for use in the extreme range for immersed sensors. Because of the wide use and increasing popularity of ceramic-packed thermocouples in metal sheaths, they are included.
Limitations of the thermocouple wires are given as to range, stability, environment included atmosphere, magnitude of thermoelectric emf, and accuracy of commercially available materials of standard and extra quality. In addition, properties of the separate elements that are pertinent to the selection or use of thermocouples have been compiled.
In the case of the ceramic-packed thermocouples the following properties are presented: temperature range of the sheath, mechanical properties of the sheath, kinds of packed insulation, resistance between thermocouple wires and between wires and sheath, minimum bending radius of the packed stock, gas-tightness of the packed insulation, and types of measuring junctions available, i.e., grounded, ungrounded, bare, totally enclosed, stagnation mounting, etc.

An equation of state for calculating the thermodynamic properties of helium at low temperatures, R. D. McCarty and R. B. Stewart, *Book, Progress in International Research on Thermodynamic and Transport Properties, pp. 107–117 (Academic Press, Inc., New York, N.Y., 1962).*
A new equation of state for helium gas with six adjustable constants is presented. This relation is adequate for the representation of the P-V-T data and for the calculation of the entropy and enthalpy for a range of temperatures from 20 to 300° K, with pressures to 100 atmospheres. A comparison of calculated volumes with the original data indicates an average arithmetic deviation of 0.07 percent and maximum deviations of 0.5 percent. A comparison of calculated pressures with original data indicates about the same average and maximum deviations. A temperature-entropy chart and a compressibility factor chart have been prepared from values calculated by this equation of state. Tabular values of density, enthalpy and entropy for even values of temperature and pressure are also included.

Thermal expansion of some engineering materials from 20° K to 293° K, V. Arp, J. H. Wilson, L. Winrich, and P. Sikora, *Cryogenics* **3,** *230 (June 1962).*
Tables are given of the thermal expansions of some materials of engineering interest. The measurements were made in the temperature range from 20° K to 293° K.

Interlaboratory evaluation of a method for indicated brightness of papers containing fluorescent brighteners, T. W. Lashof and J. M. Patek, *Tappi* **45,** *No. 7, 566 (July 1962).*
A proposed modification of the method developed by Grum and Wightman for measuring indicated brightness of papers containing fluorescent brighteners was investigated using the proposed Tappi Recommended Practice for Interlaboratory Evaluation of Test Methods. The replication error was found to be negligible compared with other sources of variability, and therefore, from a precision viewpoint, it would be wasteful to make more than one measurement on a sample unless these other sources of variability are reduced. The usefulness of the proposed method was found to be limited by the high between-laboratory variability and the relatively high random interaction, both of which may have been caused by improper lamp calibration. The high between-laboratory variability may also have been due to improper preparation and use of the MgO standards. It is believed that these elements, and therefore the precision and usefulness of the method, may be improved without much difficulty.

An intermediate size automatically controlled hydrogen refrigeration system, D. B. Chelton, D. B. Mann, and B. W. Birmingham, *Suppl. Bull. Inst. Intern du Froid, Eindhoven, Comm. 1, Annexe 1960–61, 169–178 (1969).*
Increasing interest in cryogenic systems operating in the temperature range 21° to 30° K has created a need for a simple and reliable hydrogen refrigeration system. Such a refrigeration system, developed for use with a large liquid hydrogen bubble chamber, is described. The refrigerator has a maximum capacity of 4 kilowatts at temperatures between 21 °K and 30 °K. Control is automatic and is of high sensitivity. Refrigeration may be provided at either a single zone (heat source) or multizones with temperature control of each zone.
Efficient operation of the refrigeration system depends on high performance heat exchangers. Methods used to design the heat exchangers are described. Generalized design charts which make possible the design of larger capacity systems of the same general type can be developed.

Thermal radiation standards and measurements of the Radiometry Section at the National Bureau of Standards, A. G. Maki, (*Proc. Conf. Radiative Transfer from Solid Materials, Boston, Mass., Dec. 12–13, 1960), Book, Radiative Transfer from Solid Materials, ed. H. H. Blau, Jr., and H. Fischer, Sec. III, p. 135–141 (The Macmillian Co., New York, N.Y., 1962).*
A discussion was given of two aspects of the work of the Radiometry Section at the National Bureau of Standards. Two standards of thermal radiation were described and the method of their calibration detailed. The latter half of this paper will include a description of some work currently being carried on with the aim of obtaining the normal spectral emissivity of gold, aluminum, and platinum in the infrared.

Absolute microwave refractometer, M. J. Vetter and M. C. Thompson, Jr., *Rev. Sci. Instr.* **33,** *656–660 (June 1962).*
A simple microwave refractometer has been developed using a null technique which has considerably reduced drift and other instabilities introduced by the electronic components, including the klystron. The long-term stability indicates the justification for more fundamental calibration techniques which are described. The result is an instrument in which cavity stability rather than electronic stability is the limiting factor.

Ferroelectricity in the compound $Ba_2Bi_4Ti_5O_{18}$, P. H. Fang and B. Aurivillius, *Phys. Rev.* **126,** *No. 3, 893 (May 1962).*
Some ferroelectric and crystallographical properties of the compound $Ba_2Bi_4Ti_5O_{18}$ are presented. The compound represents a new structure with the unit cell consisting of one $Bi_2O_2^{2+}$ layers. From 196° C to 580° C, a maximum in the real part of the dielectric constant was observed at +417° C. No thermal hysteresis was observed within the precission of 12° C. A remanent paralization of 2 x 10^{-6} coul/cm² and a coercive field of 10 kv/cm were observed at the room temperatures.

The ammonia beam maser as a standard of frequency, J. A. Barnes, D. W. Allan, and A. E. Wainwright, *IRE Trans. Instrumentation* **I-11,** *26–30 (June 1962).*
It has been suggested that an error in tuning of the resonant cavity in an ammonia beam maser could be detected by observing a frequency shift of the maser with the application of a magnetic field Following this suggestion, an oscillatory magnetic field was applied to the NBS double beam maser and a low noise phase demodulator was constructed to detect any phase modulation present in the maser signal. With this equipment, a servo-loop was completed to constantly control the tuning of the maser's resonant cavity. Not only did this result in the elimination of the most critical parameter of the maser's frequency dependence, but improvement of the frequency dependence upon other parameters was also observed.

Large longitudinal retarded elastic deformation of rubberlike network polymers, H. Leaderman, *J. Polymer Sci.* **59,** *No. 168, S42 (June 1962).*
Measurements of longitudinal creep under constant nominal tensile stress and of recovery, and also of creep under constant true tensile stress and recovery have been made on a specimen of plasticized polyvinyl chloride. These data have been shown to be consistent with linear superposition relations of the hereditary type. Associated with nominal stress as excitation is $(\lambda-\lambda^{-2})/3$ as the measure of response, where λ is relative length. Associated with true stress as excitation is $(\lambda^2-\lambda^{-1})\ (1+0.8\lambda^{-1})/5.4$ as the measure of response.

Magnifications of a telescope, R. E. Stephens, *J. Opt. Soc. Am.* **51,** *No. 7, 803–804 (July 1961).*
The image of a distant object formed by a telescope appears larger than the object in spite of the fact that the linear dimensions are reduced in size. This is because the image is always much nearer the observer than the object. The ratio of the image distance to the object distance approaches $1/M^2$ as both distances approach infinity, where M is the angular magnification of the telescope.

Linear thermal expansion of aluminum oxide and thorium oxide from 100° to 1100° K, J. B. Wachtman, Jr., T. G. Scuderi, and G. W. Cleek, *J. Am. Ceram. Soc.* **45,** *310–323 (July 1962).*
The linear thermal expansion of single crystal and polycrystalline aluminum oxide and polycrystalline thorium oxide was measured from 100° to 1100° K with an interferometric technique. For each substance the results are well described by Grüneisen's equation using a Nernst-Lindemann energy function.

Group theory and crystal field theory, C. M. Herzfeld and P. H. E. Meijer, Book, *Solid State Physics* **12,** *1–19 (Academic Press, Inc., New York, N.Y., 1961).*

A survey of the principal group theoretical principles and methods used in crystal field theory.

Ferroelectricity in the compound $Bi_4Ti_3O_{12}$, P. H. Fang and C. R. Robbins, *Phys. Rev.* **126,** *No. 3, 892 (May 1962).*
Some ferroelectric and crystallographical properties of the compound $Bi_4Ti_3O_{12}$ are presented. The compound has a dielectric maximum at 685°C on increasing temperature and at 670°C on decreasing temperature. At these temperatures, an endothermic peak and an exothermic peak, respectively, occur. Ferroelectricity was observed along the *c* axis of the single crystal of this compound.

Blue-glass filters to approximate the blackbody at 6500° K, D. B. Judd, *Farbe* **10,** *No. 1–4, 31 (1961).*
In 1956, Rautian, Lobanova, and Znamenskaya described a light source for precise color measurement of non-self-luminous objects with an energy distribution between 400 and 700 nm closely duplicating that of a blackbody at 6,500° K. This light source took the form of an incandescent lamp at a color temperature of 2,854° K (CIE source A) combined with a three-layer, blue-glass, filter of the Ronis type An attempt in February 1959 to purchase such Ronis filters indicated that they were not yet commercially available. At the request of the National Bureau of Standards, Corning Glass Works undertook the design and production of such a filter under the direction of their A. J. Werner, and in December 1960 delivered a supply of them. Measurements show that the degree of duplication of the blackbody energy distribution for 6,500°K available from the Corning three-layer filter is slightly better than that reported for Ronis-type filters.

Application of reflectometer techniques to accurate reflection measurements in coaxial systems, R. W. Beatty and W. J. Anson, *Proc. Inst. Elec. Engr.* **B109,** *345–348 (July 1962).*
The theory of a single directional coupler reflectometer having two auxiliary tuners is reviewed, giving emphasis to precision measurement possibilities.
Problems in setting up this system for measurements in coaxial line are discussed and a system for measurements in the frequency range 3.95–5.85 Gc/s is described.
The development of quarter wavelength short-circuit reflection standards and sliding terminations is presented.
The results of measurements of the reflection from connectors and various loads at 4 Gc/s are given.

Four methods for predicting the durability of roofing asphalts, S. H. Greenfeld and J. R. Wright, *Mater. Res. Std.* **2,** *No. 9, 738–745 (Sept. 1962).*
Four laboratory procedures (asphaltene content, filtration time, solubility parameter, and carbonyl index) for predicting the durability of 24 coating-grade roofing asphalts as determined in accelerated-weathering machines were studied. Durability tended to vary directly with filtration time, and inversely with solubility parameter, asphaltene content, and carbonyl index. There was scatter in the data in all of the correlations, but the asphalts tended to be grouped according to the source of the crudes from which they were obtained. Modifications to the asphalts produced by additives, fluxing oils, and blending stocks tended to make the asphalts deviate from their source groups.

Coring an electroform, W. H. Metzer, Jr., *Plating* **49,** *No. 8, 880 (Aug. 1962).*
Article describes novel method for removing soluble mandrels from thin walled electroforms. The electroformed part containing the mandrel is sealed, together with a reagent, in a closed system which is heated in a furnace. Mandrels have been removed from electroformed shells by this method where no ordinary means would work.

Four-place table decibels return loss to magnitude of voltage reflection coefficient, R. W. Beatty, *Microwave Eng. Handb. & Buyers Guide, p. TD188–192 (Nov. 1961).*
A four place table of the magnitude of $|\Gamma|$ of the voltage reflection coefficient corresponding to the return loss $L_R = 20 \log_{10} \frac{1}{|\Gamma|}$ is given. L_R is given to 0.01 decibel intervals over the range 0–20 decibels. A simple procedure permits use of the table outside of this range.

Insulation resistance measurements, A. H. Scott, *Proc. 4th Electrical Insulation Conf., Materials and Application, Wash., D.C., pp. 115–117 (Feb. 19–22, 1962).*
Some comments are made regarding the reasons for interest in electrical insulation-resistance measurements. A brief review of the advantages, disadvantages and sensitivity is given for various types of equipment used for making electrical insulation measurements. Also some pitfalls in making insulation measurements are mentioned. A short reference to electrode materials which can be used is given. This discussion is intended to give a background for the open discussion on Measurement of Insulation Resistances Greater than 10^{16} ohms, which will form the last part of the session.

Some tensile properties of amalgam, M. S. Rodriguez and G. Dickson, *J. Dental Res.* **41,** *No. 4, 840–852 (July–Aug. 1962).*
Methods were developed for measuring the tensile properties of dental amalgam. Specimens used were dumbbell shaped with a straight portion of 0.01 in.^{2} cross section and approximately 0.30 in. length. Tensile strengths of four amalgams ranged from approximately 7000 to 8500 psi. Elongations calculated over a 0.5 in. gage length varied from 0.3 to 0.5%. Chord moduli of elasticity from stresses of 1000 to 3000 psi for specimens of the four amalgams strained at a rate of 0.003 in. per minute averaged $3.3–4.1 \times 10^6$ psi and from 1000 to 5000 psi averaged $2.2–2.8 \times 10^6$ psi.

A study of the chemical and physical properties of magnetic recording tape, F. Nesh and R. F. Brown, Jr., *IRE Trans. Audio* **AU–10,** *No. 3, 70–71 (May–June 1962).*
A study has been made of the chemical and physical properties of magnetic recording tape. The chemical studies indicate the possible relationship between a series of solvent tests and the wear properties of commercially available tapes. The physical studies, including electron micrographs indicate a smaller unit crystal size for γ Ferric Oxide than previously supposed and a relationship between a better dispersion and improved magnetic properties. Both studies are being continued in greater detail.

Measurement of effect of moisture on heat transfer through insulated flat-roof constructions, F. J. Powell and H. E. Robinson, *Am. Soc. Testing Materials Spec. Tech. Publ.* **312,** *35–66 (1961).*
Two methods of measurement are presented for laboratory determination of the effect of moisture on the heat transfer through insulated flat-roof constructions when subjected to successive periods of simulated summer and winter temperature conditions, and daily solar heating of the top surface. The methods allow simultaneous measurements to be made on specimens of different designs. Heat-flow meters are used in the first method and a calorimeter technique in the second for observing changes in the insulating value of the entire construction and its components due to moisture. The second method includes a means for measuring the rate of change of moisture content of the specimen.
Illustrative results are given for thirteen of the fifty-four specimens tested over a period of five years. Results indicate that natural in-place drying of wetted insulation over a vapor barrier and/or a dense concrete deck is very slow, and that once wetted, such insulation will have greater heat transmission for long periods of time. Some constructions made without vapor barriers, containing materials of moderate permeance, showed good drying characteristics, so that if initially wet, or wetted later, the insulation approached dryness in a period comparable to a year's service.

APPA–TAPPI reference material program, *I. Interlaboratory investigation of TAPPI standard T 414 m–49, internal tearing resistance of paper, T. W. Lashof, Tappi* **45,** *No. 8, 656 (1962).*
The initial steps in a project to improve the reproducibility of this long established method of test are presented. These included (1) refinement of the procedure based on information that had been accumulated in the literature and by the manufacturer of the testing instrument and others over the years, and (2) an interlaboratory study involving 40 laboratories and 8 materials covering the range of the method. A within-laboratory replication error of 5.3% coefficient of variation was found. The present TAPPI standard calls for at least

5 replications, but the analysis shows that as many as 10 replications would still be useful, provided that differences between laboratories are adjusted using a standard sample. Between-laboratory variability is so large that even when only 5 replications are used to reduce the effect of within-laboratory variability, a standard sample will significantly reduce between-laboratory variability.

Properties of dental amalgams made from spherical alloy particles, N. C. Demaree and D. F. Taylor, *J. Dental Res.* **41,** *No. 4, 890–906 (July–Aug. 1962).*
Experimental dental amalgams were prepared for the first time from a typical amalgam alloy (Ag 70.6%, Sn 26.1%, Cu 2.5%, Zn 0.4%) in the form of spherical particles 2 to 150 microns in diameter rather than in the irregular particles normally employed. Properties of amalgams made, using particles of 8 size ranges, were investigated. Dimensional change on setting and setting time were greater but residual mercury content was lower for amalgam made from the larger particles. Particles between 15 and 50 microns in diameter gave maximum strength. Physical properties of some of the experimental amalgams were equal or superior to properties of dental amalgams now in use. The use of spherical particles provides a new approach to the investigation of the setting reactions of dental amalgam.

Fast-melting alloy forms water jacket for small klystrons, W. J. Anson and E. Niesen, *Electron. Design, pp. 42–45 (Mar. 1962).*
Many klystrons radiate strong external signals and often require good shielding in laboratory setups to eliminate interference between the r.f. source and the detection system. This article describes some simple approaches to both the shielding and the cooling problems.

Other NBS Publications

Journal of Research 66A (Phys. and Chem.), No. 6 (Nov.–Dec. 1962), 70 cents.
Heat of formation of nitronium perchlorate. A. A. Gilliland.
Phase equilibrium relations in the binary system bismuth sesquioxide-niobium pentoxide. R. S. Roth and J. L. Waring.
Elastic constants of rutile (TiO_2). J. B. Wachtman, Jr., W. E. Tefft, and D. G. Lam, Jr. (See above abstracts.)
Reaction of hardened portland cement paste with carbon dioxide. C. M. Hunt and L. A. Tomes. (See above abstracts.)
Titanium standards for hydrogen content. J. T. Sterling, F. J. Palumbo, and L. L. Wyman.
Ultraviolet stability of crosslinked polycaprolactam systems. S. D. Bruck.
Spectral-line intensities and *gf*-values in the first spectrum of copper. C. H. Corliss.
Batch adsorption from solution. W. V. Loebenstein.
Separation of hafnium from zirconium and their determination: Separation by anion-exchange. L. A. Machlan and J. L. Hague.

Journal of Research 66B (Math. and Math. Phys.), No. 6 (Oct.–Dec. 1962), 75 cents.
Reliability of a system in which spare parts deteriorate in storage. G. H. Weiss. (See above abstracts.)
Estimation of dispersion parameters. W. A. Thompson, Jr.
Laguerre expansions for successive generations of a renewal process. G. H. Weiss.
Bounds on ratios of means. G. T. Cargo and O. Shisha.
A model for the viscoelastic behavior of rubberlike polymers including entanglement effects. R. S. Marvin and H. Oser. (See above abstracts.)
Black box maximization of circular coverage. C. T. Zahn, Jr.
An application of information theory to the analysis of contingency tables, with a table of $2n \ln n$, $n=1(1)10{,}000$. S. Kullback, M. Kupperman, and H. H. Ku.

Journal of Research 66D (Radio Prop.), No. 6 (Nov.–Dec. 1962), 70 cents.
RF impedance probe measurements of ionospheric electron densities. J. A. Kane, J. E. Jackson, and H. A. Whale. (See above abstracts.)
Methods for applying numerical maps of ionospheric characteristics. W. B. Jones and R. M. Gallet.
Very-low-frequency radio propagation in the ionosphere. D. W. Swift.
Prolonged space-wave fadeouts in tropospheric propagation. A. P. Barsis and M. E. Johnson.
Range-error compensation for a troposphere with exponentially varying refractivity. J. J. Freeman.
On the geometrical optics of curved surfaces with periodic impedance properties. C. J. Marcinkowski and L. B. Felsen. (See above abstracts.)
On the limitations of geometrical optics solutions for curved surfaces with variable impedance properties. C. J. Marcinkowski and L. B. Felsen. (See above abstracts.)
Conversion of the amplitude-probability distribution function for atmospheric radio noise from one bandwidth to another. A. D. Spaulding, C. J. Roubique, and W. Q. Crichlow.
Some statistical properties of pulsed oblique HF ionospheric transmissions. M. Balser and W. B. Smith.
Induction in a small loop moving with a magnetostatic dipole toward a conducting half space. M. B. Kraichman.
Propagation of terrestrial radio waves of long wavelength—theory of zonal harmonics with improved summation techniques. J. R. Johler and L. A. Berry.
Terminal-zone corrections for a dipole driven by a two-wire line. K. Iizuka and R. W. P. King.
Pattern synthesis with a flush-mounted leaky-wave antenna on a conducting circular cylinder. A. Ishimaru and F. R. Beich.

Analysis of electric energy usage in Air Force houses equipped with air-to-air heat pumps, P. R. Achenbach, J. C. Davis, and W. T. Smith, NBS Mono. 51 (July 13, 1962) 30 cents.
Annotated bibliography on soft X-ray spectroscopy, H. Yakowitz and J. R. Cuthill, NBS Mono. 52 (June 29, 1962) $1.00.
Experimental transition probabilities for spectral lines of seventy elements, C. H. Corliss and W. R. Bozman, NBS Mono. 53 (July 20, 1962) $4.25.
Weights and measures administration, NBS Handb. 82 (June 22, 1962) $1.75. (Supersedes H26)
Required signal-to-noise ratios, RF signal power, and bandwidth for multichannel radio communications systems, E. F. Florman and J. J. Tary, NBS Tech. Note 100 (Jan. 1962), $1.00.
Mode conversion in the earth-ionosphere waveguide, J. R. Wait, NBS Tech. Note 151 (June 8, 1962) 20 cents.
Information selection systems retrieving replica copies: A state-of-the-art report, T. C. Bagg and M. E. Stevens, NBS Tech. Note 157 (Dec. 31, 1961) $1.25.
Efficient use of the radio spectrum, K. A. Norton, NBS Tech. Note 158 (Apr. 1962) 45 cents.
A Fortran code for calculation of eigenvalues and eigenfunctions in real potential wells, R. S. Caswell, NBS Tech. Note 159 (Aug. 1962) 25 cents.
Propagation of solar particles and the interplanetary magnetic field, C. S. Warwick, J. Geophys. Research **67,** No. 4, 1333–1346 (Apr. 1962).
Availability of machine-usable natural language material, M. E. Stevens, Proc. 3d Inst. on Information, Storage and Retrieval (American Univ., Wash., D.C.), **1,** 58–75 (Feb. 1961).
Physical measurements and experiment design, W. J. Youden, Le Plan d'Exper. Centre Natl. Recherche Sci. (Paris, France) **110,** 1–13 (Aug.–Sept. 1961).
A calculus for factorial arrangements, B. Kurkjian and M. Zelen, Annals. of Math. Statistics **33,** 600–619 (June 1962).
Modular forms whose coefficients possess multiplicative properties (II), M. Newman, Ann. of Math. **75,** 242–250 (Mar. 1962).
Transition probabilities for permitted and forbidden lines of Si X, Fe XIV and Fe X, R. H. Garstang, Extrait des Ann. d'Astrophys. **25,** No. 2, 109–117 (1962).
A note on normal matrices, M. Marcus and N. Khan, Can. Math. Bull. **4,** 23–27 (1961).
The evolution of concepts and languages of computing, R. D.

Elbourn and W. H. Ware, Proc. IRE **50,** No. 5, 1059–1066 (May 1962).

National Bureau of Standards list of IGY flares with normalized values of importance and area, C. S. Warwick, IGY Solar Activity Report Series No. 17 (Intern. Geophys. Year, World Data Center A. Solar Activity, High Altitude Observatory, University of Colorado, Boulder, Colorado, May 1, 1962).

Plural scattering of 20-kev electrons in aluminum, L. Marton, J. A. Simpson, H. A. Fowler, and N. Swanson, Phys Rev. **126,** No. 1, 182–192 (Apr. 1, 1962).

Time and its inverse, J. M. Richardson, Intern. Sci. and Tech. **1,** No. 6, 54–61 (June 1962).

Effect of crystal growth on the comparative fixation of Sr^{89} and Ca^{45} by calcified tissues, R. C. Likins, A. S. Posner, B. Paretzkin, A. P. Frost, J. Biol. Chem. 236, 2804–2806 (Oct. 1961).

Introduction, H. S. Peiser, Book, Vacuum Microbalance Techniques, Ed. R. F. Walker, **2,** 1–5 (Plenum Press, Inc., New York, N.Y., 1962).

The effect of geomagnetic activity on the F_2 region over central Africa, R. G. Rastogi, J. Geophys. Research **67,** No. 4, 1367–1374 (Apr. 1962).

Growth rates of zinc crystals from the vapor phase, R. L. Parker and L. M. Kushner, J. Chem. Phys. **35,** No. 4, 1345 (Oct. 1961).

Plastic standards in Government, F. W. Reinhart, Proc. Am. Standards Assoc. 12th Natl. Conf. Standards, pp. 44–46 (Houston, Texas, Oct. 1961).

Anisotropies in angular distributions of molecular dissociation products, G. H. Dunn, Phys. Rev. **8,** 62–64 (Jan. 15, 1962).

Heats of formation of inorganic fluorine compounds—A survey, G. T. Armstrong and L. A. Krieger, Progress on Intern. Research On Thermodynamics and Transport Properties, pp. 8–77 (ASME & Academic Press, Inc., New York, N.Y., 1962).

Plastics, G. M. Kline, The Americana Annual, p. 603 (Americana Corp., Chicago, Ill., 1961).

Vibrational-rotational spectra of BrCN, A. G. Maki and C. T. Gott, J. Chem. Phys. **35,** No. 9, 2282–2285 (1962).

Distribution of total service time for a fixed observation interval, W. S. Connor and N. C. Severo, J. Am. Stat. Assoc. **57,** 376–386 (June 1962).

Abstract shape recognition by machine, M. E. Stevens, Computers—Key to Total Systems Control, Proc. Eastern Joint Computer Conf., **20,** No. 1, 332–351 (Dec. 1961).

Determination of molecular weights and molecular weight distribution, D. McIntyre, ASD Tech. Rept. 62–283, p. 71–74 (Mar. 1962).

Environmental chemistry, F. W. Reinhart, Prevention of Deterioration Center Newsletter (Natl. Acad. Sci.-Natl. Research Council) **V,** No. 1, 1–2, 4 (Oct. 1961).

A study of solar activity associated with polar-cap absorption, C. S. Warwick and M. W. Haurwitz, J. Geophys. Research **67,** No. 4, 1317–1332 (Apr. 1962).

Stability of plastic impression trays, J. B. Woelfel and G. C. Paffenbarger, J. Am. Dental Assoc. **63,** No. 5, 705–706 (Nov. 1961).

Electron spin resonance studies of γ-irradiated small molecules at 4 °K and 77 °K, R. E. Florin, D. W. Brown and L. A. Wall, Proc. 5th Intern. Symp. on Free Radications, Paper No. 18, 1–17 (Almquist and Wiksell, Stockholm, Sweden, July 6–7, 1961).

Absolute isotopic abundance ratio and the atomic weight of chlorine, W. R. Shields, E. L. Garner and V. H. Dibeler, J. Am. Chem. Soc. **84,** 1510–1522 (1962).

Departure from the steady state in two-intermediate enzyme reactions, H. Shin, Trans. Faraday Soc. **58,** No. 475, 1439–1450 (July 1962).

Direct measurement of line intensities and widths in the first overtone band of CO, H. J. Kostkowski and A. M. Bass, J. Quant. Spectry. Radiative Transfer **1,** 177–184 (1961).

Calibration of vibration pickups at large amplitudes, E. Jones, S. Edelman, and K. S. Sizemore, J. Acoust, Soc. Am. (Errata) **34,** No. 3, 355 (Mar. 1962).

Dislocations and stacking faults in aluminum nitride, P. Delavignette, H. B. Kirkpatrick and S. Amelinckx, J. Appl. Phys. **32,** No. 6, 1098–1100 (June 1961).

Pair production as an analyzer of circular polarization of gamma rays from neutral particle decays, H. Olsen and L. C. Maximon, Il Nuovo Cimento **24,** No. 1, 186–189 (Apr. 1962).

Emission flame photometry, M. Margoshes, Anal. Chem. Suppl. **34,** No. 5, 221R–224R (Apr. 1962).

Temperature dependent of electron emission in the field emmission region, R. Klein and L. B. Leder, Phys. Rev. **124,** 1046–1049 (Nov. 1961).

Design requirements for mechanized systems in protective shelters, R. R. Achenbach, Heating, Piping and Air Conditioning **34,** No. 2, 73–79 (Feb. 1962).

Spin-lattice relaxation in two rare earth double nitrates, R. P. Hudson and B. W. Mangum, Il Nuovo Cimento **23,** 1133–1135 (Mar. 1962).

Dimensional changes in fibrous macromolecules: The system alpha-keratin-lithium bromide, L. Mandelkern, J. C. Halpin, A. F. Diorio and A. S. Posner, Am. Chem. Soc. **34,** No. 8, 1383–1391 (Apr. 1962).

Tchebycheff approximation by functions unisolvent of variable degree, J. R. Rice, Trans. Am. Math. Soc. **99,** 298–302 (1961).

Best approximations and interpolating functions, J. R. Rice, Trans. Am. Math. Soc. **101,** 477–498 (Dec. 1961).

The presence of singly-ionized gallium (Ga II) lines in stellar spectra, W. P. Bidelman and C. H. Corliss, Astrophys. J. **135,** No. 3, 968–969 (May 1962).

Theory and biomedical applications of the analog computers, H. L. Mason, Natl. Inst. of Health Workshop on Biomedical Computing, No. 1 (July 1961).

Universal-time control of the arctic and antarctic *F* region, R. A. Duncan, J. Geophys. Research **67,** 1823–1830 (May 1962).

Evaluation of the nature of the surfaces of hard tooth tissues by a surface activity test, R. L. Bowen, Proc. Workshop on Adhesive Restorative Dental Materials (Indiana Univ., Bloomington, Indiana, Sept. 28–29, 1961).

Liquid drop collisions, O. G. Engel, Symp. Erosion and Cavitation, Am. Soc. Testing Materials Spec. Tech. Publ. No. **307,** 3–16 (1961).

On the determination of disintegration rates by the coincidence method using high efficiency detectors, R. W. Hayward, Intern. J. Appl. Radiation and Isotopes **12,** 148–150 (Dec. 1961).

Field emission from niobium in the normal and superconducting states, R. Klein and L. B. Leder, Phys. Rev. **124,** No. 4, 1050–1052 (Nov. 1961).

On the self-diffusion of ions in a polyelectrolyte solution, S. Lifson and J. L. Jackson, J. Chem. Phys. **36,** No. 9, 2410–2414 (May 1962).

Mass spectrometry, R. M. Reese, Anal. Chem. **34,** No. 5, 243R–254R (Apr. 1962).

Fifteen years ACM, F. L. Alt, Commun. Assoc. Computing Machinery **5,** No. 6, 300–307 (June 1962).

Scattered radiation from large cobalt-60 calibrating sources, L. Costrell, Health Phys. J. **8,** No. 3, 261–272 (June 1962).

Measurement characteristics of the farm milk tank, M. W. Jensen, J. Milk and Food Technol. **25,** No. 4, 112–115 (Apr. 1962).

The microwave Zeeman effect of free hydroxyl radicals: $^2\Pi_{1/2}$ levels, H. E. Radford, Phys. Rev. **126,** 1035 (1962).

Effect of noncrystallizable components on the crystallization kinetics of polymers, F. Gornick and L. Mandelkern, J. Appl. Phys. **33,** No. 3, 907–913 (Mar. 1962).

Standards for plastics in the U.S.A., G. M. Kline, Proc. 13th Intern. Plastics Congress, pp. 27–33 (Turin, Italy, Sept. 28–30, 1961).

Electron resonance magnetometer for alternating magnetic fields, O. E. Spokas and M. Danos, Rev. Sci. Instr. **33,** No. 6, 613–617 (June 1962).

Traces of products of angular momentum matrices, I. Cartesian basis, E. Ambler, J. C. Eisenstein, and J. F. Schooley, J. Math. Phys. **3,** No. 1, 118–130 (Jan.–Feb. 1962).

Measurement of linear photon polarization by pair production, L. C. Maximon and H. Olsen, Phys. Rev. **126,** No. 1, 310–319 (Apr. 1962).

Standards for vinyl chloride plastics, F. W. Reinhart, Proc. SPE Regional Tech. Conf. "Vinyl Plastics" (New York, N.Y., Nov. 15, 1961); SPE J. **18,** 308–311 (Mar. 1962).

Radiation hazards in realistic perspective, L. S. Taylor, Phys. Today **15,** 32–38 (June 1962).

The molecular structure of chloroform, M. Jen and D. R. Lide, Jr., J. Chem. Phys. **36,** No. 9, 2525 (May 1962).

Device for chemically thinning crystals for transmission electron microscopy, H. B. Kirkpatrick and S. Amelinckx, Rev. Sci. Instr. **33,** No. 4, 488–489 (Apr. 1962).

Signs of nuclear resonance coupling constants in saturated aliphatic systems, H. Finegold, Proc. Chem. Soc. (London, England), No. 6, pp. 213–214 (June 1962).

Collision-induced microwave absorption in compressed gases, II. Molecular electric quadrupole moments, G. Birnbaum and A. A. Maryott, J. Chem. Phys. **36,** 2032–2036 (Apr. 1962).

Fluorescence in comets as a Markov process, T. Carrington, Astrophys, J. **135,** No. 3, 883–891 (May 1962).

Digital pattern recognition by moments, F. L. Alt, J. Assoc. Computing Mach. **9,** No. 2, 240–258 (Apr. 1962).

The nuclear photoeffect in holmium and erbium, E. G. Fuller and E. Hayward, Nuclear Phys. **30,** 613–635 (1962).

Formation constant of the 1:1 pyridine-iodine complex, A. G. Maki and E. K. Plyler, J. Phys. Chem. **66,** 766–767 (1962).

Photosensitized reaction between hydrogen (2p) atoms and molecular nitrogen, I. Tanaka and J. R. McNesby, J. Chem. Phys. **36,** No. 12 3170–3173 (June 15, 1962).

Effect of particle size on low-temperature heat capacities, A. C. Victor, J. Chem. Phys. **36,** No. 10, 2812–2813 (May 15, 1962).

Effect of molecular oxygen on the emission spectra of atomic oxygen-acetylene flames, S. L. N. G. Krishnamachari and H. P. Broida, J. Chem. Phys. **34,** 1709–1711 (1961).

Tchebycheff approximations by exponentials, J. R. Rice, J. Soc. Ind. Appl. Math. **10,** No. 1, 149–161 (Mar. 1962).

The morphology of mid-latitude 6300 angstrom arcs, T. Tohmatsu and F. E. Roach, J. Geophys. Res. **67,** No. 5, 1817–1821 (May 1962).

Some electrical properties of the porous graphite contact on *p*-type silicon, G. G. Harman, T. H. Higier, and O. L. Meyer, J. Appl. Phys. **33,** 2206 (July 1962).

The structure of the vibrational-rotational bands of an asymmetric rotor, H. C. Allen, Jr., Phil. Trans. Roy. Soc. London, Ser. B. Math. and Phys. Sci. **253,** No. 1030, 335–357 (Apr. 27, 1961).

Real representations of coordinate rotations, U. Fano, J. Math. Phys. **1,** No. 5, 417–423 (Sept.–Oct. 1960).

Structural and internal state variables in the description of scalar rate processes in fluids, R. E. Nettleton, Phys. Fluids **4,** 1488 (1961).

The types of blackout, their time variations, and the mechanisms producing them, V. Agy, J. Phys. Soc. Japan **17,** 93–97 (Sept. 1961).

Quantum-mechanical calculation of harmonic oscillator transition probabilities in a one-dimensional impulsive collision, K. E. Shuler and R. W. Zwanzig, J. Chem. Phys. **33,** No. 6, 1778–1784 (Dec. 1960).

The vapor pressure of 20 °K equilibrium hydrogen, L. C. Weber, Jr., D. E. Diller, H. M. Roder, and R. D. Goodwin, Cryogenics **3,** 236–238 (June 1962).

Programming for a closed-loop manned-machine combined system, D. C. Friedman, Proc. Combined Analog Digital Computer Systems Symp., Phila., Pa., Dec. 1960, 12th item (1960).

Studies in non-equilibrium rate processes, V. The relaxation of moments derived from a master equation, K. E. Shuler, K. Anderson, and G. H. Weiss, J. Math. Phys. **3,** No. 3, 550–556 (May–June 1962).

Kinetics of the hydrolysis of acetal in *N*-methylpropionamide-water and N, *n*-dimethylformamide-water solvents at 20, 25, 30, and 40 °, R. K. Wolford and R. G. Bates, J. Phys. Chem. **66,** No. 8, 1496–1500 (1962).

Symposium on spectroscopic excitation, B. F. Scribner, Am. Soc. Testing Materials Spec. Tech. Publ. **259,** 1 (Oct. 1960).

Path loss measurements versus prediction for long distance tropospheric scatter circuits, A. F. Barghausen and C. F. Peterson, IRE Trans. on Commun. Systems **CS-9,** No. 4, 439–445 (Dec. 1961).

Introduction to the theory of V.L.F. propagation, J. R. Wait, Proc. IRE **50,** 1624–1647 (July 1962).

Some experimental aspects of nuclear orientation, E. Ambler, Proc. Tenth Intern. Congress of Refrigeration, Copenhagen, Denmark, **I,** 195–198 (1959).

The densities of saturated liquid hydrogen, R. D. Goodwin, D. E. Diller, H. M. Roder, and L. A. Weber, Cryogenics **2,** 81–83 (Dec. 1961).

Irreversible processes in liquids and the density matrix: monatomic molecules, R. E. Nettleton, Phys. Fluids **5,** No. 6, 687–700 (June 1962).

Swtiching properties in ferroelectrics of the family $Bi_4Ba_{m-2}Ti_{m+1}O_{3(m+2)}$, P. H. Fang and E. Fatuzzo, J. Phys. Soc. Japan **17,** 238 (1962).

A derivation of the relaxation spectrum representation of the mechanical response function, R. S. Marvin, Repts. Progr. Polymer Phys. Japan **5,** 56–58 (1962).

Thermal isomerization of isopropyl-1,1,1-d_3 radicals, W. M. Jackson and J. R. McNesby, J. Chem. Phys. **36,** No. 9, 2272–2275 (May 1, 1962).

Research on light metals in the Metallurgy Division, National Bureau of Standards, T. G. Digges, (Symp. Light Metal Industry, Jamshedpur, India) Indian Construction News, p. 68 (Aug. 1961).

Attempts to eliminate fatigue damage by heat treatment, J. A. Bennett, Am. Soc. Metals, Trans. Quart. (Tech. Notes) **55,** No. 2, 362–363 (June 1962).

Graphs for bivariate normal probabilities, M. Zelen and N. C. Servero, Ann. Math. Stat. **31,** No. 3, 619–624 (Sept. 1960).

Nuclear moment of NI^{61}, L. H. Bennett and R. L. Streever, Jr., Phys. Rev. Letters **121,** No. 6, 2141–2142 (June 15, 1962).

New uses of microfilm with electronic scanners, a progress report on FOSDIC III, M. L. Greenough, Proc. 8th Annual Meeting Natl. Microfilm Assoc., Wash. D.C., Apr. 2–4, 1959, p. 278 (Annapolis, Md., 1959).

Susceptor elements for high temperature induction heating, S. Hasko and H. S. Parker, Am. Ceram. Soc. Bull. **41,** No. 7, 467 (July 1962).

Relation of solar active regions at central meridian passage to ionospheric disturbance, C. S. Warwick and J. V. Lincoln, AGARDograph Proc, Sixth AGARD Ionospheric Research Committee Meeting (Rome, Italy, May 15–18, 1961).

Radiolysis of ethane-1,1,1,-d_3, L. J. Stief and P. Ausloos, J. Chem. Phys. **36,** No. 11, 2904 (June 1, 1962).

Radiowave propagation during world war II, K. L. Norton, Proc. Re **50,** No. 5, 698–704 May 1962).

Development directions to keep leather apace, J. R. Kanagy, Leather & Shoes **142,** 34–35 (Aug. 12, 1961).

Radio propagation quality in the North Atlantic area 1953–1960, M. E. Nason, AGARDograph Proc. 6th AGARD Ionospheric Research Committee Meeting (Rome, Italy, May 15–18, 1961).

Discussion of Feldman's and Sereda's Paper Characteristics of sorption and expansion isotherms of reactive limestone aggregate, C. M. Hunt, L. A. Tomes, R. G. Pike, and D. Hubbard, J. Am. Concrete Inst. **59,** 815–818 (Mar. 1962).

The National Bureau of Standards Library, S. A. Jones, D. C. Libraries **32,** 7–10 (Jan. 1961).

Systematic errors, W. J. Youden, Ordnance **XLVI,** No. 248, 299–301 (Sept.–Oct. 1961).

Heat of formation of the most stable form of metaboric acid, HBO_2(cI), M. V. Kilday and E. J. Prosen, J. Am. Chem. Soc. Commun. to Editor **82,** 550 (1960).

The scientific contributions of William Weber Coblentz, E. K. Plyler, J. Appl. Spect. **16,** No. 3, 73–77 (1962).

Absorption spectrum of CF_2 trapped in an argon matrix, A. M. Bass and D. E. Mann, J. Chem. Phys. **36,** No. 12, 3501–3502 (June 15, 1962).

A test method for air-entrainment of standard Ottawa sand, M. R. DeFore and H. J. Corah, ASTM Bull. No. 248, 48–56 (TP162–166) (Sept. 1960).

The angular distribution of beta particles from oriented cerium-141 nuclei, D. D. Hoppes, Proc. Seventh Intern. Conf. Low Temperature Physics, University of Toronto, Canada, Aug. 1960, p. 186 (University of Toronto Press, Toronto, Canada, 1960).

Die radiometeorologie and ihre bedeutung fur die aus breitung der m-, dm- and cm- wallen auf grosse entfernungen, B. R. Bean, L. Fehlhaber, and J. Grosskopf, Nachr. Z (NTZ), pp. 9–16 (Jan. 1962).

The program at the National Bureau of Standards, L. M. Branscomb, Book, Optical Spectroscopic Measurements of High Temperatures, ed. P. J. Dickerman, p. 235 (Univ. of Chicago Press, Chicago, Ill., 1961).

Study of "valley problem" with a ray tracing program, K. Davies and A. K. Saha, Electron Density Profiles, pp. 162–166 (1962).

The extrapolation of the orthorhombic *N*-paraffin melting properties to very long chain lengths, M. G. Broadhurst, J. Chem. Phys. **36,** No. 10, 2578 (May 15, 1962).

Oscillatory phenomena, A. H. Kahn (Proc. Conf. High Magnetic Field, Mass. Inst. Tech. Cambridge, Mass., Nov. 1–4, 1961), Book, High Magnetic Fields, pp. 480–488 (Mass. Inst. Tech. Press, Cambridge, Mass., and John Wiley & Sons, Inc., New York, N.Y., 1962).

The information problem in government, S. N. Alexander, Proc. Engineering Information Symp. (Sponsored by the Engineers Joint Council), pp. 15–16 (Jan. 17, 1962).

Problems in the temperature calibration of an X-ray diffractometer furnace, F. A. Mauer and L. H. Bolz, (Proc. Tenth Annual Conf. Applications of X-ray Analysis, Denver, Colo., Aug. 7–9, 1961), Book, Advances in X-ray Analysis, p. 229 (Plenum Press, Inc., New York, N.Y., 1962).

The detection and study of solar cosmic rays by radio techniques, D. K. Bailey, (Intern. Conf. on Cosmic Rays and the Earth Storm), J. Phys. Soc. Japan **17,** Suppl. A–1, Pt. I, 106–112 (1962).

Precision and accuracy—experiment design aspects, C. Eisenhart, Conf. on Applications of Statistical Methods in the Chemical Industry, Feb. 4, 1961, (Sponsored by Am. Soc. for Quality Control, Metropolitan Section, Seaton Hall University, South Orange, N.J.), p. 1 (1961).

Games associated with a renewal process, M. M. Siddiqui, Ann. Math. Stat. **33,** 697–701 (June 1962).

Purification and vapor pressure of pure nitric oxide, E. E. Hughes, J. Chem. Phys. Letter to Editor **35,** No. 4, 1531–1532 (Oct. 1961).

Ultrasounds induce flaking of ceramics from metals, J. W. Pitts, Metal Progr. **82,** No. 2, 114–115 (Aug. 1962).

Use of gas phase chromatography for rapid determination of carbonate at low levels, F. G. Carpenter, Anal. Chem. **34,** 66 (Jan. 1962).

An experimental investigation of the scintillation of radio stars observed at frequencies of 223 and 456 megacycles per second from a location close to the auroral zone, C. G. Little, G. C. Reid, E. Stiltner, and R. P. Merritt, J. Geophys. Res. **67,** No. 5, 1763–1784 (May 1962).

The radiative formation and destruction of negative ions, L. M. Branscomb, Proc. Fifth Intern. Conf. Ionization Phenomena in Gases, Munich, Germany, I, 1–18 (North Holland Publ. Co., Amsterdam, The Netherlands, 1961).

A computer for weather data acquisition, P. Meissner, J. A. Cunningham, and C. A. Kettering, Proc. Eastern Joint Computer Conf., Dec. 13–15, 1960, p. 57 (New York, N.Y., 1960).

Position titles of chemists, W. K. Wilson, Capital Chemist 10, 145 (May 1960).

Corrected calculations of sound absorption in non-associated liquids, R. E. Nettleton, J. Acoust. Soc. Am. **34,** No. 3, 350 (Mar. 1962).

International comparisons of radioactivity standards, W. E. Perry and W. B. Mann, Proc. Ninth Intern. Congress on Radiology, Munich, Germany, July 1959, 23, VII–30. VII, 1338–1342 (Urban and Schwarzenberg, Munich, Germany, 1960).

Criteria for the reality of matrix eigenvalues, M. P. Drazin and E. V. Haynsworth, Z. Math. **78,** 449–452 (Mar. 1962).

A rapid simple method of estimating the order of chemical reactions, J. H. Flynn, Chem. Eng. **69,** No. 17, 137–140 (Aug. 20, 1962).

Paramagnetic resonance phenomena, H. E. Radford, Encyclopaedic Dictionary of Physics **5,** 293 (Pergamon Press Inc., New York, N.Y., 1962).

Chilled-air-distribution in refrigerated traliers, P. R. Achenbach, Suppl. Bull. Intern. Inst. of Refrigeration, p. 9 (1961–1962).

Mass spectrum and appearance potentials of tetrafluorohydrazine, J. T. Herron and V. H. Dibeler, J. Chem. Phys. **33,** No. 5, 1595–1596 (Nov. 1960).

A survey of polar cap absorption events (solar proton events) in the period 1952 through 1960, D. K. Bailey and J. M. Harrington, (Intern. Conf. on Cosmic Rays and the Earth Storm), J. Phys. Soc. Japan **17,** Suppl. A–II, Pt. II, 334–337 (1962).

Isotope effect in an electric field and jump frequencies for diffusion in ionic crystals, J. R. Manning, J. Appl. Phys. **33,** No. 7, 2145–2151 (July 1962).

Determination of isotope effects by "double labeling" oxidation of *d*-glucose with iodine, H. S. Isbell, L. T. Sniegoski, and H. L. Frush, Anal. Chem. **34,** No. 8, 982–984 (July 1962).

Methods of nuclear orientation, E. Ambler, Book, Progress in Cryogenics, ed. K. Mendelssohn III, 235–280 (Heywood and Co., Ltd., London, England, 1960).

Molecular collision models and transition probabilities in liquids, R. E. Nettleton, J. Chem. Phys. **38,** 2226–2227 (Apr. 1962).

Electronic development and production in the USSR, C. P. Marsden, Encylcopedia on Russia and the Soviet Union, pp. 158–160 (McGraw-Hill Book Co., Inc., New York, N.Y., 1961).

Microwave spectrum of trimethylarsine, D. R. Lide, Jr., Spectrochem. Acta **15,** 473 (1959).

Lattice frequencies and rotational barriers for inorganic carbonates and nitrates, R. A. Schroeder, C. E. Weir, and E. R. Lippincott, J. Chem. Phys. **36,** No. 10, 2803–2804 (May 1962).

Environmental characteristics of a small underground fallout shelter, P. R. Achenbach, F. J. J. Drapeau, and C. W. Phillips, ASHRAE J. **4,** No. 1, 21 (Jan. 1962).

Chemically induced vibrational excitation: hydroxyl radical emission in the 1-3-micron region produced by the $H+O_3$ atomic flame, D. Garvin, H. P. Broida, and H. J. Kostkowski, J. Chem. Phys. **37,** No. 1, 193 (July 1962).

Gas-phase radiolysis of propane, P. Ausloos and S. Lias, J. Chem. Phys. **36,** No. 12, 3163–3170 (July 15, 1962).

The absolute simplest form in digital circuit design, R. S. Ledley, Book, Digital Computers and Control Engineering, 835 pgs., (McGraw-Hill Book Co., Inc., New York, N.Y., 1960).

Infrared spectrum of dideuteroacetylene (C_2D_2), E. D. Tidwell and E. K. Plyler, J. Opt. Soc. Am. **52,** No. 6, 656–664 (June 1962).

The standards challenge, A. H. Scott, Insulation **8,** No. 2, 48–50 (Feb. 1962).

A system for generating "pronounceable" names using a computer, A. L. Leiner and W. W. Youden, J. Assoc. Computing Mach **8,** No. 1, 97–103 (Jan. 1961).

Using digital computers in the design and maintenance of new computers, A. L. Leiner, A. Weinberger, H. Loberman, and C. Coleman, IRE Trans. Electronic Computers **EC–10,** No. 4, 680–690 (Dec. 1961).

Surface preparation of solid metallic samples for X-ray spectrochemical analysis, R. E. Michaelis and B. A. Kilday, Book, Advances in X-ray Analysis **5,** 405–411 (Plenum Press, Inc., New York, N.Y., 1962).

Infrared wavelength dependence of the total absorptivity of electroplated silver, D. Cline, J. Appl. Phys. **33,** 2310–2311 (July 1962).

Simple stain gauge-based load controller, L. Mordfin and R. L. Bloss, Rev. Sci. Instr. **33,** No. 7, 772–773 (July 1962).

Quantum-mechanical calculation of harmonic oscillator transition probabilities. II. Three-dimensional impulsive collisions, F. H. Mies and K. E. Shuler, J. Chem. Phys. **37,** No. 1, 177–181 (July 1, 1962).

Remote phase control of station WWV, R. F. Fey, J. B. Milton, and A. H. Morgan, Nature **193,** No. 4820, 1063–1064 (Mar. 17, 1962).

Melting and contractility of feather keratin, L. Mandelkern, J. C. Halpin, and A. F. Diorio, J. Polymer Sci. Letter to Editor **60,** No. 169, S31–S33 (July 1962).

Wave propagation around a curved boundary which contains an obstacle, J. R. Wait, Can. J. Phys. **40,** 1010–1016 (Aug. 1962).

Duration and spacing of sferic pulses, R. F. Linfield and C. A. Samson, Proc. IRE **50,** 1841–1842 (Aug. 1962).

VHF and UHF signal characteristics observed on a long knife-edge, A. P. Barsis and R. S. Kirby, IRE Natl. Conv. Record, pp. 17–34 (1961).

Some observations on growing crystals of argon, L. H. Bolz, H. P. Broida, and H. S. Peiser, Acta Cryst. **15,** No. 8, 810–812 (Aug. 1962).

Methods and techniques of low and very low frequency monitoring at Boulder Laboratories, A. H. Morgan and D. H. Andrews, Consultative Committee for Definition of the Second Intern. Comm. on Weights and Measures, Apr. 11–12, 1961, pp. 1–10 (June 1961).

Physical measurement: Pilot of progress, A. V. Astin, Steel, p. 112 (July 23, 1962).

Vacuum photolysis of solid ethane at 77 °K, M. D. Scheer, J. McNesby, and R. Klein, J. Chem. Phys. **36**, No. 12, 3504–3505 (June 1962).

Geomagnetic and solar data, J. V. Lincoln, J. Geophys. Res. **67**, No. 5, 2035–2038 (May 1962).

Supporting evidence for solar flare effects in the *F* region of the ionosphere, R. W. Knecht and K. Davies, Nature 192, No. 4800, 348–350 (Oct. 28, 1961).

Dependence of interval between flare and associated sudden commencement storm on prestorm conditions, M. W. Haurwitz, J. Geophys. Res. Letter **67**, 2979–2982 (July 1962).

The application of NMR in determination of the structure of cyclanols, I. The structures of cyclohexane-1,3-diols, H. Finegold and H. Kwart, J. Organic Chem. **27**, 2361–2365 (1962).

Spectrophotofluorometric studies of degraded cotton cellulose, S. D. Toner and K. F. Plitt, Tappi **45**, No. 8, 681–688 (Aug. 1962).

Algorithm and rapid binary division, R. S. Ledley and J. B. Wilson, IRE Trans. Electronic Computers **EC–10**, No. 4, 662–670 (Dec. 1961).

Opportunities in dental research, G. C. Paffenbarger, J. Am. Dental Assoc. **60,** No. 3, 413–414 (Mar. 1960).

On the nature of equatorial slant sporadic *E*, R. Cohen, K. L. Bowles and W. Calvert, J. Geophys. Res. **67,** No. 3, 965–972 (Mar. 1962).

Elementary statistical design, W. J. Youden, Conf. on Applications of Statistical Methods in the Chemical Industry, Feb. 4, 1961 (Sponsored by Am. Soc. for Quality Control, Metropolitan Section, Seaton Hall University, South Orange, N.J.), p. 43 (1961).

Dielectric loss in "non-polar" polymers, A. J. Curtis, J. Chem. Phys. **36,** No. 12, 3500 (June 15, 1962).

Mobilities of positive ions in argon, E. C. Beaty, Proc. Conf. Ionization Phenomena in Gases, Aug. 28–Sept. 1, 1961, Munich, Germany, p. 183 (North Holland Publ. Co., Amsterdam, The Netherlands, 1962).

Correction to "doppler studies of the ionosphere with vertical incidence," K. Davies, Proc. IRE **50,** No. 6, 94 (June 1962).

Electron photo-detachment from ions and elastic collision cross sections for O, C, Cl and F, J. W. Cooper and J. B Martin, Phys. Rev. **126,** No. 4, 1482 (May 15, 1962).

The following articles were presented before the 1961 Cryogenic Engineering Conference and published in the Book, Advances in Cryogenic Engineering **7** (Plenum Press, Inc., New York, N.Y., 1962):

A cryostat for tensile tests in the temperature range 300 ° to 4 °K, R. P. Reed, Paper K–3, 448–454.

A method of measuring shear modulus from −424 ° to 70 °F, R. P. Mikesell and R. M. McClintock, Paper K–11, 509–513.

An electrically controlled guarded flat plate calorimeter, D. Cline and R. H. Kropschot, Paper L–5, 534–538.

An experimental investigation of the individual boiling and condensing heat transfer coefficients for hydrogen, D. E. Drayer and K. D. Timmerhaus, Paper J–6, 401–412.

Dry gas operation of ball bearings at cryogenic temperatures, L. E. Scott, D. B. Chelton, and J. A. Brennan, Paper G–3, 273–276.

Low temperature characteristics of some commercial thermocouples, R. L. Powell and L. P. Caywood, Jr., Paper L–2, 517–521.

Martensitic transformation products and mechanical properties of austenitic stainless steels at low temperatures, C. J. Guntner and R. P. Reed, Paper K–9, 500–502.

On the bulk density of boiling liquid oxygen, R. W. Arnett, Paper F–4, 214–218.

Temperature dependence of magnetic losses, J. J. Gniewek and R. L. Powell, Paper H–1, 303–310.

Testing of ball bearings with five different separator materials at 9200 RPM in liquid nitrogen, J. A. Brennan, W. A. Wilson, R. Radebaugh, and B. W. Birmingham, Paper G–2, 262–272.

The application and behavior of elastomers at cryogenic temperatures, R. F. Robbins, D. H. Weitzel, and R. N. Herring, Paper H–6, 343–352.

The application of gas-lubricated bearings to a minature helium expansion turbine, B. W. Birmingham, H. Sixsmith, and W. A. Wilson, Paper A–4, 30–42.

The efficiency of an ideal refrigerator, R. B. Jacobs, Paper L–11, 567–571.

The following papers were published in the Book:

Analytical Chemistry of Polymers, Parts II and III (Book), Ed. G. M. Kline (Vol. XII of High Polymers Series, Interscience Publ., New York, N.Y., 1962):

Part II. Analysis of molecular structure and chemical groups. 619 pages.

I. Molecular weights and sizes, S. G. Weissberg, S. Rothman, and M. Wales, pp. 1–77.
II. X-ray diffraction, A. S. Posner, pp. 79–108.
III. Optical methods, A. F. Forziati, pp. 109–157.
IV. Differential thermal analysis, H. E. Kissinger and S. B. Newman, pp. 159–179.
V. Pyrolysis, L. A. Wall, pp. 181–248.
VI. Mass spectrometry, L. A. Wall, pp. 249–268.
VII. Ultraviolet spectrophotometry, M. Tyron and E. Horowitz, pp. 269–289.
VIII. Infrared spectrophotometry, M. Tryon and E. Horowitz, pp. 291–333.
IX. Fluorescence, A. F. Forziati, pp. 335–357.
X. Chromatography, J. M. Cassel, pp. 359–404.
XI. Polarography, G. M. Brauer, pp. 405–485.
XII. Magnetic resonance spectroscopy, L. A. Wall and R. E. Florin, pp. 487–559.

Author index, subject index, pp. 561–619.

Part III. Identification procedures and chemical analysis 566 pages.

I. Systematic procedures, G. M. Brauer and E. Horowitz, pp. 1–140.
II. Color tests, G. M. Brauer and S. B. Newman, pp. 141–259.
III. Microscopy, S. B. Newman, pp. 261–348.
IV. Radiochemical analysis, R. E. Florin and L. A. Wall, pp. 349–395.
V. End-group analysis, M. Hellmann and L. A. Wall, pp. 397–411.

General References, pp. 413–419.

Cumulative subject and author index, pp. 421–566.

Emission spectra of solids condensed at very low temperatures from the electrical discharge products of nitrogen and carbon monoxide or acetylene, S. L. N. G. Krishnamachari, R. W. Nicholls, and H. P. Broida, Proc. Indian Acad. Sci. **LIV,** 61–68 (1961).

Excitation of the red and green coronal lines, C. Pecker and R. N. Thomas, Ann. Astrophys. **25,** 100–108 (Mar.-Apr. 1962).

Dependence of the ionospheric *F* region on the solar cycle, J. W. Wright, Nature **194,** No. 4827, 461–462 (May 1962).

Boolean matrix equations in digital circuit design, R. S. Ledley IRE Trans. Electronic Computers **EC–8,** No. 2, 131–139 (June 1959).

**Publications for which a price is indicated are available from the Superintendent of Documents, U.S. Government Printing Office, Washington 25, D.C. (foreign postage one-fourth additional). Reprints from outside journals and the NBS Journal of Research may often be obtained directly from the authors.*

U.S. GOVERNMENT PRINTING OFFICE:1963

UNIVERSITY MICROFILMS INC
EDITORIAL DEPARTMENT
313 NORTH FIRST ST
ANN ARBOR MICH
R 10-C JUNE

UNI
GOVERNMENT PRINTING OFFICE
DIVISION OF PUBLIC DOCUMENTS
WASHINGTON 25, D.C.
OFFICIAL BUSINESS

PENALTY FOR PRIVATE USE TO AVOID PAYMENT OF POSTAGE, $300 (GPO)

JOURNAL OF RESEARCH of the National Bureau of Standards Vol. 67C, No. 1 January–March 1963
C. Engineering and Instrumentation

Contents

	Page
Method for calibrating a standard volt box. Bernadine L. Dunfee.	1
Stability of residual thiosulfate in processed microfilm. C. I. Pope.	15
Equipment for single crystal growth from aqueous solution. John L. Torgesen, Avery T. Horton, and Charles P. Saylor.	25
An automatic multichannel correlator. Robert F. Brown, Jr.	33
Elastic constant—porosity relations for polycrystalline thoria. S. Spinner, F. P. Knudsen, and L. Stone.	39
An oxygen partial pressure warning instrument. Lewis Greenspan.	47
New fast-opening, large-aperture shutter for high-speed photography. E. C. Cassidy and D. H. Tsai.	65
Equations for the radiofrequency magnetic permeameter. Cletus A. Hoer and Alvin L. Rasmussen.	69
Publications of the National Bureau of Standards.	77

For sale by the Superintendent of Documents, U.S. Government Printing Office, Washington 25, D.C. Price 75 cents (single copy)
Subscription price: $2.25 a year; 50 cents additional for foreign mailing.

UNITED STATES GOVERNMENT PRINTING OFFICE, WASHINGTON : 1963